UNIVERSITÀ
DI PARMA

DOTTORATO DI RICERCA IN
"SCIENZE DEL FARMACO, DELLE BIOMOLECOLE E DEI PRODOTTI PER LA SALUTE"

CICLO XXX

TARGETING INTEGRINS AND BEYOND: SYNTHESIS AND BIOLOGICAL EVALUATION OF MULTIFUNCTIONAL PEPTIDOMIMETICS IN TUMOR THERAPY

Coordinatore:
Chiar.mo Prof. Marco Mor

Tutore:
Chiar.ma Prof.ssa Franca Zanardi

Dottoranda: Elisabetta Portioli

Anni 2014/2017

I wish to dedicate this thesis to Giovannino Guareschi.

Esistono cento qualità diverse di uva: c'è la bianca, la rossa, la nera, la dolce, l'aspra, l'uva moscata, la malvasia, il lambrusco, la fortana, l'uvona, l'uvetta e via discorrendo. Ma, pur se spremete cento grappoli d'uva di qualità diverse, il sugo è sempre quello: vino. A spremere uva non caverete mai benzina, latte, oppure limonata. È il succo, quello che conta, in ogni cosa.

Giovannino Guareschi, "Corrierino delle famiglie"

Table of Contents

Abstract

The work described in this PhD thesis concerns the design and synthesis of small molecular ligands targeting some subtypes of the integrin receptor family, in particular $\alpha_V\beta_3$ and $\alpha_4\beta_1$ integrins.

One major effort, which is described in Chapter 1*a*, is focused on the synthesis of dual small molecule conjugates as potential tools to impair tumor-associated angiogenesis. These constructs are formed by the covalent conjugation of a RGD unit, which is able to selectively bind to the extracellular segment of the $\alpha_V\beta_3$ integrin receptor, with a sunitinib-like moiety, a proven tyrosine kinase inhibitor (TKI) able to interact with the cytoplasmic domain of VEGFR2. Given the strict crosstalk between the VEGFR2 and $\alpha_V\beta_3$ receptors in both activated endothelial cells (ECs) and some cancer cell types, the blockage of the $\alpha_V\beta_3$/VEGFR2 couple may assume high anti-angiogenic and anti-tumor potential. On these bases, three dual conjugates were designed, synthesized and fully characterized, and subsequently tested *in vitro* to assess their properties as $\alpha_V\beta_3$ binders and VEGFR2 kinase inhibitors. All the conjugated compounds showed interesting anti-angiogenesis properties *in vitro* and one of them demonstrated a significant angiogenesis impairment *in vivo*, which proved superior to the action of the single RGD or sunitinib modules and their simple combinations.

In Chapter 1*b* the work done during my period abroad is described. The coordination of platinum to DNA is an area of intense research that allowed the development of valuable platinum-based chemotherapeutics such as cisplatin and carboplatin. Besides DNA, platinum(II) is able to coordinate other biomolecules such as proteins, and this binding ability was exploited in bioconjugation reactions. In particular, extensive research in this area showed that some *N*-heteroaryl and *S*-donor groups in the side chains of suitable amino acids are preferential coordination sites for platinum in proteins. My work focused on the exploitation of the binding properties of Pt(II) versus suitable amino acids in order to synthesize cyclic peptides. In particular, four new cyclopeptides were prepared, where the central Pt(II) metal ion coordinates to different bidentate amine ligands and diverse RGD-based peptide sequences embedding suitable *N*-heteroaryl and *S*-donor groups. This coordination-based approach testifies that the platinum(II) ion may exert a double function: *i*) to favour peptide cyclization by exploiting its coordinative ability; and *ii*) to furnish peptide-Pt(II) complexes, which could be valuable tools for anti-cancer and anti-angiogenic interventions.

As a further therapeutic target of interest, another integrin receptor, $\alpha_4\beta_1$, was considered, given its primary role in mediating chronic inflammation, autoimmune diseases and cancer-related inflammation. In Chapter 2, our efforts in this field are described. In particular, the design and synthesis of seven new cyclic peptidomimetics are reported, all of which containing an aminoproline core scaffold grafted into key $\alpha_4\beta_1$-recognizing peptide sequences. This work constitutes a first step towards further studies aiming at the evaluation of these small molecules as effective and selective $\alpha_4\beta_1$ binders, with the final goal of gaining insights about the structural and functional aspects of this important biological target.

For clarity's sake, this thesis is organized into three main chapters – chapter 1*a*, 1*b*, and 2- with self-consistent numbering of compound formulas, figures, schemes and references.

Name of Amino Acid*	Three letter code	One letter code
Alanine	Ala	A
Arginine	Arg	R
Asparagine	Asn	N
Aspartic Acid	Asp	D
Cysteine	Cys	C
Glutamic Acid	Glu	E
Glutamine	Gln	Q
Glycine	Gly	G
Histidine	His	H
Isoleucine	Ile	I
Leucine	Leu	L
Lysine	Lys	K
Methionine	Met	M
Phenylalanine	Phe	F
Proline	Pro	P
Serine	Ser	S
Threonine	Thr	T
Tryptophan	Trp	W
Tyrosine	Tyr	Y
Valine	Val	V

*D-amino acids are described by D-Xaa in the three-letter code and with the small letter in the one-letter code.

Chapter 1. Targeting integrin $\alpha_V\beta_3$

1a. Dual conjugates

Part of the work described in this Chapter was published in the following article:

Sartori, A.; Portioli, E.; Battistini, L.; Calorini, L.; Pupi, A.; Vacondio, F.; Arosio, D.; Bianchini, F.; Zanardi, F. Synthesis of Novel *c*(AmpRGD)−Sunitinib Dual Conjugates as Molecular Tools Targeting the $\alpha_V\beta_3$ Integrin/VEGFR2 Couple and Impairing Tumor-Associated Angiogenesis. *J. Med. Chem.* **2017**, *60* (1), 248–262.

1*a*.1 Introduction

1*a*.1.1 Angiogenesis

Blood vessels are fundamentally composed of endothelial cells (ECs), which interconnect with each other to form the tubes that direct and maintain blood flow and tissue perfusion.[1] Several modes of vessel formation have been identified, as shown schematically in Figure 1.

In the developing mammalian embryos, blood vessels form through *vasculogenesis* (Fig. 1b), a process which involves the *de novo* production of ECs from mesoderm-derived angioblast and endothelial precursors, which are recruited to differentiate in response to local cues. Distinct signals then specify either arterial or venous differentiation. Vasculogenesis is typically followed by classical *sprouting angiogenesis* (Fig. 1a), which involves the ECs on pre-existing vasculature to form new blood vessels, ensuring the expansion of the vascular network. *Arteriogenesis* then occurs, in which endothelial cell channels become covered by pericytes or vascular smooth muscle cells (VSMCs), which provide stability and control perfusion. Moreover, angiogenesis occurs during development and vascular remodeling according to a tightly controlled dynamic process leading to neovascularization, which supports the requirements of the changing tissue. After plain development, the vasculature rarely extend further.[1] In the adult, physiological angiogenesis occurs during wound healing and in the female reproductive cycles (ovulation, menstruation, implantation, pregnancy) and it is usually focal, such as in blood coagulation in a wound, and self-limited in time, taking days (ovulation), weeks (wound healing) or months (placentation).[2,3] By contrast, pathological angiogenesis can persist for years. During pathological angiogenesis the vessel growth is deregulated, contributing to the pathogenesis of many disorders. To name just a few, *insufficient vessel growth* can lead to heart and brain ischemia, ulcerative disorders and neurodegeneration, while *abnormal vessel growth* may fuel cancer, inflammatory disorders, pulmonary hypertension and blinding eye diseases.[3,4]

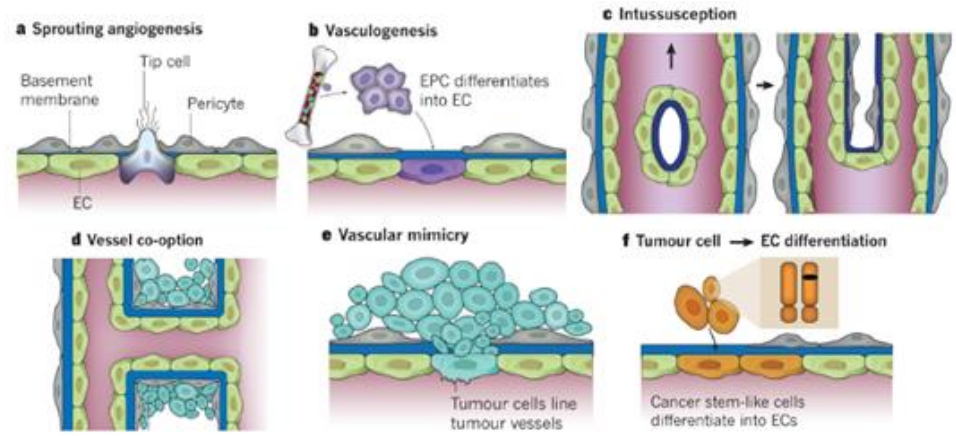

Figure 1. Known methods of blood vessel formation in normal tissues (**a-c**) and tumors (**a-f**). Figure reprinted from ref.[1].

Tissues can also become vascularized by other mechanisms, but the relevance of these processes is not well understood (Fig. 1).[1,5] Endothelial progenitor cells (EPCs), which can either reside in the vascular wall or migrate from bone marrow in response to chemoattractants from the tumor cells, can differentiate into ECs and contribute to vessel formation (a process known *postnatal vasculogenesis*). *Vascular mimicry* can also occur, whereby tumor cells can act as replacement cells for ECs. Another possibility is that chromosomal abnormalities in putative cancer stem cells allow tumor cells to differentiate into ECs. Other mechanisms by which tumor cells can obtain a blood flow include *vessel co-option*, whereby the tumor cell arises near to (or migrates toward) a preexisting blood vessel, or the process of *intussusception*, whereby a preformed vessel splits into two daughter vessels by the insertion of a tissue pillar. Unlike normal tissues, which use sprouting angiogenesis, vasculogenesis and intussusception (Fig. 1, **a**-**c**), tumours can use all six modes of vessel formation (Fig. 1, **a**-**f**).

The most investigated vascularization mode is the *sprouting angiogenesis*, which is a complex process. In response to an appropriate stimulus, the quiescent vasculature can become activated to induce formation of new capillaries.[1]

- **Sprouting angiogenesis: vessel branching, maturation and quiescence**

In a healthy adult, quiescent ECs have long half-lives and are protected against insults by the autocrine action of maintenance signals, such as vascular endothelial growth factor (VEGF), NOTCH, angiopoietin-1 (ANG-1) and fibroblast growth factors (FGFs).[1,5] Because vessels supply oxygen, endothelial cells are equipped with *oxygen sensors* and *hypoxia-inducible factors,* such as prolyl hydroxylase domain 2 (PHD2) and hypoxia-inducible factor-2α (HIF-2α), respectively, which allow the vessels to re-adjust their shape to optimize blood flow. Quiescent ECs form a monolayer of cells interconnected by junctional molecules, such as VE-cadherin and claudins. These endothelial cells are ensheathed by pericytes, which suppress ECs proliferation and release cell-survival signals, such as VEGF and ANG-1. ECs and pericytes at rest produce a common basement membrane.

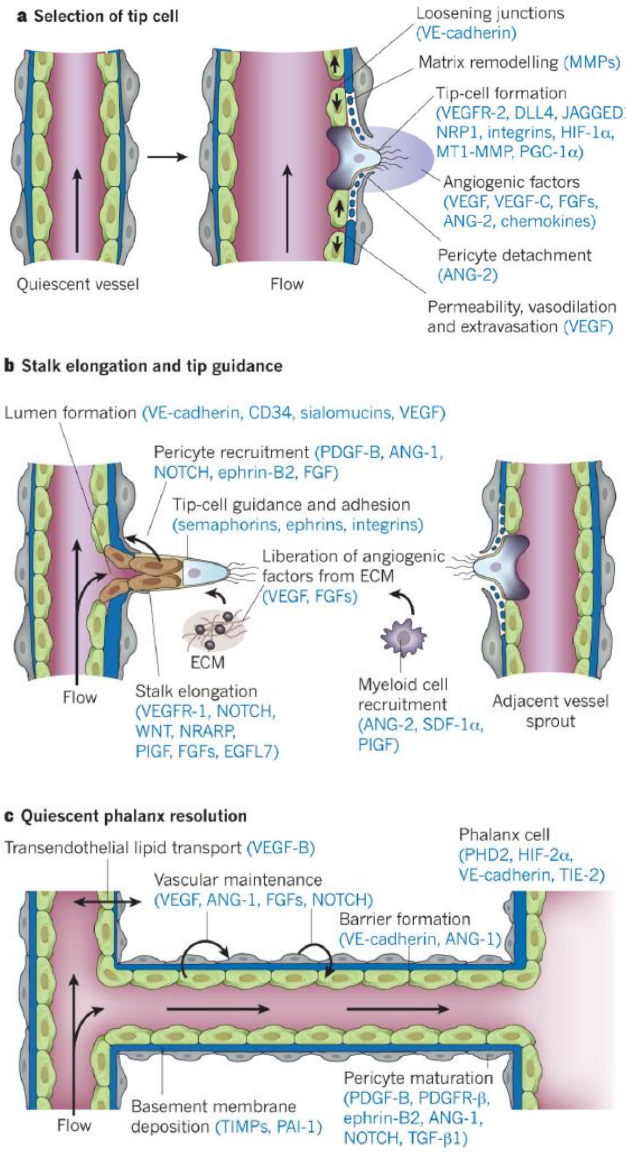

Figure 2. Molecular basis of vessel branching. The consecutive steps (**a-c**) of blood vessel branching are shown, with the key molecular players involved denoted in parentheses. Adapted from ref.[1].

When a quiescent vessel senses an **angiogenic signal** (such as VEGF, ANG-2, FGFs) *released by a hypoxic, inflammatory or tumour cell,* pericytes first detach from the vessel wall (in response to ANG-2) and liberate themselves from the basement membrane by proteolytic degradation, which is mediated by matrix metalloproteinases (MMPs) (Fig. 2a). ECs loosen their junctions, and the nascent vessel dilates. **VEGF** increases the permeability of the endothelial cell layer, causing plasma proteins (such as fibrinogen and fibronectin) to extravasate and lay down a provisional extracellular matrix (ECM) scaffold. In response to integrin signalling, ECs migrate onto this ECM surface. Proteases liberate angiogenic molecules stored in the ECM (such as VEGF and FGF) and remodel the ECM into an angio-competent milieu (Fig. 2b). To build a perfused tube and prevent ECs from moving en masse towards the angiogenic signal, one endothelial cell, known as the **tip cell**, becomes selected to lead the tip in the presence of factors such as VEGF receptors, neuropilins (NRPs), and the NOTCH ligands DLL4 and JAGGED1 (Fig. 2a). The neighbours of the tip cell assume subsidiary positions as **stalk cells**, which divide to elongate the stalk [stimulated by NOTCH, NOTCH-regulated ankyrin repeat protein (NRARP), placental growth factor (PlGF) and FGFs] and establish the lumen (mediated by VE-cadherin, sialomucins, VEGF) (Fig. 2b).

Tip cells are equipped with filopodia to sense and navigate in response to environmental guidance signals, such as semaphorins and ephrins, and adhere to the extracellular matrix (mediated by integrins) to migrate. Instead, stalk cells release molecules (such as EGFL7) into the ECM to convey spatial information about the position of their neighbours, so that the stalk elongates (Fig. 2b).
A hypoxia-inducible program, driven by HIF-1α, renders endothelial cells responsive to angiogenic signals. Myeloid bridge cells aid the fusion of neighbouring vessel branches, allowing the initiation of blood flow. For a vessel to become functional, it must become mature and stable. Endothelial cells resume their quiescent state (Fig. 2c), and signals [such as platelet-derived growth factor B (PDGF-B), ANG-1, transforming growth factor-β (TGF-β), ephrin-B2 and NOTCH] cause the cells to become covered by pericytes. Protease inhibitors [known as tissue inhibitors of metalloproteinases (TIMPs) and plasminogen activator inhibitor-1 (PAI-1)] cause the deposition of a basement membrane, and junctions are re-established to ensure optimal flow distribution. Vessels regress if they are unable to become perfused.

Therefore, *sprouting angiogenesis* is a complex and tightly controlled dynamic process that can occur physiologically in those tissues that undergo active remodelling in response to stress and hypoxia. However, in pathological situations, such as cancer, the same angiogenic signaling pathways are induced and exploited.

- **Tumor angiogenesis**

Environmental or genetic events transform normal epithelial cells into tumor cells, which grow and divide with little effect on their surroundings until their size exceeds 1-2 mm.[6]

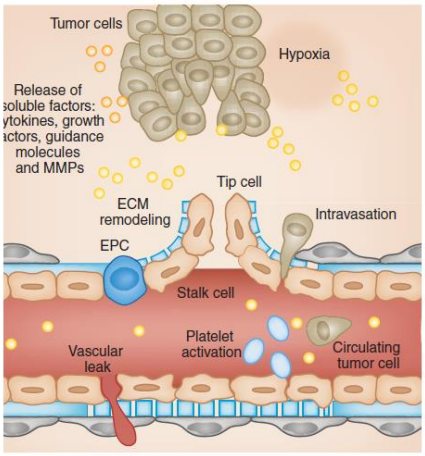

Figure 3. Tumor-associated angiogenesis. Figure reprinted from ref.[6].

Once a tumor lesion exceeds a few millimeters in diameter, hypoxia and nutrient deprivation trigger an "angiogenic switch", through up-regulation of the transcription factor hypoxia inducible factor-1α (HIF-1α), which in turn increases the expression of many angiogenesis inducers and suppresses the expression of endogenous angiogenesis inhibitors as well. Thus, tumor cells release soluble growth factors, chemokines and cytokines in their microenvironment, which create a concentration gradient that initiates the sprouting and proliferation of formerly quiescent endothelial cells on nearby blood vessels (Fig. 3). These signals also recruit a variety of cell types that compose the tumor microenvironment (Fig. 4). Their activation initiates a cascade of events that quickly become dysregulated, influencing the angiogenic response to a tumor.[6]

For example, the combination of stimulatory signals within the tumor microenvironment prompts perivascular cells to detach from the mature blood vessels, compromising their integrity, permitting their remodeling and promoting an activated phenotype. Once the vascular barrier is disrupted, multiple cell types are exposed to angiogenic and inflammatory stimuli to escalate the response. In particular, platelets are recruited to sites of exposed basement membrane, where they become activated and release their stores of stimulatory factors into the tumor microenvironment. Endothelial progenitor cells (EPCs) and myeloid cells from the bone marrow move to the perceived wound, where they release even more soluble factors locally. The remodeling response, required for tumor expansion, is further driven by recruitment of tumor-associated fibroblasts, which aberrantly deposit extracellular matrix (ECM) proteins and release stimulatory factors. Matrix metalloproteinases (MMPs) cleave and remodel the ECM to form fragments that affect the function of integrin on neighboring cells, or to expose previously hidden epitopes that function as endogenous inhibitors of angiogenesis, for example, tumstatin (TUMS) or endostatin (END) (Fig. 4).

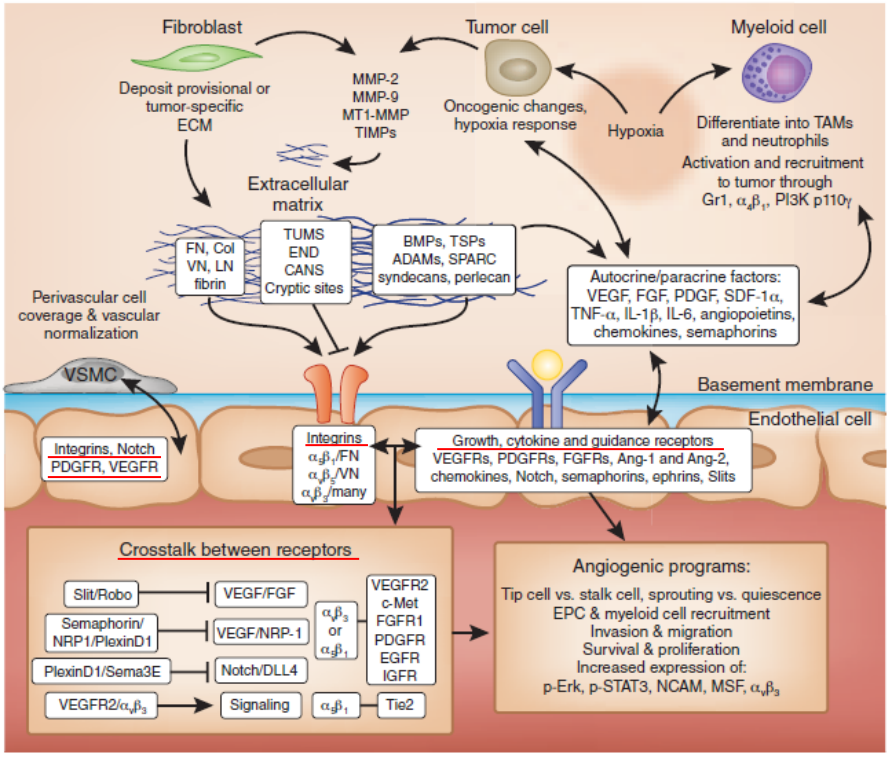

Figure 4. Variety of cell types and components of the stroma which compose tumor microenvironment, together with mediators of endothelial activation involved in the tumor angiogenic response. Figure reprinted from ref.[6].

Each cell in the tumor microenvironment is affected by its neighboring cells, as well as by the components of the tumor stroma (Fig. 4).[6] Within this dynamic environment, integrins and other receptors on the surface of endothelial cells recognize and bind factors that initiate intracellular signalling pathways, leading to phenotypic changes that promote the migration, invasion, survival and proliferation required for sprouting angiogenesis. Receptors from different pathways can crosstalk to either suppress or augment cellular activation (Fig. 4).

Targeting angiogenesis through therapeutics requires consideration of these signaling components among the different cell types and consideration of how receptor crosstalk might affect the net result. These complicated interactions govern angiogenic remodeling and can contribute to *de novo* or acquired resistance to a targeted anti-angiogenic therapy.

Given the specific and crucial role exerted by certain integrin subfamilies and vascular growth factor receptors in tumor-related angiogenesis, an emphasis will be placed upon these two receptor classes in the following paragraphs.

1*a*.1.2 Receptors involved in angiogenesis: Integrins and VEGFRs

1*a*.1.2.1 Integrin receptors and ligands

The integrins are a large family of cell adhesion molecules that have the crucial task of integrating (hence the name integrins) mechanochemical cues from the cytoskeleton or the extracellular matrix (ECM) across the plasma membrane.[7–9] Integrins, which are found on nearly all cells, mediate cell-cell and cell-substrate interactions. This extensive family of cell surface receptors, which in humans includes 24 subtypes formed by the noncovalent combination of 18 α-subunits and 8 β-subunits, binds to a diverse collection of ligands that are mostly large molecules, usually found in the subendothelial matrix, including fibronectin, vitronectin and collagen. Other ligands are plasma proteins, including complement factors and fibrinogen.[7] The biggest integrin subfamily, constituted by α_V integrins, $\alpha_{IIb}\beta_3$, $\alpha_5\beta_1$ and $\alpha_8\beta_1$, recognize the tripeptide sequence Arg-Gly-Asp (RGD) on their respective ligands (Fig. 5).[10,11] Then there are collagen receptors, that recognize the triple helical GFOGER sequence in their ligands, leukocyte-specific receptors with, for example, the LDV binding motif, and laminin receptors.

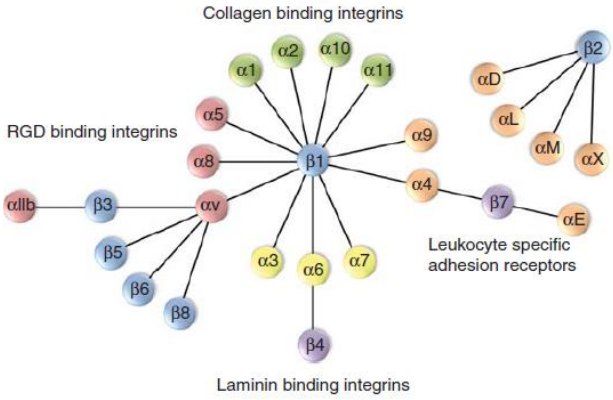

Figure 5. The integrin family. Reprinted from ref.[10].

Integrins possess a large extracellular domain, a transmembrane domain and a short cytoplasmatic region (with the exception of β_4 which has a cytoplasmatic domain of over 1000 amino acid residues).[7,12] Half of all α-subunits contain an extra 200-residue module toward the *N*-terminus, named α-I domain, which contains the metal-ion-dependent-adhesion-site (MIDAS) involved in the binding site for ligands. The *N*-terminus of the β-subunit also contains an interactive domain (I domain, also known as the β-I domain) with a MIDAS motif. In integrins lacking the α-I domain, the ligand binding site is formed at the interface between the α and the β subunits and, in this case, the β subunit contributes to modulate the ligand specificity.

The field of integrin research was advanced enormously by the publication of the crystal structure of the extracellular domain of $\alpha_V\beta_3$ alone or in complex with the RGD-containing cyclopeptide ligand Cilengitide (see infra). The integrin-ligand complex crystal structure showed that RGD peptide binds at the α,β-interface, with its arginine residue contacting the α-subunit propeller and its aspartate helping to coordinate the divalent cation at the β MIDAS site.[13]

Many integrins are not constitutively active, and the adhesion of cells to matrix proteins needs to be strictly controlled and regulated in response to environmental changes.[7,14] Integrins exist in at least three states, inactive (bent-closed conformation), active (extended-closed) and ligand-bound (extended-open) (Fig. 6).
The switching of integrins from an inactive to an active state involves long-range conformational changes not only in the ligand-binding pocket, but also across the whole of the extracellular domain and in the cytoplasmic face. Thus, upon binding of proteins to the intracellular domain of the β-subunit, a conformational switch is induced in the external portion, accompanied by increasing affinity for ligands and binding. This event, named "inside-out signaling", controls processes like cell adhesion and migration. Conversely, during "outside-in signaling", ligand binding leads to dissociation of the transmembrane units and induce integrin clustering, forming the so-called focal adhesion. This lead to initiation of the intracellular signaling cascade that is involved in the regulation of a variety of biological processes such as cell polarity, cytoskeletal structure, and cell survival (Fig. 6).

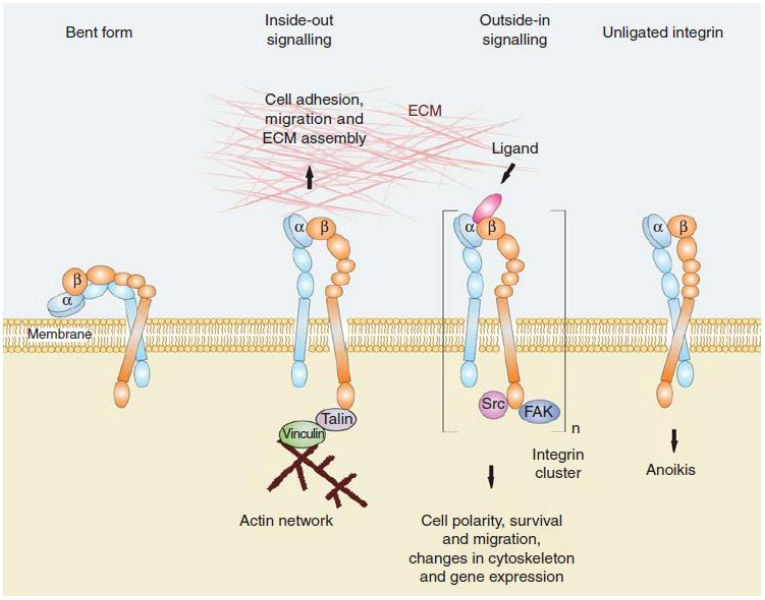

Figure 6. Schematic representation of integrin activation states and signaling mechanisms. Figure reprinted from ref.[10].

In addition, the functionality of integrins in not confined to themselves and, once ligation to a specific ECM ligand occurs, integrin-mediated signalling typically develops as a function of cooperative interactions (crosstalk) between integrins and growth factors or neighboring cell surface receptors (e.g. EGFR, VEGFR). These complex and intertwined signalling mechanisms affect many crucial aspects of cell life and behavior, including regulation of cell growth, development and proliferation, cell motility and migration, cell differentiation, cell survival and apoptosis.[6,7,15,16]

Integrins are found to be expressed on almost all cell types in a strongly varying distribution pattern. Given their fundamental contribution in human physiology, specific integrin dysregulation phenomena are linked to the pathogenesis of many disease states (including cancer, osteoarthritis, osteoporosis, thrombosis, vascular diseases, autoimmune diseases), and this renders them attractive targets for pharmaceutical research.[7,17] In particular, the repertoire of integrins in endothelial cells of angiogenic vessels differs from the integrins expressed in resting endothelial cells.[11,13] Both integrins $\alpha_V\beta_3$ and $\alpha_V\beta_5$ are expressed in various cell types (such as: endothelial cells, fibroblasts, epithelial cells, osteoblasts and smooth muscle cells), and are upregulated in endothelial cells undergoing angiogenesis. Additionally, they are highly upregulated on endothelium during tumor angiogenesis. In the cancer-related field, the expression of particular integrins is correlated with disease progression and decreased patient survival in various tumor types, including glioblastoma ($\alpha_V\beta_3$, $\alpha_V\beta_5$), melanoma ($\alpha_V\beta_3$, $\alpha_5\beta_1$), breast carcinoma ($\alpha_6\beta_4$, $\alpha_V\beta_3$), prostate and pancreatic carcinoma ($\alpha_V\beta_3$), ovarian carcinoma ($\alpha_V\beta_3$, $\alpha_4\beta_1$), non-small-cell lung carcinoma ($\alpha_5\beta_1$), and cervical carcinoma ($\alpha_V\beta_3$, $\alpha_V\beta_6$), rendering these integrin families appealing targets for cancer therapy.[11]

Up to now, no FDA-approved drugs for cancer-related integrin receptors exist; however, given the potential that such integrins have as therapeutic targets, a number of specific antibodies, peptide or peptidomimetic small molecule antagonists have been developed so far, which are currently used in preclinical or clinical trials in several oncology programs.[10,13,17–19]

- **$\alpha_V\beta_3$-integrin antagonists**

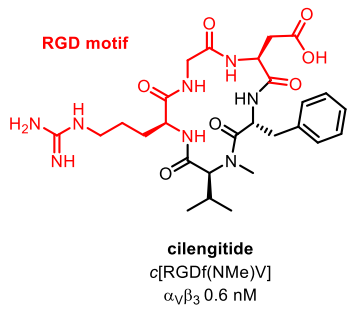

Figure 7. Biological activity (IC_{50}) of cilengitide in inhibiting the binding of vitronectin (Vn) to isolated integrin $\alpha_V\beta_3$. Ref.[13].

Among antiangiogenic $\alpha_V\beta_3$-integrin inhibitors, the small molecule Cilengitide, *c*[RGDf(N-Me)V], a cyclic pentapeptide which incorporates the key RGD tripeptide recognizing motif, is the most widely studied (Fig. 7). Cilengitide shows subnanomolar affinity for $\alpha_V\beta_3$ and activity in the low nanomolar range for $\alpha_V\beta_5$ and $\alpha_5\beta_1$. In this peptide, cyclization, incorporation of a D amino acid and *N*-methylation led to a significantly enhanced receptor affinity and *in vivo* stability against enzymatic degradation.[10] As Cilengitide revealed promising antitumor and antiangiogenic properties in early clinical studies as well as good stability profile, it was chosen by Merck as drug candidate in several advanced clinical trials as either single agent or in combination with chemo- or radiotherapy.[13,20–22]

Despite the promising results shown by Cilengitide in many studies, it failed in an advanced phase III clinical trial for the treatment of patients with newly diagnosed glioblastoma.[20] The reasons of this failure are still not fully understood. Evidences have been disclosed, however, that very low concentrations of Cilengitide in preclinical models paradoxically stimulate tumor growth and angiogenesis by promoting VEGF-stimulated angiogenesis.[23–26] This is consistent with other evidences in which inhibitors of VEGF increased tumor perfusion resulting in enhanced tumor progression,[27,28] and this points to the conclusion that blockage of one target alone might not be sufficient to inhibit the angiogenesis for a prolonged period of time, as tumor could react through activation of compensatory pathways.[23–29]

Besides their role as biological targets for direct therapeutic intervention, integrins which are overexpressed on selected tumor cells and their neighboring cells may be regarded as useful biomarkers of the tumor pathology; thus ligands (small molecules or antibodies) which bind to them with high affinity and specificity may be conveniently exploited as smart tools delivering attached active cargos to the tumor site.[11,30–35] Along this line, several reports exist illustrating the potential of multifunctional integrin ligand-containing systems associated with therapeutic agents, diagnostic tools, or both, under the shape of either conventional covalent bioconjugates or supramolecular assemblies.[11,30–35]
In the domain of *targeted therapeutics*,[19,30–35] active and specific directioning of the loaded drug by the integrin ligand allows for: (*i*) improved action specificity, (*ii*) lowered application doses, (*iii*) reduced toxicity on healthy tissues, and (*iv*) minimization of multi-drug resistance often witnessed in non-targeted administration. In the *targeted diagnosing field*,[36–38] on the other hand, delivering of imaging active probes at the site of interest may result in real-time tumor diagnosing, and *in vivo* noninvasive, quantitative assessment of individual biomarker expression and image-guided surgery.

In recent past years, the research group where I carried out most of my PhD studies developed a series of γ-aminocyclopentanecarboxylic acid (Acpca)-based[39] or γ-aminoproline (Amp)-based RGD-cyclotetrapeptides[40] which turned out to be very potent $\alpha_V\beta_3$ and/or $\alpha_V\beta_5$ binders (IC_{50} ligand affinities towards isolated receptors in the low nanomolar range; see Fig. 8).

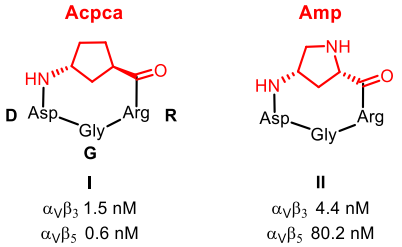

Figure 8. Two examples of integrin inhibitors and relative integrin affinity. IC_{50} values were calculated as the concentration of compound required for 50% inhibition of [^{125}I]-echistatin binding to isolated receptors $\alpha_V\beta_3$ and $\alpha_V\beta_5$.

In particular, for Amp-based cyclopeptides (Fig. 9), the Amp scaffold (4-aminopyrrolidine-2-carboxylic acid) shows a multifaceted structure, which merges the structural features of a γ-aminobutirric acid with those of a proline resulting in an unnatural but natural-like, conformationally constrained α,γ-amino acid.[41]

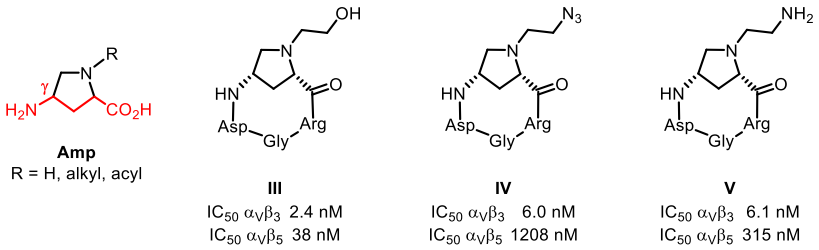

Figure 9. General formula of the γ-aminoproline (Amp) scaffold to be incorporated in the targeted cyclopeptides of this study. Compounds **III-V** are previously reported *c*AmpRGD cyclotetrapeptides exhibiting good competence as $\alpha_V\beta_3$ integrin ligands (IC_{50} values were calculated as the concentration of compound required for 50% inhibition of biotinylated vitronectin binding to isolated receptor).

The primary amine group and carboxylic acid functionalities of Amp can be grafted onto the peptide sequence of interest and foster the following intramolecular cyclization reaction. As known, the cyclic analogues of bioactive peptides are much more stable to enzymatic degradation with respect to the native linear peptides and their often defined conformational behaviour may potentially impart higher target binding and selectivity.[42] Moreover, the Amp nucleus possesses a N^{α}-proline site free for further covalent bonding to useful additional functional units, as shown in the structure of compounds **III**-**V** in Figure 9.

The covalent conjugation of these ligands with ancillary units (e.g. DOTA, fluorescein) resulted in overall preservation of their binding capability.[41] In the targeted chemotherapy, our group constructed bioconjugates where the cytotoxic paclitaxel drug (PTX) was covalently linked to monomeric or dimeric RGD prototypes via efficient and viable chemistry (e.g.: compound **VI**, Fig. 10).[43] *In vitro* cytotoxicity tests on various human tumor cell lines showed interesting results, with antiproliferative activity approaching or even surpassing that of PTX alone. Moreover, in 2015 our research group also reported the synthesis of a ^{111}In-labelled *c*(AmpRGD)-DOTA bioconjugate, which was used as radiotracer in preclinical models of tumor melanoma (compound **VII**, Fig. 10).[44] This construct demonstrated to be a promising starting point in the search for new SPECT-imaging small-molecular probes for non-invasive visualization of tumor angiogenesis, human melanoma and other $\alpha_V\beta_3/\alpha_5\beta_1$-positive tumors.

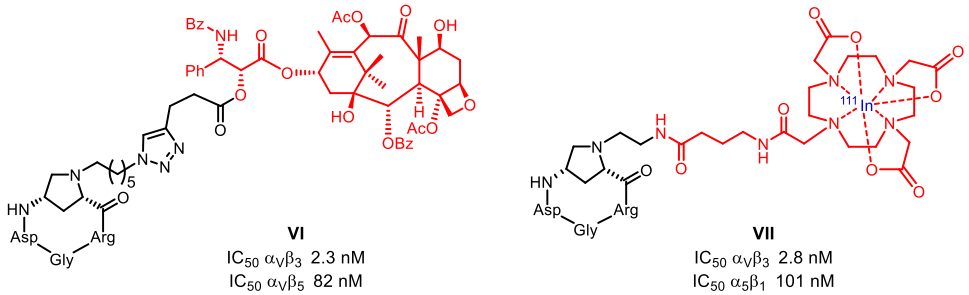

Figure 10. Structure of *c*(AmpRGD)-containing covalent bio-conjugates (IC_{50} values were calculated as the concentration of compound required for 50% inhibition of biotinylated vitronectin binding to isolated receptor.

Also, construction of $\alpha_V\beta_3$-specific *c*(AmpRGD)-based liposomal nanoparticles was devised and subsequent loading with anticancer doxorubicin was performed; preliminary biological evaluation of these supramolecular assemblies *in vitro* indicated the effective and selective delivery of doxorubicin to $\alpha_V\beta_3$-positive cells, with subsequent cell-internalization and exercise of its cytotoxic action.[45]

1*a*.1.2.2 VEGF/VEGFR system and ligands

The vascular endothelial growth factor (VEGF) and its receptors (VEGFRs) play crucial roles in both physiological and pathological angiogenesis.[46]

The VEGF family is divided into five members having a homodimer structure: VEGF-A, VEGF-B, VEGF-C, VEGFD and placental growth factor (PlGF). In addition, VEGF ligands can be present in mammals in several different splice variants and processed forms.[47] For example, VEGF-A, which is generally called VEGF because is the master regulator of angiogenesis, exists in four isoforms: VEGF121, VEGF165, VEGF189 and VEGF206. Among VEGF-A isoforms, VEGF165 is quantitatively dominant and it's overexpressed in a variety of human tumors.[46] The VEGF family members bind, in an overlapping pattern, to three different but structurally correlated VEGF receptors (VEGFRs), which are transmembrane tyrosine kinases (TKs).[47,48] VEGFRs consist of three subtypes, VEGFR-1, VEGFR-2 and VEGFR-3, and are structurally related to platelet-derived growth factor receptors (PDGFRs). All subtypes possess seven immunoglobulin-like domains in the extracellular region followed by a single transmembrane segment. The intracellular portion of the receptor is constituted by a juxtamembrane (JM) segment, a TK domain, which is divided into proximal and distal kinase domains by an insert domain of about 70 amino acid residues, and a carboxy-terminal tail (Fig. 11).[47,49]

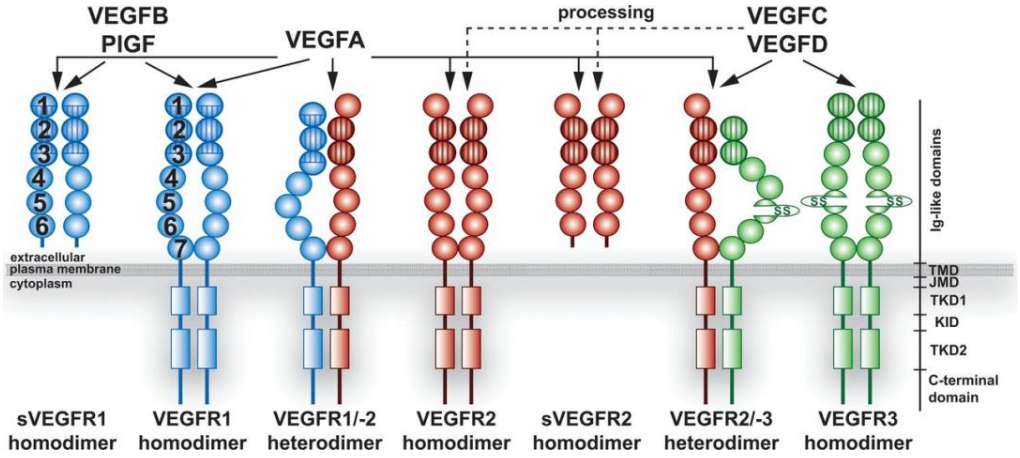

Figure 11. VEGF binding specificities towards homo- and heterodimeric VEGFRs. JMD, juxtamembrane domain; KID, kinase insert domain; TMD, transmembrane domain; TKD1, ATP-binding domain; TKD2, phosphotransferase domain. Figure reprinted from ref.[47].

VEGFR-1 and VEGFR-2 are expressed in vascular endothelial and hematopoietic stem cells. VEGFR-1 is also expressed in monocytes and macrophages.[46] The expression of VEGFR-3, instead, is largely restricted to lymphatic endothelial cells.

The VEGF family members have different affinities toward the three VEGFR subtypes (Fig. 11). In general, VEGF-A activates VEGFR-1 and VEGFR-2, whereas VEGF-B and PlGF bind only to VEFGR-1. VEGF-C and VEGF-D bind to VEGFR-3 although upon proteolysis of specific chains in the early proteins, they are allowed to bind both VEGFR-2 and VEGFR-3. Guided by the binding properties of the ligands, the VEGFRs are able to form both homodimers and heterodimers (Fig. 11).[50] Receptor dimerization, induced by the binding of VEGFs to VEGFRs, causes modification in the intracellular domain conformation.[49] These conformational changes lead to the exposure of the ATP-binding site, followed by ATP binding and auto- or transphosphorylation on specific tyrosine residues on the receptor dimers and on downstream signal transducer proteins. This mechanism leads to the initiation of a typical receptor signal transduction cascade, which activates several downstream enzymatic pathways, including p38MAPK, Raf/MEK/ERK and PI3K/PKB pathways. Tyrosine phosphorylation on VEGFRs is tightly regulated both by internalization and degradation, and by dephosphorylation through different protein tyrosine phospatases.

It was reported that **VEGFR-1** mediates proliferation of endothelial cells, migration of monocytes and macrophages and recruitment of bone marrow-derived endothelial and hematopoietic precursor cells.[46,49] However, the precise role of VEGFR-1 functions is still emerging; several studies in recent years have suggested that this receptor may play both negative and positive roles in angiogenesis. In fact, VEGFR-1 negatively regulates physiological vasculogenesis during embryogenesis, while it is weakly involved in mediating the physiological angiogenic response to VEGF. Moreover, VEGFR-1 acts primarily as a decoy receptor, modulating the availability of VEGF-A and reducing its bioavailability to other receptors, in particular to VEGFR-2, which is the principal receptor in VEGF signalling. Importantly, VEGFR-1-dependent signalling was shown to play a role in the angiogenesis of certain tumors as well as in the progression of rheumatoid arthritis and atherosclerosis. VEGFR-1 is up-regulated in several tumor cell lines, including malignant prostate cells, pancreatic cancer cells, malignant melanoma cells and lung adenocarcinoma cells. Furthermore, VEGFR-1 is involved in tumor metastasis; however, it seems that selective inhibition of VEGFR-1 activity does not change the rate of spontaneous metastasis formation after surgical removal of primary tumors. Finally, VEGFR-1 and VEGFR-2 also exist in soluble forms (as shown in Fig. 11), that are involved in both angiogenesis and different human diseases. High levels of soluble VEGFR-1 have been detected in several cancers, including breast, pancreatic, lung and ovarian cancers and leukemias. On the other hand, administration of soluble VEGFR-1 has demonstrated antitumor effects, probably because the soluble receptor intercepts VEGF-A.

VEGFR-2 has a more potent tyrosine kinase activity than VEGFR-1, despite a 10-fold lower affinity for VEGF-A.[46,49] VEGFR-2 is the major regulator of VEGF-driven responses in endothelial cells under both physiological and pathological conditions. Stimulation of VEGFR-2 promotes growth, migration, and tubular formation of endothelial cells and enhances vascular permeability (Fig. 12).

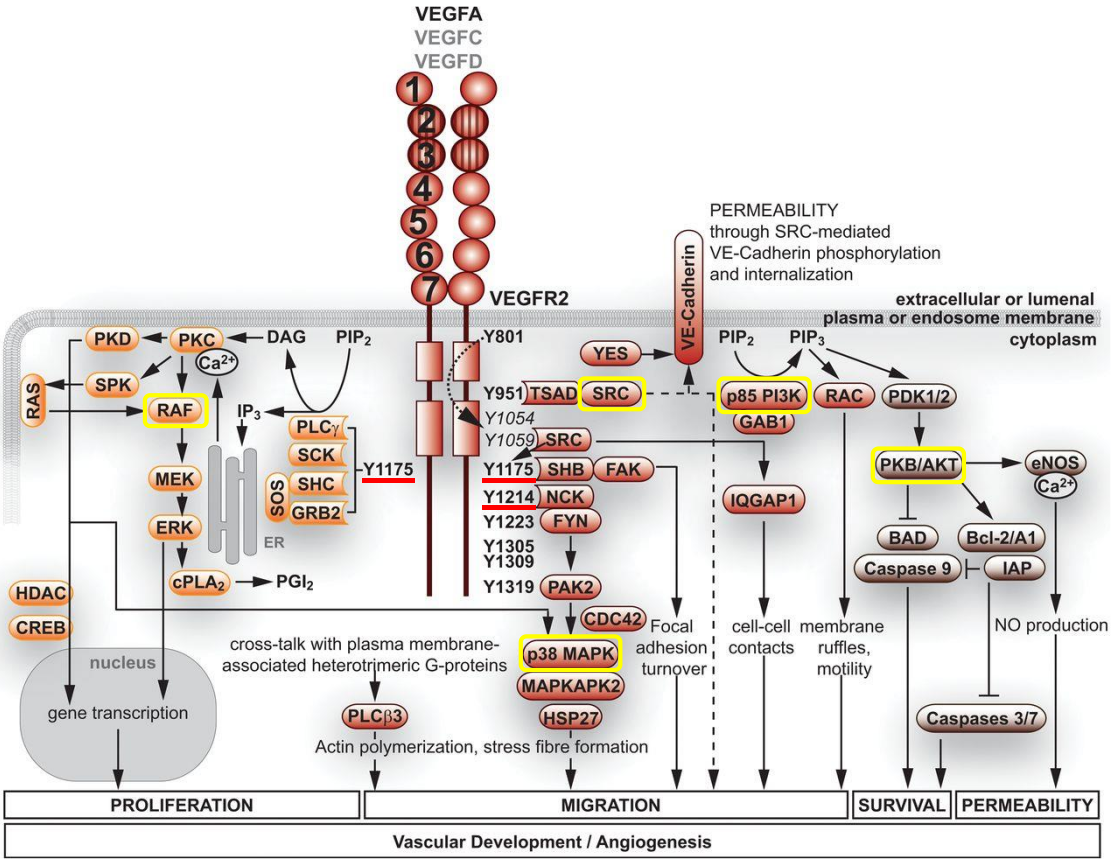

Figure 12. VEGFR2 tyrosine phosphorylation sites and signal transduction. Figure adapted from ref.[47].

Its signaling pathways are relatively well understood, with Y1175 and Y1214 in human VEGFR-2 being the main autophosphorylation sites following VEGF binding. Autophosphorylated VEGFR-2 is required for activation of several downstream pathways, including PI3K, p38MAPK, FAK, Src, Akt, which are usually hyperactivated in several tumors. VEGFR-2 is overexpressed in several malignancies, including ovarian and thyroid cancer, melanoma and medulloblastoma. VEGFR-2 and VEGFR-3 are primarily located and significantly up-regulated on the tumor vasculature (blood and/or lymphatic) that supports the majority of solid cancers. Moreover, the signal intensity of both receptors is significantly higher in vessels associated with malignant colorectal, lung and breast tumor tissues than in adjacent nontumor tissues.

Concerning **VEGFR-3**, its expression in the adult seems to be largely restricted to lymphatic endothelial cells, regulating lymphangiogenesis in response to VEGF-C and VEGF-D.[46,49] Furthermore, VEGFR-3 is strongly expressed in several human malignancies, including lung, cervical, breast and colorectal cancers. Its higher levels are correlated with increased metastasis formation and shorter patient survival, since the lymphatic vessels surrounding the tumor play important roles in metastasis formation.

- **VEGF/VEGFR inhibitors**

Therapeutic strategies based on the inhibition of VEGF or its receptor signalling systems are an attractive approach for the treatment of different diseases, primarily tumors.[51,52]

Since Folkman proposed that antiangiogenesis would be a novel antitumor strategy, angiogenesis has become an attractive drug target.[53] Especially, VEGF-A and VEGFR-2 are currently the main targets for antiangiogenic therapy. Currently, antiangiogenic agents belong either to monoclonal antibodies or synthetic small molecules classes.[51]

Antibodies as angiogenesis-related protein inhibitors

Three protein inhibitors of the VEGF-A pathway have been approved for cancer therapy: (*i*) *bevacizumab* (Avastin; Genentech/Roche), a recombinant humanized VEGFA-specific monoclonal antibody; (*ii*) *aflibercept* (zvi-aflibercept, Eylea; Regeneron Pharmaceuticals), a recombinant VEGFR fusion protein that binds to, and inhibits VEGFA, VEGFB and PIGF; and (*iii*) *ramucirumab*, a fully human monoclonal antibody that inhibits VEGFR2 (Fig. 13).[51,54,55]

Bevacizumab, inhibiting the binding of VEGF-A to its receptors, prevents VEGFR activation and the subsequent signalling cascades.[51,54,55] Bevacizumab has been approved for the treatment of metastatic colorectal cancer (mCRC) by the United States Food and Drug Administration (FDA) in 2004, and by the European Medicines Agency (EMA) in 2006. Subsequently, bevacizumab has been approved by the FDA for treatment of metastatic nonsquamous non-small cell lung cancer (NSCLC), renal cell carcinoma (RCC), ovarian cancer, cervical cancer, and glioblastoma multiforme (GBM). In the European Union, bevacizumab is approved for breast cancer, NSCLC, ovarian cancer and renal cell cancer but not for GBM or cervical cancer.

Aflibercept, another VEGF ligand inhibitor, is approved in both the United States (2012) and Europe in combination with chemotherapy for recurrent mCRC.[51,54,55]

Ramucirumab is instead a recombinant monoclonal antibody of the immunoglobulin G1 (IgG1) class, that binds to the VEGFR-2, blocking receptor activation. It has been approved for use in advanced gastric cancer and NSCLC in both the United States and Europe, and for mCRC in the United States.[51,54,55]

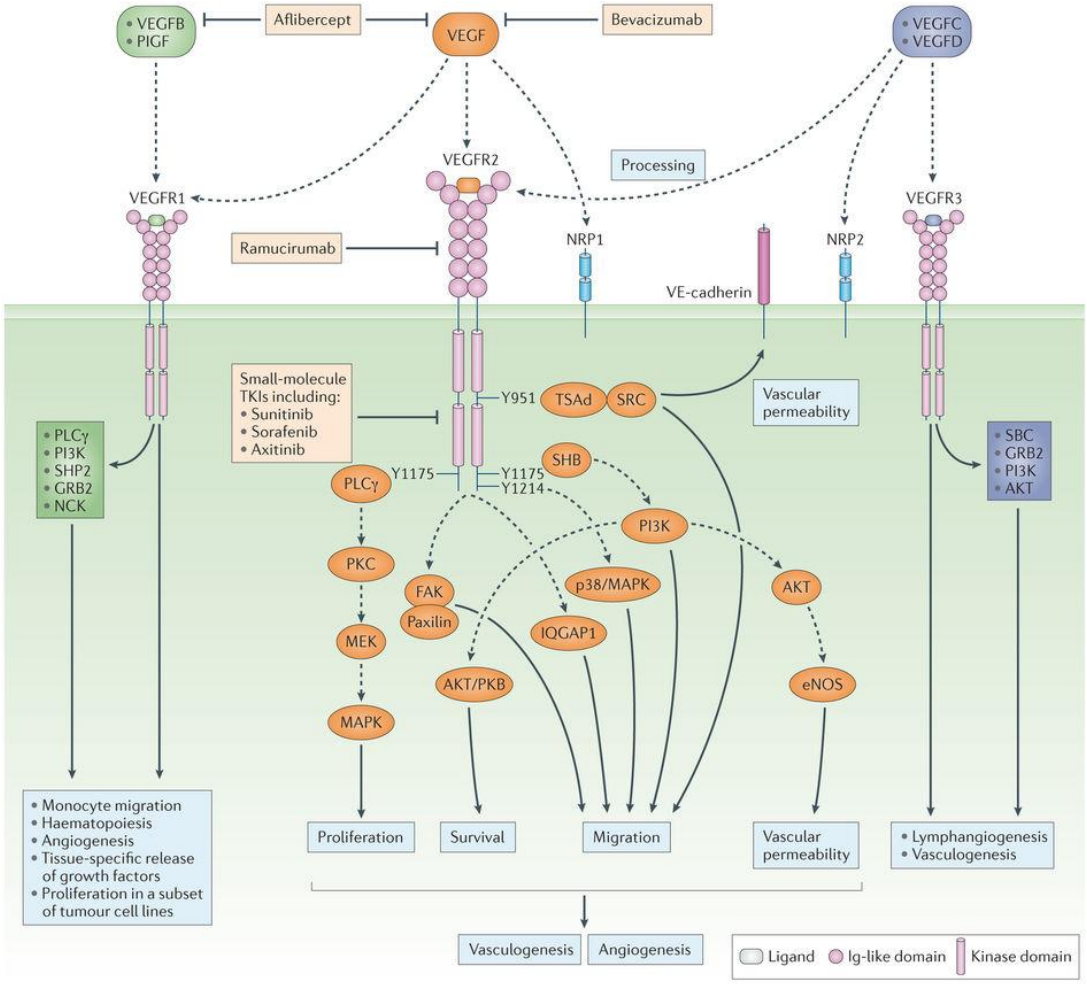

Figure 13. VEGF signalling pathways and inhibitors. Figure adapted from ref.[51]

Small molecule RTKIs

In addition to using monoclonal antibodies, alternative approaches of inhibiting the VEGFA-VEGFR pathway for the treatment of cancer led to discovery of a number of compounds known as receptor tyrosin kinase inhibitors (RTKIs).[49,51]

Generally, RTKIs are small synthetic molecules that act with an ATP-competitive mechanism by binding the ATP poket of the protein kinase domain. TK inhibitors that target VEGFRs, often target more than one member of the VEGFR family because of the structural similarity shared by VEGFR-1, -2 and -3. Moreover, since a number of receptor TK families (such as: PDGFRs, CSFR, c-Kit and FLT3) share a substantial sequence homology with VEGFRs in their catalytic domains, several TK inhibitors are not selective for VEGFRs and are defined as multikinase inhibitors. However, their poor selectivity among different TK families seems to offer different opportunities in cancer treatment. In fact, several independent biological pathways that are vital for tumor proliferation and metastasis can be disrupted using multitargeted inhibitors.

A number of VEGFR/multitargeted inhibitors are under clinical trials and several compounds are currently approved for clinical use, including sunitinib, sorafenib, pazopanib, vandetanib, cabozantinib, axitinib, ponatinib, lenvatinib, and regorafenib.[49,54,55] Figure 14 shows just an overview of some of these compounds currently used in clinical settings.

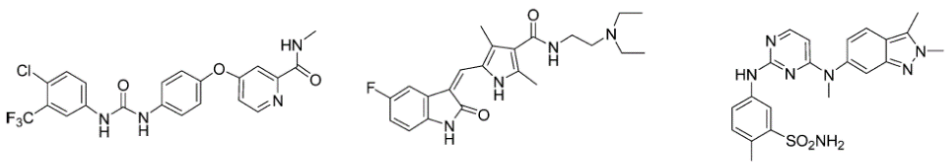

VIII
sorafenib

IX
sunitinib

X
pazopanib

Figure 14. Some selected VEGFR/multitargeted inhibitors approved for clinical use.

Sorafenib, **VIII** (trade name Nexavar, co-developed and co-marketed by Bayer and Onyx Pharmaceuticals), is a biarylurea multitargeted kinase inhibitor. It inhibits, among others, VEGFR-2 and VEGFR-3, PDGFRβ, c-Kit, and Raf.[49] Sorafenib was approved by U.S. FDA in 2005 for the treatment of advanced renal cell carcinoma (RCC), in 2007 for the treatment of hepatocellular carcinoma (HCC), and in 2013 for the treatment of thyroid cancer.[51] Three more VEGFR RTKIs, cabozantinib (Cometriq; Exelixis), vandetanib (Caprelsa; Astra Zeneca) and lenvantinib (E7080; Eisai), have been approved for thyroid cancer, based in part on their ability to inhibit the RTK RET.[51]

Sunitinib, **IX** (trade name Sutent, by Sugen-Pfizer), is a multikinase indol-2-one inhibitor targeting VEGFR-1 and VEGFR-2, PDGFRβ, and other kinases, including FLT3, which has been shown to be involved, especially in mutated forms, in acute leukemia. It also inhibits c-Kit, hyperactivated by mutations in gastrointestinal stromal tumor (GIST).[49,51] Sunitinib is indicated as first-line therapy for metastatic renal cell carcinoma,[56] pancreatic neuroendocrine tumors (PNET),[57] and as second-line therapy for imatinib-resistant gastrointestinal stromal tumors (GIST).[58]

Pazopanib, **X** (trade name Votrient, by GlaxoSmithKline), is a potent pan-VEGFR inhibitor; indeed it inhibits VEGFR-1, -2 and -3. Its chemical structure is quite unusual among kinase inhibitors, bearing a 2,4-pyrimidinediamine core substituted by an indazole ring and a 2-methylbenzenesulfonamide moiety. Pazopanib also inhibits PDGFRα/β and c-Kit. It was approved by the FDA (2009) and by EMA (2010) for first- and second-line treatment of advanced renal cell carcinoma, and by FDA for soft tissue sarcoma in 2012. Pazopanib also appears to be effective in the treatment of ovarian and in NSCLC.[49,51]

Sorafenib, sunitinib, and pazopanib are orally administered as tosylate, malate and hydrochloride salts, respectively. Common doses, $T_{1/2}$, and T_{max} of these inhibitors are reported in Table 1.[49]

				pharmacokinetics	
Compound	**Trade name**	**Administration**	**Salt**	**$T_{1/2}$**	**T_{max} (h)**
sorafenib (VIII)	Nexavar	400 mg orally twice daily	tosylate	25-48 h	3
sunitinib (IX)	Sutent	50 mg orally once daily	malate	40-60 h	6-12
pazopanib (X)	Votrient	800 mg orally once daily	hydrochloride	30.9 h	2-4

Table 1. Comparison of some pharmacokinetic parameters for approved compounds sorafenib, sunitinib and pazopanib.

With the expanding use of agents that target the VEGF signalling pathway in cancer therapy, it is increasingly recognized that they are associated with a wide spectrum of toxicities.[49,54,55] VEGFR inhibitors are generally less toxic than conventional chemotherapeutic agents, with the most common adverse effects being thromboembolic events, congestive heart failure, gastrointestinal perforation and hypertension.

1*a*.1.3 Antiangiogenesis therapy and resistance mechanisms

As angiogenesis is a prerequisite for tumor growth and may contribute to tumor progression, invasion and metastasis, the angiogenic process is generally accepted as an indicator of tumor prognosis. Therefore, targeting tumor angiogenesis has become of high clinical relevance, as testified by the number of clinically approved anti-angiogenic agents shown in the last paragraph, all targeting the VEGF signalling axis.[51,52,59]

Despite the demonstrable clinical benefits of anti-angiogenic therapy, the preclinical and clinical data of the current therapeutic settings clearly indicate the transient efficacy, restoration of tumor progression and aggressive recurrence of tumor invasion after the withdrawal of anti-angiogenic therapy. Therefore, the impact of this therapeutic regime on improving overall survival of patients has been disappointing in clinic.

The reason is to be ascribed to the insurgence of compensatory angiogenic mechanisms that confer tumor resistence to anti-angiogenic agents.[59–61]

- **Modes of resistance to anti-angiogenic therapy**

Recent advances in pathophysiology of tumor angiogenesis, together with related molecular and cellular underpinnings, have suggested that two modes of unconventional resistance underlie such results: (*i*) evasive resistance, an adaptation to circumvent the specific angiogenic blockade; and (*ii*) intrinsic or pre-existing indifference (Fig. 15).[59,61] These two general modes of cancer resistance to angiogenesis inhibitors are called "unconventional", because are not acquired by mutational alteration of the gene encoding for a drug target or by alterations in drug uptake and efflux.[61] Multiple mechanisms underlie both modes of resistance.

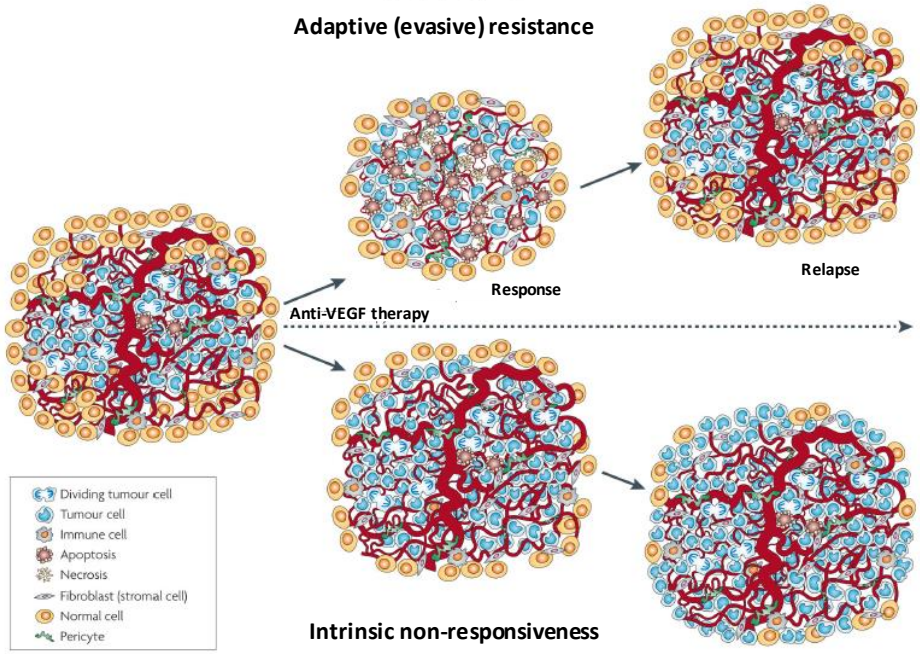

Figure 15. Two modes of resistance in response to anti-angiogenic therapy: (*i*) adaptive (evasive) and (*ii*) intrinsic tumor resistance. Figure adapted from ref.[61].

Intrinsic non-responsiveness is a pre-existing condition defined by the absence of any (even transitory) beneficial effect of an anti-angiogenic therapy, ranging from the inability to shrink or stabilize tumours to the lack of improvement in quality of life. By contrast, *adaptive* (or *evasive*) *resistance* refers to the ability of a tumour, after an initial response phase, to adapt so as to evade the therapeutic blockade (*i*) by inducing or accentuating mechanisms that enable neovascularization despite the therapeutic blockade, (*ii*) or reduce dependence on such growth of new blood vessels by other means, leading to renewed tumour growth and progression.

Concerning the activation and/or upregulation of alternative pro-angiogenic signalling circuits within the tumor, clinical and experimental settings have identified several pro-angiogenic growth factors having a key role in driving compensatory angiogenesis during blockade of VEGF axis (Fig. 16).[59] Some of the key angiogenic factors include fibroblast growth factors 1 and 2 (FGF1 and FGF2, respectively), hepatocyte growth factor/cMet pathway, angiopoietins, platelet-derived growth factor (PDGF)-C, interleukins, Ephrins.

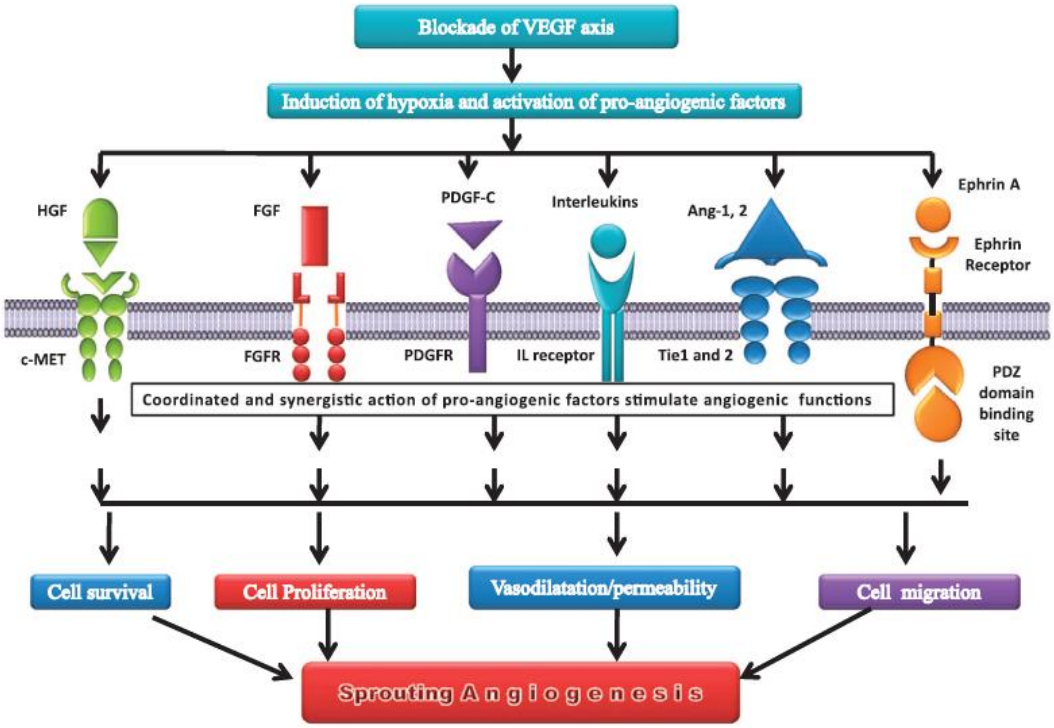

Figure 16. Role of pro-angiogenic factors in driving compensatory angiogenesis during blockade of VEGF axis. Figure reprinted from ref.[59].

Concerning the reduction of tumor growth dependence toward sprouting angiogenesis, as already mentioned (see paragraph 1*a*.1.1), tumors can sustain their growth, invasion and metastasis, recruiting blood vessels through angiogenesis-independent mechanisms, such as *vessel co-option*, vessel remodeling through *intussusception* and *vascular mimicry*.[59,61] These mechanisms seem to vary not only spatially and temporally within a tumor, but also between a primary tumor and its metastases and among tumor types.[60] Moreover, tumors may switch from one mechanism to another during growth and in response to treatment. While VEGF seems to be a central player in sprouting angiogenesis, our knowledge of the molecular players in other mechanisms is still in its infancy.
Understanding these mechanisms in more detail will allow development of novel agents to target all types of tumor vessels and augment responses to currently available antiangiogenic (AA) agents.

Another explanation of the disappointing performance of antiangiogenic therapy in the clinic can be ascribed to the induced hypoxic condition by anti-angiogenic agents, as consequence of their effect of "vascular regression".[59] Reducing blood supply, the impaired blood perfusion in tumors can produce an abnormal microenvironment characterized by hypoxia and acidosis, which help cancer cells to evade the immune system, increase their invasive and metastatic potential, and apply selective survival pressures to which cancer cell populations may adapt (Fig. 17).[60]

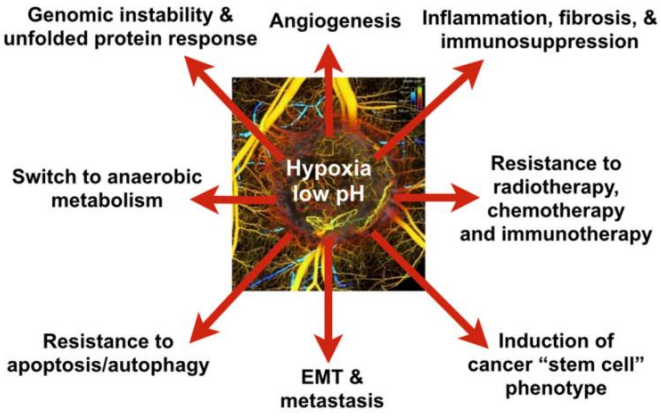

Figure 17.Consequence of hypoxia and acidosis resulting from impaired perfusion due to tumor progression and treatment resistance. Epithelial to mesenchymal transition (EMT). Figure reprinted from ref.[60].

Under physiological conditions, immune cells constantly patrol tissues to identify and destroy pathogens, foreign antigens and abnormal cells. In contrast, a hypoxic and acidic microenvironment reprograms the resident macrophages (phagocytes) – whose job is to recognize, engulf and remove dying cells – into a protumorigenic and immunosuppressive phenotype.[60,62] Hypoxia and acidosis can also attenuate the killing potential of immune effector cells within the tumor microenvironment. Specifically, growth factors and chemokines (e.g., TGFβ, VEGF) induced by hypoxia or acidosis suppress the activity of T lymphocytes, and inhibit the ability of dendritic cells to process tumor antigens and present them to lymphocytes.[60,63]
In addition to protection from the immune system, hypoxia may select for more malignant cells, as cells that respond to physiological cues normally undergo apoptosis under hypoxic conditions.[64] Hypoxia can increase the invasive potential of cancer cells by inducing the production of pro-migratory proteins (e.g., SDF1α, HGF) and pro-invasive extracellular matrix molecules.[65] Hypoxia also provides a niche for so-called cancer stem cells and facilitates inflammation, while also conferring resistance to radiation and many widely used therapeutic agents.[64] Collectively, these observations may explain why intratumoral hypoxia correlates with poor prognosis in many human cancers.[64]

Elevated interstitial fluid pressure (IFP) resulting from compression of lymphatic vessels also fuels tumor progression and resistance to treatment, but via distinct mechanisms.[60,66] Tumor vessel leakiness worsens interstitial hypertension, causes edema and leads to sluggish blood flow due to clogging of red blood cells concentrated by the leakage of plasma.[60] Tumor vessel leakiness and compression thereby collaborate in creating a vicious cycle responsible for both acute and chronic hypoxia as well as acidosis.
Thus, normalizing the tumor microenvironment by repairing the function of tumor vessels may be a promising strategy to slow tumor progression and enhance cancer treatment.

While the debate about the actual usefulness of antiangiogenesis therapy remains open,[54,55,59–61] current researches suggest that possible solutions could entail the use of drugs capable of hitting multiple targets/pathways and cell types involved in the tumor microenvironment[6,52,59,61] while possessing supplemental selective targeting moieties. Indeed, the use of (*i*) targeted therapy, which selectively address specific cell types (such as, tumor-associated stromal and endothelial cells, tumor cells) allowing optimal distribution into tumor site while limiting off-target effects of therapeutic drugs, as well as the use (*ii*) of angiogenesis inhibitors in combination with other anticancer drugs (combinatory therapy), able to perturb multiple molecular targets and signalling pathway, are arising privileged therapeutic options.[52]

1*a*.1.4 Crosstalk VEGFR2- $\alpha_V\beta_3$

Among the intricate, often overlapping cell signalling networks regulating angiogenesis (paragraph 1*a*.1.1), growing evidence emerged for the existence of a strict crosstalk between the VEGFR2 and $\alpha_V\beta_3$ receptors.[16,29,67–70] These two receptors are physically and functionally connected in common cell populations (e.g., endothelial cells and several cancer cell types), and their interactions are important for both integrin activation and mutual regulation of the kinase activity.[16]

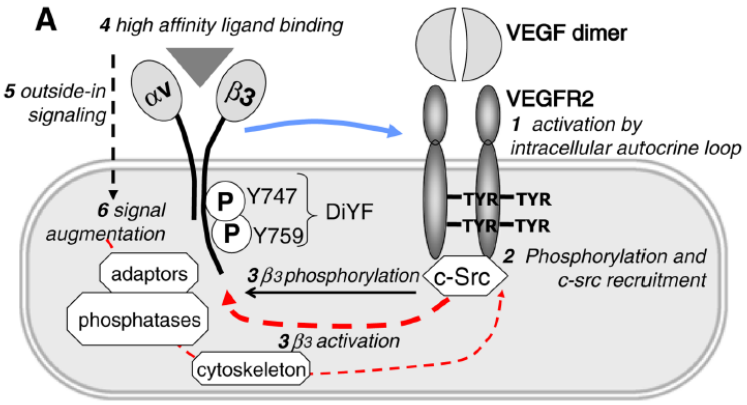

Figure 18. Molecular events involved in interaction between VEGFR2 and $\alpha_V\beta_3$. Figure reprinted from ref.[16].

As shown in Figure 18, VEGF induces auto-phosphorylation and activation of VEGFR2, causing the recruitment of c-Src, a member of the Src family of kinases.[16] c-Src kinase is responsible for the phosphorylation of tyrosine residues Y747 and Y759 within the integrin β_3-cytoplasmic domain, an event that leads to the formation of the complex between VEGFR2 and $\alpha_V\beta_3$. Moreover, the phosphorylation of the cytoplasmic domain of $\alpha_V\beta_3$ promotes the activation of this integrin (inside-out signaling) which basically results in its conformational changes and increase in ligand binding affinity. Ligation of integrin triggers outside-in signalling, which further augments cell activation. The association of $\alpha_V\beta_3$ with VEGFR2 promotes the full activation of each receptor, leading to maximal angiogenesis in response to VEGF. Blockage of the $\alpha_V\beta_3$/VEGFR2 couple may thus be of high therapeutic potential.[71–74]

1*a*.2 Aim of the work

Based on the wealth of information given in the introduction, one could conclude that the still unmet full clinical success of anti-integrin and/or anti-VEGFR anti-angiogenic therapeutics could be ascribed to the highly complex *in vivo* regulation involving these receptors, whose intertwined relationship suggests that a dual-specific agent capable of inhibiting them simultaneously would have great therapeutic potential.[15,16,68,71–73]

In fact, the combined use of two small molecules, cilengitide and a sunitinib analogue, SU5416 (Fig. 19, A), showed antiangiogenic effect and inhibition of melanoma tumor growth and metastasis during *in vivo* preclinical studies.[71] In this instance, however, the two drugs were independently delivered, with possible differences in localization and pharmacokinetics.

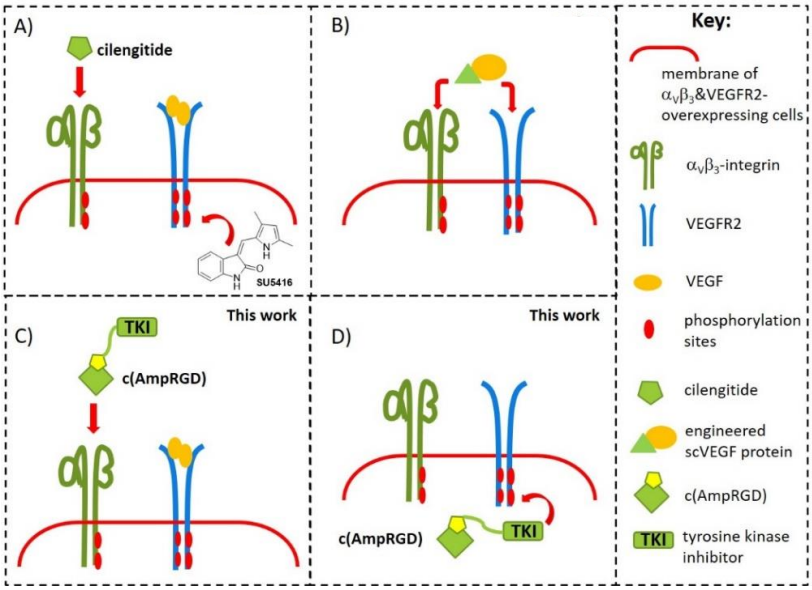

Figure 19. (**A**) $\alpha_V\beta_3$ antagonist cilengitide (outside cell)+VEGFR2 antagonist (inside), two discrete small molecules, different localization. (**B**) One engineered dual-specific protein (outside), simultaneous $\alpha_V\beta_3$/VEGFR2 inhibition. (**C**, **D**) One small molecule, the *c*(AmpRGD)-TKI conjugate, recognizing $\alpha_V\beta_3$ (outside), partially entering the cell (possibly via $\alpha_V\beta_3$), and antagonizing VEGFR2 (inside) (this work, ref.[90]).

In a subsequent enlightening study,[72] a dual specific scVEGF protein was engineered, capable of binding the extracellular portions of $\alpha_V\beta_3$ and VEGFR2 simultaneously, showing promise for effective *in vitro* and *in vivo* antiangiogenic action (Fig. 19, B). Though highly promising, this work had the limitation of dealing with complex engineered 25 kDa proteins.

A complementary and conceptually different approach is proposed in the work of my PhD research program, according to which a selective binder of the extracellular segment of $\alpha_V\beta_3$ could be covalently linked to a proven TKI such as sunitinib, whose interaction with the cytoplasmic domain of VEGFR2 is widely recognized, as described before. As $\alpha_V\beta_3$ binder, we could rely on the recently discovered series of aminoproline-based RGD cyclotetrapeptides of type *c*(AmpRGD)-X (where X=H, alkyl, acyl groups) which in many cases showed remarkable and selective binding capability toward the $\alpha_V\beta_3$ integrin receptor in both cell-free and cell assays (vide supra, Fig. 8 and 9).[40,41]

On the bases of the premises illustrated in the introduction, and relying on the good results of AmpRGD cyclopeptides as integrin $\alpha_V\beta_3$ binders, we herein proposed that the covalent assemblage of an anchorable sunitinib-like moiety to the *c*(AmpRGD) portion through a suitable linker would furnish dual conjugates (Fig. 19, C and D; schematic representation) wherein the RGD unit would possibly provide: (*i*) EC-selective targeting by $\alpha_V\beta_3$-RGD recognition, (*ii*) $\alpha_V\beta_3$-dependent antiangiogenic effect, and (*iii*) $\alpha_V\beta_3$-mediated cell internalization. On the other hand, the sunitinib unit could exert its intracellular TKI effect after internalization, while playing a role in overall perturbation of the $\alpha_V\beta_3$-VEGFR2 crosstalk.

Thus, my PhD work focused on the design and synthesis of three novel covalent prototypes **1-3** (Fig. 20), which were then subjected to biological activity evaluation in order to prove their possible effectiveness as dual anti-angiogenic agents.

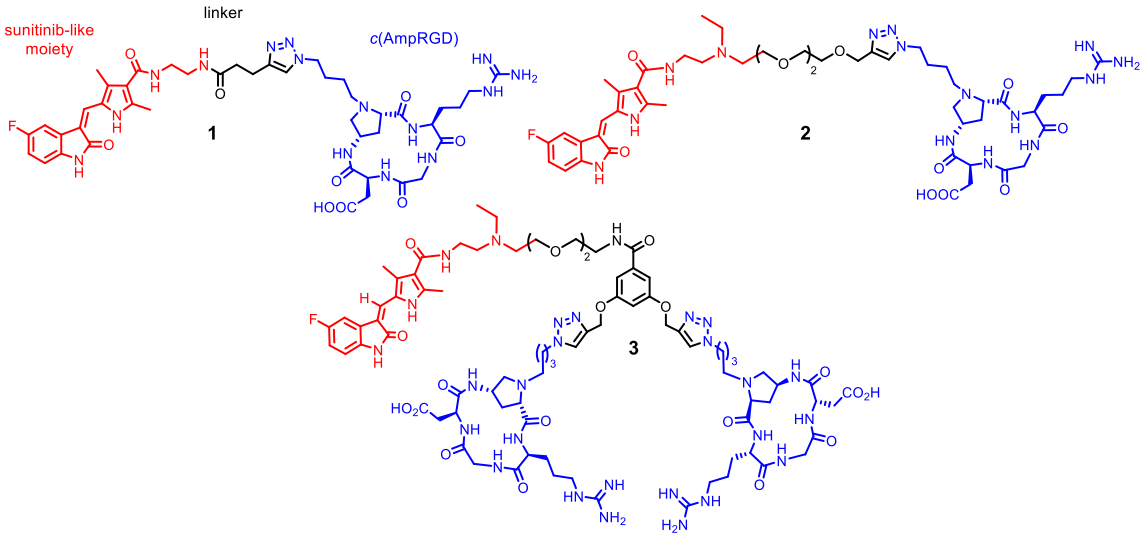

Figure 20. Structure of the targeted dual conjugates **1**–**3**.

In particular, the binding properties toward $\alpha_V\beta_3$ integrin, the kinase inhibitory activity, cell uptake and antiangiogenesis potential *in vitro* of all the three conjugates have been evaluated, vis-à-vis the behavior of the single modules and their simple combinations. Finally, the *in vivo* antiangiogenesis potential of the dimeric-RGD conjugate **3** was evaluated.

In the next paragraphs, the structural design requirements of compounds **1-3**, and the results and discussion of the whole work are illustrated.

1*a*.3 Results and Discussion

1*a*.3.1 Design of Sunitinib-*c*(AmpRGD) conjugates 1-3

To fulfil the objectives of this work (Fig. 19, C and D), the projected dual conjugates had to embody several stringent requisites. *First*, the active units should not disturb each other, that is, the sunitinib moiety should not compromise the RGD-binding capability while the RGD unit should not impede the tyrosine kinase activity of sunitinib. *Second*, to exclude premature detachment of the two active units (outside the targeted cells), the linker between them should be either uncleavable or cleavable within cells exclusively; *third*, the conjugate should enter the targeted cells possibly via $\alpha_V\beta_3$-mediated endocytosis.

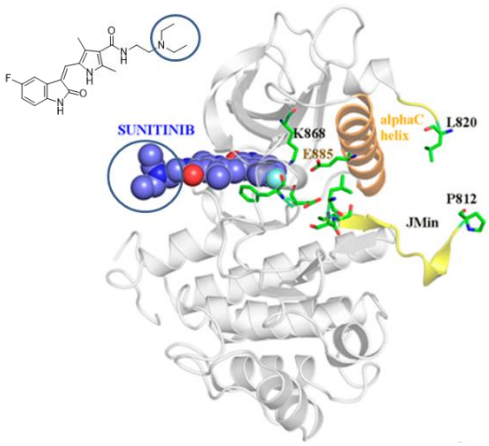

Figure 21. Overview of the crystal complex of sunitinib bound to the catalytic and JM domains of VEGFR2. Figure adapted from ref.[76].

As a background, extensive structure-activity relationship studies on sunitinib analogues[49,75] and X-ray analysis of the complex between the drug and the tyrosine kinase domain of the VEGFR2 active site (Fig. 21)[76,77] revealed that the aromatic portion of the molecule is directly involved in the binding, while the terminal tertiary amine stands outside the pocket and may allow certain margins of structural modifications. Thus, connection of sunitinib to the linker exploiting this amine terminal would likely be uninfluential toward the tyrosine kinase activity. Furthermore, we were aware of the binding capability and selectivity toward the $\alpha_V\beta_3$ integrin of *c*(AmpRGD)-based ligands and related conjugates,[40,41,43–45] anticipating that the conjugation of these ligands with the ancillary sunitinib moiety would not hardly compromise their $\alpha_V\beta_3$-integrin binding ability. Lastly, the cell internalization potential of *c*(AmpRGD)-conjugates was preliminarily assayed using a *c*(AmpRGD)-fluorescein conjugate, which demonstrated complete $\alpha_V\beta_3$-dependent internalization in A375 melanoma cells within 25 min exposure (vide infra). The synthetic details of the fluorescent construct are discussed in the next section.

With these clues at hand, conjugates **1-3** were designed, wherein the two active units are positioned 11-22 bonds away (Fig. 22, N^{α} to N^{ω}) and are connected via robust triazole/ether/amide linkages (Fig. 22).

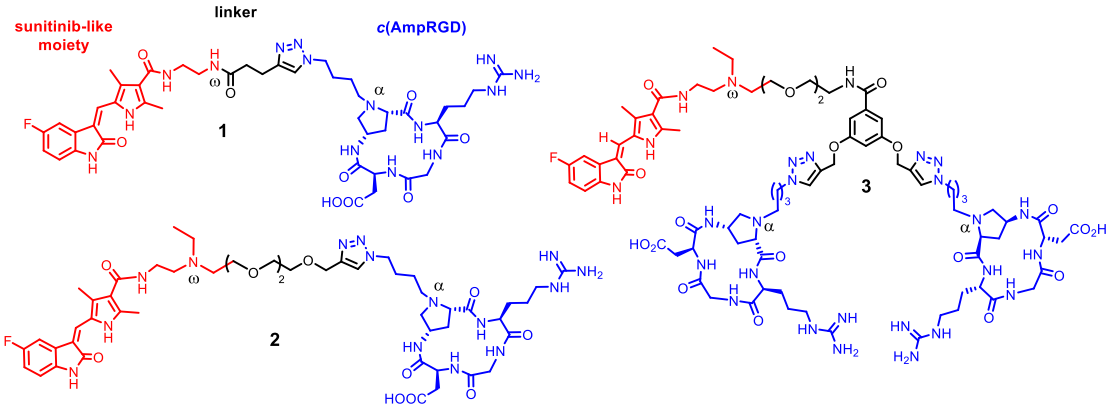

Figure 22. Structure of the targeted dual conjugates **1**-**3**.

Monomeric compounds **1** and **2** differ from each other in the linker length and type; compounds **2** and **3** share a common pegylated linker and maintain the tertiary amine functionality of the parent drug, while compound **1** replaces this amine with a secondary amide. Finally, compound **3** features a dimeric RGD presentation, which could be important for enhanced integrin recognition and integrin-mediated cell internalization.[78–81]

1*a*.3.2 Synthesis of Sunitinib-*c*(AmpRGD) conjugates 1-3

The synthesis of the dual constructs **1-3** began with the preparation of three constitutive modules namely, the *c*(AmpRGD)-azide, representing the directing unit (Scheme 1), the sunitinib analogue (Scheme 5), and the linker moieties (Fig. 23).

- **Synthesis of the *c*(AmpRGD) modules**

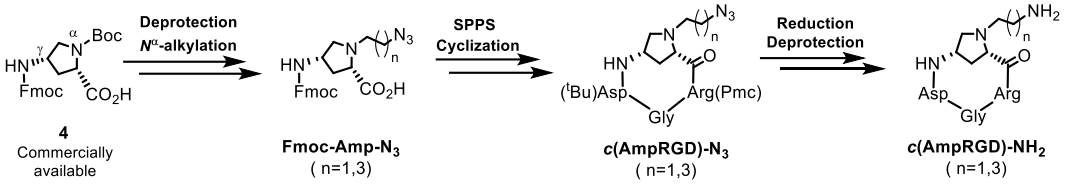

Scheme 1. General synthetic plan of the *c*(AmpRGD)-N_3 and *c*(AmpRGD)-NH_2 modules.

The general synthetic plan to access to *c*(AmpRGD)-azide modules and their reduced counterparts *c*(AmpRGD)-amine is described in Scheme 1. It has been possible to obtain the functionalization of the N^{α}-proline site with two short alkyl chains (two- and four-carbon long), both ending with an azido group which will be useful for further handling in the field of click chemistry or to furnish the amino derivatives. However, the N^{α}-installation of the longer alkyl chain proved to be more desirable (vide infra). To the aim of synthesize the *c*(AmpRGD) unit, commercial 4-aminoproline nucleus **4** was N^{α}-functionalised with short alkyl chains to give *N*-alkylated aminoproline scaffolds **Fmoc-Amp-N_3**, suitable for the following solid phase peptide synthesis (Fmoc-SPPS). After cleavage from the resin, the synthesized linear peptides were cyclized, giving the protected azido-terminating cyclotetrapeptides ***c*(AmpRGD)-N_3**, ready to be used in the construction of the dual conjugates. The reduced and deprotected counterparts ***c*(AmpRGD)-NH_2** were used as reference compounds during biological assays.

Concerning the synthesis of Fmoc-Amp-N_3 scaffolds **7** and **9** (Scheme 2), which differ in the *N*-alkyl chain length, a long optimization work was required. First, the commercial orthogonally protected *cis*-amino-L-proline **4** was selected as the starting point. This γ-amino acid, equipped with the proper N^{γ}-Fmoc protecting group, was selectively deprotected at the N^{α}-site by acidic treatment, affording quantitatively the aminoproline scaffold **5**, which represents the common precursor to *N*-alkylated aminoprolines **7** and **9** (Scheme 2).

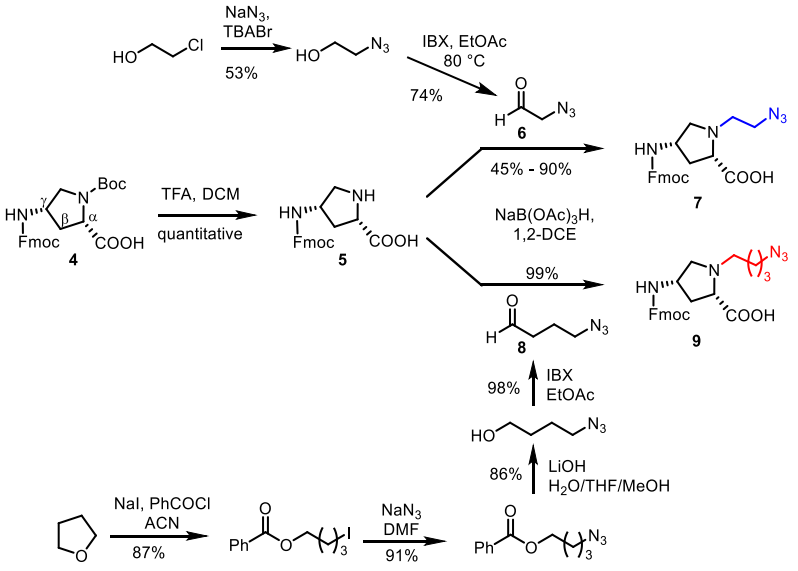

Scheme 2. Synthesis of the *N*-alkylated aminoproline scaffolds **7** and **9**.

The following N^{α}-site functionalization of proline **5** was accomplished according to the two different paths, outlined in Scheme 2. The azido-acetaldehyde (**6**), required to install the two-carbon long alkyl chain by reductive amination on proline **5**, was obtained in two steps starting from the commercial 2-chloroetanol. This alcohol, according to literature procedure,[82] was subjected to nucleophilic substitution with sodium azide (NaN_3) giving 2-azidoetanol in modest yield, which was treated, in turn, with the mild oxidant IBX (*o*-iodoxybenzoic acid). The resulting 2-azidoacetaldehyde (**6**) was recovered by simple filtration of the reaction mixture, since IBX and IBX-derived by-products are insoluble in EtOAc at room temperature.[83] The reaction required high temperature (80 °C) to solubilize IBX and allow the oxidation of the alcohol to the corresponding carbonyl compound. In our case, solid by-products were filtered-off at room temperature, allowing simple and clean recovery of the 2-azidoacetaldehyde (**6**). However, given its low molecular weight, this aldehyde proved to be extremely volatile and solvent removal (under reduced pressure at 0.8 bar and low temperatures below 40 °C) was never complete. The following *N*-alkylation step of **5** with aldehyde **6** by reductive amination using sodium triacetoxyborohydride [$NaB(OAc)_3H$], led to compound **7** in variable yields ranging from 45 to 90%. These results could probably be explained by the uncertainty of the effective amount of compound **6** added to the reaction and/or by possible interference deriving from residual EtOAc.

In an attempt to overcome this issue, we decided to functionalize the aminoproline **5** with a four carbon-long alkyl chain, deriving from the less volatile 4-azidobutanal (**8**). According to the procedure described in literature,[84] the precursor 4-azidobutanol was obtained in three synthetic steps starting from tetrahydrofuran. The ring opening with sodium iodide (NaI) in the presence of benzoyl chloride allowed the simultaneous installation of the ester and iodo-groups, giving to the 4-iodobutyl benzoate intermediate. The displacement of iodide with an azido-group, followed by saponification, quickly led to 4-azidobutanol, which was subjected to the oxidation step by IBX treatment. After filtration and solvent removal under reduced pressure (keeping temperature below 45 °C and pressure at 0.8 bar), the desired compound 4-azidobutanal (**8**) was recovered in a quantitative yield. In this case, the *N*-alkylation step of scaffold **5** with aldehyde **8** in the presence of [$NaB(OAc)_3H$], led to compound **9** in a reproducible 99% isolated yield. Both the synthesized *N*-alkylated aminoproline scaffolds **7** and **9** were then used in the following SPPS procedure for the preparation of linear AmpRGD tetrapeptides **10** and **11** (Scheme 3).

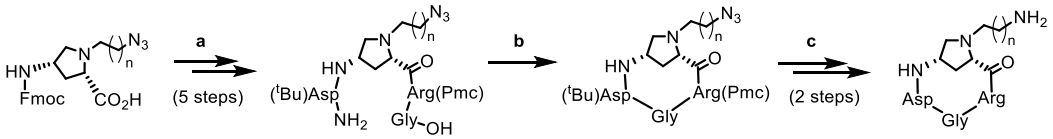

7: n=1
9: n=3

10: n=1 (96%)
11: n=3 (94%)

12: n=1 (67%)
13: n=3 (67%)

14: n=1 (82%)
15: n=3 (82%)

Scheme 3. Synthesis of the *c*(AmpRGD)-azide modules (12 and 13), and their reduced counterparts (14 and 15). Reagents and conditions: (**a**) Fmoc-SPPS: (*i*) Cl-cTrt-O-Gly-(Pmc)Arg-NH_2, **7** (or **9**), HATU, HOAt, collidine, DMF, rt; (*ii*) piperidine, DMF, rt; (*iii*) Fmoc-Asp(*t*Bu)-OH, HATU, HOAt, collidine, DMF, rt; (*iv*) piperidine, DMF, rt; (*v*) AcOH, TFE, DCM, rt; (**b**) HATU, HOAt, collidine, DCM/DMF, rt; (**c**) (*i*) H_2, Pd/C, EtOH, rt; (*ii*) TFA/TIS/H_2O (95:2.5:2.5), rt.

The syntheses of linear precursors **10** and **11** were carried out by means of the SPPS Fmoc-strategy exploiting acid-labile *o*-chlorotrityl chloride resin preloaded with Gly amino acid. In this way, the Amp unit would likely assume a central critical position, creating a local constraint that pre-organizes the peptide backbone toward the following macrocyclization step. Using standard Fmoc-SPPS chemistry, *N*-Fmoc-protected amino acids were coupled stepwise using the HATU/HOAt activating system in the presence of collidine as a base. After each coupling, the Fmoc *N*-protecting group was easily removed by standard piperidine/DMF procedure and, once completed, linear peptide sequences were readily cleaved from the resin using the usual AcOH/TFE/DCM system. This mild acidic treatment allowed to preserve the acid-labile protecting groups *tert*-butyl (*t*Bu) and 2,2,5,7,8-pentamethylchroman-6-sulfonyl (Pmc) in the amino acid side chains of aspartic acid and arginine, respectively. The crude linear peptides were obtained in high yields (94-96%) for the entire solid phase sequence.

Compounds **10** and **11** were then subjected to in-solution head-to-tail cyclisation. As well known, macrocyclization of peptides is generally considered a significant synthetic challenge.[85] Ring-closing (intramolecular) reactions are often plagued by low yields[86] and usually are much slower as compared to intermolecular bond formations. Competing side reactions, such as dimerization or cyclodimerization of linear peptide precursors, often predominate for certain ring sizes. Since this problem can be suppressed by leading the reaction under diluted conditions,[87] we performed the cyclization reaction at 2.3 mM peptide concentration in dry DCM/DMF solvent mixture (13:1). The expedient of keeping low the amount of the high boiling solvent (DMF) allowed an easier evaporation of the solvent under vacuum, thus avoiding high temperature and prolonged time, which can lead to the degradation of the cyclized product (e.g., oxidation at the N^{α}-proline). Moreover, since the half-life of HATU under basic conditions is in the range of minutes,[87] we decided to add dropwise the solution of each linear peptide and collidine in dry DCM to a previously prepared solution of HATU/HOAt reagent couple in dry DCM/DMF mixture. In this way, the HATU coupling reagent should be reactive for enough time and the slow addition of the precursor contributes to keep low its concentration in the reaction mixture.

The crude cyclized peptides were purified by reverse phase flash chromatography [H_2O (0.1% TFA)/MeCN: linear gradient 80:20 to 20:80] furnishing the novel azide module **13** in overall eight-step sequences and rewarding 63% overall yield from proline **4**, while compound **12** was obtained in variable yields (30-60% overall yields). Azides **12** and **13** could be also conveniently converted to free amines **14** and **15**, respectively, via reduction and acidic deprotection (82%, two steps), which served as reference compounds in the biological assays. It is worth to note that the synthesis of similar *c*(AmpRGD)-azide/amine congeners, reported by us in previous works,[41,44] required longer linear synthetic sequences (14-15 steps) and were obtained in lower yields (10-16% overall yields).

- **Synthesis of the fluorescein-*c*(AmpRGD) conjugate 20**

As previously mentioned, the ability of *c*(AmpRGD) units to mediate internalization of the dual constructs in $\alpha_V\beta_3$-overexpressing melanoma cell lines was investigated by confocal fluorescence microscopy. To this aim, the fluorescein-labelled conjugate **20** was synthesized starting from azido-ethyl derivative **12**, fluorescein isothiocyanate and linker **17** (Scheme 4).

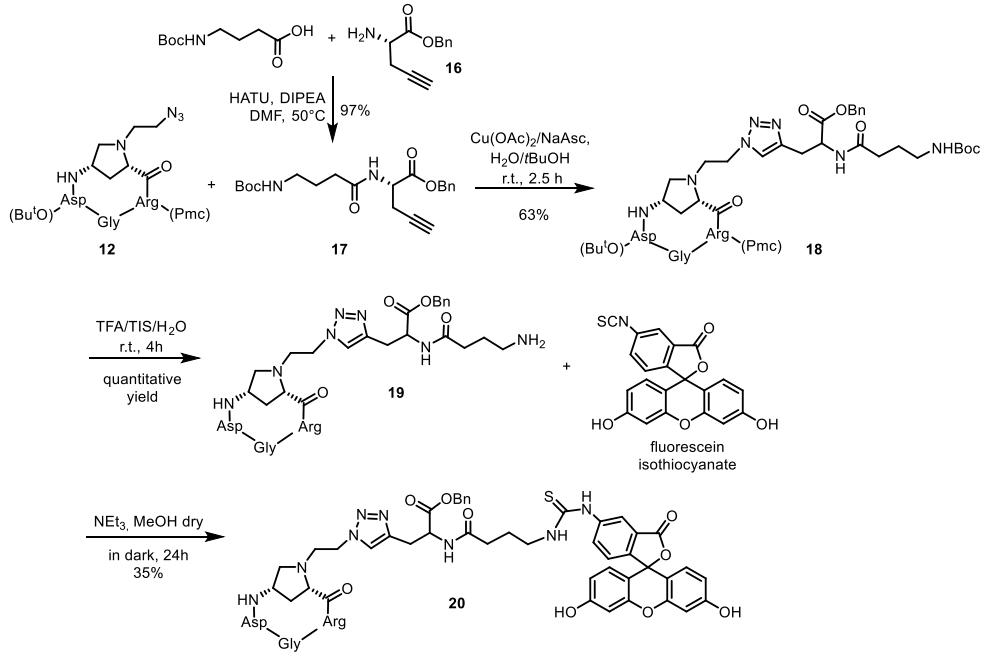

Scheme 4. Synthetic pathway to the RGD-fluorescein compound **20**.

By reacting the commercial Boc-protected γ-aminobutyric acid with L-propargylglycine benzyl ester **16** in the presence of HATU/DIPEA coupling system, compound **17** was obtained in high isolated yield after flash chromatography purification. The alkyne linker module **17** was then conjugated to Amp-based cyclopeptide **12** via copper-catalyzed azide-alkyne cycloaddition fournishing the intermediate **18** in a 63% isolated yield. After acidic treatment, that allowed to deblock the side chain protecting groups and terminal primary amine, compound **19** was quantitatively obtained and then coupled with fluorescein isothiocianate. The coupling reaction was conducted in dark under basic conditions leading to conjugate **20**, which was recovered in a modest 35% yield, by reverse phase HPLC purification. After structural characterization, compound **20** was utilized in internalization studies, as detailed in the biological evaluation section.

- **Synthesis of the sunitinib-Like Module 23**

Concerning the sunitinib portion, carboxylic acid **23** (Scheme 5) was judged a good precursor. The synthesis of this precursor was accomplished following the reported procedure by Sun et al. in 2003.[75]

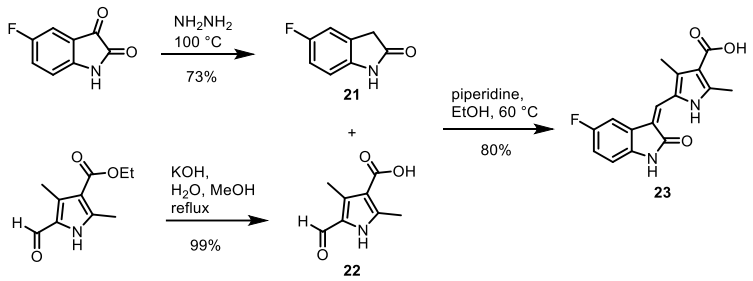

Scheme 5. Synthesis of the sunitinib-like module **23**.

As shown in Scheme 5, compound **23** derived from Knoevenagel condensation between oxindole **21** and pyrrole acid **22**, in turn obtained from commercially available sources. Indeed, fluorooxindole **21** was efficiently prepared by Wolff-Kishner reduction of commercial 5-fluoroisatin (73% yield), while saponification of the corresponding commercial ethyl ester produced acid **22** in high yields (99%). The base-promoted condensation of **21** to the formyl moiety in **22** consigned 3-alkylidene 2-oxindole **23** in a good 80% yield as the sole detectable *Z*-configured isomer.[1]

- **Synthesis of the linker moieties 24-26**

Concerning the linkers needful for connecting Amp-based targeting unit to sunitinib analogue, simple chemistry was used to access alkyne-terminating amine **24**, pegylated counterpart **25** and bis-alkyne amine **26** (Fig. 23).

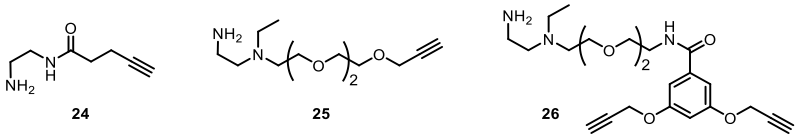

Figure 23. Structures of the linkers **24**-**26**.

These linkers share two functional groups: (*i*) a primary amino group, that will be exploited to bind the sunitinib-like moiety **23** via amide linkage; and (*ii*) a terminal alkyne, that will react by a copper-catalyzed azide-alkyne cycloaddition with the azido group of the *c*(AmpRGD)-azide **13** module. Hereafter, their preparation from commercial starting materials is described.

[1] The photoinduced *Z*-*E* isomerization of sunitinib drug is renowned as it is known that dark conditions promote reversible reconversion to the biologically active *Z*-isomer. In our hands, all "sunitinib-containing" compounds were pure *Z*-configured compounds and were treated under dark conditions to prevent possible isomerization. For more information, see ref.[95].

The first linker **24** was prepared in just two synthetic steps, as detailed in Scheme 6.

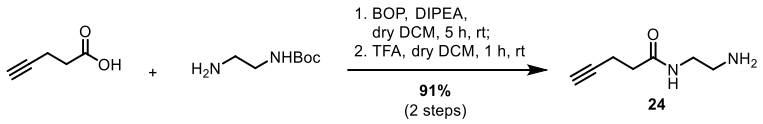

Scheme 6. Synthesis of linker **24**.

The BOP-promoted coupling reaction between the carboxylic group of the 4-pentynoic acid and the primary amino group of the *N*-Boc-ethylenediamine furnished the corresponding *N*-Boc protected intermediate that, after exposure to TFA/DCM mixture, gave the desired linker **24**, as TFA salt, in 91% isolated yield over two steps.

On the contrary, the synthesis of the second linker **25**, featuring a short pegylated chain and a tertiary amino group, was more demanding as far as synthetic work was concerned (Scheme 7). The *N*-ethyl derivative **27** was obtained by reductive amination of *N*-Boc-ethylenediamine with acetaldehyde, using the usual reducing agent sodium triacetoxyborohydride, in presence of a catalytic amount of magnesium sulfate ($MgSO_4$), as drying agent. This latter fosters the formation of the iminium ion reaction during the amination step, which is preferentially reduced by sodium triacetoxyborohydride, with respect to the starting aldehyde. The *N*-ethyl derivative **27** was obtained in a modest isolated 54% yield by flash chromatography purification accompanied by significant amount of *N,N*-diethyl derivative, as by-product of the reaction. In order to limit this drawback, the aldehyde has to be added in a just small excess (1.2 equiv) compared to *N*-Boc-ethylenediamine (1 equiv). Since acetaldehyde is particularly volatile, a precise addition of the required amount resulted quite difficult. To overcome this issue, acetaldehyde was cooled in liquid nitrogen thus reducing volatility and increasing manageability for a short time. Addition of cool acetaldehyde allowed to avoid the flash chromatography purification, and the desired product **27** was recovered just by extractive steps.[2]

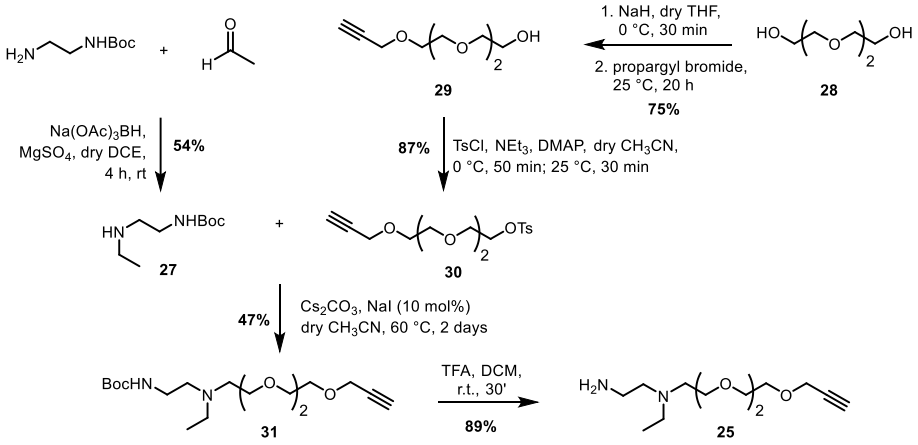

Scheme 7. Synthesis of the second linker **25**.

The alkyne-tosylate **30** was prepared according to a reported procedure,[88] starting from commercial triethylene glycol **28**. Selective mono-substitution of hydroxy groups was accomplished by treating compound **28** (1 eq) with the strong base sodium hydride (0.65 equiv), in order to favor the formation of the mono-activated nucleophile species. After addition of propargyl bromide (0.5 equiv), compound **29** was recovered in a good 75% isolated yield by flash chromatographic purification. The free hydroxy group in **29** was then

[2] As an alternative procedure, after reaction completion, the reaction mixture was simply filtered, and the retentate washed with DCM (x 2). Treating the filtrate with water (pH = 4), after extraction with DCM (x 4), the product remained in the aqueous phase while the organic impurities passed in the organic phase. Adding sodium carbonate to water (until pH = 12), the product passed in the organic phase (DCM, x 4). After removal of the solvent under reduced pressure, compound **27** was isolated in a 78% yield.

subjected to tosylation, giving the desired compound **30** in a high isolated yield, ready for the following nucleophilic substitution step. Given the poor nucleophilic character of the secondary amine **27**, substitution was performed with the following cautions: (*i*) using the inorganic base cesium carbonate (Cs_2CO_3), which displayed both good basicity and solubility in organic solvents, enhancing nucleophilicity of **27** while preserving the alkyne-proton of **30**; (*ii*) reducing the solvent volumes and (*iii*) warming the reaction mixture to 60 °C. Also, a catalytic amount of sodium iodide (NaI) was added in order to promote the overall nucleophilic substitution. Despite all these precautions, the reaction furnished compound **31** in a modest isolated yield of 47%, accompanied by the unreacted substrate **30**, which was quantitatively recovered in the purification step. After the acidic deprotection step, the desired linker **25** was quantitatively obtained, as a TFA salt.

Finally, concerning the synthesis of the third linker **26**, the *bis*-alkyne precursor **32** was prepared starting from the commercial 3,5-diidroxybenzoic acid according to a known procedure (Scheme 8).[89] 3,5-diidroxybenzoic acid was protected as a methyl ester and then reacted with propargyl bromide in the presence of potassium carbonate. After restoration of the carboxylic functionality by saponification, compound **32** was recovered in a satisfying isolated 71% yield over 3 steps.

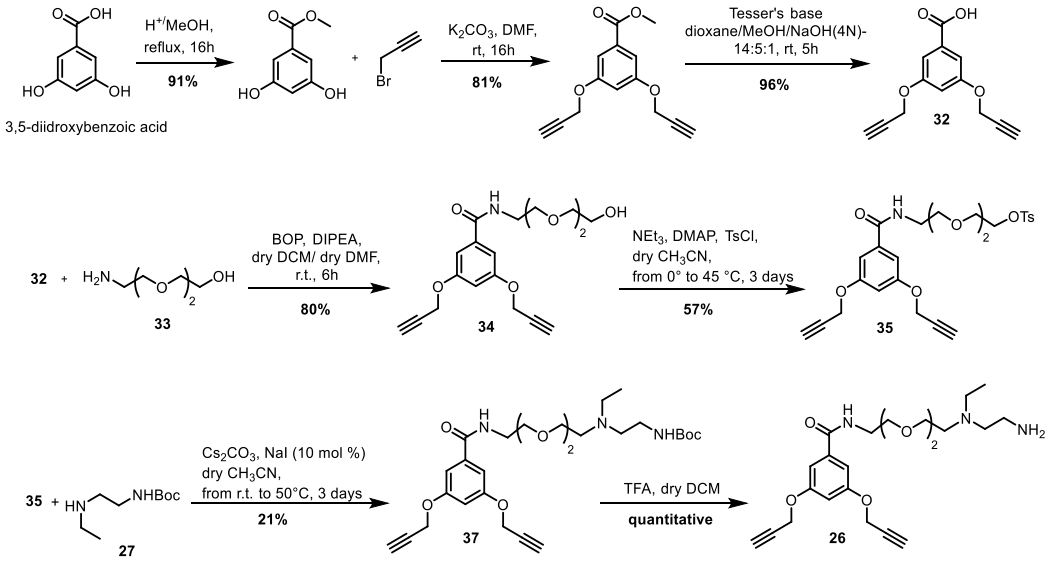

Scheme 8. Synthesis of the third linker **26**.

The coupling reaction between the carboxylic functionality within **32** and the amino group of the commercial compound **33**, promoted by BOP/DIPEA activating system, furnished compound **34** in good isolated yield (80%). Since compound **32** was found to be insoluble in DCM, addition of a minimal amount of DMF proved to be necessary. Tosylation reaction of compound **34**, performed according to the optimized conditions previously disclosed for the synthesis of linker **25**, proved to be inefficient probably due to poor reactivity of the substrate. However, prolonging the reaction time (stirring at 45-50 °C for three days) delivered compound **35** in a respectable 57% isolated yield. Flash chromatographic purification allowed to partially recover the unreacted starting compound **34** accompanied by the chloro-derivative **36** (Scheme 9). These results could be explained by the mechanism displayed in Scheme 9.

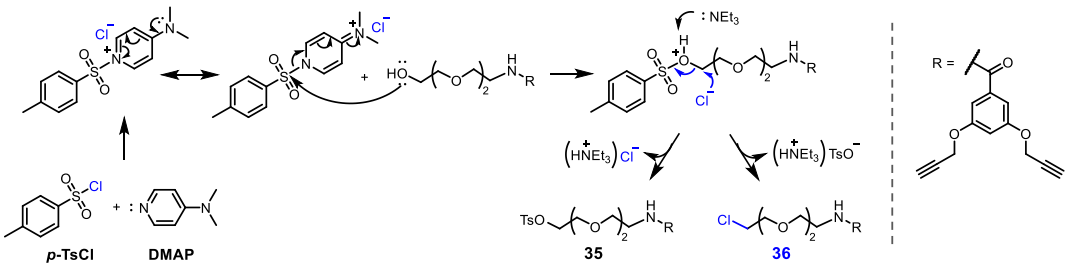

Scheme 9. Possible mechanism to explain the formation of chloro-derivative **36**.

In attempting to improve the tosylation step, some aspects were considered: (*i*) longer reaction time (stirring the mixture at 50 °C for several days) did not improve the reaction outcome; (*ii*) performing the reaction under reflux (~80 °C) led to increased formation of the chloro-derivative **36**; *(iii)* using a carefully dried acetonitrile enhanced the reaction yield.

The substitution reaction between the poor nucleophile **27** and the tosylate **35** proved to be even more difficult as compared to the substitution leading to compound **31** (Scheme 7). Using the same synthetic conditions, compound **37** was obtained in scarce yield (21%) with partial recovery of the starting tosylate **35** by flash chromatography. No improvement was observed when leaving the system to react for longer reaction time (more than 3 days), warming the reaction to reflux (at least 80 °C), nor performing the reaction in DMF. Final deprotection upon exposure of compound **37** to TFA quantitatively led to the linker **26**.

At this point, all was ready for preparation of the three dual conjugates **1**-**3**, where the main modules could be connected through common synthesis pathways. Thus, as shown in Scheme 10, parallel BOP-promoted condensation of carboxylic acid **23** with either amines **24**, **25** or **26** provided access to the respective alkyne-terminating amides **38**, **39**, or **40** in good isolated yields ranging from 64% to 88%.

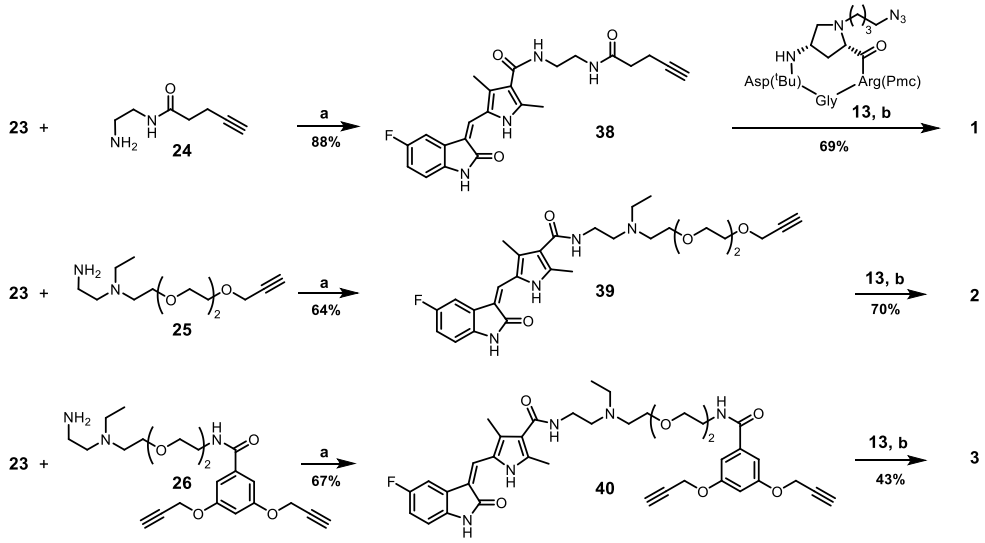

Scheme 10. Modular synthesis of the sunitinib-*c*(AmpRGD) conjugates 1-3. Reagents and conditions: (**a**) BOP, DIPEA, DCM/DMF (2:3), rt; (**b**) (*i*) azide **13**, $Cu(OAc)_2$, Na L-Asc, H_2O/DMF, rt; (*ii*) TFA/TIS/H_2O (95:2.5:2.5), rt.

Copper-catalyzed 1,3-dipolar cycloaddition between these alkynes and the previous *c*(AmpRGD)-azide **13** (2-fold equivalents in case of the dimeric execution involving compound **40**), followed by acidic deprotection and preparative reverse-phase HPLC purification, gave conjugates **1**-**3** as TFA salts in 69%, 70%, and 43% yields, respectively, and good purity (96-98%).

The conjugates **1**-**3** were evaluated in different biological assays to explore their potential as dual targeted anti-angiogeneic molecular tools, as detailed in the following section.

1*a*.3.3 Biological evaluation of Sunitinib-*c*(AmpRGD) conjugates 1-3

While the focus of this study was the design and synthesis of the sunitinib-*c*(AmpRGD) conjugates, a subsequent work was carried out on these compounds, in order to evaluate them as possible anti-angiogenic tools, as described in the aims of the work.

The following sub-sections describe the results of the analytical and biological measures for the sake of completeness and in order to place the synthesis efforts in the more complex scenario of the work.

These analyses were carried out by Prof. Federica Vacondio of the Food and Drug Department of the University of Parma (*in vitro* stability, lipophilicity and cell uptake), Dr. Daniela Arosio of the Molecular Science and Technology Institute of CNR, Milan (solid phase receptor binding assays), and Dr. Francesca Bianchini, of the CISPIM Centre, University of Florence (*in cell* inhibition of adhesion, cell proliferation tests, *in cell* TKI activity measurement, *in vitro* and *in vivo* inhibition of angiogenesis).

For experimental details on this section, the reader is addressed to the published article.[90]

- ***In vitro* stability of conjugates 1-3**

The *in vitro* stability of conjugates **1**-**3** in 80% v/v rat and human plasma was firstly evaluated by HPLC-UV-Vis analysis. The cyclopeptides were incubated and analyzed up to 8 h, as detailed in Table 2. Invariably and regardless of their intimate structure, compounds **1**-**3** showed complete resistance to rat and human plasma degradation during the observed time. This demonstrated that the covalent connection of the modules resulted in robust conjugates anticipating that, whatever the biological response, it would be the result of the interaction of the cell environment with the integral, preserved structure of the conjugates and not the individual detached components.

Table 2. In Vitro Plasma Stability of Compounds 1-3 vs Sunitinib

Compound	Rat plasma (% compd at 8h)[a]	Human plasma (% compd at 8h)[a]
sunitinib	97.3 (±9.1)	102.3 (±5.2)
1	88.2 (±12.7)	99.0 (±10.9)
2	104.1 (±3.3)	106.6 (±11.5)
3	108.8 (±10.5)	98.6 (±15.4)

[a]Percentage of compound remaining after 8 h of incubation in 80% v/v plasma, 37 °C, protected from light. Reported are means ± SD.

- **Cell internalization studies of fluorescent conjugate 20**

The cell internalization potential of *c*(AmpRGD) conjugates was preliminarily assayed using the *c*(AmpRGD)-fluorescein conjugate **20**. Thus, A375M melanoma cells overexpressing $\alpha_V\beta_3$ were incubated at 37 °C, and exposed for 25 min to a 10 μM *c*(AmpRGD)-fluorescein **20** solution in phosphate buffered saline (PBS). In addition, to investigate the specific $\alpha_V\beta_3$-mediated internalization of the *c*(AmpRGD)-fluorescein **20**, cells were also pretreated for 30 min with the $\alpha_V\beta_3$ blocking antibody (Millipore LM609) 1 mg/mL. As shown in Figure 24 and 25A, compound **20** entered the cells and localized in the cytoplasmic region, as revealed by confocal fluorescence microscopy. When instead cells were pre-treated by an anti-$\alpha_V\beta_3$ antibody (1 mg/mL) before the incubation with **20**, the green fluorescence of *c*(AmpRGD)-fluorescein **20** was not registered inside the cell (Fig. 25B), proving that internalization was $\alpha_V\beta_3$-dependent.

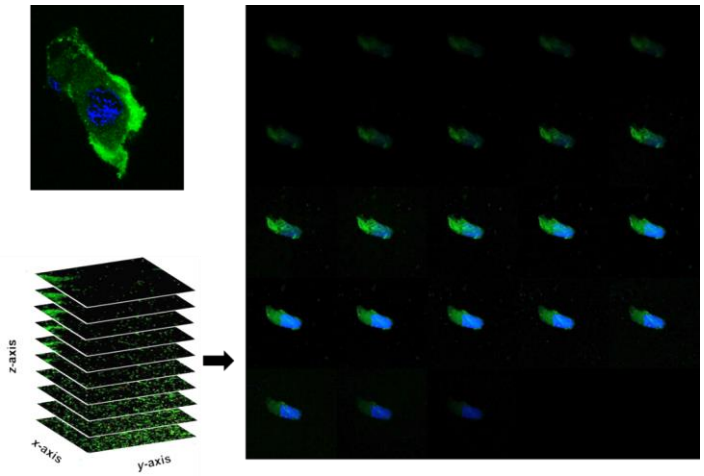

Figure 24. Confocal fluorescence microscopy analysis of a A375 melanoma cell exposed for 25 min to a 10 µM solution of *c*(AmpRGD)-fluorescein **20** (green emission). Nucleus stained with DAPI (blue emission). *c*(AmpRGD)-fluorescein **20** is localized inside the cell.

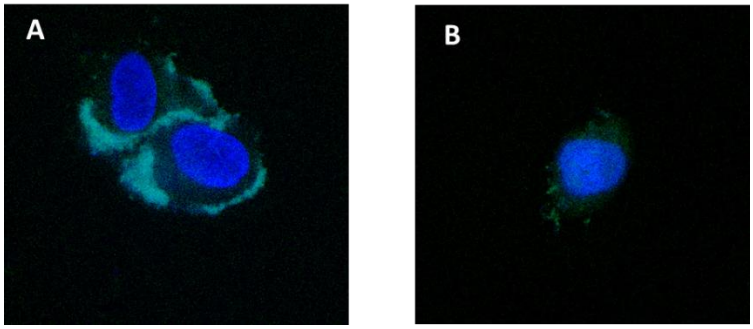

Figure 25. Fluorescence microscopy images of a A375 melanoma cells exposed for 25 min to a 10 µM solution of *c*(AmpRGD)-fluorescein **20** (green emission). Nucleus stained with DAPI (blue emission). **A**) Compound **20** entered the cell and localized in the cytoplasmic region. **B**) The green fluorescence of *c*(AmpRGD)-fluorescein **20** is not registered inside the cell, as a result of the cell treatment with an anti-$\alpha_v\beta_3$ antibody (1 mg/mL) before incubation with **20**.

Though these preliminary internalization experiments were promising in terms of cell uptake efficiency, we were aware that the scenario related to the *c*(AmpRGD)-sunitinib conjugates could have been different. The chemical structures of these conjugates are similar in the RGD moiety but different in the appended moieties (fluorescein versus sunitinib); furthermore, the cell uptake could be dependent upon the cell type, e.g. A375 melanoma versus endothelial progenitor cells (EPCs). Thus, the cell uptake of conjugates **1-3** was evaluated, quantitatively, as described in the next sub-section.

- **Lipophilicity and cellular uptake of conjugates 1-3**

At physiological pH, compounds **1**-**3** proved highly hydrophilic in accordance with the measured negative values of the Log$D_{oct,7.4}$ (i.e. the distribution coefficient in *n*-octanol/buffer at pH 7.4, Table 3). As expected, attachment of the *c*(AmpRGD) module to the sunitinib-like portion turned the lipophilic character of the drug to hydrophilic, which was magnified by the pegylated linker (compounds **2** and **3** vs **1**) and the dipeptide presentation (**3** vs **1** and **2**).

Table 3. Lipophilicity and Cellular Uptake of Compounds 1-3 and Sunitinib in EPCs

Compound	Log $D_{oct,7.4}$[a]	MW	Intracellular Content (nmol/mg prot) (1 h)[b]	Cell uptake (pmol/min /mg prot) (1 h)	Log Cell Uptake (1 h)	Intracellular Content (nmol/mg prot) (8 h)[b]
sunitinib	2.51	398.5	5.72 (±0.71)	95.3	1.98	2.90 (±0.40)
1	– 2.03	960.0	0.26 (±0.02)	4.3	0.64	0.22 (±0.02)
2	– 2.56	1078.2	0.48 (±0.07)	8.0	0.90	0.43 (±0.09)
3	– 3.02	1788.9	0.94 (±0.02)	15.7	1.19	0.54 (±0.03)

[a]Distribution coefficient in the *n*-octanol/buffer system, pH 7.4. Reported are means ± SD. [b]EPCs were incubated with 1 μM final concentration of test compound. After 1 h, the medium containing the tested compounds was removed and intracellular content was quantified immediately and after 8 h. Experiments were conducted in triplicate and data were expressed as nmol/mg of total cell proteins in each sample.

The capability of endothelial progenitor cells (EPCs) to internalize conjugates **1**-**3** as compared to free sunitinib was next investigated. Total intracellular concentrations of **1**-**3** and sunitinib were measured by HPLC-ESI-MS/MS. EPCs were incubated in standard conditions for 1 h in the presence of the different compounds at 1 μM final concentration. As illustrated in Table 3, all compounds were detected in the intracellular extracts, with the small-sized sunitinib drug showing maximum levels at 1 h, while conjugates **1**-**3** were found in the cell extract to a much lesser extent. In particular, compound **1** showed a scarce entrance in cells after 1 h treatment, which remained almost invariable after 8 h. Pegylated counterpart **2**, having similar molecular weight, almost doubled its ability to enter cells as compared to **1** at both 1 h and 8 h treatment. Finally, dimeric RGD conjugate **3**, notwithstanding its higher molecular weight, showed a 4-fold and 2-fold ability to enter cells as compared to **1** and **2**, respectively.

These data are quite interesting since they emphasize the following points: (*i*) the requisite delivery of the sunitinib-like moiety inside cells is provided by conjugates **1**-**3**, even if the internalization is not as efficient as the free drug, and (*ii*) the amount of each conjugate (expressed as pmol/min/mg prot) which passes through the EPC membrane in the first hour is, on a log scale, inversely related to its lipophilicity. The more hydrophilic and bulkier **3** is more efficiently internalized than **1**; the dependence of the internalized content upon the RGD presentation (monomeric vs dimeric) suggests a direct involvement of the RGD moiety during the internalization process possibly via $\alpha_v\beta_3$-mediated endocytosis.[78–81] The assay was repeated for compounds **2** and **3** in the presence of excess $\alpha_v\beta_3$ integrin ligand **15** (100 μM). Significant decrease of cell uptake was witnessed for both compounds (not shown) further corroborating the notion of an active role of this integrin during internalization.

- **Solid-phase receptor binding assay**

The integrin activity and selectivity profile of compounds **1**-**3** were firstly evaluated by measuring their ability to bind to human, isolated $\alpha_v\beta_3$ and $\alpha_5\beta_1$ integrin receptors by competitive displacement assays using either biotinylated vitronectin VN (for $\alpha_v\beta_3$) or biotinylated fibronectin FN (for $\alpha_5\beta_1$). To better evaluate the impact of the sunitinib moiety on binding capability, the results were compared to those obtained for the unconjugated counterpart *c*(AmpRGD)-$(CH_2)_2NH_2$ (**14**) and commercial ligand *c*(RGDfV). As shown in Table 4, compounds **1**-**3** exhibited one-digit nanomolar affinity toward $\alpha_v\beta_3$ integrin, which was even superior to the unconjugated AmpRGD-based counterpart and showed in all cases an appreciable $\alpha_v\beta_3/\alpha_5\beta_1$ selectivity. Compound **3**, bearing a 2-fold RGD repeat, showed an increased binding affinity as compared to monomer **2**, even if it was lower than **1**. Overall, the presence of a sunitinib-linker cargo attached to the integrin-recognizing RGD unit did not compromise the exquisite binding affinity and selectivity of these conjugates.

Table 4. Inhibition of biotinylated VN and FN binding to $\alpha_v\beta_3$ and $\alpha_5\beta_1$ receptors, respectively[a]

Compound	IC_{50} (nM) ± SD for $\alpha_v\beta_3$	IC_{50} (nM)±SD for $\alpha_5\beta_1$
1	1.24±0.01	30.7±17.7
2	5.1±0.6	101.3±31.3
3	3.8±0.6	95.8±46.7
c(AmpRGD)-$(CH_2)_2NH_2$ (**14**)	6.1±1.6[b]	151.6±67.6[b]
c(RGDfV)	3.2±1.3[b]	166.0±28.0[c]

[a] IC_{50} values were calculated as the concentration of compound required for 50% inhibition of biotinylated VN or FN binding to human, isolated receptors. Each data point represents the average of triplicate wells; data analysis was carried out by nonlinear regression analysis using GraphPad Prism software. Each experiment was repeated in duplicate. [b] Ref.[41]. [c] Ref.[44].

- **Inhibition of EPC adhesion to the $\alpha_v\beta_3$-ligand vitronectin using conjugates 1-3**

The synthesized compounds **1**-**3** were evaluated for their ability to inhibit the adhesion of natural ligand vitronectin (VN) to $\alpha_v\beta_3$-overexpressing cells. Endothelial progenitor cells (EPCs) were chosen due to their abundant $\alpha_v\beta_3$ integrin receptor expression (as certified by flow cytometric analysis),[3] and for their recognized role in tumor angiogenesis.[91,92] The assay of adhesion inhibition was performed in the presence of 2.0 mmol/L $MnCl_2$ to switch $\alpha_v\beta_3$ integrin to its activated form with increasing concentrations of compounds **1**, **2** and **3** (1, 10, 100, 1000, 10000 nM); for comparison purposes, sunitinib alone, unconjugated *c*(AmpRGD) **15**, and a combination of both were also assayed.

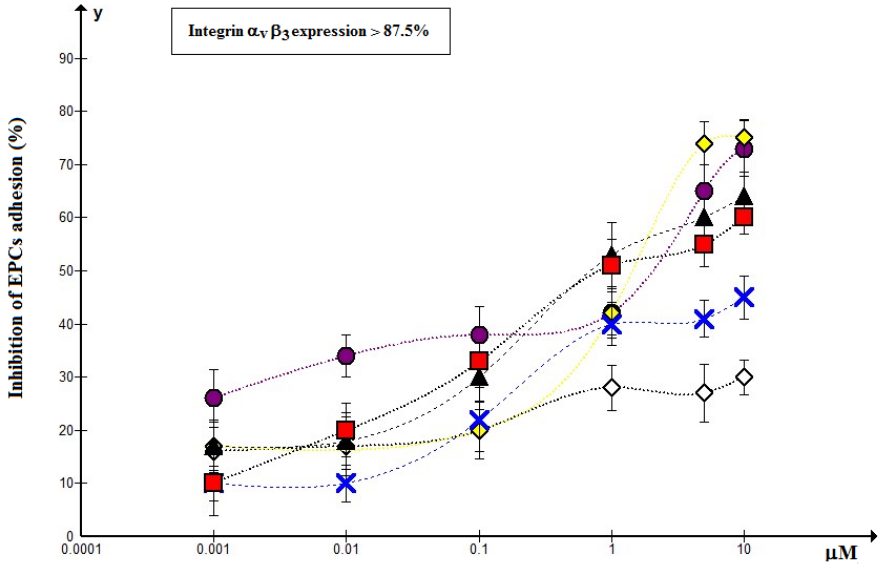

Figure 26. Inhibition of EPCs adhesion to VN in the presence of compounds **1**-**3**, **15**, sunitinib, and the combination sunitinib+**15** (▲ compound **1;** ✖ compound **2;** ■ compound **3;** ● compound **15;** ◇ sunitinib; ◆ compound **15**+sunitinib**)**. Top insert indicates the percentage of $\alpha_v\beta_3$ integrin expression in EPCs. The inhibitory activity was calculated as percentage of cell adhesion to VN in untreated cells and was expressed as mean ± SD. Experiments were carried out in triplicate.

[3] The expression of β_1 integrins (e.g., $\alpha_5\beta_1$) in EPCs was also evaluated; it was determined to be about 35-40%, lower than the expression of $\alpha_v\beta_3$ (>87.5%).

As shown in Figure 26, conjugated cyclopeptides **1** and **3** strongly inhibited cell adhesion in a dose-related manner with IC_{50} values nearly approaching 500 nM, while conjugate **2** showed a less efficient activity (IC_{50} *ca* 10 µM); notably, the inhibitory capability of compounds **1** and **3** was even better than the unconjugated counterpart **15** (IC_{50} 1.8 µM). As expected, the inhibitory capability of sunitinib alone remained negligible at these concentrations, a result consistent with the IC_{50} value observed for the combination sunitinib+**15**, having an IC_{50} value similar to that of compound **15** alone. Overall, the covalent conjugation of the *c*(AmpRGD) portion to the sunitinib-like moiety as described in the diverse topologies of compounds **1**-**3** does not significantly alter the ligand binding capability towards these endothelial $\alpha_v\beta_3$-overexpressing cells.

- **Effect of conjugates 1-3 on cell proliferation and cell viability**

The effect of the different compounds was evaluated on EPCs in a proliferation assay performed in the presence of VEGF-A (20 ng/mL), and the various compounds **1**-**3**, **15**, sunitinib, and **15**+sunitinib at 1 µM concentration every 24 h. The effect was followed after 24 h, 48 h and 72 h exposure. Cell proliferation was measured by cell count and cell viability was evaluated using trypan blue exclusion assay (Fig. 27).

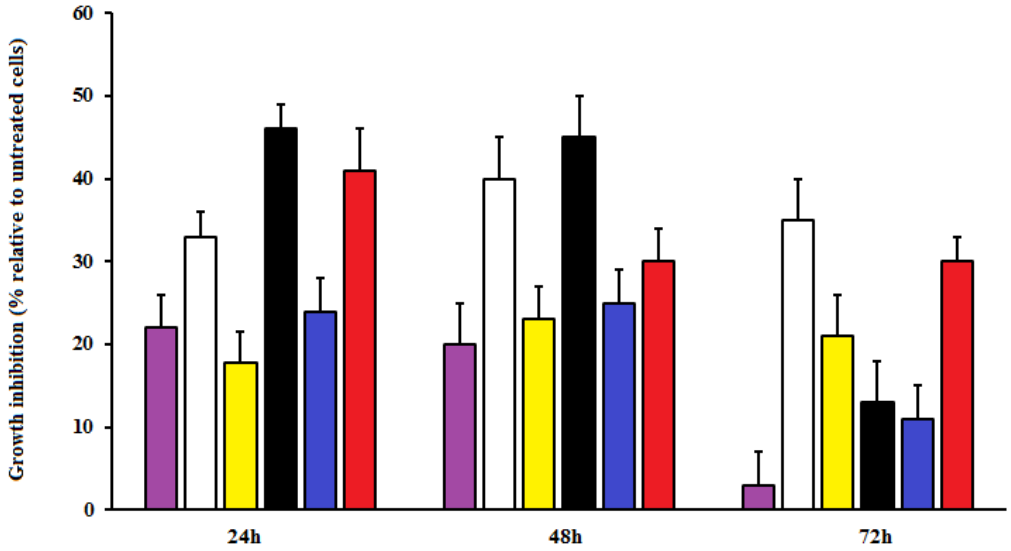

Figure 27. Effect of the different compounds on VEGF-mediated EPCs proliferation. EPCs were grown in a serum and growth factor-free medium containing 20 ng/mL VEGF-A. Cells were exposed to 1 µM concentration of different compounds every 24 h (compound **15**, sunitinib; compound **15**+sunitinib, compound **1**, compound **2**, compound **3**). After 24 h, 48 h, and 72 h incubation, cells were counted and cell viability was assessed. Representative of three independent experiments.

After the first 24 h treatment, conjugates **1**-**3** showed inhibition of VEGF-induced proliferation of 46%, 24%, and 41%, respectively, with respect to untreated cells. On the other hand, sunitinib inhibited cell proliferation of 33%, and the combination of sunitinib with compound **15** poorly impacted cell proliferation. After 48 h treatment, conjugates **1**-**3** and sunitinib alone maintained almost the same level of inhibition of proliferation. Interestingly, the combination of sunitinib and compound **15** revealed a 23% of inhibition. After 72 h, inhibition of EPCs proliferation found in cells treated with compound **3** was similar to that of cells exposed to sunitinib, while other treatments did not show a significant inhibition of proliferation.

During the entire experiment, cell viability was monitored and no significant difference was found in EPCs exposed either to the conjugated compounds or to separate drugs.

- **Inhibition of TKI activity by conjugates 1-3**

To evaluate whether conjugation within **1**-**3** would affect the TKI activity of the sunitinib-like portion toward its targeted kinases, the inhibitory activity of representative compound **3** against human recombinant PDGFRβ and VEGFR2 was evaluated. As shown in Table 5, IC_{50} values were in the nanomolar range, slightly superior than those reported for sunitinib,[75] demonstrating that appendage of the two RGD moieties and linker was not detrimental for TKI activity *in vitro*.

Table 5. Inhibition of TKI Activity for Compound 3 and the Reference Compound Sunitinib against Human Recombinant PDGFRβ and VEGFR2[a]

Compound	PDGFRβ (nM)	VEGFR2 (nM)
3	9	420
sunitinib	2[b]	80[b]

[a]IC_{50} values for **3** were calculated as the concentration of compound required for 50% inhibition of control specific activity (staurosporine). Each data point represents the average of duplicate wells; data analysis was carried out by nonlinear regression analysis using software developed at Cerep (Hill software). [b]Ref.[75].

The ability of compounds **1**-**3** to inhibit VEGF-stimulated VEGFR2 phosphorylation was then investigated by Western blotting using EPCs, which were proven to express high levels of VEGFR2 (besides $\alpha_V\beta_3$). Sunitinib alone, *c*(AmpRGD) **15** alone, and a combination of the two were also assayed for comparison purposes. Percent inhibition at 1 µM concentration is reported in the densitometric analysis histogram (Fig. 28). EPCs were treated for 1 h with the different compounds and then activated with 50 ng/mL VEGF-A for 5 min[93] before cell lysis for VEGFR2 phosphorylation detection.

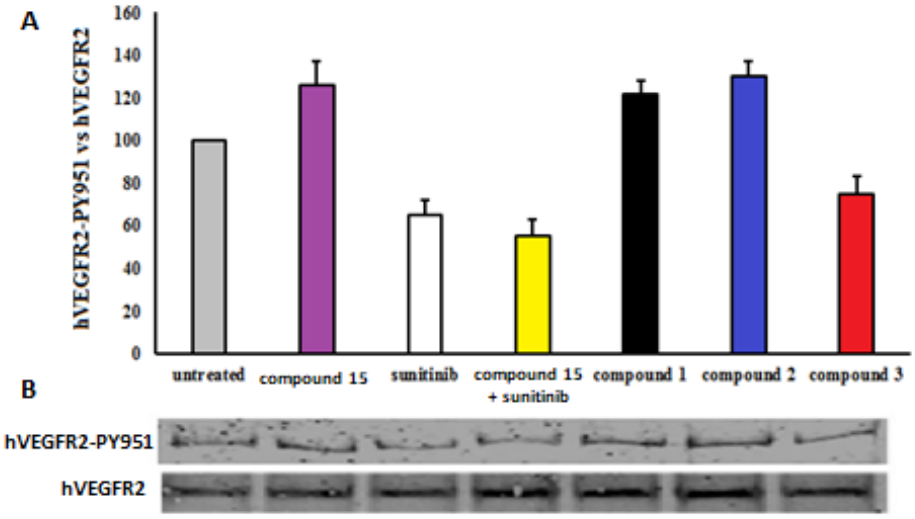

Figure 28. Inhibition of VEGFR2 phosphorylation in EPCs treated for 1 h with 1 µM concentration of different compounds, followed by VEGF-A activation (50 ng/mL) for 5 min. **A**) Densitometric analysis of the inhibition of VEGF-induced VEGFR2 phosphorylation. **B**) Western blot analysis. Results are reported as the mean ± SD of percent of inhibition of VEGFR2 phosphorylation compared to VEGF-treated cells. Representative of three independent experiments.

Among the different compounds, **1**, **2** and **15** showed a weak induction of VEGFR2 phosphorylation, that might be the result of the synergistic intracellular interaction between $\alpha_V\beta_3$ and VEGFR2 probably through Src domains leading to a mild activation of the VEGF receptor.[67–69,94]

As mentioned before, the biological behavior of monomeric compounds **1** and **2** might be influenced more by their RGD moiety rather than the sunitinib moiety, as a consequence of their weak propensity to enter EP cells. Interestingly, dimeric compound **3** induced a marked reduction of VEGFR2 phosphorylation, comparable to that found in EP cells exposed to sunitinib alone or to the combination of sunitinib + **15**; and this would support the notion that the biological behavior of compound **3** is heavily influenced by its sunitinib moiety, likely due to the enhanced ability to be delivered to the intracellular compartment through the double RGD moieties. Overall, the TKI activity of compound **3** is attributable to the direct interaction with the Y951 domain of VEGFR2 (as sunitinib does) supporting the evidence that **3** acts as genuine VEGFR2 antagonist.

- **Conjugates 1-3 inhibit the angiogenic process *in vitro* and *in vivo***

The ability of conjugates **1**-**3** to interfere with EP cells in organizing capillary network *in vitro* was determined. Cells were seeded on Matrigel and exposed to a medium containing VEGF-A (20 ng/mL). Cells were incubated for 6 h in the presence of conjugates **1**-**3**, unconjugated *c*(AmpRGD) **15**, sunitinib, and the combination **15**+sunitinib at 0.01, 0.1, and 1.0 μM concentrations. As shown in Figure 29A, a significant or even dramatic reduction in the number of newly formed tubules was observed when EP cells were incubated on Matrigel with the various compounds. The quantification was performed by measuring the number of loops formed by connecting capillary projections (branches) and expressed as percentage of reduction compared to untreated cells, as reported in Figure 29B.

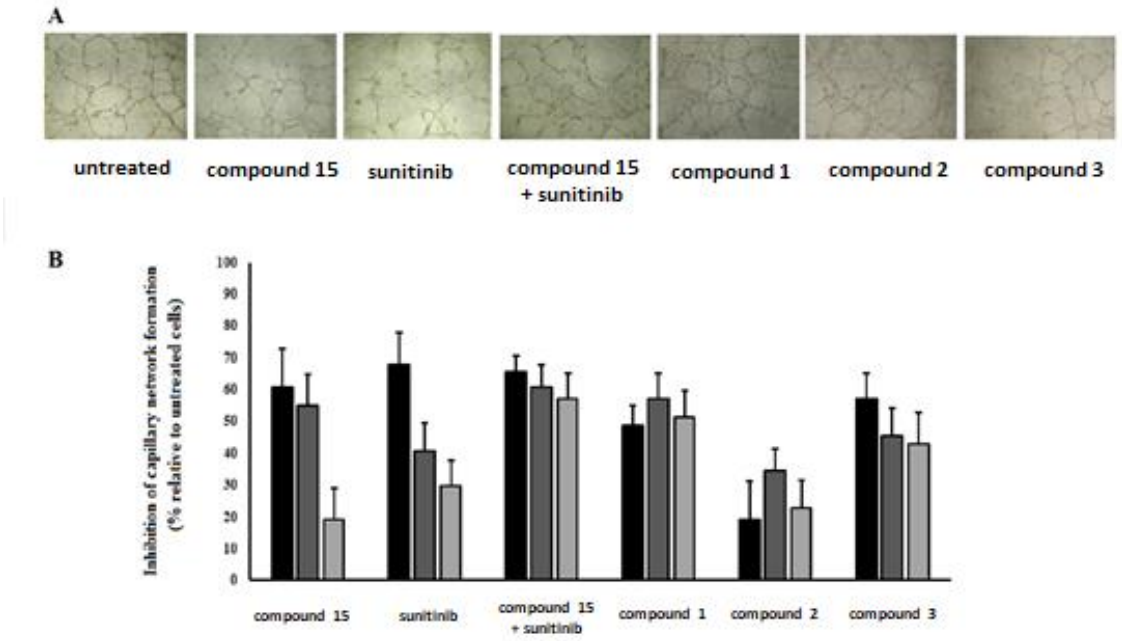

Figure 29. *In vitro* inhibition of tubulogenesis in VEGF-A activated (20 ng/mL) EPCs seeded on Matrigel and incubated for 6 h with compounds **1**-**3**, *c*(AmpRGD) **15**, sunitinib, and **15**+sunitinib at 1 μM (black), 0.1 μM (dark grey), and 0.01 μM (grey) concentrations. **A**) Representative images of the different treatments at 1 μM concentration. **B**) Histograms refer to the inhibition of branches development as compared to untreated cells and expressed as percentage. Representative of three independent experiments.

Unconjugated *c*(AmpRGD) **15** shows a good and dose-related anti-angiogenic activity which is likely due to the inhibitory interaction between the RGD moiety and the extracellular binding domain of $\alpha_V\beta_3$ integrin. Slightly superior anti-angiogenic response is witnessed with sunitinib alone, which clearly owes this behavior to its interaction with the intracellular domain of different kinases, including VEGFR2. Treating EPCs with the combination **15**+sunitinib results in a remarkable dose-dependent (slightly sloped) anti-angiogenic trend, with an exceptional 60% inhibition at 10 nM, much higher than that observed in **15** (19%) and sunitinib (30%) separately.

Passing to conjugates **1**-**3**, the inhibitory activity of angiogenesis is more pronounced for **1** and **3** than for **2**. In particular, for monomeric compound **1** and dimeric derivative **3**, the anti-angiogenesis activity is similar to that of the single **15** or sunitinib at both 1 µM and 0.1 µM concentrations, while it is highly improved (52% for **1** and 43% for **3**) at 10 nM, somehow paralleling the behavior of the combination. This demonstrates that for both the combined and conjugated ingredients, a favorable synergy could exist, given by both the extracellular RGD-integrin interaction (likely provided by the non-internalized fraction of compounds) and the sunitinib-VEGFR2 kinase interaction (provided by the amount of internalized compound, see also uptake data). Indeed, the partial internalization of the conjugates may be considered a benefit allowing the contemporary action both outside and inside cells.

Overall, the association of the two active modules either in the guise of a combination or as a covalent conjugate is beneficial to gain anti-angiogenic effect *in vitro*. Which of the two options is better has to be judged after *in vivo* anti-angiogenesis evaluation, which is able to measure the putative targeting effect within the covalent conjugates.

Next, the ability of conjugate **3** (as compared to **15**, sunitinib and their combination) to block angiogenesis *in vivo* using a Matrigel plug assay was measured. We chose compound **3** for this study as it had the strongest binding to EPCs, it was best internalized, it was the most effective in inhibiting VEGFR2 phosphorylation and capillary tube formation. Despite the very preliminary character of the data obtained, we found that *in vivo* angiogenesis is scarcely impaired by unconjugated compound **15**, while it is downregulated by sunitinib treatment (Fig. 30). This inhibition was comparable to that obtained in the co-treatment, while the injection of compound **3** revealed a consistent reduction of *in vivo* angiogenesis. These results corroborate the substantial role of conjugate **3** as an anti-angiogenic tool *in vivo* and substantiate the hypothesis according to which the covalent conjugation of two key angiogenesis-related players (as in **3**) results in a synergic action, even superior to their simple combination.

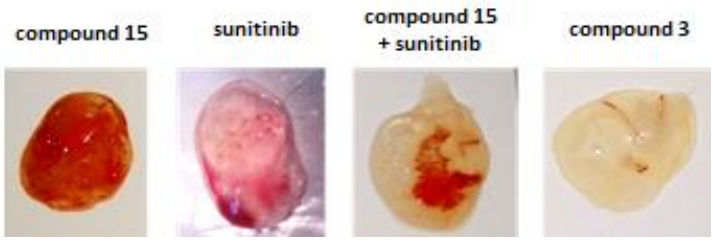

Figure 30. Inhibition of *in vivo* angiogenesis in Matrigel plugs implanted in FVB mice. Matrigel plugs contained VEGF-A/heparin+10 mg/kg sunitinib or equivalent quantity within **15** or **3** (compound **15**, sunitinib, sunitinib+**15,** compound **3**). Plugs were removed from mice and photographed after 4 days.

1*α*.4 Conclusions

Three novel molecules, compounds **1**-**3**, were efficiently synthesized and characterized, which featured the robust covalent linkage of a sunitinib-like portion to one or two cyclic aminoproline RGD moieties. Subsequent biological investigations gave important clues about the relative weight of the active modules within the conjugates. Overall, compound **3** seems to best summarize the structural characteristics required for optimal biological response, where both the RGD and the sunitinib modules may exert an active role. The preliminary, relevant anti-angiogenic effect of compound **3** in mice assesses its potential as an effective tool against tumor-associated angiogenesis and is even superior than the simple combination of the two discrete modules. This work stands as a proof-of-concept of how anti-angiogenic small molecules may be selectively delivered to cells through simple, super-targeted anti-angiogenic conjugated molecules to be used in tumor-related or angiogenesis-related therapy.

1*α*.5 Experimental Part

Experimental synthetic procedures and characterization data

General. All chemicals were of the highest commercially available quality and were used without further purification. Solvents were dried by standard procedures and reactions requiring anhydrous conditions were performed under nitrogen or argon atmosphere. H-Gly-2-ClTrt resins (loading 0.63 mmol/g and 0.58 mmol/g) were purchased from Novabiochem, (2*S*,4*S*)-Fmoc-4-amino-1-Boc-pyrrolidine-2-carboxylic acid from PolyPeptide and all other reagents from Alfa Aesar, TCI and Sigma-Aldrich. Analytical thin layer chromatography (TLC) was performed on silica gel 60 F_{254} pre-coated plates with visualization under short-wavelength UV light and by dipping the plates with molybdate reagent (aqueous H_2SO_4 solution of ceric sulphate/ammonium molybdate) followed by heating. Flash column chromatography was performed using 40-63 µm silica gel using the indicated solvent mixtures. Automated flash column chromatography was carried out with the Biotage Isolera One system using Biotage KP-Sil cartridges (direct phase) or KP-C18-HS (reverse phase). Melting points (mp) were measured with an optical Optiphot2-Pol thermo-microscope and are uncorrected. Optical rotations were measured using a Perkin-Elmer model 341 polarimeter at ambient temperature using a 100 mm cell with a 1 mL capacity and are given in units of 10^{-1} deg cm^2 g^{-1}. ESI-mass spectra were recorded on API 150EX apparatus and are reported in the form of (*m/z*). HPLC purifications were performed on a Prostar 210 apparatus (Varian, UV detection) equipped with C_{18}-10 µm columns (Discovery BIO Wide Pore 10 × 250 mm or 21.2 × 250 mm). Routine NMR spectra were recorded on Avance 300 or 400 or 600 (Bruker) NMR spectrometers. Chemical shifts (*δ*) are reported in parts per million (ppm) with TMS ($CDCl_3$), CD_2HOD, and HOD resonance peaks set at 0, 3.31, and 4.80 ppm, respectively. Multiplicities are indicated as s (singlet), d (doublet), t (triplet), q (quartet), m (multiplet), and b (broad). Coupling constants, *J*, are reported in Hertz. ^1H and ^{13}C NMR assignments are corroborated by 1D and 2D experiments (gCOSY and gHSQC sequences). High resolution mass analysis (ESI) was performed on LTQ ORBITRAP XL Thermo apparatus. Purity of all tested compounds was determined by analytical high-pressure liquid chromatography (HPLC) and was in the 96 - >99% range.

Abbreviations. Ac, acetyl; Amp, 4-amino-L-proline; Bn, benzyl; Boc, *tert*-butoxycarbonyl; Bz, benzoyl; Pmc, 2,2,5,7,8-pentamethylchroman-6-sulfonyl; Fmoc, 9-fluorenylmethoxycarbonyl; SPPS, solid phase peptide synthesis; IBX, 2-iodoxybenzoic acid; DCE, 1,2-dichloroethane; DCM, dichloromethane; DMF, *N*,*N*-dimethylformamide; DIPEA, diisopropylethylamine; TFA, trifluoroacetic acid; TFE, trifluoroethanol; HATU, *O*-(7-azabenzotriazol-1-yl)-*N*,*N*,*N*',*N*'-tetramethyluronium hexafluorophosphate; HOAt, 1-hydroxy-7-azabenzotriazole; BOP, (benzotriazol-1-yloxy)tris(dimethylamino)phosphonium hexafluorophosphate; TIS, triisopropylsilane; $NaB(OAc)_3H$, sodium triacetoxyborohydride; *p*-TsCl, *p*-toluenesulfonyl chloride; DMAP, 4-(dimethylamino)pyridine; $Cu(OAc)_2$, copper(II) acetate; Na L-Asc, (+)-sodium L-ascorbate.

Starting Materials. H-Gly-2-ClTrt resin, (2*S*,4*S*)-Fmoc-4-amino-1-Boc-pyrrolidine-2-carboxylic acid (**4**), Fmoc-Asp(*t*Bu)-OH; Fmoc-Arg (Pmc)-OH, 2,4,6-collidine, piperidine, glacial acetic acid, *N*-Boc-4-aminobutyric acid, L-propargylglycine benzyl ester 4-pentynoic acid, 5-fluoroisatin, ethyl 5-formyl-2,4-dimethylpyrrole-3-carboxylate, triethylene glycol, *N*-Boc-ethylenediamine, propargyl bromide, acetaldehyde, 2-[2-(2-aminoethoxy)ethoxy]ethanol, 3,5-dihydroxybenzoic acid were commercially available and were used as such without further purification. Sunitinib malate salt was purchased by LC Laboratories (USA) with a purity of > 99%.

2-Azidoethanol,[82] 4-azidobutanol,[84] 3-alkylidene 2-oxindole **23**,[75] alkyne-terminating polyethylene glycol **30**,[88] and 3,5-dipropynyloxy benzoic acid **32**[89] were prepared according to literature procedures.

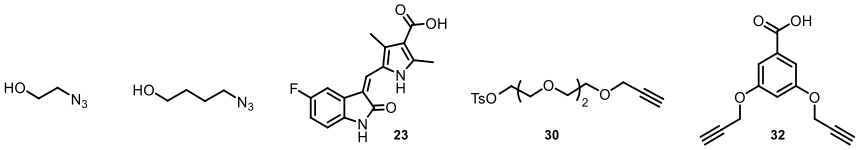

2-Azidoacetaldehyde (6)

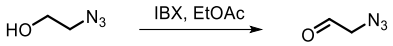

6

To a stirred solution of 2-azidoethanol (150 mg, 2.72 mmol, 1 equiv) in EtOAc (12 mL), IBX (1.45 g, 5.16 mmol, 3 equiv) was added. The heterogeneous reaction mixture was refluxed for 3 h, then it was allowed to cool to room temperature and the white solid removed by filtration. The filtrate was evaporated under reduced pressure, keeping the temperature under 45 °C, affording 2-azidoacetaldehyde **6** (111 mg, yield 74%) as a colourless oil. Spectroscopic charachterization data are in accordance to literature.

4-Azidobutanal (8)

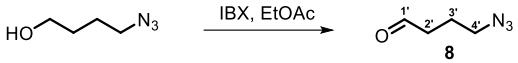

8

To a stirred solution of 4-azidobutanol (300 mg, 2.61 mmol, 1 equiv) in EtOAc (22.5 mL), IBX (2.19 g, 7.82 mmol, 3 equiv) was added. The heterogeneous reaction mixture was refluxed for 3 h, then it was allowed to cool to room temperature and the white solid removed by filtration. The filtrate was evaporated under reduced pressure, keeping the temperature under 45 °C, affording 4-azidobutanal **8** (292 mg, yield 99%) as a colourless oil.

^{1}H NMR (400 MHz, $CDCl_3$) δ 9.80 (t, J = 1.1 Hz, 1H, H1'), 3.35 (t, J = 6.8 Hz, 2H, H4'), 2.58 (td, J = 6.8, 1.1 Hz, 2H, H2'), 1.91 (quint, J = 6.8 Hz, 2H, H3'). ^{13}C NMR (100 MHz, $CDCl_3$) δ 200.9 (Cq), 50.5 (CH_2), 40.8 (CH_2), 21.4 (CH_2).

(2*S*,4*S*)-4-*N*-(9-Fluorenylmethoxycarbonyl)aminoproline (5)

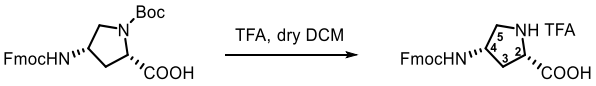

4 5

To a solution of protected aminoproline **4** (1 g, 2.21 mmol) in dry DCM (20 mL) at 0 °C, TFA (5 mL) was added dropwise. The ice bath was removed and the reaction was kept under stirring at room temperature for 1 h. The solvent was evaporated under reduced pressure and Et_2O (4 ×) was used to favour the complete removal of TFA. The N^{α}-deprotected aminoproline **5** (1.03 g, as TFA salt, quantitative yield) was obtained as a white solid; mp 172.5-173.0 °C.

^{1}H NMR (400 MHz, DMSO-d_6) δ 7.89 (d, J = 7.4 Hz, 2H, ArH), 7.67 (d, J = 7.4 Hz, 2H, ArH), 7.43 (dd, J = 7.4, 7.4 Hz, 2H, ArH), 7.33 (dd, J = 7.4, 7.4 Hz, 2H, ArH), 4.35 (m, 2H, CH_2 Fmoc), 4.23 (dd, J = 6.6, 6.6 Hz, 1H, CH Fmoc), 4.08 (m, 1H, H4), 3.85 (dd, J = 8.1, 8.1 Hz, 1H, H2), 3.28 (m, 1H, H5a), 3.02 (m, 1H, H5b), 2.42 (m, 1H, H3a), 1.86 (m, 1H, H3b). ^{13}C NMR (100 MHz, DMSO-d_6) δ 170.0 (Cq), 156.1 (Cq), 144.3 (2C, Cq), 141.2 (2C, Cq), 128.1 (2C, CH), 127.6 (2C, CH), 125.5 (2C, CH), 120.6 (2C, CH), 65.9 (CH_2), 59.4 (CH), 50.3 (CH), 49.4 (CH), 47.1 (CH_2), 34.5 (CH_2). MS (ESI$^+$) m/z = 353.2 $[M+H]^+$.

(2*S*,4*S*)-1-(2-Azidoethyl)-4-*N*-(9- fluorenylmethoxycarbonyl) aminoproline (7)

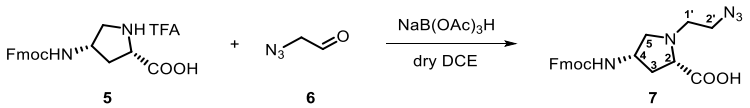

5 6 7

To a solution of N^{α} deprotected aminoproline **5** (186 mg, 0.53 mmol, 1 equiv) in dry DCE (13 mL), $NaB(OAc)_3H$ (343 mg, 1.62 mmol, 3 equiv) was added and, after 5 min, a solution of 4-azidoacetaldehyde **6** (62 mg, 0.73 mmol, 1.4 equiv) in dry DCE (2.5 mL) were added. The reaction was stirred under argon at room temperature for 5 h, quenched with a saturated aqueous $NaHCO_3$ solution and extracted with DCM (1 ×) and EtOAc (4 ×). The combined organic layers were dried, filtered and concentrated under reduced pressure giving a crude residue that was purified by SNAP cartridge flash chromatography (EtOAc/MeOH, linear gradient 95:5 to 60:40) to afford *N*-alkylated aminoproline **7** (206 mg, yield 93%) as a white-yellow solid; mp 87.7-88.0 °C.

^{1}H NMR (400 MHz, MeOD) δ 7.80 (d, *J* = 7.4 Hz, 2H, ArH), 7.64 (d, *J* = 7.4 Hz, 2H, ArH), 7.40 (dd, *J* = 7.4, 7.4 Hz, 2H, ArH), 7.32 (dd, *J* = 7.4, 7.4 Hz, 2H, ArH), 4.40 (m, 2H, CH_2 Fmoc), 4.26-4.17 (m, 2H, CH Fmoc, H4), 3.68-3.59 (m, 3H, H2, H2'a,b), 3.43 (bd, *J* = 10.6 Hz, 1H, H5a), 3.28 (m, 1H, H1'a), 3.11 (m, 1H, H5b), 2.99 (m, 1H, H1'b), 2.67 (m, 1H, H3a), 1.98 (m, 1H, H3b). ^{13}C NMR (100 MHz, MeOD) δ 174.2 (Cq), 157.0 (Cq), 144.0 (2C, Cq), 141.4 (2C, Cq), 127.6 (2C, CH), 127.0 (2C, CH), 124.9 (2C, CH), 119.8 (2C, CH), 68.9 (CH_2), 66.5 (CH), 60.3 (CH_2), 59.3 (CH_2), 54.8 (CH), 49.4 (CH_2), 47.2 (CH), 35.5 (CH_2). MS (ESI$^+$) *m/z* = 422.2 $[M+H]^+$, 444.3 $[M+Na]^+$.

(2*S*,4*S*)-1-(4-Azidobutyl)-4-*N*-(9-fluorenylmethoxycarbonyl)aminoproline (9)

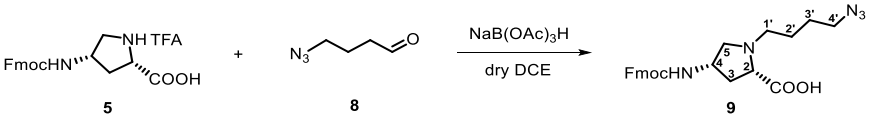

To a solution of N^{α} deprotected aminoproline **5** (498 mg, 1.07 mmol, 1 equiv) in dry DCE (38 mL), $NaB(OAc)_3H$ (634 mg, 2.99 mmol, 2.8 equiv) was added and, after 5 min, a solution of 4-azidobutanal **8** (181 mg, 1.60 mmol, 1.5 equiv) in dry DCE (4 mL) were added. The reaction was stirred under argon at room temperature for 5 h, quenched with a saturated aqueous $NaHCO_3$ solution and extracted with DCM (1 ×) and EtOAc (4 ×). The combined organic layers were dried, filtered and concentrated under reduced pressure giving a crude residue that was purified by SNAP cartridge flash chromatography (EtOAc/MeOH, linear gradient 95:5 to 60:40) to afford *N*-alkylated aminoproline **9** (441 mg, yield 95%) as a white solid; mp 87.7-88.0 °C.

^{1}H NMR (400 MHz, MeOD) δ 7.79 (bd, *J* = 7.5 Hz, 2H, ArH), 7.63 (dd, *J* = 7.4, 3.0 Hz, 2H, ArH), 7.39 (t, *J* = 7.5 Hz, 2H, ArH), 7.31 (t, *J* = 7.4 Hz, 2H, ArH), 4.39 (d, *J* = 7.1 Hz, 2H, CH_2 Fmoc), 4.30 (m, 1H, H4), 4.18 (t, *J* = 7.1 Hz, 1H, CH Fmoc), 3.85 (t, *J* = 8.2 Hz, 1H, H2), 3.62 (dd, *J* = 12.0, 3.2 Hz, 1H, H5a), 3.36 (t, *J* = 6.5 Hz, 2H, H4'), 3.34–3.24 (m, 2H, H5b + H1'a), 3.07 (m, 1H, H1'b), 2.75 (dt, *J* = 13.5, 8.3 Hz, 1H, H3a), 2.08 (dt, *J* = 13.5, 7.2 Hz, 1H, H3b), 1.77 (m, 2H, CH_2), 1.64 (quint, *J* = 7.0 Hz, 2H, CH_2). ^{13}C NMR (100 MHz, MeOD) δ 172.2 (Cq), 157.0 (Cq), 144.0 (2C, Cq), 141.4 (2C, Cq), 127.6 (2C, CH), 127.0 (2C, CH), 124.9 (2C, CH), 119.8 (2C, CH), 68.9 (CH_2), 66.6 (CH_2), 58.6 (CH), 55.1 (CH_2), 50.6 (CH), 49.4 (CH), 35.2 (CH_2), 25.8 (CH_2), 23.2 (CH_2). $[\alpha]_D^{25} = -35.0$ (*c* 1.0; MeOH). HRMS (ESI$^+$) $C_{24}H_{27}N_5O_4$ calcd for $[M+H]^+$ 450.2136, found 450.2154.

H-Asp(*t*Bu)-1-(4-azidobutyl)Amp-Arg(Pmc)-Gly-OH (11)

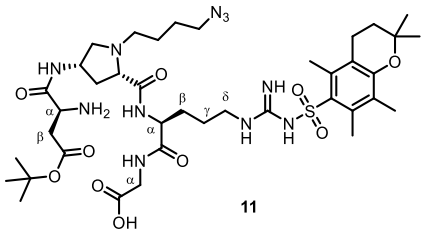

The synthesis of linear tetrapeptide H-Asp(*t*Bu)-1-(4-azidobutyl)Amp-Arg(Pmc)-Gly-OH (**11**) was performed using the preloaded 2-chlorotrityl-Gly-H resin (loading 0.63 mmol/g).

Resin swelling: the resin (530 mg, 0.33 mmol, 1 equiv) was swollen in a solid phase reaction vessel with dry DMF (5 mL) under mechanical stirring; after 40 min the solvent was drained and the resin was washed with DCM (2 ×) and DMF.

Peptide coupling: a preformed solution of Fmoc-Arg(Pmc)-OH (332 mg, 0.50 mmol, 1.5 equiv) in dry DMF (4 mL) was treated with HATU (254 mg, 0.67 mmol, 2 equiv), HOAt (1.11 mL, 0.67 mmol, 2 equiv) and 2,4,6-collidine (88 µL, 0.67 mmol, 2 equiv) and stirred for 10 min before adding to the resin. The mixture was shaken at room temperature for 5 h. Completion of the reaction was checked by the Kaiser test.[4]

[4] General procedure for Kaiser test. A few drops of *solution A* (80% phenol solution in ethanol), *solution B* (6% ninhydrin solution in ethanol) and *solution C* (98:2 – pyridine/KCN aq. 0.1 mM) were added to a small sample of the resin [pre-washed with DCM (2 x)], and then heated to 100 °C for 2 min. If resin beads maintained their yellow color, quantitative coupling was achieved. In case of blue resin beads, the coupling step was not fully completed and it was then repeated.

The solution was drained and the resin was washed several times with DMF (2 ×), *i*PrOH, (2 ×), Et_2O (2 ×), DCM (2 ×). The resin was treated with 20% v/v piperidine in DMF (5 mL) and the mixture was stirred for 30 min. The solution was drained and the resin was washed with DMF (2 ×), *i*PrOH, (3 ×), Et_2O (2 ×), DCM (2 ×). The coupling of the Fmoc-1-(4-azidobutyl)Amp-OH **9** (225 mg, 0.50 mmol, 1.5 equiv) and Fmoc-Asp(*t*Bu)-OH (206 mg, 0.50 mmol, 1.5 equiv) were carried out under the same conditions.

Resin cleavage: the resin was treated with 5 mL of the cleavage mixture DCM/TFE/glacial AcOH (3:1:1) kept under mechanical stirring for 20 min at room temperature. The solution was recovered and the resin was carefully washed with DCM (2 ×). This protocol was repeated twice. The combined solution was evaporated under reduced pressure affording linear tetrapeptide **11** (272 mg, yield 94%) as a light yellow solid, which was used in the following step without further purification. MS (ES^+) *m/z* = 878.5 $[M+H]^+$.

H-Asp(*t*Bu)-1-(2-azidoetil)Amp-Arg(Pmc)-Gly-OH (10)

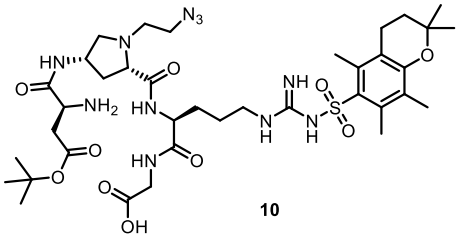

10

Compound **10** was prepared in accordance to the procedure described for compound **11**, starting from 2-chlorotrityl-Gly-H resin (loading 0.58 mmol/g, 568 mg), fournishing the linear terapeptide **10** (275 mg, yield 98%) as white solid. Compound **10** was used in the following step without further purification.
MS (ESI^+) *m/z* = 850.5 $[M+H]^+$, 872.5 $[M+Na]^+$.

***c*(AmpRGD) Azide (13)**

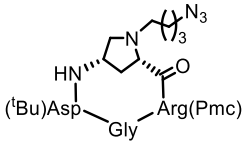

13

To a solution of linear tetrapeptide **11** (137 mg, 0.16 mmol, 1 equiv) in dry DCM (35 mL), 2,4,6-collidine (52 µL, 0.39 mmol, 2.5 equiv) was added. The mixture was stirred under argon at room temperature, and added dropwise to a solution of HATU (119 mg, 0.31 mmol, 2 equiv) and HOAt (43 mg, 0.31 mmol, 2 equiv) in dry DMF (5mL) and dry DCM (30 mL). The reaction mixture was degassed by argon/vacuum cycles (3 ×) and left to stir under argon at room temperature for 5 h. After completion, the solution was concentrated under vacuum, treated with aq $NaHCO_3$ saturated solution and extracted with EtOAc (4 ×). The combined organic layers were dried with $MgSO_4$, filtered and evaporated under reduced pressure, keeping the temperature under 50 °C. The crude was purified by reverse phase flash chromatography [H_2O (0.1% TFA)/MeCN: linear gradient 80:20 to 20:80] furnishing the protected c(AmpRGD)-N_3 **13** (90 mg, yield 67%) as a white solid; mp 118.6 °C; $[\alpha]_D^{25}$ = + 19.2 (*c* 0.5; MeOH).

^{1}H NMR (400 MHz, MeOD) δ 4.64 (dd, *J* = 6.3, 5.6 Hz, 1H, Hα Asp), 4.44 (ddd, *J* = 6.9, 6.9, 2.0 Hz, 1H, H4), 4.16 (d, *J* = 13.9 Hz, 1H, Hα Gly), 4.08 (t, *J* = 7.5 Hz, 1H, Hα Arg), 3.64 (d, *J* = 9.2 Hz, 1H, H2), 3.34 (d, *J* = 13.9 Hz, 1H, Hα Gly), 3.30 (t, *J* = 6.6 Hz, 2H, Hδ Arg), 3.27-3.13 (m, 3H, H1'a,b + H5a), 3.04 (bd, *J* = 9.6 Hz, 1H, H5b), 2.76-2.63 (m, 6H, Hβ Asp + CH_2 Pmc + H4'a,b), 2.59 (s, 3H, CH_3 Pmc), 2.57 (s, 3H, CH_3 Pmc), 2.41 (ddd, *J* = 13.6, 9.5, 7.1 Hz, 1H, H3a), 2.12 (s, 3H, CH_3 Pmc), 1.99 (d, *J* = 13.6 Hz ,1H, H3b), 1.86 (t, 2H, CH_2 Pmc), 1.74-1.69 (m, 2H, Hβ Arg), 1.65-1.62 (m, 6H, Hγ Arg + H2' + H3'), 1.46 (s, 9H, *t*Bu), 1.33 (s, 6H, CH_3 Pmc). ^{13}C NMR (75 MHz, MeOD) δ 177.3 (Cq), 175.4 (Cq), 170.6 (Cq), 170.1 (Cq), 169.8 (Cq), 156.8 (Cq), 153.5 (Cq), 138.5 (Cq), 135.3 (Cq), 134.9 (Cq), 133.5 (Cq), 123.8 (Cq), 118.2 (Cq), 81.0 (Cq), 73.7 (CH_2), 62.7 (CH_2), 60.0 (CH_2), 55.1 (CH), 52.3

(CH_2), 51.0 (CH_2), 49.8 (CH), 49.1 (CH), 44.4 (CH_2), 40.1 (CH), 37.3 (CH_2), 36.1 (CH_2), 32.6 (CH_2), 27.1 (3C, CH_3), 26.9 (CH_2), 26.5 (CH_2), 25.8 (2C, CH_3), 25.7 (CH_2), 21.2 (CH_2), 17.8 (CH_3), 16.7 (CH_3), 11.1 (CH_3). HRMS (ESI$^+$) $C_{39}H_{61}N_{11}O_9S$ calcd for $[M+H]^+$ 860.4447, found 860.4470.

***Cyclo*[Arg(Pmc)-Gly-Asp(*t*Bu)-1-(2-azidoethyl)Amp] (12)**

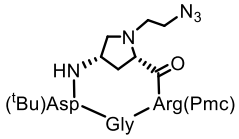

12

Compound **12** was prepared in accordance to the procedure described for compound **13**, using linear tetrapeptide **10** (30 mg, 0.03 mmol, 1 equiv), fournishing the cyclic peptide **12** (18.4 mg, yield 67%) as white solid.

^{1}H NMR (400 MHz, MeOD) δ 4.64 (dd, *J* = 5.6, 5.6 Hz, 1H, Hα Asp), 4.45 (m, 1H, H4 Amp), 4.16 (d, *J* = 13.8 Hz, 1H, Hα Gly), 4.10 (dd, *J* = 7.1, 7.1 Hz, 1H, Hα Arg), 3.75 (d, *J* = 8.8 Hz, 1H, H2 Amp), 3.46-3.30 (m, 3H, Hα Gly, H2'a,b), 3.21 (m, 2H, H1'a,b), 3.07 (bd, *J* = 8.7 Hz, 1H, H5a Amp), 2.98 (m, 3H, H5b Amp, Hδ Arg), 2.70 (m, 4H, CH_2 Pmc, Hβ Asp), 2.59 (s, 3H, CH_3 Pmc), 2.58 (s, 3H, CH_3 Pmc), 2.43 (m, 1H, H3a Amp), 2.12 (s, 3H, CH_3 Pmc), 2.02 (d, *J* = 11.4 Hz, 1H, H3b Amp), 1.86 (dd, *J* = 6.7, 6.7 Hz, 2H, CH_2 Pmc), 1.77–1.68 (m, 2H, Hβ Arg,), 1.68–1.50 (m, 2H, Hγ Arg), 1.46 (s, 9H, *t*Bu), 1.33 (s, 6H, CH_3 Pmc). MS (ESI$^+$) *m/z* = 832.6 $[M+H]^+$, 854.6 $[M+Na]^+$

***c*(AmpRGD) Amine (15)**

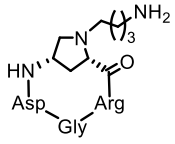

15

The cyclic tetrapeptide **13** (29 mg, 0.03 mmol) was dissolved in EtOH (4 mL) and a catalytic amount of 10% palladium on carbon was added. The reaction vessel was degassed under vacuum and thoroughly purged with hydrogen (3 ×). The resulting heterogeneous mixture was stirred overnight under hydrogen at room temperature, then the catalyst was filtered off and the filtrate was concentrated under vacuum. The protected intermediate AmpRGD-NH_2 (27 mg, 0.03 mmol) was dissolved in 1.6 mL of a TFA/TIS/H_2O (95:2.5:2.5) mixture and stirred at room temperature for 2.5 h. Then, the solvent was evaporated and the crude residue was thoroughly washed with Et_2O (4 ×) and petroleum ether (2 ×). Preparative RP-HPLC purification was performed [C_{18}-10 µm column, 21.2 × 250 mm; solvent A: H_2O (0.1% TFA) and solvent B: MeCN, flow rate 8 mL/min; detection 220 nm] using a linear gradient from 100% A to 25% B in 25 min. The removal of the solvent under vacuum, keeping the temperature under 50 °C, furnished c(AmpRGD)-NH_2 **15** (18.4 mg, TFA salt, yield 91%) as a colourless glassy solid; $[\alpha]_D^{25}$ = –13.3 (*c* 1.0, H_2O).

^{1}H NMR (400 MHz, D_2O) δ 4.60 (dd, *J* = 6.2, 6.2 Hz, 1H, Hα Asp), 4.52 (d, *J* = 10.8 Hz, 1H, H2), 4.26 (bt, *J* = 4.9 Hz, 1H, H4), 4.12 (dd, *J* = 7.5, 7.5 Hz, 1H, Hα Arg), 3.94 (d, *J* = 13.9 Hz, 1H, Hα Gly), 3.93 (m, 1H, H5a), 3.37 (bd, *J* = 8.8 Hz, 1H, H5b), 3.21 (m, 2H, H4'), 3.09 (t, *J* = 6.8 Hz, 2H, Hδ Arg), 2.90–2.81 (m, 3H, H1' + H3a), 2.80 (d, *J* = 5.9 Hz, 2H, Hβ Asp), 2.42 (bd, *J* = 15.2 Hz, 1H, H3b), 1.68–1.46 (m, 8H, Hβ Arg + Hγ Arg + H2' + H3'). ^{13}C NMR (100 MHz, D_2O) δ 176.2 (Cq), 174.5 (Cq), 172.7 (Cq), 171.2 (2C, Cq), 156.9 (Cq), 66.0 (CH), 60.2 (CH_2), 56.1 (CH), 49.9 (CH), 44.6 (CH_2), 40.6 (CH_2), 38.8 (CH_2), 35.1 (CH_2), 35.0 (CH_2), 34.9 (CH_2), 26.5 (CH_2), 24.6 (CH_2), 23.8 (CH_2), 22.3 (CH_2). HRMS (ESI$^+$) $C_{21}H_{37}N_9O_6$ calcd for $[M+H]^+$ 512.2940, found 512.2932.

***c*(AmpRGD) Amine (14)**

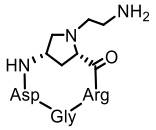

14

Compound **14** was prepared according to the procedure described for compound **15** starting from azide **12**. Colourless glassy solid. $[\alpha]_D^{25}$ = –13.3 (*c* 1.0, H_2O).

^{1}H NMR (600 MHz, D_2O) δ 4.64 (m, 1H, H2 Amp), 4.58 (dd, *J* = 6.0, 6.0 Hz, 1H, Ha Asp), 4.27 (dd, *J* = 5.4, 5.4 Hz, 1H, H4 Amp), 4.15 (dd, *J* = 7.8, 7.8 Hz, 1H, Hα Arg), 3.99 (bd, *J* = 12.0 Hz, 1H, H5 Amp), 3.92 (d, *J* = 13.8 Hz, 1H, Hα Gly), 3.57 (m, 2H, H2'Amp), 3.46 (dd, *J* = 12.6, 4.2 Hz, 1H, H5 Amp), 3.45 (d, *J* = 13.8 Hz, 1H, Hα Gly), 3.26 (ddd, *J* = 13.8, 7.2, 7.2 Hz, 1H, H1'Amp), 3.19 (ddd, *J* = 13.8, 7.2, 7.2 Hz, 1H, H1' Amp), 3.08 (dd, *J* = 6.6, 6.6 Hz, 2H, Hδ Arg), 2.88 (ddd, *J* = 15.0, 11.4, 6.0 Hz, 1H, H3 Amp), 2.79 (m, 2H, Hβ Asp), 2.47 (bd, *J*. = 15.0 Hz, 1H, H3 Amp), 1.65 (m, 2H, Hβ Arg), 1.58 (m, 1H, Hγ Arg), 1.49 (m, 1H, Hγ Arg). ^{13}C NMR (150 MHz, D_2O) δ 66.9 (CH, C2 Amp), 60.3 (CH2, C5 Amp), 56.2 (CH, Cα Arg), 51.6 (CH2, C2'Amp), 50.3 (CH, C4 Amp), 50.0 (CH, Cα Asp), 44.7 (CH2, Cα Gly), 40.6 (CH2, Cδ Arg), 35.1 (CH2, C1'Amp), 35.0 (CH2, C3 Amp), 34.9 (CH2, Cβ Asp), 26.5 (CH2, Cβ Arg), 24.7 (CH2, Cγ Arg). HRMS (ESI$^+$) $C_{19}H_{34}N_9O_6$ calcd for $[M+H]^+$ 484.2632, found 484.2619.

(*S*)-Benzyl 2-(4-(*tert*-butoxycarbonylamino)butanamido)pent-4-ynoate (17)

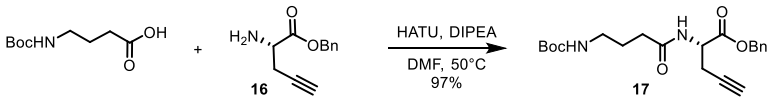

To the solution of *N*-Boc-4-aminobutyric acid (42 mg, 0.21 mmol, 1 equiv) and **16** (63 mg, 0.31 mmol, 1.5 equiv) in DMF (0.6 mL), HATU (157 mg, 0.41 mmol, 2 equiv) and DIPEA (180 µL, 1.03 mmol, 5 equiv) were added and the reaction mixture was stirred at 50 °C for 3.5 h. H_2O (10 mL) was then added to the reaction and the aqueous phase was extracted with EtOAc (3 ×). The organic layers were collected and evaporated under reduced pressure. The crude was purified by silica gel flash chromatography (hexanes/EtOAc from 60:40 to 50:50) to obtain compound **17** (78 mg, 97% yield) as a pale yellow solid.

^{1}H NMR (300 MHz, $CDCl_3$) δ 7.37 (m, 5H, ArH), 6.71 (bd, *J* = 7.6 Hz, 1H, NH), 5.25 (d, *J* = 12.2 Hz, 1H, CHaPh), 5.20 (d, *J* = 12.2 Hz, 1H, CHbPh), 4.80 (dt, *J* = 7.9, 4.9 Hz, 1H, CHN), 4.74 (bs, 1H, NH), 3.19 (m, 2H, CH_2N), 2.80 (dd, *J* = 5.0, 2.8 Hz, 2H, $CH_2C\equiv$), 2.32 (t, *J* = 7.0 Hz, 2H, CH_2CO), 2.02 (t, *J* = 2.8 Hz, 1H, ≡CH), 1.83 (quint, *J* = 7.0 Hz, CH_2), 1.46 (s, 9H, *t*Bu). ^{13}C NMR (100 MHz, $CDCl_3$) δ 174.5 (Cq), 170.5 (Cq), 135.9 (Cq), 128.4 (2C, CH), 128.2 (CH), 128.1 (2C, CH), 78.8 (2C, Cq), 71.3 (CH), 67.0 (CH_2), 51.7 (CH), 39.5 (CH_2), 32.7 (CH_2), 27.6 (CH_3), 26.1 (CH_2), 21.0 (CH_2).

Compound 18

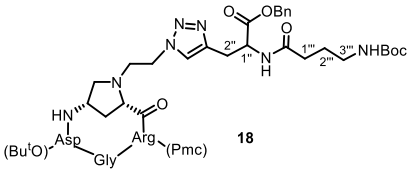

A stirred solution of **12** (6.7 mg, 0.0081 mmol, 1 equiv) and **17** (4.7 mg, 0.012 mmol, 1.5 equiv) in H_2O/*t*BuOH 1:1 (800 µL) was degassed by argon/vacuum cycles (3 ×). To this solution, a freshly prepared aqueous mixture (50 µL) of $Cu(OAc)_2$ (0.48 mg, 0.0024 mmol, 0.3 equiv) and sodium ascorbate (0.96 mg, 0.0048 mmol, 0.6 equiv) was added, previously degassed by argon/vacuum cycles (3 ×). The reaction mixture was degassed again and left to stir at room temperature, protected from light, under argon for 3 h. The solvent was evaporated under reduced pressure, MeOH was added (2 mL) and the solution filtered to remove the copper salts. The methanol was evaporated and the crude purified by silica gel flash chromatography (EtOAc/MeOH from 95:5 to 90:10) to give compound **18** (6.2 mg, 63%) as an orange resin. $[\alpha]_D^{25}$ = + 14.4 (*c* 1.0; MeOH).

^{1}H NMR (400 MHz, MeOD) δ 7.82 (s, 1H, =CH), 7.34 (m, 5H, ArH), 5.18 (d, *J* = 12.2 Hz, 1H, CHaPh), 5.12 (d, *J* = 12.2 Hz, 1H, CHbPh), 4.79 (dd, *J* = 8.2, 5.8 Hz, 1H, H1''), 4.64 (dd, *J* = 5.8, 5.8 Hz, 1H, Hα Asp), 4.42 (ddd, *J* = 6.5, 6.5, 1.6 Hz, 1H, H4 Amp), 4.39 (t, *J* = 5.8 Hz, 2H, H2'), 4.15 (d, *J* = 14.3 Hz, 1H, Hα Gly), 4.05 (t, *J* = 7.5 Hz, 1H, Hα Arg), 3.48 (d, *J* = 9.3 Hz, 1H, H2 Amp), 3.34 (d, *J* = 14.3 Hz, 1H, Hα Gly), 3.29–3.11 (m, 7H, H2' + H1' + H5a Amp+ Hδ Arg), 3.02 (m, 2H, H3'''), 2.92 (bd, *J* = 9.6 Hz, 1H, H5b Amp), 2.72–2.66 (m, 4H, Hβ Asp + CH_2 Pmc), 2.58 (s, 3H, CH_3 Pmc), 2.57 (s, 3H, CH_3 Pmc), 2.34 (ddd, *J* = 13.8, 9.0, 7.2 Hz, 1H, H3a Amp), 2.24 (t, *J* = 7.4 Hz, 2H, H1'''), 2.11 (s, 3H, CH_3 Pmc), 1.98 (d, *J* = 13.8 Hz, 1H, H3b Amp), 1.85 (t, *J* = 7.0 Hz, 2H, CH_2 Pmc), 1.74–1.50 (m, 6H, H2''' + Hβ + Hγ Arg), 1.46 (s, 9H, *t*Bu), 1.44 (s, 9H, *t*Bu), 1.32 (s, 6H, CH_3 Pmc). MS (ESi$^+$) *m/z* = 1220.7 $[M+H]^+$, 1242.7 $[M+Na]^+$

Compound 19

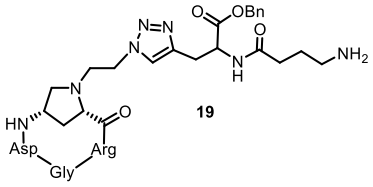

19

Compund **18** (7.8 mg, 0.0064 mmol) was dissolved in a solution of TFA/TIS/H_2O (95:2.5:2.5, 320 µL) and the reaction mixture was stirred at room temperature for 3 h. The solvent was evaporated under reduced pressure and the crude was washed with Et_2O and DCM to give compound **19** as pale yellow glassy solid (5.1 mg, quantitative yield). $[\alpha]_D^{25}$= – 7.9 (*c* 0.5; MeOH).

^{1}H NMR (400 MHz, D_2O/MeOD 90:10) δ 7.56 (s, 1H, =CH), 7.30 (m, 3H, ArH), 7.22 (m, 2H, ArH), 5.09 (d, *J* = 12.1 Hz, 1H, CHaPh), 5.01 (d, *J* = 12.1 Hz, 1H, CHbPh), 4.63–4.57 (m, 2H, H1'' + Hα Asp), 4.53 (bt, *J* = 4.9 Hz, 2H, H1'), 4.26 (bt, *J* = 4.9 Hz, 1H, H4 Amp), 4.20 (bd, *J* = 10.2 Hz, 1H, H2 Amp), 4.05 (t, *J* = 6.7 Hz, 1H, Hα Arg), 3.95 (d, *J* = 13.9 Hz, 1H, Hαa Gly), 3.79 (bd, *J* = 11.9 Hz, 1H, H5a Amp), 3.69 (bt, *J* = 4.9 Hz, 2H, H2'), 3.43 (d, *J* = 13.9 Hz, 1H, Hαb Gly), 3.38 (m, 1H, H5b Amp), 3.15–3.07 (m, 4H, H2'' + Hδ Arg), 2.83 (t, *J* = 7.4 Hz, 2H, H3'''), 2.75 (d, *J* = 5.5 Hz, 2H, Hβ Asp), 2.79–2.70 (m, 1H, H3a Amp), 2.32 (d, *J* = 15.0 Hz, 1H, H3b Amp), 2.27 (t, *J* = 7.3 Hz, 2H, H1'''), 1.77 (quint, *J* = 7.4 Hz, 2H, H2'''), 1.68–1.46 (m, 4H, Hβ e Hγ Arg). MS (ESI$^+$) *m/z* = 798.5 $[M+H]^+$

Fluorescein-c(AmpRGD) Conjugate 20

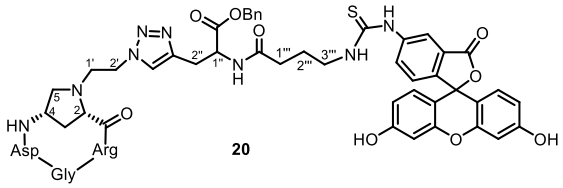

20

To a solution of compound **19** (5.1 mg, 0.0064 mmol, 1 equiv) in MeOH (0.6 mL) cooled at 0 °C, fluorescein isothiocyanate (2.5 mg, 0.0064 mmol, 1 equiv) and Et_3N (2.7 µL, 0.019 mmol, 3 equiv) were added. The reaction was stirred at room temperature for 24 h protected from light. The solvent was then evaporated and the crude was precipitated by the addition of Et_2O. The solid was washed with a mixture Et_2O:MeOH (80:20) and then purified by semipreparative RP-HPLC (C_{18}-10 µm 250 × 10 mm; solvent A: H_2O (0.1% TFA) and solvent B: MeCN, flow rate 3.0 mL/min) using the following gradient elution: 0-1 min 5% B, 1-24 min 5-35% B, 24-30 min 35% B; affording compound **20** (1.8 mg, 35% yield) as orange solid. $[\alpha]_D^{25}$ = – 18.7 (*c* 0.2; MeOH).

^{1}H NMR (400 MHz, MeOD) δ 8.24 (d, *J* = 1.8 Hz, 1H, ArH), 7.77 (s, 1H, =CH), 7.72 (m, 1H, ArH), 7.37 (m, 5H, ArH), 7.21 (d, *J* = 8.0 Hz, 1H, ArH), 6.76 (m, 4H, ArH), 6.61 (bd, *J* = 9.0 Hz, 2H, ArH), 5.22 (d, *J* = 12.2 Hz, 1H, CHaPh), 5.19 (d, *J* = 12.2 Hz, 1H, CHbPh), 4.81 (dd, *J* = 8.7, 4.7 Hz, 1H, H1''), 4.72 (m, 3H, H1' + Hα Asp), 4.33

(bt, *J* = 5.2 Hz, 1H, H4 Amp), 4.23 (m, 2H, H2 + Hα Arg), 4.09 (d, *J* = 13.6 Hz, 1H, Hαa Gly), 3.97 (bd, *J* = 11.0 Hz, 1H, H5a Amp), 3.91–3.81 (m, 2H, H2'), 3.60 (bm, 2H, H3'''), 3.50 (m, 1H, H5b Amp), 3.40 (d, *J* = 13.6 Hz, 1H, Hαb Gly), 3.23 (m, 3H, H2''a + Hδ Arg), 3.14 (dd, *J* = 15.0, 8.9 Hz, 1H, H2''b), 2.85–2.81 (m, 1H, H3a Amp), 2.83 (d, *J* = 5.7 Hz, 2H, Hβ Asp), 2.56 (d, *J* = 14.6 Hz, 1H, H3b Amp), 2.36 (t, *J* = 6.8 Hz, 2H, H1'''), 1.93 (m, 2H, H2'''), 1.82–1.65 (m, 4H, Hβ + Hγ Arg). MS (ESI$^+$) *m/z* = 798.5 $[M+H]^+$.

***N*-(2-Aminoethyl)-4-pentynamide (24)**

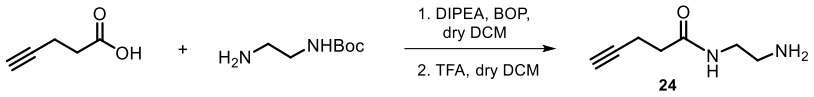

To a solution of 4-pentynoic acid (150 mg, 1.53 mmol, 1 equiv) in dry DCM (15 mL), BOP (879 mg, 1.99 mmol, 1.3 equiv) and DIPEA (1.07 ml, 6.12 mmol, 4 equiv) were added and, after 5 min, a solution of *N*-Boc-ethylenediamine (312 µL, 1.99 mmol, 1.3 equiv) in dry DCM (5 ml) was added. The reaction was stirred for 5 h under nitrogen at room temperature and after completion the solvent was evaporated under reduced pressure. The residue was redissolved in EtOAc and this solution was subsequently washed with a saturated aqueous NH_4Cl solution (2 ×), a saturated aqueous $NaHCO_3$ solution (2 ×) and H_2O (2 ×). The organic layer was collected, dried with $MgSO_4$, filtered and concentrated to afford a crude residue which was purified by flash chromatography (EtOAc/MeOH, 14.5:0.5) furnishing the *N*-Boc intermediate (334 mg, 91% yield) as white solid. This intermediate was dissolved in dry DCM (2 ml) and TFA (1 ml) was added dropwise. After 1 h at room temperature, the reaction mixture was concentrated under reduced pressure and the crude residue was treated with Et_2O (4 ×) in order to remove the excess TFA, giving the product **24** (195 mg, TFA salt, quantitative yield) as a colourless oil.

^{1}H NMR (400 MHz, MeOD) (mixture of rotamers, major isomer) *δ* 3.48 (bt, *J* = 5.6 Hz, 2H, CH_2), 3.07 (bt, *J* = 5.6 Hz, 2H, CH_2), 2.52–2.42 (m, 4H, CH_2), 2.30 (t, *J* = 2.3 Hz, 1H, ≡CH). ^{13}C NMR (75 MHz, MeOD) *δ* 173.9 (Cq), 82.0 (Cq), 68.9 (CH), 39.4 (CH_2), 36.8 (CH_2), 34.3 (CH_2), 14.0 (CH_2). MS (ESI$^+$) *m/z* = 141.1 $[M+H]^+$.

***N*^{1}-*tert*-Butoxycarbonyl-*N*^{2}-ethylethane-1,2-diamine (27)**

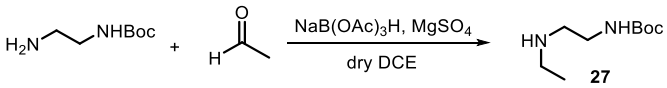

To a stirred solution of *N*-Boc-ethylenediamine (197µL, 1.25 mmol, 1 equiv) in 1,2-DCE (4 mL), a catalytic amount of anhydrous $MgSO_4$ (15 mg, 0.125 mmol) and acetaldehyde (105 µL, 1.87 mmol, 1.5 equiv) were added and, after 1 h, $NaB(OAc)_3H$ (529 mg, 2.50 mmol, 2 equiv) was added. The reaction was stirred overnight under argon at room temperature and then quenched by the addition of water (10 mL) and extracted with DCM (3 ×). The aqueous layer was treated with a saturated $NaHCO_3$ solution and re-extracted with DCM (3 ×). These latter organic layers were collected, dried with $MgSO_4$, filtered and concentrated under reduced pressure. The crude residue was purified by silica gel flash chromatography [EtOAc/MeOH(NH_3), gradient elution 95:5 to 90:10] affording product **27** (127 mg, 54% yield) as a pale yellow solid.

^{1}H NMR ($CDCl_3$, 300 MHz) *δ* 5.16 (bs, 1H, NH), 3.19 (q, *J* = 5.9 Hz, 2H, $CONHCH_2$), 2.70 (t, *J* = 5.9 Hz, 2H, $CONHCH_2CH_2$), 2.63 (q, *J* = 7.3 Hz, 2H, $NHCH_2CH_3$), 1.41 (s, 9H), 1.07 (t, *J* = 7.0 Hz, 3H, $NHCH_2CH_3$).
^{13}C NMR ($CDCl_3$, 75 MHz) *δ* 156.2 (Cq), 79.2 (Cq), 49.3 (CH_2), 44.1 (CH_2), 40.7 (CH_2), 28.7 (3C, CH_3), 15.7 (CH_3).

***N*^{1}-*tert*-Butoxycarbonyl-*N*^{2}-ethyl-*N*^{2}-{2-[2-(2-(prop-2-ynyloxy)ethoxy)ethoxy]ethyl}ethane-1,2-diamine (31)**

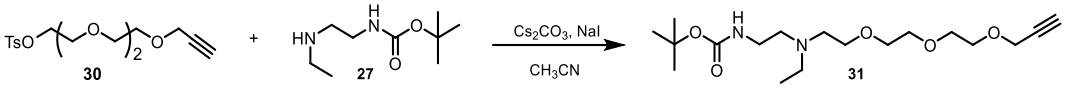

To a stirred solution of **30** (20 mg, 0.11 mmol, 1 equiv) and **27** (40 mg, 0.12 mmol, 1.1 equiv) in dry MeCN, Cs_2CO_3 (35 mg, 1 equiv) and NaI (3.3 mg, 0.2 equiv) were added. The reaction was left to stir under argon at room temperature for 2 days and at 60 ° C for one further day. After evaporation of the solvent, the crude was purified by silica gel flash chromatography [elution gradient from EtOAc/petroleum ether 80:20 to EtOAc/MeOH(NH_3) 95:5] to afford compound **31** (17.8 mg, 47% yield) as a colourless oil.

^{1}H NMR (400 MHz, $CDCl_3$) δ 4.21 (d, *J* = 2.3 Hz, 2H, -OC*H*$_2$C≡CH), 3.73–3.57 (bm, 10H, -OC*H*$_2$), 3.25–3.18 (m, 2H, -CONHC*H*$_2$), 2.78–2.71 (m, 2H, -NC*H*$_2$), 2.71–2.62 (m, 4H, -NC*H*$_2$), 2.44 (t, *J* = 2.4 Hz, 1H, ≡CH), 1.45 (s, 9H, Boc), 1.07 (t, *J* = 7.1 Hz, 3H, CH_3). ^{13}C NMR (100 MHz, $CDCl_3$) δ 156.3 (Cq), 79.8 (Cq), 79.3 (Cq), 74.8 (CH), 70.7 (CH_2), 70.5 (2C, CH_2), 69.3 (CH_2), 68.7 (CH_2), 58.5 (CH_2), 53.2 (CH_2), 53.0 (CH_2), 49.0 (CH_2), 37.9 (CH_2), 28.6 (3C, CH_3), 11.0 (CH_3). HRMS (ES$^+$) $C_{18}H_{34}N_2O_5$ calcd for $[M+H]^+$ 359.2540, found 359.2547.

***N*^{1}-ethyl-*N*^{1}-{2-[2-(2-(prop-2-yn-1-yloxy)ethoxy)ethoxy]ethyl}ethane-1,2-diamine (25)**

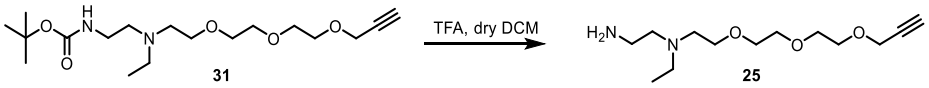

TFA (400 µL) was added to a solution of **31** (29 mg, 0.08 mmol) in dry DCM (800 µL) and the reaction mixture was left to stir at room temperature for 30 min. The solvent and the acid were evaporated under vacuum, and the crude was treated with Et_2O (4 ×), affording **25** (27 mg, TFA salt, yield 89%) as pale yellow oil.

^{1}H NMR (400 MHz, $CDCl_3$) δ 4.19 (m, 2H, -OC*H*$_2$C≡CH), 3.90 (m, 2H, -OC*H*$_2$CH$_2$N), 3.77–3.56 (m, 12H, -OC*H*$_2$, -C*H*$_2$NH$_2$), 3.46 (m, 2H, -NCH$_2$), 3.35 (bq, *J* = 7.0 Hz, 2H, -NC*H*$_2$CH$_3$), 2.55 (m, 1H, ≡CH), 1.39 (t, *J* = 7.0 Hz, 3H, CH_3). ^{13}C NMR (100 MHz, $CDCl_3$) δ 78.9 (Cq), 75.7 (CH), 70.1 (CH_2), 69.9 (CH_2), 69.8 (CH_2), 69.0 (CH_2), 65.2 (CH_2), 58.5 (CH_2), 53.1 (CH_2), 52.3 (CH_2), 52.1 (CH_2), 36.6 (CH_2), 8.9 (CH_3). HRMS (ESI$^+$) $C_{13}H_{26}N_2O_3$ calcd for $[M+H]^+$ 259.2016, found 259.2032.

***N*-{2-[2-(2-Hydroxyethoxy)ethoxy]ethyl}-3,5-bis(prop-2-yn-1-yloxy)benzamide (34)**

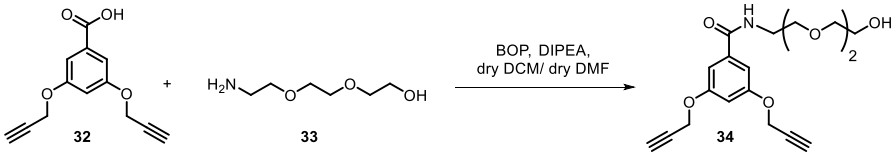

To a stirred solution of 3,5-bis(prop-2-yn-1-yloxy)benzoic acid **32** (80 mg, 0.35 mmol, 1 equiv) in dry DMF (0.7 mL) and dry DCM (0.3 mL), BOP (200 mg, 0.45 mmol, 1.3 equiv) and DIPEA (121 µL, 0.69 mmol, 2 equiv) were added and, after 5 min, triglycolamine **33** (53 µL, 0.38 mmol, 1.1 equiv) was added. The reaction was stirred under argon for 6 h at room temperature; then the solvent was evaporated under reduced pressure. The residue was redissolved in EtOAc (4 mL) and the organic phase was extracted with saturated aqueous NH_4Cl solution (2 ×), saturated aqueous $NaHCO_3$ solution (2 ×) and H_2O (2 ×). The organic layer was collected, dried with $MgSO_4$, filtered and concentrated. The crude residue was purified by silica gel flash chromatography (EtOAc/MeOH, gradient elution from 100% EtOAc to 95:5), giving **34** (100 mg, yield 80%) as pale yellow oil.

^{1}H NMR (300 MHz, $CDCl_3$) δ 7.07 (d, ^4J = 2.2 Hz, 2H, ArH), 6.73 (t, ^4J = 2.2 Hz, 1H, ArH), 4.71 (d, ^4J = 2.4 Hz, 4H, ArOC*H*$_2$), 3.75–3.58 (bm, 12H, -OC*H*$_2$, -CONHC*H*$_2$), 2.57 (t, ^4J = 2.4 Hz, 2H, ≡CH). ^{13}C NMR (75 MHz, $CDCl_3$) δ 166.9 (Cq), 158.6 (2C, Cq), 136.8 (Cq), 106.8 (2C, CH), 105.3 (CH), 78.1 (2C, Cq), 76.0 (2C, CH), 72.5 (CH_2), 70.3

(2C, CH_2), 69.9 (CH_2), 61.6 (CH_2), 56.1 (2C, CH_2), 39.8 (CH_2). HRMS (ESI$^+$) $C_{19}H_{23}NO_6$ calcd for $[M+H]^+$ 362.1598, found 362.1613.

2-(2-{2-[3,5-Bis(prop-2-ynyloxy)benzamido]ethoxy}ethoxy)ethyl-4-methylbenzenesulfonate (35)

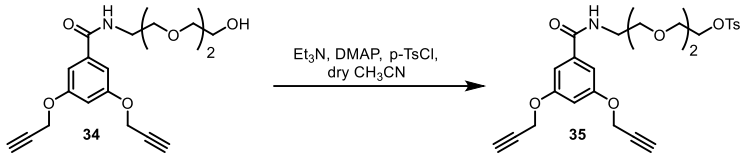

To a stirred solution of **34** (27 mg, 0.07 mmol, 1 equiv) and Et_3N (21 µL, 0.15 mmol, 2 equiv) in dry MeCN (400 µL), at 0 °C under argon atmosphere, DMAP (1.8 mg, 0.01 mmol, 0.2 equiv) and *p*-TsCl (29 mg, 0.15 mmol, 2 equiv) were added. The reaction was left to stir at 0 °C for 10 min and at 45 °C for 3 days, then it was treated with water (2 mL) and extracted with EtOAc (3 ×). The organic layers were collected and concentrated to give a crude residue which was purified by silica gel flash chromatography (EtOAc/hexane, 80:20) furnishing compound **35** (22 mg, yield 57%) as a colourless glassy solid.

^{1}H NMR (300 MHz, $CDCl_3$) δ 7.79 (d, J = 8.4 Hz, 2H, Ts), 7.34 (d, J = 8.0 Hz, 2H, Ts), 7.03 (d, ^4J = 2.3 Hz, 2H, ArH), 6.75 (t, J = 2.3 Hz, 1H, ArH), 4.72 (d, ^4J = 2.4 Hz, 4H, ArOCH_2), 4.20–4.16 (m, 2H, -CH_2OTs), 3.75–3.69 (m, 2H, -OCH_2CH$_2$OTs), 3.69–3.59 (m, 8H, -OCH$_2$, -CONHCH_2), 2.56 (t, ^4J = 2.4 Hz, 2H, ≡CH), 2.45 (s, 3H, CH_3).
^{13}C NMR (75 MHz, $CDCl_3$) δ 166.8 (Cq), 158.7 (2C, Cq), 144.9 (Cq), 137.0 (Cq), 133.0 (Cq), 129.8 (2C, CH), 127.9 (2C, CH), 106.8 (2C, CH), 105.2 (CH), 78.0 (2C, Cq), 76.0 (2C, CH), 70.8 (CH_2), 70.3 (CH_2), 69.8 (CH_2), 69.2 (CH_2), 68.8 (CH_2), 56.1 (2C, CH_2), 39.8 (CH_2), 21.6 (CH_3). HRMS (ESI$^+$) $C_{26}H_{29}NO_8S$ calcd for $[M+H]^+$ 516.1687, found 516.1679.

***N*-{2-[2-(2-{[2-(*tert*-Butoxycarbonylamino)ethyl](ethyl)amino}ethoxy)ethoxy]ethyl}-3,5-bis(prop-2-ynyloxy)benzamide (37)**

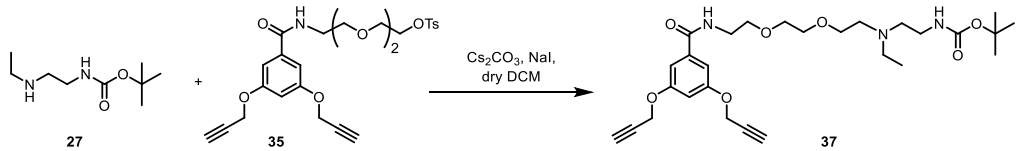

To a stirred solution of **35** (36 mg, 0.07 mmol, 1 equiv) and **27** (24 mg, 0.13 mmol, 1.8 equiv) in dry MeCN (400 µL) at room temperature, Cs_2CO_3 (45 mg, 0.14 mmol, 2 equiv) and NaI (2.1 mg, 20 mol %) were added. The reaction was left to stir at 50 °C under argon for 3 days. The solvent was evaporated, the residue was dissolved in EtOAc (3 mL) and this solution was washed with saturated aqueous NH_4Cl solution (2 ×) and with saturated aqueous $NaHCO_3$ solution (2 ×). The organic layer was collected and concentrated under vacuum, affording a crude residue which was purified by silica gel flash chromatography [gradient elution from EtOAc/hexane 80:20 to EtOAc/MeOH(NH_3) 90:10] to give **37** (7.8 mg, yield 21%) as a pale yellow oil.

^{1}H NMR (400 MHz, MeOD) δ 7.11 (d, ^4J = 2.3 Hz, 2H, ArH), 6.82 (t, ^4J = 2.3 Hz, 1H, ArH), 4.79 (d, ^4J = 2.4 Hz, 4H, ArOCH_2), 3.70–3.63 (m, 6H, -OCH$_2$), 3.61–3.56 (m, 4H, -OCH$_2$, -CONHCH_2), 3.13 (t, J = 6.8 Hz, 2H, -CH_2NHBoc), 3.00 (t, ^4J = 2.4 Hz, 2H, ≡CH), 2.68 (t, J = 5.8 Hz, 2H, -OCH$_2$CH_2N-), 2.60 (q, J = 7.1 Hz, 2H, -NCH_2CH$_3$), 2.59 (t, J = 6.8 Hz, 2H, -NCH$_2$), 1.45 (s, 9H, Boc), 1.04 (t, J = 7.1 Hz, 3H, CH_3). ^{13}C NMR (100 MHz, MeOD) δ 168.2 (Cq), 158.9 (2C, Cq),157.0 (Cq), 136.3 (Cq), 106.7 (2C, CH), 104.9 (CH), 78.6 (Cq), 78.0 (2C, Cq), 75.8 (2C, CH), 70.0 (2C, CH_2), 69.1 (CH_2), 69.0 (CH_2), 55.6 (2C, CH_2), 52.8 (CH_2), 52.6 (CH_2), 48.2 (CH_2), 39.6 (CH_2), 37.7 (CH_2), 27.4 (3C, CH_3), 10.5 (CH_3). HRMS (ESI$^+$) $C_{28}H_{41}N_3O_7$ calcd for $[M+H]^+$ 532.3017, found 532.3011.

***N*-[2-(2-{2-[(2-aminoethyl)(ethyl)amino]ethoxy}ethoxy)ethyl]-3,5-bis(prop-2-ynyloxy) benzamide (26)**

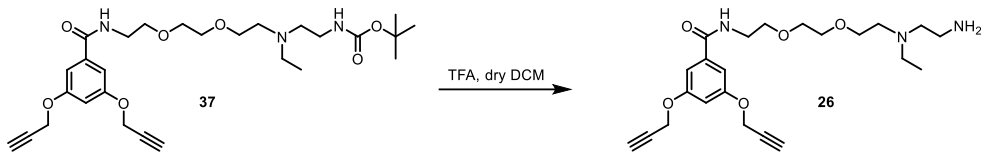

To a solution of **37** (12.9 mg, 0.02 mmol) in dry DCM (250 µL), TFA (100 µL) was added. The mixture was left to stir for 30 min at room temperature, and then concentrated to afford a crude residue. Et_2O (4 ×) was added and evaporated in order to completely remove the excess of TFA. Compound **26** (11.7 mg, yield 91%) was obtained as TFA salt, as a pale brown oil.

^{1}H NMR (300 MHz, MeOD) δ 7.10 (d, ^4J = 2.3 Hz, 2H, ArH), 6.85 (t, ^4J = 2.3 Hz, 1H, ArH), 4.80 (d, ^4J = 2.4 Hz, 4H, ArOCH_2), 3.83 (t, J = 5.0 Hz, 2H, -OCH_2CH$_2$N), 3.72–3.66 (m, 6H, -OCH$_2$), 3.61–3.56 (m, 2H, -CONHCH_2), 3.52–3.49 (m, 2H, -CH_2NH$_2$), 3.45–3.40 (m, 4H, -NCH$_2$, -OCH$_2$CH_2N), 3.31–3.28 (m, 2H, -NCH_2CH$_3$), 3.02 (t, ^4J = 2.3 Hz, 2H, ≡CH), 1.03 (t, J = 7.1 Hz, 3H, CH$_3$). ^{13}C NMR (75 MHz, MeOD) δ 168.6 (Cq), 159.1 (2C, Cq), 136.4 (Cq), 106.9 (2C, CH), 105.0 (CH), 78.1 (2C, Cq), 76.0 (2C, CH), 70.2 (CH$_2$), 70.0 (CH$_2$), 69.5 (CH$_2$), 65.1 (CH$_2$), 55.7 (2C, CH$_2$), 52.6 (CH$_2$), 49.9 (CH$_2$), 49.6 (CH$_2$), 39.6 (CH$_2$), 34.5 (CH$_2$), 8.3 (CH$_3$). HRMS (ESI$^+$) $C_{23}H_{33}N_3O_5$ calcd for $[M+H]^+$ 432.2493, found 432.2497.

Compound 38

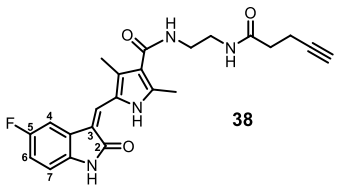

To a solution of **23** (94 mg, 0.31 mmol, 1 equiv) in dry DCM (1.5 mL) and dry DMF (2.5 mL), BOP (70 mg, 0.16 mmol, 1.3 equiv) and DIPEA (85 µL, 0.49 mmol, 4 equiv) were added and, after 5 min, a solution of **24** (103 mg, 0.41 mmol, 1.3 equiv) in dry DCM (1.5 mL) and dry DMF (1 mL) was added. The reaction was stirred under argon at room temperature, protected from light. A yellow precipitate started to form after 1 h. After 5 h the reaction was over and Et_2O (3 mL) and petroleum ether (3 mL) were added to the mixture. The solid was collected by vacuum filtration and washed with H_2O (3 ×) furnishing compound **38** (116 mg, yield 88%) as an orange solid; mp> 220 °C.

^{1}H NMR (400 MHz, DMSO-d$_6$) δ 13.69 (s, 1H, NH), 10.89 (s, 1H, NH), 8.02 (bt, J = 4.5 Hz, 1H, NH), 7.76 (dd, J = 9.5, 2.0 Hz, 1H, H4), 7.72 (s, 1H, H1'), 7.60 (bt, J = 5.0 Hz, 1H, NH), 6.92 (ddd, J = 8.8, 8.8, 2.0 Hz, 1H, H6), 6.85 (dd, J = 9.2, 4.4 Hz, 1H, H7), 3.28 (m, 2H, CH$_2$), 3.24 (m, 2H, CH$_2$), 2.76 (t, J = 2.4 Hz, ≡CH), 2.44 (s, 3H, CH$_3$), 2.42 (s, 3H, CH$_3$), 2.37 (m, 2H, CH$_2$), 2.29 (t, J = 7.1 Hz, 2H, CH$_2$). ^{13}C NMR (100 MHz, DMSO-d$_6$) δ 171.1 (Cq), 170.0 (Cq), 165.4 (Cq), 158.6 (d, $^1J_{CF}$ = 233 Hz, Cq), 137.1 (Cq), 135.0 (Cq), 130.8 (Cq), 127.6 (d, $^3J_{CF}$ = 10 Hz, Cq), 126.3 (CH), 125.3 (Cq), 121.0 (Cq), 115.1 (Cq), 112.8 (d, $^2J_{CF}$ = 25 Hz, CH), 110.4 (d, $^3J_{CF}$ = 8 Hz, CH), 106.3 (d, $^2J_{CF}$ = 26 Hz, CH), 84.2 (Cq), 71.7 (CH), 46.6 (CH$_2$), 34.8 (CH$_2$), 19.3 (CH$_2$), 14.7 (CH$_2$), 13.8 (CH$_3$), 11.0 (CH$_3$). HRMS (ES$^+$) $C_{23}H_{23}FN_4O_3$ calcd for $[M+H]^+$ 423,1827, found 423,1823.

Compound 39

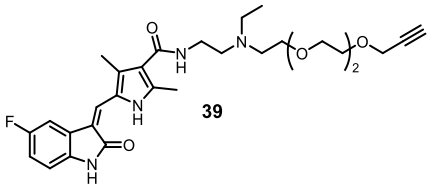

To a stirred suspension of **23** (11 mg, 0.04 mmol, 1 equiv) in dry DMF (500 µL), BOP (21 mg, 0.05 mmol, 1.3 equiv) and DIPEA (26 µL, 0.15 mmol, 4 equiv) were added and, after 5 min, a solution of **25** (15 mg, 0.04 mmol, 1.1 equiv) in dry DCM (400 µL) was added. The reaction mixture was stirred under argon at room temperature for 3 h protected from light. After reaction completion, the solvent was evaporated under reduced pressure, the residue was washed with water (3 ×), and the solvent was removed by a Pasteur pipette. The yellow-orange crude was purified by silica gel flash chromatography [gradient elution from 100% EtOAc to 90:10 EtOAc/MeOH(NH_3)] affording **39** (12.7 mg, yield 64%) as a yellow-orange glassy solid.

^{1}H NMR (400 MHz, MeOD) δ 7.58 (s, 1H, =CH), 7.45-7.39 (m, 1H, ArH), 6.90–6.83 (m, 2H, ArH), 4.14 (d, ^4J = 2.4 Hz, 2H, -OCH_2C≡CH), 3.65–3.53 (m, 10H, -OCH_2), 3.50 (t, J = 6.5 Hz, 2H, -CONHCH_2), 2.81 (t, ^4J = 2.4 Hz, 1H, ≡CH), 2.81–2.76 (bm, 4H, -NCH_2), 2.72 (q, J = 7.1 Hz, 2H, -NCH_2CH$_3$), 2.52 (s, 3H, CH_3), 2.49 (s, 3H, CH_3), 1.12 (t, J = 7.1 Hz, 3H, CH_3). ^{13}C NMR (75 MHz, MeOD) δ 171.8 (Cq), 168.5 (Cq), 160.6 (d, $^1J_{CF}$ = 236 Hz, Cq), 138.3 (Cq), 136.0 (Cq), 131.7 (Cq), 128.8 (d, $^3J_{CF}$ = 9 Hz, Cq), 127.6 (Cq), 125.5 (CH), 121.2 (Cq), 116.9 (Cq), 113.9 (d, $^2J_{CF}$ = 25 Hz, CH), 111.3 (d, $^3J_{CF}$ = 8 Hz, CH), 106.5 (d, $^2J_{CF}$ = 26 Hz, CH), 80.7 (Cq), 76.1 (CH), 71.6 (CH_2), 71.5 (2C, CH_2), 71.5 (CH_2), 70.8 (CH_2), 70.2 (CH_2), 59.1 (CH_2), 54.0 (CH_2), 53.9 (CH_2), 49.7 (CH_2), 38.5 (CH_2), 13.7 (CH_3), 12.2 (CH_3), 11.1 (CH_3). HRMS (ESI$^+$) $C_{29}H_{37}FN_4O_5$ calcd for $[M+H]^+$ 541.2821, found 541.2817.

Compound 40

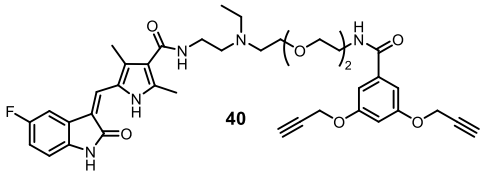

To a stirred suspension of **23** (7.7 mg, 0.026 mmol, 1.2 equiv) in dry DMF (200 µL), BOP (13.3 mg, 0.03 mmol, 1.4 equiv) and DIPEA (15 µL, 0.09 mmol, 4 equiv) were added and, after 5 min, a solution of **26** (11.7 mg, 0.21 mmol, 1 equiv) in dry DCM (200 µL) and dry DMF (100 µL) was added. The reaction mixture was left to stir under argon at room temperature for 16 h, protected from light. After reaction completion, the solvent was evaporated under reduced pressure and the residue was re-dissolved in EtOAc (2 mL) and the solution was washed with H_2O (2 ×) and saturated aqueous $NaHCO_3$ solution (2 ×). The organic layer was collected and concentrated under vacuum, affording an orange crude residue which was purified by silica gel flash chromatography [EtOAc/MeOH(NH_3), 95:5] affording compound **40** (10.2 mg, yield 67%) as yellow glassy solid.

^{1}H NMR (400 MHz, MeOD) δ 7.47 (bs, 1H, =CH), 7.35 (m, 1H, H4 suni), 7.05 (d, ^4J = 2.3 Hz, 2H, ArH), 6.86–6.80 (m, 2H, H6, H7 suni), 6.75 (t, J = 2.3 Hz, 1H, ArH), 4.74 (d, ^4J = 2.3 Hz, 4H, ArOCH_2), 3.63–3.57 (m, 8H, -OCH_2), 3.52–3.44 (m, 4H, -CONHCH_2), 2.99 (t, ^4J = 2.3 Hz, 2H, -≡CH), 2.77–2.69 (m, 6H, -NCH_2), 2.48 (s, 3H, CH_3), 2.43 (s, 3H, CH_3), 1.08 (t, ^3J = 7.1 Hz, 3H, -NCH$_2$CH_3). ^{13}C NMR (100 MHz, MeOD) δ 170.1 (Cq), 168.0 (Cq), 166.9 (Cq), 159.0 (d, $^1J_{CF}$ = 236.5 Hz, Cq), 158.8 (2C, Cq), 136.7 (Cq), 136.2 (Cq), 134.4 (Cq), 130.0 (Cq), 127.3 (d, $^3J_{CF}$ = 9 Hz, Cq), 126.1 (Cq), 123.8 (CH), 119.5 (Cq), 115.3 (d, $^4J_{CF}$ = 2.9 Hz, Cq), 112.3 (d, $^2J_{CF}$ = 24.3 Hz, CH), 109.8 (d, $^3J_{CF}$ = 8.5 Hz, CH), 106.6 (2C, CH), 104.9 (d, $^2J_{CF}$ = 27.3 Hz, CH), 104.8 (CH), 78.0 (2C, Cq), 75.8 (2C, CH), 70.0 (CH_2), 69.9 (CH_2), 69.1 (CH_2), 69.0 (CH_2), 55.6 (2C, CH_2), 52.4 (2C, CH_2), 48.1 (CH_2), 39.5 (CH_2), 36.9 (CH_2), 12.2 (CH_3), 10.6 (CH_3), 9.6 (CH_3). HRMS (ESI$^+$) $C_{39}H_{44}FN_5O_7$ calcd for $[M+H]^+$ 714.3298, found 714.3290.

Synthesis of the Sunitinib-*c*(AmpRGD) Conjugates 1-3

Conjugate 1

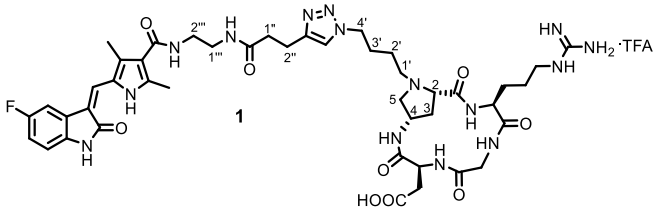

A stirred solution of compounds **13** (20 mg, 0.02 mmol, 1 equiv) and **38** (12.8 mg, 0.03 mmol, 1.3 equiv) in dry DMF (2 mL) was degassed at room temperature by argon/vacuum cycles (3 ×). To this solution was added a freshly prepared aqueous mixture (1 mL) of $Cu(OAc)_2$ (1.39 mg, 0.007 mmol, 0.3 equiv) and sodium ascorbate (2.8 mg, 0.014 mmol, 0.6 equiv), previously degassed by argon/vacuum cycles (3 ×). The reaction mixture was degassed again and left to stir, protected from light, under argon at room temperature for 20 h. After reaction completion, the mixture was concentrated under vacuum, keeping the temperature under 50 °C. The crude was dissolved with 5 drops of MeOH, and a yellow precipitate adhering to the round-bottom flask walls was obtained by means of the dropwise addition of Et_2O and petroleum ether. The organic solvents were removed by a Pasteur pipette. Subsequently, the residue was treated with water (3 ×), and the solvent was removed by a Pasteur pipette, affording a yellow-orange solid, which was used in the following step without further purification. The crude intermediate (30 mg, 0.02 mmol) was treated with a solution (1.2 mL) of TFA/TIS/H_2O (95:2.5:2.5) and the reaction mixture was left to stir for 2 h under argon at room temperature, protected from light. After solvent evaporation, the crude residue was washed thoroughly with Et_2O (4 ×) and petroleum ether (2 ×). Preparative RP-HPLC purification was performed [C_{18}-10 µm column, 21.2 × 250 mm; solvent A: H_2O (0.1% TFA) and solvent B: MeCN; flow rate 8.0 mL/min; detection 421 nm] using the following gradient elution: 0-1 min 5% B, 1-20 min 5-35% B, 20-28 min 35% B; R_t = 26.9 min. Product **1** (17.3 mg, as TFA salt, yield 69%) was obtained as an orange glassy solid. $[\alpha]_D^{25}$ = – 7.70 (*c* 1.0; MeOH).

^{1}H NMR (400 MHz, MeOD) δ 7.77 (s, 1H, ArH), 7.55 (s, 1H, =CH), 7.40 (m, 1H, ArH), 6.87 (m, 2H, ArH), 4.72 (t, *J* = 5.9 Hz, 1H, Hα Asp), 4.53 (d, *J* = 11 Hz, 1H, H2 Amp), 4.38 (t, *J* = 6.4 Hz, 2H, H1'), 4.31 (bm, 1H, H4 Amp), 4.25 (t, *J* = 7.3 Hz, 1H, Hα Arg), 4.08 (d, *J* = 13.6 Hz, 1H, Hαa Gly), 4.03 (m, 1H, H5a Amp), 3.50 (m, 2H, H1'''), 3.47–3.40 (m, 3H, H2''' + H5b Amp), 3.41 (d, *J* = 13.6 Hz, 1H, Hαb Gly), 3.31–3.20 (m, 4H, Hδ Arg + H4'), 3.03 (t, *J* = 7.2 Hz, 2H, H2''), 2.90 (m, 1H, H3a Amp), 2.84 (d, *J* = 5.8 Hz, 2H, Hβ Asp), 2.71–2.56 (m, 3H, H3b Amp + H1''), 2.48 (s, 3H, CH_3), 2.44 (s, 3H, CH_3), 2.02–1.86 (m, 2H, H2'), 1.86–1.48 (m, 6H, Hβ Arg + H3' + Hγ Arg).

^{13}C NMR (100 MHz, MeOD) δ 175.6 (Cq), 173.7 (Cq), 172.9 (Cq), 171.8 (Cq), 170.9 (Cq), 170.1 (Cq), 170.0 (Cq), 167.3 (Cq), 159.0 (d, $^1J_{CF}$ = 236 Hz, Cq), 157.3 (Cq), 146.6 (Cq), 136.7 (Cq), 134.4 (Cq), 130.1 (Cq), 127.2 (d, $^3J_{CF}$ = 9 Hz, Cq), 126.1 (Cq), 123.7 (CH), 122.3 (CH), 119.4 (Cq), 115.3 (Cq), 112.3 (d, $^2J_{CF}$ = 25 Hz, CH), 109.8 (d, $^3J_{CF}$ = 8 Hz, CH), 104.8 (d, $^2J_{CF}$ = 26 Hz, CH), 65,9 (CH), 60.3 (CH_2), 55.8 (CH), 54.6 (CH_2), 50.0 (CH), 49.7 (CH), 48.8 (CH_2), 44.5 (CH_2), 40.5 (CH_2), 39.0 (CH_2), 38.9 (CH_2), 34.9 (CH_2), 34.8 (CH_2), 34.7 (CH_2), 26.9 (CH_2), 26.5 (CH_2), 25.2 (CH_2), 22.3 (CH_2), 21.1 (CH_2), 12.1 (CH_3), 9.5 (CH_3). HRMS (ESI$^+$) $C_{44}H_{58}FN_{15}O_9$ calcd for $[M+H]^+$ 960.4599, found 960.4576.

Conjugate 2

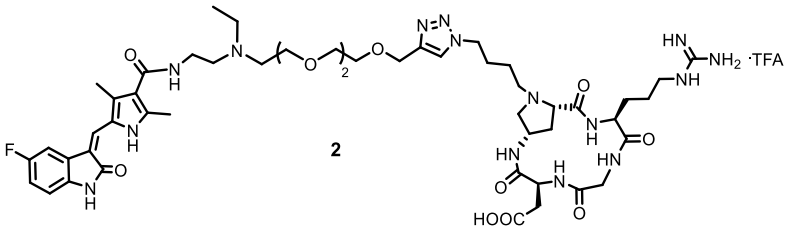

2

Compound **2** was prepared according to the procedure described for the synthesis of compound **1**, starting from **13** (6.5 mg, 0.0076 mmol, 1 equiv) and **39** (5.3 mg, 0.0098 mmol, 1.3 equiv) in dry DMF (700 µL) and using $Cu(OAc)_2$ (0.45 mg, 0.002 mmol, 0.3 equiv), sodium ascorbate (0.9 mg, 0.0045 mmol, 0.6 equiv) in H_2O (300 µL). After 24 h, the protected intermediate (9 mg, 0.006 mmol) was treated with a solution of TFA/TIS/H_2O (321 µL). Preparative RP-HPLC purification was performed [C_{18}-10 µm column, 21.2 × 250 mm; solvent A: H_2O (0.1% TFA) and solvent B: MeCN, flow rate 8.0 mL/min; detection 421 nm] using the following gradient elution: 0-1 min 5% B, 1-20 min 5-35% B, 20-28 min 35% B; R_t = 26.4 min. Conjugate **2** (6.3 mg, as TFA salt, yield 70% for two steps) was obtained as yellow-orange glassy solid. $[\alpha]_D^{20} = -8.75$ (*c* 0.16; MeOH).

^{1}H NMR (400 MHz, MeOD) δ 7.96 (s, 1H, CH triazole), 7.63 (s, 1H, =CH),7.49–7.45 (m, 1H, ArH), 6.93–6.88 (m, 2H, ArH), 4.72 (t, *J* = 6.0 Hz, 1H, Hα Asp), 4.60 (s, 2H, -OC*H*$_2$-triazole), 4.56 (bd, *J* = 11 Hz, 1H, H2 Amp), 4.43 (t, *J* = 6.0 Hz, 2H, H1'), 4.30 (m, 1H, H4 Amp), 4.24 (t, *J* = 7.2 Hz, 1H, Hα Arg), 4.11–4.00 (bm, 2H, Hαa Gly, H5a Amp), 3.93–3.88 (m, 2H, -OCH_2), 3.80–3.73 (m, 2H, -CONHC*H*$_2$), 3.71–3.62 (m, 8H, -OCH_2), 3.55–3.36 (bm, 8H, -NCH_2, Hαb Gly, H5b Amp), 3.31–3.22 (bm, 4H, Hδ Arg, H4'), 2.97–2.82 (bm, 3H, H3a Amp, Hβ Asp), 2.68 (bd, *J* = 14.4 Hz, 1H, H3b Amp), 2.55 (s, 3H, CH_3), 2.51 (s, 3H, CH_3), 2.01–1.91 (bm, 2H, H2'), 1.86–1.58 (bm, 6H, Hβ Arg, H3', Hγ Arg), 1.41 (t, *J* = 7.2 Hz, 3H, CH_3).

^{13}C NMR (100 MHz, MeOD) δ 175.7 (Cq), 172.8 (Cq), 171.8 (Cq), 170.9 (Cq), 170.3 (Cq), 170.1 (Cq), 168.7 (Cq), 159.1 (d, $^1J_{CF}$ = 236 Hz, Cq), 157.3 (Cq), 146.5 (Cq), 137.4 (Cq), 134.6 (Cq), 130.2 (Cq), 127.1 (d, $^3J_{CF}$ = 9 Hz, Cq), 126.2 (Cq), 123.8 (2C, CH), 118.1 (Cq), 116.1 (Cq), 112.7 (d, $^2J_{CF}$ = 25 Hz, CH), 110.0 (d, $^3J_{CF}$ = 9 Hz, CH), 105.2 (d, $^2J_{CF}$ = 26 Hz, CH), 70.0 (2C, CH_2), 69.4 (2C, CH_2), 66.1 (CH), 64.3 (CH_2), 63.5 (CH_2), 60.2 (CH_2), 55.9 (CH), 54.7 (CH_2), 53.6 (CH_2), 52.7 (CH_2), 50.1 (CH), 49.7 (CH), 49.2 (CH_2), 48.9 (CH_2), 44.5 (CH_2), 40.5 (CH_2), 35.2 (CH_2), 34.7 (CH_2), 34.0 (CH_2), 26.9 (CH_2), 26.6 (CH_2), 25.2 (CH_2), 22.4 (CH_2), 12.4 (CH_3), 9.6 (CH_3), 7.9 (CH_3).
HRMS (ESI$^+$) $C_{50}H_{72}FN_{15}O_{11}$ calcd for $[M+H]^+$ 1078.5593, found 1078.5585.

Conjugate 3

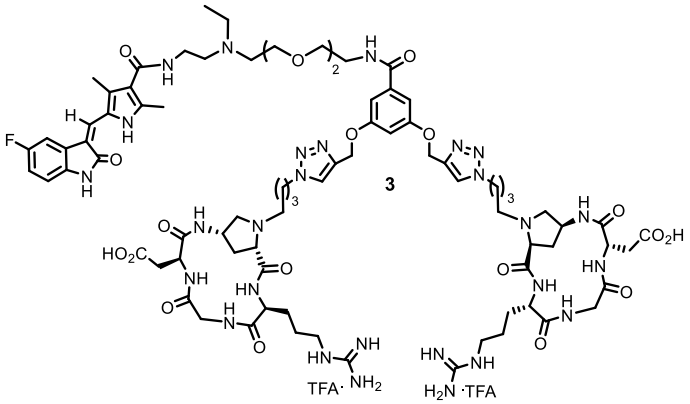

Compound **3** was prepared according to the procedure described for the synthesis of compound **1**, starting from **13** (28.1 mg, 0.033 mmol, 2.3 equiv) and **40** (10.2 mg, 0.014 mmol, 1 equiv) in dry DMF (2 mL) and using $Cu(OAc)_2$ (1.7 mg, 0.01 mmol, 0.6 equiv), sodium ascorbate (3.4 mg, 0.02 mmol, 1.2 equiv) in H_2O (0.9 mL). After 24 h, the protected intermediate (32.3 mg, 0.013 mmol) was treated with a solution of TFA/TIS/H_2O (321 µL). Preparative RP-HPLC purification was performed [C_{18}-10 µm column, 21.2 × 250 mm; solvent A: H_2O (0.1% TFA) and solvent B: MeCN, flow rate 8.0 mL/min; detection 421 nm] using the following gradient elution: 0-1 min 5% B, 1-23 min 5-40% B, 23-28 min 40% B; R_t = 21.8 min. Conjugate **3** (12.4 mg, as TFA salt, yield 43%) was obtained as a yellow glassy solid. $[\alpha]_D^{20} = -6.92$ (*c* 0.39; MeOH).

^{1}H NMR (400 MHz, MeOD) δ 8.06 (s, 2H, =CH triazole), 7.54 (s, 1H, =CH), 7.41 (m, 1H, H4 suni), 7.07 (d, ^4J = 2.0 Hz, 2H, ArH), 6.91–6.86 (m, 2H, H6 + H7 suni), 6.70 (bt, ^4J = 2.0 Hz, 1H, ArH), 5.21 (d, ^2J = 12.2 Hz, 2H, ArOCHa), 5.15 (d, ^2J = 12.2 Hz, 2H, ArOCHb), 4.69 (t, J = 5.8 Hz, 2H, Hα Asp), 4.59 (bd, J = 10.6 Hz, 2H, H2 Amp), 4.51–4.44 (m, 4H, H1'), 4.33 (bs, 2H, H4 Amp), 4.22 (bt, J = 6.6 Hz, 2H, Hα Arg), 4.13–4.01 (bm, 4H, Hαa Gly + H5a Amp), 3.93–3.87 (bm, 2H, -OCH_2), 3.79–3.63 (bm, 8H, -CONHCH_2,-OCH_2), 3.60–3.38 (bm, 12H, -CONHCH_2, Hαb Gly, H5b Amp + -NCH_2), 3.31 (bm, 4H, Hδ Arg), 3.26–3.21 (bm, 4H, H4'), 3.00–2.88 (bm, 2H, H3a Amp), 2.88–2.74 (m, 4H, Hβ Asp), 2.73–2.65 (bd, J = 14.7 Hz, 2H, H3b Amp), 2.50 (s, 3H, CH_3), 2.46 (s, 3H, CH_3), 2.04–1.92 (bm, 4H, H2'), 1.84–1.57 (bm, 12H, Hβ Arg, H3', Hγ Arg), 1.39 (t, J = 7.2 Hz, 3H, -NCH_2CH$_3$).

^{13}C NMR (100 MHz, MeOD) δ 175.6 (Cq), 172.8 (Cq), 171.8 (Cq), 171.0 (Cq), 170.2 (Cq), 169.9 (Cq), 168.7 (Cq), 168.4 (Cq), 159.4 (2C, Cq), 159.1 (d, $^1J_{CF}$ = 236.7 Hz, Cq), 157.3 (2C, Cq), 143.5 (2C, Cq), 137.4 (Cq), 136.4 (Cq), 134.6 (Cq), 130.2 (Cq), 127.2 (d, $^3J_{CF}$ = 9.1 Hz, Cq), 126.2 (Cq), 124.1 (2C, CH), 123.8 (CH), 118.0 (Cq), 115.9 (d, $^4J_{CF}$ = 2.9 Hz, Cq), 112.6 (d, $^2J_{CF}$ = 24.0 Hz, CH), 110.0 (d, $^3J_{CF}$ = 8.3 Hz, CH), 106.3 (2C, CH), 105.1 (d, $^2J_{CF}$ = 26.0 Hz, CH), 104.9 (CH), 70.2 (CH_2), 69.8 (CH_2), 69.1 (CH_2), 65.9 (2C, CH), 64.3 (CH_2), 61.2 (2C, CH_2), 60.5 (2C, CH), 55.9 (2C, CH), 54.6 (2C, CH_2), 52.7 (CH_2), 50.1 (2C, CH), 49.6 (2C, CH), 49.1 (4C, CH_2), 44.6 (2C, CH_2), 40.5 (2C, CH_2), 39.5 (CH_2), 35.3 (CH_2), 34.9 (2C, CH_2), 34.7 (2C, CH_2), 26.9 (2C, CH_2), 26.5 (2C, CH_2), 25.2 (2C, CH_2), 22.4 (2C, CH_2), 12.4 (CH_3), 9.6 (CH_3), 7.9 (CH_3). HRMS (ESI$^+$) $C_{81}H_{114}FN_{27}O_{19}$ calcd for $[M+2H]^{2+}$ 894.9457, found 894.9479.

1*α*.6 References

(1) Carmeliet, P.; Jain, R. K. *Nature* **2011**, *473* (7347), 298–307.
(2) Hanahan, D.; Folkman, J. *Cell* **1996**, *86* (3), 353–364.
(3) Folkman, J. *Nat. Rev. Drug Discov.* **2007**, *6*, 273–286.
(4) Carmeliet, P. *Nat. Med.* **2003**, *9* (6), 653–660.
(5) Welti, J.; Loges, S.; Dimmeler, S.; Carmeliet, P. *J. Clin. Invest.* **2013**, *123* (8), 3190–3200.
(6) Weis, S. M.; Cheresh, D. A. *Nat. Med.* **2011**, *17* (11), 1359–1370.
(7) Cox, D.; Brennan, M.; Moran, N. *Nat. Rev. Drug Discov.* **2010**, *9* (10), 804–820.
(8) Gahmberg, C. G.; Fagerholm, S. C.; Nurmi, S. M.; Chavakis, T.; Marchesan, S.; Grönholm, M. *Biochim Biophys Acta.* **2009**, *1790* (6), 431–444.
(9) Arnaout, M. A.; Goodman, S.; Xiong, J.-P. *Curr Opin Cell Biol.* **2007**, *19* (5), 495–507.
(10) Kapp, T. G.; Rechenmacher, F.; Sobahi, T. R.; Kessler, H. *Expert Opin. Ther. Pat.* **2013**, *23* (10), 1273–1295.
(11) Desgrosellier, J. S.; Cheresh, D. A. *Nat. Rev. Cancer* **2010**, *10* (1), 9–22.
(12) Shimaoka, M.; Springer, T. A. *Nat. Rev. Drug Discov.* **2003**, *2* (9), 703–716.
(13) Mas-Moruno, C.; Rechenmacher, F.; Kessler, H. *Anticancer. Agents Med. Chem.* **2010**, *10* (10), 753–768.
(14) Millard, M.; Odde, S.; Neamati, N. *Theranostics* **2011**, *1*, 154–188.
(15) Somanath, P. R.; Ciocea, A.; Byzova, T. V. *Cell Biochem. Biophys.* **2009**, *53* (2), 53–64.
(16) Somanath, P. R.; Malinin, N. L.; Byzova, T. V. *Angiogenesis* **2009**, *12* (2), 177–185.
(17) Ley, K.; Rivera-Nieves, J.; Sandborn, W. J.; Shattil, S. *Nat. Rev. Drug Discov.* **2016**, *15* (3), 173–183.
(18) Paolillo, M.; Russo, M. a; Serra, M.; Colombo, L.; Schinelli, S. *Mini Rev. Med. Chem.* **2009**, *9* (12), 1439–1446.
(19) Liu, Z.; Wang, F.; Chen, X. *Drug Dev. Res.* **2008**, *69* (6), 329–339.
(20) Stupp, R.; Hegi, M. E.; Gorlia, T.; Erridge, S. C.; Perry, J.; Hong, Y. K.; Aldape, K. D.; Lhermitte, B.; Pietsch, T.; Grujicic, D.; Steinbach, J. P. ete.; Wick, W.; Tarnawski, R.; Nam, D. H.; Hau, P.; Weyerbrock, A.; Taphoorn, M. J. B.; Shen, C. C.; Rao, N.; Thurzo, L.; Herrlinger, U.; Gupta, T.; Kortmann, R. D.; Adamska, K.; McBain, C.; Brandes, A. A.; Tonn, J. C. hristia.; Schnell, O.; Wiegel, T.; Kim, C. Y.; Nabors, L. B. ur.; Reardon, D. A.; van den Bent, M. J.; Hicking, C.; Markivskyy, A.; Picard, M.; Weller, M. *Lancet. Oncol.* **2014**, *15* (10), 1100–1108.
(21) O'Donnell, P. H.; Karovic, S.; Karrison, T. G.; Janisch, L.; Levine, M. R.; Harris, P. J.; Polite, B. N.; Cohen, E. E. W.; Fleming, G. F.; Ratain, M. J.; Maitland, M. L. *Clin Cancer Res.* **2015**, *21* (22), 5092–5099.
(22) Vansteenkiste, J.; Barlesi, F.; Waller, C. F.; Bennouna, J.; Gridelli, C.; Goekkurt, E.; Verhoeven, D.; Szczesna, A.; Feurer, M.; Milanowski, J.; Germonpre, P.; Lena, H.; Atanackovic, D.; Krzakowski, M.; Hicking, C.; Straub, J.; Picard, M.; Schuette, W.; O'Byrne, K. *Ann. Oncol.* **2015**, *26* (8), 1734–1740.
(23) Reynolds, A. R.; Hart, I. R.; Watson, A. R.; Welti, J. C.; Silva, R. G.; Robinson, S. D.; Da Violante, G.; Gourlaouen, M.; Salih, M.; Jones, M. C.; Jones, D. T.; Saunders, G.; Kostourou, V.; Perron-Sierra, F.; Norman, J. C.; Tucker, G. C.; Hodivala-Dilke, K. M. *Nat. Med.* **2009**, *15* (4), 392–400.
(24) Weller, M.; Reardon, D.; Nabors, B.; Stupp, R. *Nat. Med.* **2009**, *15* (7), 726.
(25) Weis, S. M.; Stupack, D. G.; Cheresh, D. A. *Cancer Cell* **2009**, *15* (5), 359–361.
(26) Yamada, S.; Bu, X. Y.; Khankaldyyan, V.; Gonzales-Gomez, I.; McComb, J. G.; Laug, W. E. *Neurosurgery* **2006**, *59* (6), 1304–1312.
(27) Ebos, J. M. L.; Lee, C. R.; Cruz-Munoz, W.; Bjarnason, G. A.; Christensen, J. G.; Kerbel, R. S. *Cancer Cell* **2009**, *15* (3), 232–239.
(28) Pàez-Ribes, M.; Allen, E.; Hudock, J.; Takeda, T.; Okuyama, H.; Viñals, F.; Inoue, M.; Bergers, G.; Hanahan, D.; Casanovas, O. *Cancer Cell* **2009**, *15* (3), 220–231.
(29) Reynolds, A. R.; Reynolds, L. E.; Nagel, T. E.; Lively, J. C.; Robinson, S. D.; Hicklin, D. J.; Bodary, S. C.; Hodivala-Dilke, K. M. *Cancer Res.* **2004**, *64*, 8643–8650.
(30) Schottelius, M.; Laufer, B.; Kessler, H.; Wester, H. J. *Acc. Chem. Res.* **2009**, *42* (7), 969–980.
(31) Garanger, E.; Boturyn, D.; Dumy, P. *Anticancer. Agents Med. Chem.* **2007**, *7* (5), 552–558.
(32) Dufort, S.; Sancey, L.; Hurbin, A.; Foillard, S.; Boturyn, D.; Dumy, P.; Coll, J.-L. *J. Drug Target.* **2011**, *19* (7), 582–588.
(33) Eldar-Boock, A.; Miller, K.; Sanchis, J.; Lupu, R.; Vicent, M. J.; Satchi-Fainaro, R. *Biomaterials* **2011**, *32* (15), 1–22.

(34) Morales-Avila, E.; Ferro-Flores, G.; Ocampo-García, B. E.; De León-Rodríguez, L. M.; Santos-Cuevas, C. L.; García-Becerra, R.; Medina, L. A.; Gómez-Oliván, L. *Bioconjug. Chem.* **2011**, *22* (5), 913–922.
(35) Dal Pozzo, A.; Esposito, E.; Ni, M.; Muzi, L.; Pisano, C.; Bucci, F.; Vesci, L.; Castorina, M.; Penco, S. *Bioconjug. Chem.* **2010**, *21* (11), 1956–1967.
(36) Kelderhouse, L. E.; Chelvam, V.; Wayua, C.; Mahalingam, S.; Poh, S.; Kularatne, S. A.; Low, P. S. *Bioconjug. Chem.* **2013**, *24* (6), 1075–1080.
(37) Wenk, C. H. F.; Ponce, F.; Guillermet, S.; Tenaud, C.; Boturyn, D.; Dumy, P.; Watrelot-Virieux, D.; Carozzo, C.; Josserand, V.; Coll, J. L. *Cancer Lett.* **2013**, *334* (2), 188–195.
(38) Altai, M.; Strand, J.; Rosik, D.; Selvaraju, R. K.; Eriksson Karlström, A.; Orlova, A.; Tolmachev, V. *Bioconjug. Chem.* **2013**, *24* (6), 1102–1109.
(39) Casiraghi, G.; Rassu, G.; Auzzas, L.; Burreddu, P.; Gaetani, E.; Battistini, L.; Zanardi, F.; Curti, C.; Nicastro, G.; Belvisi, L.; Motto, I.; Castorina, M.; Giannini, G.; Pisano, C. *J. Med. Chem.* **2005**, *48* (24), 7675–7687.
(40) Zanardi, F.; Burreddu, P.; Rassu, G.; Auzzas, L.; Battistini, L.; Curti, C.; Sartori, A.; Nicastro, G.; Menchi, G.; Cini, N.; Bottonocetti, A.; Raspanti, S.; Casiraghi, G. *J. Med. Chem.* **2008**, *51* (6), 1771–1782.
(41) Battistini, L.; Burreddu, P.; Carta, P.; Rassu, G.; Auzzas, L.; Curti, C.; Zanardi, F.; Manzoni, L.; Araldi, E. M. V; Scolastico, C.; Casiraghi, G. *Org. Biomol. Chem.* **2009**, *7* (23), 4924–4935.
(42) Gentilucci, L.; De Marco, R.; Cerisoli, L. *Curr. Pharm. Des.* **2010**, *16*, 3185–3203.
(43) Pilkington-Miksa, M.; Arosio, D.; Battistini, L.; Belvisi, L.; De Matteo, M.; Vasile, F.; Burreddu, P.; Carta, P.; Rassu, G.; Perego, P.; Carenini, N.; Zunino, F.; De Cesare, M.; Castiglioni, V.; Scanziani, E.; Scolastico, C.; Casiraghi, G.; Zanardi, F.; Manzoni, L. *Bioconjug. Chem.* **2012**, *23* (8), 1610–1622.
(44) Sartori, A.; Bianchini, F.; Migliari, S.; Burreddu, P.; Curti, C.; Vacondio, F.; Arosio, D.; Ruffini, L.; Rassu, G.; Calorini, L.; Pupi, A.; Zanardi, F.; Battistini, L. *Med. Chem. Commun.* **2015**, *6* (12), 2175–2183.
(45) Battistini, L.; Burreddu, P.; Sartori, A.; Arosio, D.; Manzoni, L.; Paduano, L.; D'Errico, G.; Sala, R.; Reia, L.; Bonomini, S.; Rassu, G.; Zanardi, F. *Mol. Pharm.* **2014**, *11* (7), 2280–2293.
(46) Takahashi, S. *Biol. Pharm. Bull.* **2011**, *34* (12), 1785–1788.
(47) Koch, S.; Tugues, S.; Li, X.; Gualandi, L.; Claesson-Welsh, L. *Biochem. Soc.* **2011**, *437*, 169–183.
(48) Simons, M.; Gordon, E.; Claesson-Welsh, L. *Nat. Rev. Mol. Cell Biol.* **2016**, *17* (10), 611–625.
(49) Musumeci, F.; Radi, M.; Brullo, C.; Schenone, S. *J. Med. Chem.* **2012**, *55* (24), 10797–10822.
(50) Olsson, A.-K.; Dimberg, A.; Kreuger, J.; Claesson-Welsh, L. *Nat. Rev. Mol. Cell Biol.* **2006**, *7*, 359–371.
(51) Ferrara, N.; Adamis, A. P. *Nat. Rev. Drug Discov.* **2016**, *15* (6), 385–403.
(52) El-Kenawi, A. E.; El-Remessy, A. B. *Br. J. Pharmacol.* **2013**, *170* (4), 712–729.
(53) Folkman, J. *N. Engl. J. Med.* **1971**, *285* (21), 1182–1186.
(54) Choueiri, T. K.; Sonpavde, G. Toxicity of molecularly targeted antiangiogenic agents: Non-cardiovascular effects. UpToDate, 2017; https://www.uptodate.com/contents/toxicity-of-molecularly-targeted-antiangiogenic-agents-non-cardiovascular-effects (Jul 25, 2017) (accessed Jan 1, 2017).
(55) Choueiri, T. K.; Sonpavde, G. Toxicity of molecularly targeted antiangiogenic agents: Cardiovascular effects. UpToDate, 2017; https://www.uptodate.com/contents/toxicity-of-molecularly-targeted-antiangiogenic-agents-cardiovascular-effects (Aug 21, 2017).
(56) Bagcchi, S. *Lancet Oncol.* **2014**, *15* (10), e420.
(57) Raymond, E.; Dahan, L.; Raoul, J.-L.; Bang, Y.-J.; Borbath, I.; Lombard-Bohas, C.; Valle, J.; Metrakos, P.; Smith, D.; Vinik, A.; Chen, J.-S.; Hörsch, D.; Hammel, P.; Wiedenmann, B.; Van Cutsem, E.; Patyna, S.; Lu, D. R.; Blanckmeister, C.; Chao, R.; Ruszniewski, P. *N. Engl. J. Med.* **2011**, *364* (6), 501–513.
(58) Faivre, S.; Demetri, G.; Sargent, W.; Raymond, E. *Nat. Rev. Drug Discov.* **2007**, *6* (9), 734–745.
(59) Gacche, R. N. *Oncogenesis* **2015**, *4* (e153), 1–8.
(60) Jain, R. K. *Cancer Cell.* **2014**, *26* (5), 605–622.
(61) Bergers, G.; Hanahan, D. *Nat. Rev. Cancer* **2008**, *8* (8), 592–603.
(62) Casazza, A.; Di Conza, G.; Wenes, M.; Finisguerra, V.; Deschoemaeker, S.; Mazzone, M. *Oncogene* **2014**, *33* (14), 1743–1754.
(63) Barsoum, I. B.; Smallwood, C. A.; Siemens, D. R.; Graham, C. H. *Cancer Res.* **2014**, *74* (3), 665–674.
(64) Wilson, W. R.; Hay, M. P. *Nat. Rev. Cancer* **2011**, *11* (6), 393–410.
(65) Semenza, G. L. *Annu. Rev. Pathol. Mech. Dis.* **2014**, *9* (1), 47–71.
(66) Jain, R. K. *J. Clin. Oncol.* **2013**, *31* (17), 2205–2218.
(67) Mahabeleshwar, G. H.; Feng, W.; Phillips, D. R.; Byzova, T. V. *J. Exp. Med.* **2006**, *203* (11), 2495–2507.
(68) Mahabeleshwar, G. H.; Feng, W.; Reddy, K.; Plow, E. F.; Byzova, T. V. *Circ Res.* **2007**, *101* (6), 570–580.

(69) Mahabeleshwar, G. H.; Chen, J.; Feng, W.; Somanath, P. R.; Razorenova, O. V.; Byzova, T. V. *Cell Cycle* **2008**, *7* (3), 335–347.
(70) Robinson, S. D.; Hodivala-Dilke, K. M. *Curr. Opin. Cell Biol.* **2011**, *23* (5), 630–637.
(71) Strieth, S.; Eichhorn, M. E.; Sutter, A.; Jonczyk, A.; Berghaus, A.; Dellian, M. *Int. J. Cancer* **2006**, *119* (2), 423–431.
(72) Papo, N.; Silverman, A. P.; Lahti, J. L.; Cochran, J. R. *Proc. Natl. Acad. Sci.* **2011**, *108* (34), 14067–14072.
(73) Kim, T. J.; Landen, C. N.; Lin, Y. G.; Mangala, L. S.; Lu, C.; Nick, A. M.; Stone, R. L.; Merritt, W. M.; Armaiz-Pena, G.; Jennings, N. B.; Coleman, R. L.; Tice, D. A.; Sood, A. K. *Cancer Biol. Ther.* **2009**, *8* (23), 2263–2272.
(74) Zanella, S.; Mingozzi, M.; DalCorso, A.; Fanelli, R.; Arosio, D.; Cosentino, M.; Schembri, L.; Marino, F.; Dezotti, M.; Formaggio, F.; Pignataro, L.; Belvisi, L.; Piarulli, U.; Gennari, C. *ChemistryOpen* **2015**, *4* (5), 633–641.
(75) Sun, L.; Liang, C.; Shirazian, S.; Zhou, Y.; Miller, T.; Cui, J.; Fukuda, J. Y.; Chu, J.; Nematalla, A.; Wang, X.; Chen, H.; Sistla, A.; Luu, T. C.; Tang, F.; Wei, J.; Tang, C. *J. Med. Chem.* **2003**, *46*, 1116–1119.
(76) McTigue, M.; Murray, B. W.; Chen, J. H.; Deng, Y.-L.; Solowiej, J.; Kania, R. S. *Proc. Natl. Acad. Sci.* **2012**, *109* (45), 18281–18289.
(77) Capelli, A. M.; Costantino, G. *J. Chem. Inf. Model.* **2014**, *54* (11), 3124–3136.
(78) Boturyn, D.; Coll, J. L.; Garanger, E.; Favrot, M. C.; Dumy, P. *J. Am. Chem. Soc.* **2004**, *126* (18), 5730–5739.
(79) Sancey, L.; Garanger, E.; Foillard, S.; Schoehn, G.; Hurbin, A.; Albiges-Rizo, C.; Boturyn, D.; Souchier, C.; Grichine, A.; Dumy, P.; Coll, J.-L. *Mol. Ther.* **2009**, *17* (5), 837–843.
(80) Ivaska, J.; Heino, J. *Annu. Rev. Cell Dev. Biol.* **2011**, *27* (1), 291–320.
(81) Liu, S. *Bioconjug. Chem.* **2015**, *26* (8), 1413–1438.
(82) Norberg, O.; Deng, L.; Aastrup, T.; Yan, M.; Ramström, O. *Anal. Chem.* **2011**, *83* (3), 1000–1007.
(83) More, J. D.; Finney, N. S. *Org. Lett.* **2002**, *4* (17), 3001–3003.
(84) Bates, R. W.; Dewey, M. R. *Org. Lett.* **2009**, *11* (16), 3706–3708.
(85) Thakkar, A.; Trinh, T. B.; Pei, D. *ACS Comb. Sci.* **2013**, *15*, 120–129.
(86) Marsault, E.; Peterson, M. L. *J. Med. Chem.* **2011**, *54* (7), 1961–2004.
(87) Malesevic, M.; Strijowski, U.; Bächle, D.; Sewald, N. *J. Biotechnol.* **2004**, *112*, 73–77.
(88) Lu, G.; Lam, S.; Burgess, K. *Chem. Commun.* **2006**, *15*, 1652–1654.
(89) Dijkgraaf, I.; Rijnders, A. Y.; Soede, A.; Dechesne, A. C.; van Esse, G. W.; Brouwer, A. J.; Corstens, F. H. M.; Boerman, O. C.; Rijkers, D. T. S.; Liskamp, R. M. J. *Org. Biomol. Chem.* **2007**, *5* (6), 935–944.
(90) Sartori, A.; Portioli, E.; Battistini, L.; Calorini, L.; Pupi, A.; Vacondio, F.; Arosio, D.; Bianchini, F.; Zanardi, F. *J. Med. Chem.* **2017**, *60* (1), 248–262.
(91) Ribatti, D. *J Cell Mol Med* **2004**, *8* (3), 294–300.
(92) Marçola, M.; Rodrigues, C. E. *Stem Cells Int.* **2015**, 832649.
(93) Chen, P.-Y.; Qin, L.; Zhuang, Z. W.; Tellides, G.; Lax, I.; Schlessinger, J.; Simons, M. *Proc. Natl. Acad. Sci.* **2014**, *111* (15), 5514–5519.
(94) Somanath, P. R.; Malinin, N. L.; Byzova, T. V. *Angiogenesis* **2009**, *12* (2), 177–185.
(95) Sistla, A.; Shenoy, N. *Drug Dev. Ind. Pharm.* **2005**, *31* (10), 1001–1007.

Chapter 1. Targeting integrin $\alpha_V\beta_3$

1b. Platinum(II) complexes[5]

[5] The work described in this chapter is CONFIDENTIAL.

1*b*.1 Introduction

The coordination of platinum to DNA is an area of intense research that has allowed the development of valuable platinum-based chemotherapeutics.[1] Amongst clinically approved platinum anticancer agents, three are approved worldwide for treating cancer in human (cisplatin, carboplatin and oxaliplatin), and an additional three are approved for use in specific countries: nedaplatin (Japan), lobaplatin (China), and heptaplatin (Korea) (Fig. 1). Despite having been introduced into the market almost 40 years ago, these platinum complexes remain among the most widely used anticancer chemotherapeutics, representing one of the great successes in the field of medicinal inorganic chemistry. One notable mark of the success of the platinum drugs is the fact that, since the introduction of cisplatin into the treatment regimen of testicular cancer patients, cure rates for this disease have exceeded 95%.[1] Cisplatin is currently used primarily to treat testicular, ovarian, and bladder cancers, but has also been used in the treatment of head and neck cancers, lung cancer, malignant pleural mesothelioma, neuroblastoma, tumors of the brain, and esophageal and cervical cancers.[2] The clinical trials database maintained by the U.S. National Institutes of Health (NIH), which lists >186 000 clinical trials in over 180 countries, cites cisplatin as a component in more active clinical trials than any other anticancer agent (Fig. 2). Similar trends hold for the European Union Clinical Trial Register, which is maintained by the European Medicines Agency (EMA) and lists over 25 000 trials with a European clinical trials database (EudraCT) protocol, as well as the International Clinical Trials Registry Platform of the WHO.[1]

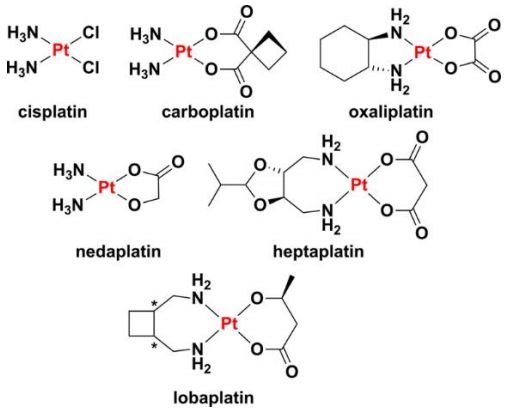

Figure 1. Chemical structures of clinically approved and marketed platinum anticancer drugs.

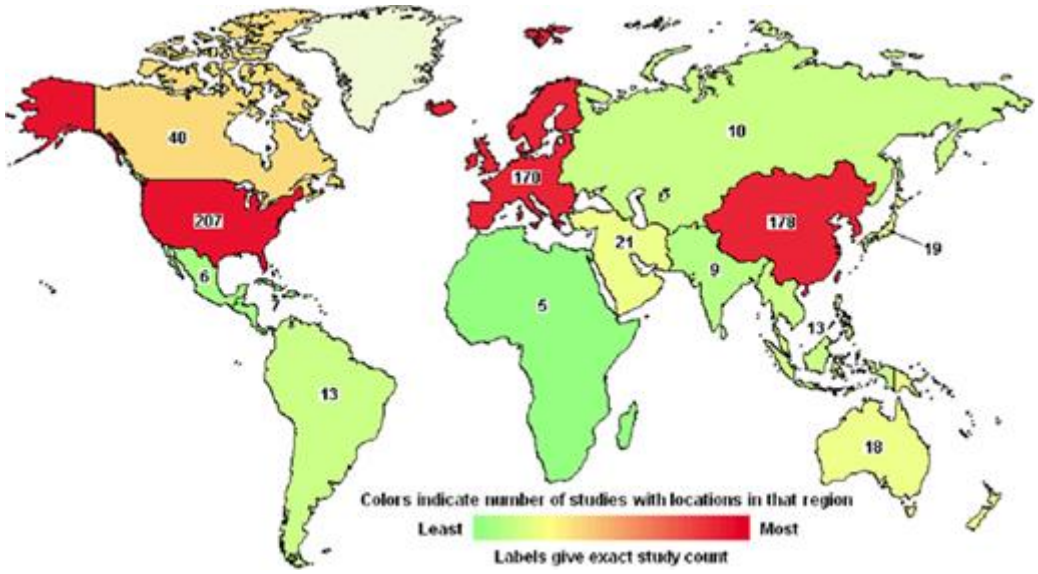

Figure 2. NIH-registered clinical trials involving cisplatin in various parts of the world as of 2015. The numbers reflect only those trials that are open and the activity of which has been verified by the NIH within the past two years. Picture reprinted from ref.[1].

Despite the widespread use of these drugs, a new platinum agent has not received worldwide approval in over a decade. However, research activity toward new platinum anticancer agents has remained intense,[1,3] focusing mainly on the development of targeted Pt(II) agents, Pt(IV) prodrugs and nanoparticle delivery.

Cisplatin and its analogous compounds are neutral and square-planar platinum (II) complexes, in which the central metal ion, Pt(II), coordinates two *cis* amine and two *cis* anionic ligands.[1] The amine ligands can be chelating or nonchelating and are referred to as the "nonleaving group" ligand(s) because they remain bound to the metal center throughout the course of intracellular transformations. In contrast, the "leaving group" ligand(s), which can be monodentate anionic or chelating dianionic fragments, leave the platinum(II) coordination sphere.

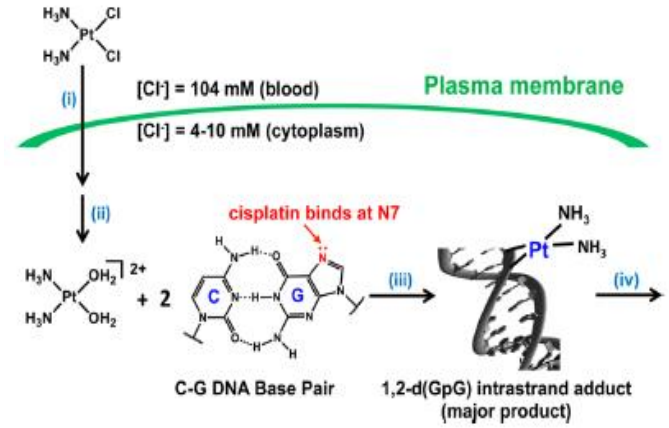

Figure 3. Four steps of the mechanism of action of cisplatin and related platinum anticancer drugs. (*i*) Cellular uptake, (*ii*) aquation/ activation, (*iii*) DNA binding, and (*iv*) cellular processing of DNA lesions leading to apoptosis. Figure reprinted from ref.[1].

After cell internalization, cisplatin (and related platinum anticancer drugs) undergoes a ligand substitution, a process called aquation, in which a chloride ligand is replaced by a water molecule (Fig. 3). This drug activation process (aquation) is suppressed in the bloodstream, where the chloride ion concentration is high (~100 mM), but occurs more readily in the cytoplasm, where the chloride ion concentration falls below 20 mM. The aquated platinum complex assumes positive charge, which attracts them to the negatively charged nuclear DNA, where the metal-coordinated water molecule can be substituted by a heterocylic DNA base, forming *intra*-strand and *inter*-strand DNA cross-links, mainly interacting with N^7 atoms of neighbouring guanine bases. These DNA adducts distort the structure of DNA in a substantial manner; in fact, upon platination, the double helix results bend and unwind. Cellular processing of these DNA lesions leads to apoptosis.[1]

Besides DNA, platinum(II) also readily coordinates to other biomolecules, such as proteins.[4] Extensive research in this area has shown that, among the various potential binding sites for platinum(II) in proteins, the most likely are those containing the amino acids cysteine, methionine, and histidine.[5–8] However, although the protein binding properties of Pt(II) have been extensively studied, they still remain largely underexploited. In recent years, a cisplatin-type complex, [Pt(en)Cl_2], (en = ethylenediamine), has found application as linker in bio-conjugation reactions.[9–12]

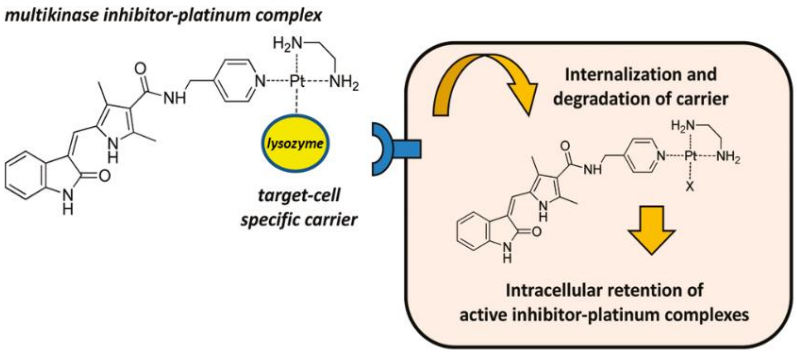

Figure 4. Platinum coordinated multikinase inhibitor bioconjugate. Figure reprinted from ref.[10].

For example, the complex [Pt(en)Cl_2] has been used as bifunctional linker for the conjugation of a multikinase inhibitor to lysozyme for specific renal targeting (Fig. 4).[10] Since lysozyme is: (*i*) freely filtered through the glomerular barrier into the tubular lumen, and (*ii*) reabsorbed by proximal tubular cells via megalin and cubilin receptor-mediated endocytosis, it can be used as carrier toward renal tubular cells. The linkage of the multikinase inhibitor to its carrier using a platinum(II)-based linker ensured the formation of a conjugate that can be dissociated within cells by competitive displacement of the platinum ligands by endogenous thiols, such as glutathione (GSH).

Moreover, the complexation of Pt(II) to an oxindole-based multikinase inhibitor showed to not affect its pharmacological activity but additionally improving its retention in the target cells, thereby prolonging the pharmacological activity of the delivered compound. This developed cell-selective multikinase inhibitor bioconjugate may eventually provide a safe and efficient way to administrate multikinase inhibitors in less life-threatening diseases than cancer (such as: liver cirrhosis, chronic airway inflammation and idiopathic pulmonary fibrosis), without inducing dose-limiting off-organ toxicities.[10]

As highlighted in the work by Waalboer et al. in 2015,[13] the potential of platinum(II) as a bifunctional linker in the coordination of small molecules, such as imaging agents or (cytotoxic) drugs, to monoclonal antibodies (mAbs), could be promising to the preparation of antibody-drug conjugates (ADCs), for selectively targeting diagnostic or therapeutic agents to tumors or other diseases. In particular, Waalboer and co-workers investigated the use of the [Pt(en)Cl_2] complex in the coordination of an imaging agent, such as a 4-nitrobenzo-2-oxa-1,3-diazole (NBD) fluorophore, to the monoclonal antibody trastuzumab (Herceptin). To investigate the effect of the type of coordinating group on the efficiency of the conjugation reaction, diverse sets of NBD ligands, covering *N*-heteroaromatic, *N*-aliphatic amine and thioether coordinating groups, were synthesized and complexed with [Pt(en)Cl_2] (Fig. 5).

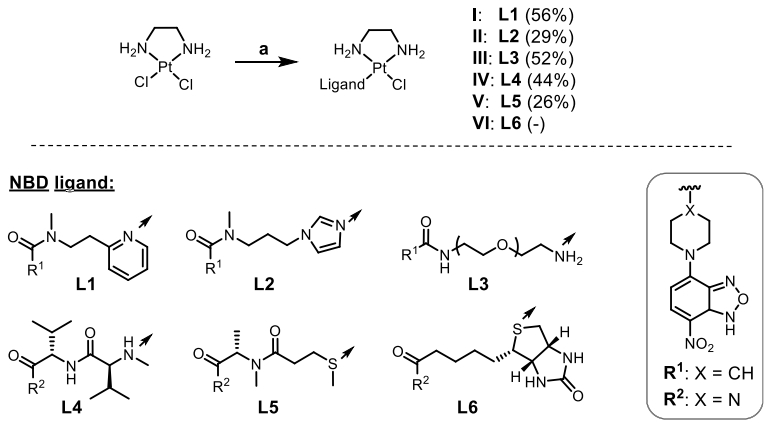

Figure 5. Synthesis of complexes **I**-**VI**. Reagents and conditions: **a**) $AgNO_3$, DMF, r.t., 16 h, then ligands L1-L6, r.t.- 60 °C, 24-48 h. Figure adapted from ref.[13].

Reaction of *N*-coordinated complexes (20 equiv) with trastuzumab at 37 °C for 2 h, followed by removal of weakly bound complexes with excess thiourea, afforded conjugates with an NBD/mAb ratio of 1.5-2.9, that were stable in phosphate-buffered saline at room temperature for at least 48 h. In contrast, thioether-coordinated complexes afforded unstable conjugates. Finally, surface plasmon resonance analysis showed no loss in binding affinity of trastuzumab after conjugation, illustrating that further investigations on the use of [Pt(en)Cl_2] as linker in the field of antibody-drug conjugates are warranted.

In the field of drug discovery, cyclic peptides are of considerable interest, representing a large, privileged and yet underexploited class of molecules.[14–16] Cyclic peptides are important tools in medicinal chemistry because they exhibit, compared with their linear precursors, a reduced conformational flexibility, resulting in improved metabolic stability and bioavailability, which can also impart an enhanced biological activity, with higher receptor binding and selectivity.[17] To date, several naturally occurring as well as synthetic cyclic peptides have advanced to the clinic.[18,19]

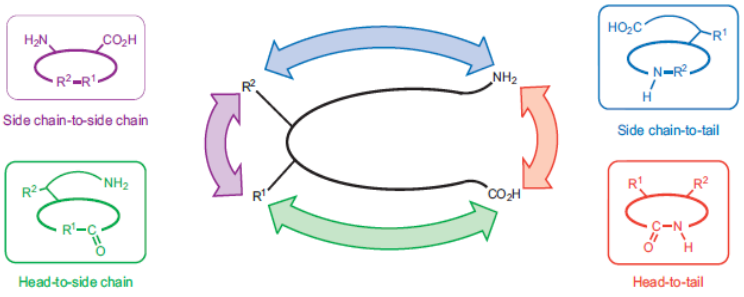

Figure 6. The four possible ways a peptide can be constrained in a macrocycle. Figure reprinted from ref.[17].

The synthesis of cyclic peptides, also called macrocyclization, is generally considered a significant synthetic challenge.[17]

Indeed, the macrocyclization step is usually characterized by low yields, as affected by several factors including the ring size, peptide sequence and the reaction conditions,[20] and often requires high dilution conditions to avoid the formation of dimers, trimers and oligomers. Depending on its functional groups, a peptide can be cyclized in four different ways: (*i*) head-to-tail (*C*-terminus to *N*-terminus), (*ii*) head-to-side chain, (*iii*) side chain-to-tail or (*iv*) side-chain-to-side-chain (Fig. 6). Traditional methodologies, such as lactamization, lactonization and the formation of a disulfide bridge, are among the most utilized approaches of synthesizing cyclic peptides,[16,17] but, over the years, a number of reactions have been developed for the synthesis of macrocyclic structures, such as, for example: azide-alkyne cycloadditions, ring-closing metathesis and multicomponent macrocyclization strategies.[21,22]

In addition to these covalent-bond-based methods, coordination-based approaches may provide alternative strategies for structural constraining of peptides. In a work of 2014,[23] a novel luminogenic peptide cyclization approach was described utilizing histidine-iridium(III) complex coordination chemistry (Fig. 7). Through the coordination of the transition metal iridium(III) to the imidazole group of histidine side chains, an RGD-based peptide, having histidine residues flanking each terminus, was cyclized. The cyclic peptide thus obtained showed very promising biological results demonstrating, among other things, the validity of the coordination-based approaches to provide structural constrained peptides.

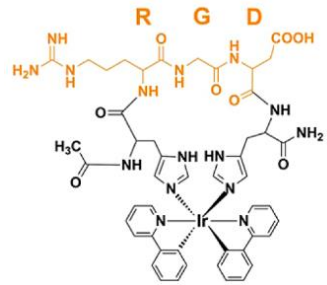

Figure 7. Structure of the cyclic peptide Ir–HRGDH developed by Ma and co-workers in 2014. Ref.[23].

To the best of our knowledge, the coordination between transition metal Pt(II) complexes and *N*-aryl or *S*-donor groups of side chains of suitable amino acids, has never been exploited in order to synthesize potentially bioactive cyclic peptides.

1*b*.2 Aim of the work

In this research work I reported the first use of a coordination-based approach to provide cyclic peptides, exploiting the binding properties of platinum(II) *versus* *N*-heteroaryl and *S*-donors groups to cyclize RGD-based pentapeptides. As well-known, the RGD sequence is a universal cell-recognition sequence of several extracellular matrix proteins bound to integrins, which are involved in different important physiologically processes like cell differentiation, platelet aggregation and tumour metastasis.[24] Incorporation of this sequence into cyclic pentapeptides could lead to useful bioactive compounds.

1*b*.3 Results and Discussion

During my six months-period abroad, spent in the research group led by Prof. Matteo Zanda at the IMS (Institute of Medical Sciences, Aberdeen, UK), I was involved in a research project aimed at the chemical synthesis of a collection of diverse square planar platinum(II) complexes, as shown in Figure 8.

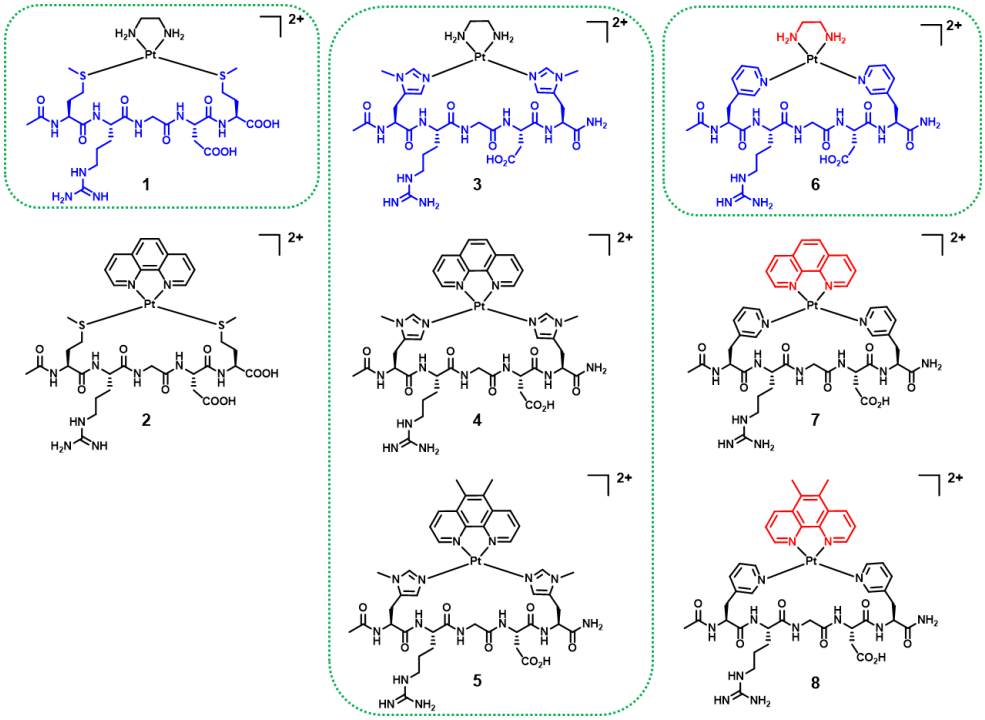

Figure 8. Platinum(II)-peptide complexes under investigation in this study. The compounds enclosed in dashed green boxes were synthesized, isolated by RP-HPLC purification (as TFA salts) and characterized by ES-MS analysis and NMR spectroscopy.

These compounds were designed based on the following structural criteria: they are all characterized by a central Pt(II) metal ion, which forms coordinative bonds with two bidentate neutral ligands. One ligand consists in the linear peptide sequence to be cyclised, in order to obtain the corresponding cyclic peptide; for this purpose, three different RGD-based pentapeptide sequences were considered, possessing Pt(II) coordinative groups in the side chains of the two amino acids flanking each terminus of the RGD motif. Concerning the second ligand, it was decided to investigate three different bidentate molecules: 1,2-ethanediamine (en), 1,10-phenanthroline (phen) and its *bis*-methylated derivative, namely 5,6-dimethyl-1,10-phenanthroline, (5,6-Me_2-phen). In particular, compounds **1** and **2** feature the presence of a Ac-MRGDM-OH pentapeptide coordinated to a Pt(II)-en (compound **1**) or Pt(II)-phen (compound **2**) moiety; compounds **3**, **4** and **5** are characterized by the Ac-(Me)HRGD(Me)H-$CONH_2$ pentapeptide sequence coordinated to a Pt(II)-en (compound **3**), Pt(II)-phen (compound **4**), or Pt(II)-Me_2phen (compound **5**) moiety. Compounds **6**, **7** and **8** feature the presence of a Ac-(Py)ARGD(Py)A-$CONH_2$ pentapeptide sequence coordinated to a Pt(II)-en (compound **6**), Pt(II)-phen (compound **7**), or Pt(II)-Me_2phen (compound **8**) moiety, respectively.

Initial successful synthetic results were obtained by Dr. Chiara Zanato, a postdoctoral research member of the Zanda's group, who synthesized the prototypical compound **1** in a good 51% isolated yield, as a TFA salt. In these initial studies, concerns arose during the synthesis of compounds **2**, **7** and **8**; indeed their formation was observed during the monitoring of the respective cyclization reactions, but it was not possible to isolate them, likely because of their instability under the purification conditions.

All the coordination complexes presented in Figure 8 are square planar species, due to the presence of the Pt(II) centre. Since both ligands which form coordinative bonds with the central metal ion are neutral, the synthesized platinum(II) complexes possess a double positive charge, that of the central Pt(II) ion. Indeed, as previously seen for cisplatin, the substitution of two negatively charged ligands (chloride ions) with two neutral water molecules led to the formation of positively charged complexes.[1]

In order to explore the potential of platinum(II) as bivalent linker to cyclise peptide sequences of interest, which contain amino acids with suitable coordinating sites, it was decided to start the study by exploiting the same cisplatin-type complex, [Pt(en)Cl_2], already seen and used in several bioconjugation reactions,[9–13] and endowed with the 1,2-ethanediamine bidentate ligand.

Moreover, it was also decided to evaluate Pt(II) coordination properties when platinum(II) is complexed with other type of bidentate ligands, such as phenanthrolines. 1,10-Phenanthroline (phen) is a classic ligand in coordination chemistry, which has been extensively used as a chemically versatile module exhibiting a fortunate combination of structural and chemical properties.[25,26] Phen is a rigid planar, hydrophobic, electron-poor heteroaromatic system characterized by two inward-pointing nitrogen donor atoms, beautifully placed to act cooperatively in cation binding. Despite the lower σ-donor ability of its nitrogen atoms, in agreement with the electron-poor characteristics of the heteroaromatic rings, phen ligand displays a noticeable coordination ability for transition metals and the resulting complexes show great stability.
Taking advantage of their peculiar structural features (such as planarity, rigidity and hydrophobicity), phen derivatives have been used to form metallointercalators, in which the planar heteroaromatic system use π-π stacking and dipole-dipole interactions to intercalate between base pairs in double-stranded DNA.[1,25] Metallointercalators can unwind, bend, and distort DNA topology, and it is their structural effect on DNA that is thought to mediate their antiproliferative properties. Systematic studies of charged platinum(II) complexes of general formula $[Pt(I_L)(A_L)]^{2+}$, where I_L is an *intercalating ligand* and A_L is an *ancillary ligand*, have yielded to some of the most promising results.[27] Combinations of phenanthroline-based ligands (I_L) and 1,2-diaminocycloalkane ligands (A_L) gave impressive cytotoxicities against L1210 murine leukemia cells. The most cytotoxic complex of this group possesses a 5,6-dimethyl-1,10-phenanthroline as the intercalating ligand. Another important property of 1,10-phenanthrolines is connected to their propensity to afford luminescent molecules.[26] The unmodified 1,10-phenanthroline nucleus is a weakly fluorescent compound but, following several routes, it can be variously substituted giving a wide range of highly luminescent phenanthroline compounds with emission bands ranging from the UV to the near infrared region (NIR). Suitably designed phenantroline ligands could thus be used in a variety of biological applications, for instance as biological probes.

- **Synthesis of linear peptides 9-11**

Concerning the peptide ligands to be cyclized, three linear RGD-based pentapeptide sequences were firstly synthesized (compounds **9**, **10** and **11**, Scheme 1), having three different amino acid couples at the *N*- and *C*-terminus of the RGD core, endowed of platinum(II) coordinating groups on their side chains.

As already said in the introduction, Pt(II) shows high reactivity mainly with sulfur containing groups, such as free thiols in cysteine (Cys, C) and the thioether sulphur in methionine (Met, M), or the imidazole nitrogen atoms of histidine (His, H).[5,13] In order to exploite the Pt(II) binding capability toward *N*-heteroaryl and *S*-donor groups, we used the following three amino acids: (*i*) Met, that can coordinate platinum(II) by the side chain thioether sulphur; (*ii*) N^1-methyl-His, which can coordinate Pt(II) only through the N^3 of the imidazole ring; and (*iii*) a modified L-alanine (Ala, A), (3-pyridyl)-Ala, having a nonconventional pyridyl coordinating group. The pyridine group seems to be very effective as Pt(II)-coordinating group, as shown in the work of Waalboer et al.[13]

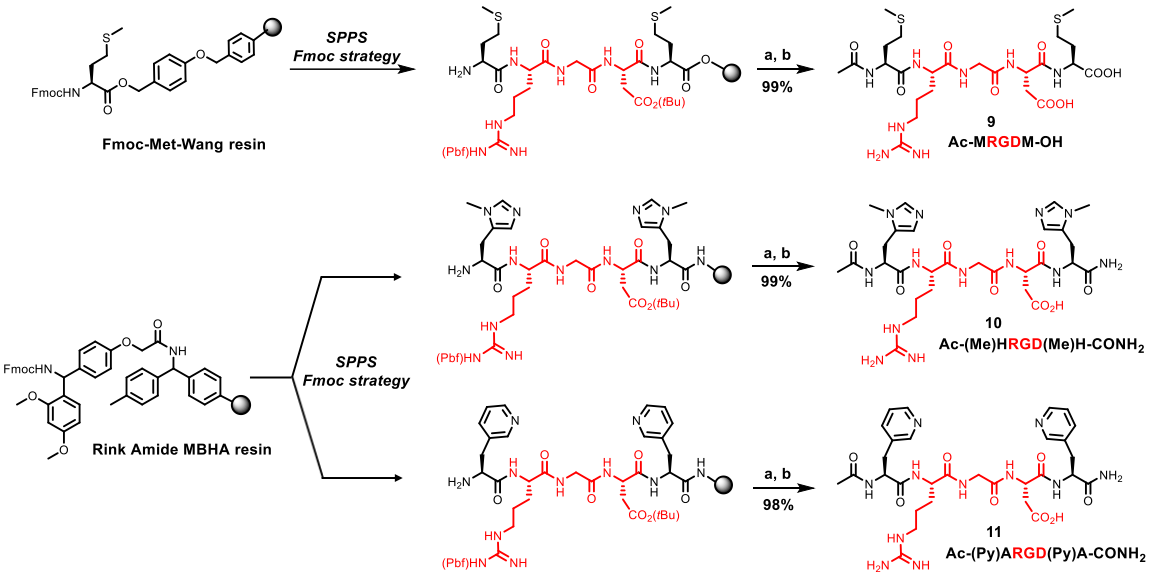

Scheme 1. SPPS Fmoc strategy: (Fmoc cleavage) 20% piperidine in DMF, rt, 10 min. (Coupling) Fmoc-amino acid, HATU, DIPEA, DMF, rt, 2 h (2x). *Sequence of addition for **9***: Fmoc-Asp(O*t*Bu)-OH, Fmoc-Gly-OH, Fmoc-Arg(Pbf)-OH, Fmoc-Met-OH. *Sequence of addition for **10***: Fmoc-3-methyl-L-histidine, Fmoc-Asp(O*t*Bu)-OH, Fmoc-Gly-OH, Fmoc-Arg(Pbf)-OH, Fmoc-3-methyl-L-histidine. *Sequence of addition for **11***: Fmoc-β-(3-pyridyl)-Ala-OH, Fmoc-Asp(O*t*Bu)-OH, Fmoc-Gly-OH, Fmoc-Arg(Pbf)-OH, Fmoc-β-(3-pyridyl)-Ala-OH. **a)** (Acetylation) DCM/acetic anhydride/DIPEA 20:4:1, rt, 2 h. **b)** (Cleavage) TFA/TIS/H_2O-95:2.5:2.5, rt, 2 h (2x).

For the synthesis of the three RGD-based pentapeptide sequences **9**-**11**, the SPPS Fmoc-strategy was followed, using two different types of acid-labile resins, the Fmoc-Met preloaded Wang resin or a Rink-amide resin (Scheme 1). Peptide **9** was assembled starting from the commercially available Fmoc-Met preloaded Wang resin while, for the synthesis of compounds **10** and **11**, a Rink-amide resin was used, on which it was necessary to install the unusual Fmoc-3-methyl-L-histidine and Fmoc-β-(3-pyridyl)-Ala-OH amino acids, respectively. The Fmoc-protected amino acids were coupled in sequence using HATU as a coupling agent. Once added the last amino acid and performed the last basic cleavage (Fmoc deprotection), the NH_2 group at the *N*-terminus of each linear peptide sequence was masked by acetylation. We selected the acid-labile *t*Bu and Pbf (Pbf = 2,2,4,6,7-pentamethyldihydrobenzofurane) groups to protect aspartate (Asp, D) and arginine (Arg, R) side chains respectively, which could be removed simultaneously during the cleavage of the linear precursors from the resin. After the acid treatment, the detachment from the Wang resin released compound **9** with a free COOH group at the *C*-terminus, while the cleavage from the Rink-amide resin produced compounds **10** and **11**, in which the terminal COOH group was substituted by an amide.

- **Cyclization reactions**

The exploration of this new coordination-based cyclization strategy started using the commercially available [Pt(en)Cl_2] complex, in the attempt to cyclize the RGD-based pentapeptide **9** through the formation of coordination bonds between Pt(II) and the sulphur atoms of thioether groups of the two Met residues.

The following synthetic procedure is an adjustment of the "general procedure for the synthesis of Pt(II) complexes" reported by Waalboer et al.[13] First of all, [Pt(en)Cl_2] was treated with silver nitrate ($AgNO_3$, 2 equiv), an effective reagent for replacing halides with nitrates, that are more effective leaving groups (Scheme 2). This activation reaction occurs in a minimum amount of dry DMF and required 16 h of stirring in the dark, leading to the formation of a pale yellow solution and a white-grey AgCl precipitate. After removal of the insoluble AgCl salt, by filtration of the reaction mixture over Celite, the linear peptide **9** was added to the solution of the activated Pt(II) complex, [Pt(en)$(NO_3)_2$].

The cyclization reaction was monitored by LC/MS analysis and once no increase in conversion was observed, in this case after 12 h of stirring, the reaction solvent was removed by freeze-drying procedure. Compound **1** was obtained in a good isolated yield (51%, as TFA salt) by reverse phase-HPLC purification.

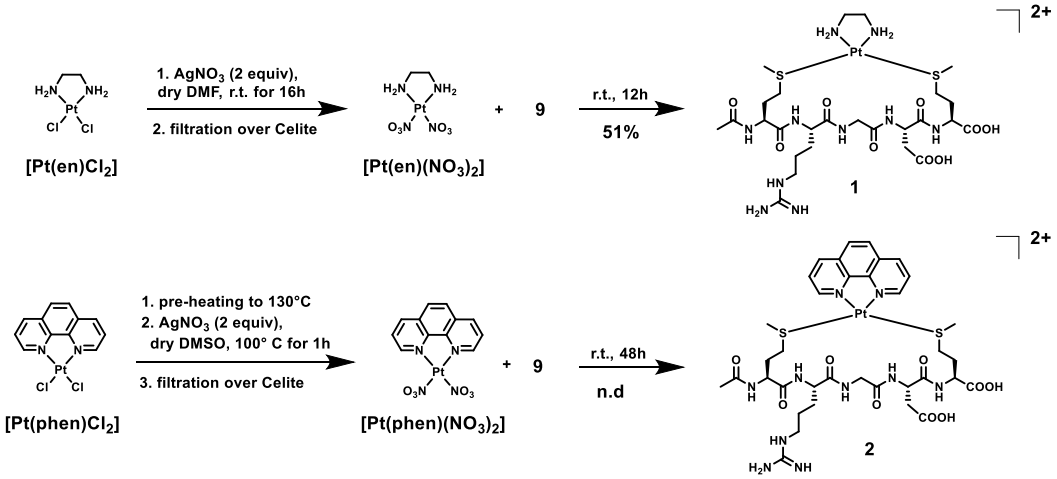

Scheme 2. Synthetic procedure of [Pt(en)(**9**)]$^{2+}$ (compound **1**) and [Pt(phen)(**9**)]$^{2+}$ (compound **2**) complexes, as TFA salts.

Encouraged by this success, we tried to cyclize compound **9** using the commercially available [Pt(phen)Cl_2] complex. As previously said, the phen ligand can represent an interesting starting point, in particular toward the development of phenantroline-based luminescent molecules, which could lead to the development of potential imaging agents. Disappointingly, by following the aforesaid synthetic procedure, during the activation step, the white-grey precipitate of AgCl salt was just formed in traces. After some failed synthetic attempts, in which modified activation procedures were tried (for example: using increased amounts of silver nitrate or heating the reaction mixture up to 40 °C), alternative activation procedures were attempted by adapting a synthetic protocol found in literature.[28] Thus, suspending the [Pt(phen)Cl_2] complex in dry DMSO and then heating the reaction system until 130 °C, the formation of a very fine yellow suspension was observed, almost resembling a very dense yellow solution. After the addition $AgNO_3$ (2 equiv) the reaction system immediately produced a white-grey precipitate of AgCl and a pale yellow solution. The reaction mixture was left to stir for 1 h at 100 °C and then, after filtration over Celite, peptide **9** was added (Scheme 2). LC-MS monitoring of the reaction revealed the formation of compound **2** and, after reaction completion, the solvent was removed by freeze-drying. However, after RP-HPLC purification, it was not possible to recover compound **2**, likely because intrinsically unstable. Further RP-HPLC purification attempts of compound **2** were performed, but the compound still continued to show impurities. These experimental observations led us to conclude that compound **2** is coordinatively unstable.

Given this structural instability, the reaction using the Pt(II) complex bearing the analogous bis-methylated phenantrolin ligand, [Pt(5,6-Me_2-phen)Cl_2], was not attempted. The quite different stability of Pt(II) complexes **1** and **2** could be certainly due to the different properties of the en vs phen ligands (given their very different structure), but it could be overcome by a judicious choice of the coordinating amino acid residues of the peptide.

Indeed, a number of studies indicate that binding of platinum(II) to methionine is kinetically controlled, whereas the binding toward histidine is thermodynamically controlled.[5,13,29,30] Therefore, in principle, Pt(II) complexes with His coordinating sites should be more stable than the complexes with Met, even if the rate of their formation should be slower. However, the imidazole ring of Hys side chain provides a bidentate ligand, having two competitive donor atoms. Thus, in order to avoid the formation of both possible N^1 and N^3 linkage isomers during the coordination-based cyclization strategy with platinum(II) complexes, the two His residues of RGD-based pentapeptide **10** bear an N^1-methylated imidazole ring.

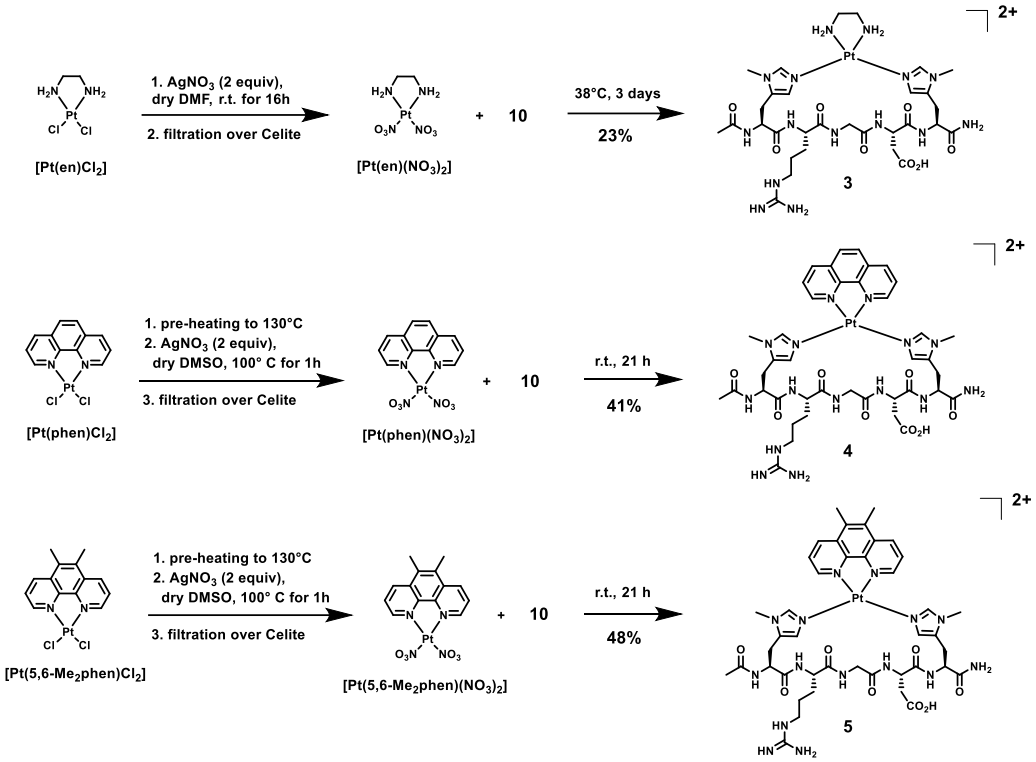

Scheme 3. Synthesis of [Pt(en)(**10**)]$^{2+}$ (compound **3**), [Pt(phen)(**10**)]$^{2+}$ (compound **4**), and [Pt(5,6-Me$_2$-phen)(**10**)]$^{2+}$ (compound **5**) complexes, as TFA salts.

For the synthesis of compound **3**, the synthetic procedure used for the preparation of compound **1** was followed. The rate of the cyclization reaction proved to be actually slower than compound **1**, and required heating (up to 40 °C, to avoid the possible degradation of the linear peptide). However, the reaction did not go to completion and, after RP-HPLC purification, compound **3** was recovered in a low cyclisation yield (23%) as TFA salt (Scheme 3).

For the synthesis of compound **4**, instead, the procedure optimized during the preparation of compound **2** was followed. In this instance, the cyclization reaction to complex **4** proceeded better than **3**; it went to completion after 21 hours at room temperature, giving the desired product in a moderate 41% isolated yield, as TFA salt.

As the Pt(II) complex with 5,6-dimethyl-1,10-phenanthroline, [Pt(5,6-Me$_2$-phen)Cl$_2$], is not commercially available, it was easily synthesized by starting from compounds K_2PtCl_4 and (5,6-Me$_2$-phen), by following literature procedures (see the experimental part).[31,32] By paralleling the same procedure used for compound **4**, complex **5** was obtained in a quite good 48% isolated yield (TFA salt) after two sequential RP-HPLC purification steps. All the isolated compounds **3-5** were characterized by NMR spectroscopy (^{1}H, COSY, ^{13}C, HSQC and ^{195}Pt) and ESI-MS analysis, and proved to be >98% pure compounds.

In the previous mentioned work by Waalboer et al.,[13] among a set of NMD ligands toward the [Pt(en)Cl$_2$] complex, pyridine group seems to be very effective as Pt(II)-coordinating group. Thus, we decided to carry out the coordination-based cyclization strategy with platinum(II) complexes using the RGD-based pentapeptide **11**, which possesses two (3-pyridyl)-L alanine residues, at both the *N*- and *C*-terminus of the RGD core (Scheme 4).

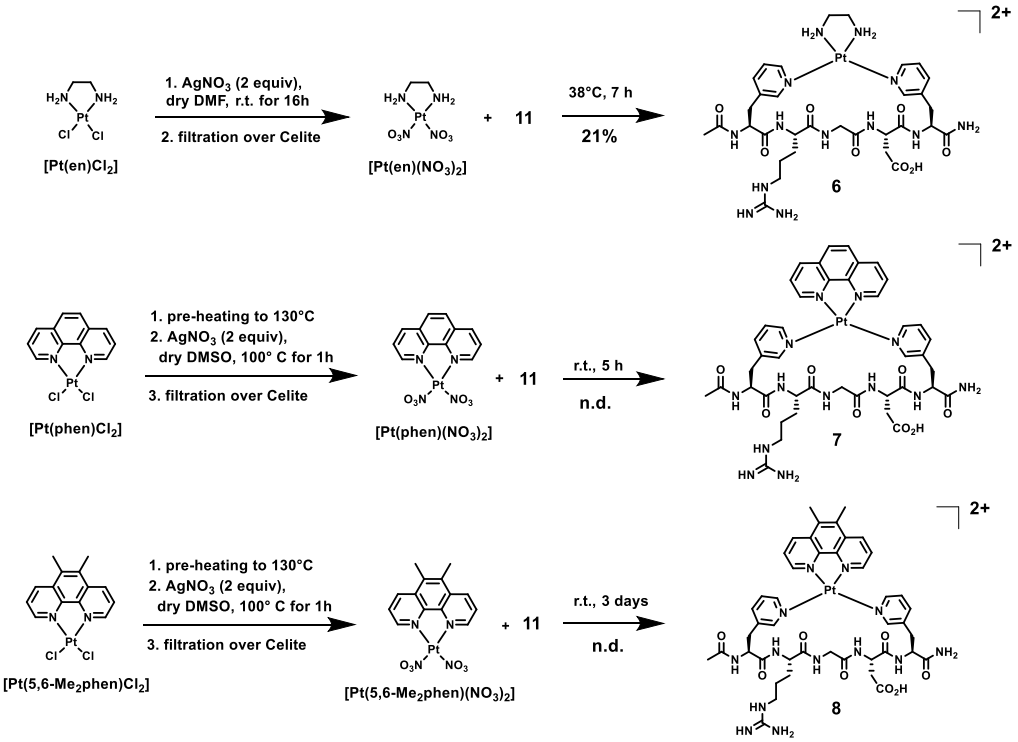

Scheme 4. Synthesis of [Pt(en)(**11**)]$^{2+}$ (compound **6**), [Pt(phen)(**11**)]$^{2+}$ (compound **7**), [Pt(5,6-Me$_2$-phen)(**11**)]$^{2+}$ (compound **8**) complexes, as TFA salts.

Compound **6** was obtained by following the same synthetic procedure shown for the synthesis of the complexes **1** and **3**, all sharing the 1,2-ethylendiamine ligand. Also in this case, the cyclization step was carried out at 38 °C, and proved faster than before; it went to completion in seven hours, as revealed by LC-MS monitoring. After removal of the solvent by freeze-drying and RP-HPLC purification, compound **6** was recovered in a 21% isolated yield, as TFA salt. Compounds **6** was characterized by NMR spectroscopy (^{1}H, COSY, ^{13}C, HSQC and ^{195}Pt) and ESI-MS analysis.

Concerning the synthesis of compounds **7** and **8**, as seen for compound **2**, it proved to be unsuccessful. Despite the LC-MS monitoring of the cyclization step revealed the formation of the desired target compounds and the progressive disappearance of the limiting reagent (peptide **11**) during the progression of the reaction, no pure compound could be obtained after removal of the solvent by freeze-drying and subsequent RP-HPLC purification, demonstrating an intrinsic instability for these products. Indeed, analysis of the impurities present after the purification step revealed that some of them showed the isotopic pattern of Pt. Further RP-HPLC purification attempts of compounds **7** and **8** were performed, but both compounds still continued to show impurities. These experimental observations led us to conclude that these types of Pt(II) complexes are unstable.

1*b*.4 Conclusions

In conclusion, conditions were found to achieve the preparation of four new cyclopeptides where different bidentate amine ligands and diverse RGD-based peptide sequences coordinate to a central Pt(II) metal ion. Crucial for optimal cyclization was the judicious choice of the coordinating groups within the peptide chain, with histidine moieties giving the best results in terms of cyclization efficiency. Some preliminary biological assays on the synthesized cyclopeptides were performed, including cytotoxicity and cell adhesion tests; the results of the biological evaluation are not reported here due to the very preliminary character of the collected data.

This work represents one rare example of coordination-based approach where the platinum(II) ion may exert a double function: *i*) to favour peptide cyclization by exploiting its coordinative ability; and *ii*) to furnish peptide-Pt(II) complexes endowed of potential biological activity.

1*b*.5 Experimental Part

Experimental synthetic procedures and characterization data

General. All chemicals were of the highest commercially available quality and were used as such without further purification. Reactions requiring anhydrous conditions were performed under nitrogen atmosphere using commercially available anhydrous solvents. Rink Amide MBHA resin LL (100-200 mesh), Rink Amide MBHA resin HL (100-200 mesh) and Fmoc-amino acids were purchased from Novabiochem (Merck). Platinum(II) complexes used as starting materials were purchased from Sigma-Aldrich (Merck). All other reagents were purchased from Alfa Aesar, TCI, or Sigma-Aldrich (Merck). ^{1}H NMR, ^{13}C NMR and ^{195}Pt NMR spectra were recorded on a Bruker AVANCE III 400 NMR spectrometer. Chemical shifts (δ) are reported in parts per million (ppm) with HOD resonance peaks set at 4.80 ppm. Multiplicities are indicated as s (singlet), d (doublet), t (triplet), q (quartet), m (multiplet), and b (broad). Coupling constants, *J*, are reported in Hertz. ^{1}H and ^{13}C NMR assignments were corroborated by 1D and 2D experiments (gCOSY and gHSQC sequences). Mass analyses were performed using Agilent 1200 HPLC system coupled to Agilent G6120 single quadrupole detector equipped with an electrospray ionization (ESI) source in direct infusion modality. ESI-MS spectra were recorded in positive mode. RP (reverse phase) HPLC-MS analyses were performed with an Agilent 1200 HPLC system equipped with a DAD and an ESI-MS detector. HPLC conditions for analytical analyses: Phenomenex Luna C18 column, 5 µm, 100 Å, 250 × 4.6 mm (L × ID), inj. volume 20 µL, flow rate 1 mL/min. HPLC conditions for preparative purification: Phenomenex Luna C18 column, 5 µm, 100 Å, 250 × 21.6 mm (L × ID), flow rate 20 mL/min.

Abbreviations. Boc, *tert*-butoxycarbonyl; Pbf, 2,2,4,6,7-pentamethyldihydrobenzofuran-5-sulfonyl; Fmoc, 9-fluorenylmethoxycarbonyl; SPPS, solid phase peptide synthesis; DCM, dichloromethane; DMF, N,Ndimethylformamide; DMSO, dimethyl sulfoxide; Et_2O, ethyl ether; DIPEA, diisopropylethylamine; TFA, trifluoroacetic acid; Ac_2O, acetic anhydride; TIS, triisopropylsilane; HATU, O-(7-azabenzotriazol-1-yl)-N,N,N′,N′,N′-tetramethyluronium hexafluorophosphate; en, 1,2-ethanediamine; phen, 1,10-phenanthroline; 5,6-Me_2-phen, 5,6-Dimethyl-1,10-phenanthroline; [Pt(en)Cl_2], dichloro(ethylenediamine)platinum(II).

Starting Materials. Fmoc-Met-Wang resin (100-200 mesh), Rink Amide MBHA resin LL (100-200 mesh), Rink Amide MBHA resin HL (100-200 mesh), Fmoc-3-methyl-L-histidine, Fmoc-Asp(O*t*Bu)-OH, Fmoc-Gly-OH, Fmoc-Arg(Pbf)-OH, Fmoc-*β*-(3-pyridyl)-Ala-OH, $Ag(NO)_3$, K_2PtCl_4, 5,6-Dimethyl-1,10-phenanthroline, dichloro(ethylenediamine)platinum(II), and dichloro(1,10-phenanthroline)platinum(II) were commercially available and were used as such without further purification.

Ac-MRGDM-OH (9)

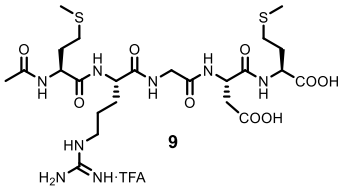

The synthesis of linear pentapeptide Ac-MRGDM-OH (**9**) was performed using the preloaded Fmoc-Met-Wang resin (loading 0.64 mmol/g). *Resin swelling*: the resin (84 mg, 0.13 mmol, 1 equiv) was swollen in a solid phase reaction vessel with dry DMF (2 mL) under mechanical stirring; after 40 min the solvent was drained and the resin was washed with DCM (2 ×) and DMF (2 ×). *Fmoc deprotection*: the resin was treated with 20% v/v piperidine in DMF (2 mL) and the mixture was shaken for 20 min. The solution was drained and the resin was washed with DCM (2 ×) and DMF (2 ×). *Peptide coupling*: a preformed solution of Fmoc-(N^3-methyl)-Hys-OH (68 mg, 0.17 mmol, 2 equiv) in dry DMF (2 mL) was treated with HATU (66 mg, 0.17 mmol, 2 equiv) and DIPEA (61 µL, 0.35 mmol, 4 equiv) and stirred for 5 min before adding to the resin. The mixture was shaken at room temperature for 2 h. The solution was drained and the resin was washed with DCM (3 ×) and DMF (3 ×). The peptide coupling was repeated a second time. Completion of the reaction was checked by the Kaiser test (see Experimental Part, Chapter 1*a*). The solution was drained and the resin was washed with DCM (3 ×) and DMF (3 ×). The resin was treated with 20% v/v piperidine in DMF (2 mL) and the mixture was stirred for 30 min. The solution was drained and the resin was washed with DCM (2 ×) and DMF (2 ×).

The coupling of the Fmoc-Asp(*t*Bu)-OH (72 mg, 0.17 mmol, 2 equiv), Fmoc-Gly-OH (52 mg, 0.17 mmol, 2 equiv), Fmoc-Arg(Pbf)-OH (113 mg, 0.17 mmol, 2 equiv) and Fmoc-(N^3-methyl)-Hys-OH (68 mg, 0.17 mmol, 2 equiv) were carried out under the same conditions. *Acetylation*: after the last coupling procedure, a solution of DCM/Acetic anhydride/DIPEA (20:4:1) (2.5 mL) was added to the resin. The mixture was shaken at room temperature for 1 h, then was drained and the resin was washed with DCM (2 ×) and DMF (2 ×). This protocol was repeated twice. *Resin cleavage*: the resin was finally treated with 2.5 mL of the cleavage mixture TFA/TIS/H_2O (95:2.5:2.5) kept under mechanical stirring for 2 h at room temperature. The solution was recovered and the resin was carefully washed with DCM (4 ×). The combined solution was concentrated (by N_2 flux) and Et_2O was added to precipitate the crude peptide.
The linear pentapeptide **9** was lyophilized and obtained as a bulky white solid (70 mg, as TFA salt, 99% yield based on the estimated loading of the resin), which was used in the following step without further purification. MS (ESI$^+$) *m/z* = 690.3 $[M+H]^+$.

Ac-(Me)HRGD(Me)H-CONH$_2$ (10)

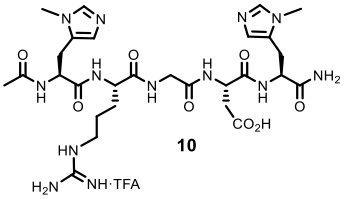

The synthesis of linear pentapeptide Ac-(N^3-methyl)-Hys-Asp(*t*Bu)-Arg(Pbf)-Gly-(N^3-methyl)-Hys-$CONH_2$ (**10**) was performed using the Rink Amide MBHA resin LL (substitution 0.56 mmol/g). *Resin swelling*: the resin (155 mg, 0.09 mmol, 1 equiv) was swollen in a solid phase reaction vessel with dry DMF (2 mL) under mechanical stirring; after 40 min the solvent was drained and the resin was washed with DCM (2 ×) and DMF (2 ×). *Fmoc deprotection*: the resin was treated with 20% v/v piperidine in DMF (2 mL) and the mixture was shaken for 20 min. The solution was drained and the resin was washed with DCM (2 ×) and DMF (2 ×). *Peptide coupling*: a preformed solution of Fmoc-Asp(*t*Bu)-OH (108 mg, 0.26 mmol, 2 equiv) in dry DMF (2 mL) was treated with

HATU (99 mg, 0.26 mmol, 2 equiv) and DIPEA (91 µL, 0.52 mmol, 4 equiv) and stirred for 5 min before adding to the resin. The mixture was shaken at room temperature for 2 h. The solution was drained and the resin was washed with DCM (3 ×) and DMF (3 ×). The peptide coupling was repeated a second time. Completion of the reaction was checked by Kaiser test. The solution was drained and the resin was washed with DCM (3 ×) and DMF (3 ×). The resin was then treated with 20% v/v piperidine in DMF (2 mL) and the mixture was stirred for 30 min. The solution was drained and the resin was washed with DCM (2 ×) and DMF (2 ×). The coupling of the Fmoc-Gly-OH (78 mg, 0.26 mmol, 2 equiv), Fmoc-Arg(Pbf)-OH (170 mg, 0.26 mmol, 2 equiv) and Fmoc-Met-OH (97 mg, 0.26 mmol, 2 equiv) were carried out under the same conditions. *Acetylation*: after the last coupling procedure, a solution of DCM/Acetic anhydride/DIPEA (20:4:1) (2.5 mL) was added to the resin. The mixture was shaken at room temperature for 1 h, then was drained and the resin was washed with DCM (2 ×) and DMF (2 ×).This protocol was repeated twice. *Resin cleavage*: the resin was finally treated with 2.5 mL of the cleavage mixture TFA/TIS/H_2O (95:2.5:2.5) kept under mechanical stirring for 2 h at room temperature. The solution was recovered and the resin was carefully washed with DCM (4 ×). The combined solution was concentrated (by N_2 flux) and Et_2O was added to precipitate the crude peptide.

The linear pentapeptide **10** was lyophilized and obtained as a bulky white solid (99 mg, as TFA salt, 99% yield based on the estimated loading of the resin), which was used in the following step without further purification. MS (ESI^+) *m/z* = 690.4 $[M+H]^+$.

Ac-(Py)ARGD(Py)A-$CONH_2$ (11)

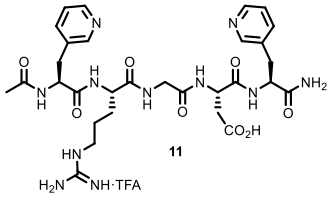

11

The synthesis of linear pentapeptide Ac-(3-pyridyl)-Ala-Asp(*t*Bu)-Arg(Pbf)-Gly-(3-pyridyl)-Ala-$CONH_2$ (**11**) was performed using the Rink Amide MBHA resin HL (substitution 0.87 mmol/g). *Resin swelling*: the resin (100 mg, 0.09 mmol, 1 equiv) was swollen in a solid phase reaction vessel with dry DMF (2 mL) under mechanical stirring; after 40 min the solvent was drained and the resin was washed with DCM (2 ×) and DMF (2 ×). *Fmoc deprotection*: the resin was treated with 20% v/v piperidine in DMF (2 mL) and the mixture was shaken for 20 min. The solution was drained and the resin was washed with DCM (2 ×) and DMF (2 ×). *Peptide coupling*: a preformed solution of Fmoc-(3-pyridyl)-Ala-OH (68 mg, 0.18 mmol, 2 equiv) in dry DMF (2 mL) was treated with HATU (67 mg, 0.18 mmol, 2 equiv) and DIPEA (61 µL, 0.35 mmol, 4 equiv) and stirred for 5 min before adding to the resin. The mixture was shaken at room temperature for 2 h. The solution was drained and the resin was washed with DCM (3 ×) and DMF (3 ×). The peptide coupling was repeated a second time. Completion of the reaction was checked by the Kaiser test. The solution was drained and the resin was washed with DCM (3 ×) and DMF (3 ×). The resin was treated with 20% v/v piperidine in DMF (2 mL) and the mixture was stirred for 30 min. The solution was drained and the resin was washed with DCM (2 ×) and DMF (2 ×). The coupling of the Fmoc-Asp(*t*Bu)-OH (72 mg, 0.18 mmol, 2 equiv), Fmoc-Gly-OH (52 mg, 0.18 mmol, 2 equiv), Fmoc-Arg(Pbf)-OH (114 mg, 0.18 mmol, 2 equiv) and Fmoc-(3-pyridyl)-Ala-OH (68 mg, 0.18 mmol, 2 equiv) were carried out under the same conditions. *Acetylation*: after the last coupling procedure, a solution of DCM/Acetic anhydride/DIPEA (20:4:1) (2.5 mL) was added to the resin. The mixture was shaken at room temperature for 1 h, then was drained and the resin was washed with DCM (2 ×) and DMF (2 ×).This protocol was repeated twice. *Resin cleavage*: the resin was finally treated with 2.5 mL of the cleavage mixture TFA/TIS/H_2O (95:2.5:2.5) kept under mechanical stirring for 2 h at room temperature. The solution was recovered and the resin was carefully washed with DCM (4 ×). The combined solution was concentrated (by N_2 flux) and Et_2O was added to precipitate the crude peptide.

The linear pentapeptide **11** was lyophilized and obtained as a bulky white solid (69 mg, as TFA salt, 98% yield based on the estimated loading of the resin), which was used in the following step without further purification. MS (ESI$^+$) *m/z* = 684.3 $[M+H]^+$.

[Pt(en)(10)](CF$_3$CO$_2$)$_2$, compound 3:

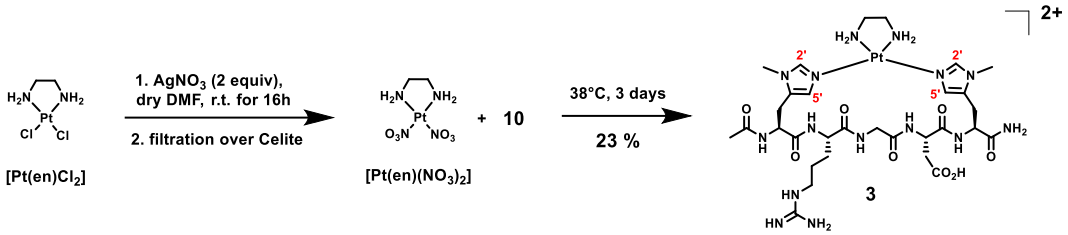

$[Pt(en)Cl_2]$ (4.7 mg, 0.01 mmoL, 1 equiv) was reacted with $AgNO_3$ (4.9 mg, 0.03 mmoL, 2 equiv) in dry DMF (0.2 mL) for 16 h in the dark and nitrogen atmosphere. The suspension was filtered over Celite and the filter rinsed with dry DMF (0.2 mL, 2 ×). The linear peptide **10** (12 mg, as TFA salt, 0.01 mmoL, 1 equiv) was then added as a solid to the filtrate and the mixture was degassed by nitrogen/ vacuum cycles (3 ×) and left to stir in the dark at 38 °C for 72 h. The reaction was monitored by HPLC-MS analysis and once no increase in conversion was observed, the reaction mixture was frozen and lyophilized. The resulting white solid (12.2 mg) was purified by preparative RP-HPLC (Solvent A: H_2O 0.1% TFA, Solvent B: CH_3CN 0.1% TFA, flow 20 mL/min, detection 210 nm) using the following gradient elution: 0 - 15 min, 5 -25% B; R_t = 7.3 min. The purified compound **3** was lyophilized and obtained as a white powder (3.9 mg, as TFA salt, 23% yield).

^{1}H NMR (400 MHz, D_2O) δ 7.58 (s, 1H, H2'), 7.51 (s, 1H, H2'), 6.73 (s, 1H, H5'), 6.68 (s, 1H, H5'), 4.70 (m, 1H, Hα Hys$_A$), 4.66-4.61 (m, 2H, Hαa Gly + Hα Hys$_B$), 4.35-4.27 (m, 2H, Hα Asp + Hα Arg), 4.04 (d, *J* = 16.9 Hz, 1H, Hαb Gly), 3.55 (s, 6H, 2·CH_3 Hys), 3.24-3.15 (m, 1H, Hβa Hys$_B$),3.11 (t, *J* = 6.9 Hz, 2H, Hδ Arg), 3.07-2.89 (m, 3H, Hβ Asp + Hβb Hys$_B$), 2.88-2.66 (m, 6H, 2·CH_2 (en) + Hβ Hys$_A$), 1.96 (s, 3H, CH_3 Ac), 1.76-1.40 (bm, 4H, Hβ Arg + Hγ Arg).

^{13}C NMR (100 MHz, D_2O) δ 175.1 (Cq), 174.4 (Cq), 173.9 (Cq), 173.0 (Cq), 172.7 (Cq), 171.9 (Cq), 169.8 (Cq), 156.7 (Cq), 139.6 (CH), 139.4 (CH), 130.0 (Cq), 128.7 (Cq), 127.1 (CH), 125.5 (CH), 53.4 (CH), 52.7 (CH), 50.9 (CH), 49.9 (CH), 47.5 (2C, 2·CH_2 en), 42.8 (CH_2), 40.4 (CH_2), 35.8 (CH_2), 32.1 (CH_3), 32.0 (CH_3), 28.1 (CH_2), 25.1 (CH_2), 24.9 (CH_2), 24.2 (CH_2), 21.5 (CH_3). ^{195}Pt (86 MHz, D_2O) δ -2676.
ESI-MS (m/z) $C_{30}H_{51}N_{15}O_8Pt$ calcd for $[M]^{2+}$ 472.2, found 472.5.

[Pt(phen)(10)](CF$_3$CO$_2$)$_2$, compound 4:

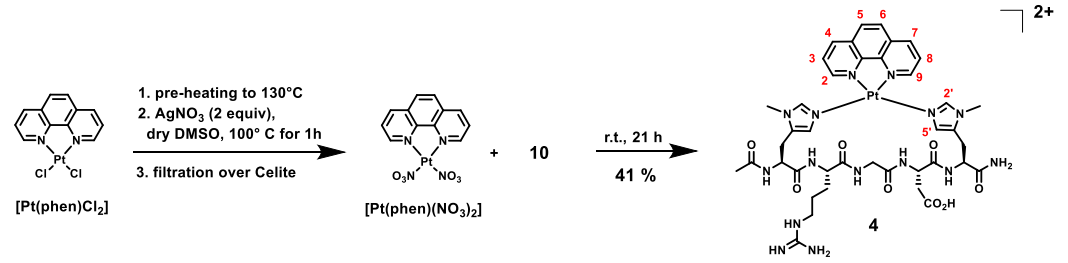

$[Pt(phen)Cl_2]$ (11 mg, 0.02 mmoL, 1 equiv) was dissolved in a minimum amount of dry DMSO (500 µL) with heating at 130 °C. To this fine yellow suspension an amount of $AgNO_3$ (8.2 mg, 0.05 mmoL, 2 equiv) was added twice giving immediately a white-grey precipitate of AgCl and a yellow solution. The mixture was left to stir at 100 °C for 1 h, in the dark and nitrogen atmosphere, and then was filtered over Celite and the filter rinsed with dry DMSO (0.25 mL, 2 ×). The linear peptide **10** (19 mg, as TFA salt, 0.02 mmoL, 1 equiv) was then added as a solid to the filtrate and the mixture was degassed by nitrogen/vacuum cycles (3 ×) and left to stir in the

dark at room temperature for 21 h. The reaction was monitored by HPLC-MS analysis and once no increase in conversion was observed, the reaction mixture was frozen and lyophilized. The resulting white solid was purified by preparative RP-HPLC (Solvent A: H_2O 0.1% TFA, Solvent B: CH_3CN 0.1% TFA, flow 20 mL/min, detection 210 nm) using the following gradient elution: 0 - 20 min, 5 -40% B; R_t = 10.3 min. The purified compound **3** was lyophilized and obtained as a white powder (12.5 mg, as TFA salt, 41% yield).

^{1}H NMR (400 MHz, D_2O) δ 8.88-8.82 (m, 2H, H2 +H9), 8.23-8.19 (d, *J* = 5.1 Hz, 1H, H4 or H7), 8.17 (s, 1H, H2'), 8.12 (s, 2H, H5 + H6), 8.11-8.08 (d, *J* = 5.1 Hz, 1H, H7 or H4), 8.00 (s, 1H, H2'), 7.95-7.87 (m, 2H, H3 + H8), 7.18 (s, 1H, H5'), 7.13 (s, 1H, H5'), 4.72 (m, 2H, Hα Hys_A + Hα Hys_B), 4.53 (t, *J* = 7.2 Hz, 1H, Hα Asp), 4.25 (m, 1H, Hα Arg), 4.10 (d, *J* = 17.1 Hz, 1H, Hαa Gly), 3.72 (s, 6H, 2·CH_3 Hys), 3.58 (d, *J* = 17.1 Hz, 1H, Hαb Gly), 3.36-3.28 (m, 1H, Hβa Hys_A), 3.16-3.00 (m, 5H, Hβ Asp + Hδ Arg + Hβb Hys_A), 2.89-2.80 (m, 1H, Hβa Hys_B), 2.72-2.63 (m, 1H, Hβb Hys_B), 2.01 (s, 3H, CH_3 Ac), 1.71-1.40 (bm, 4H, Hβ Arg + Hγ Arg).

^{13}C NMR (100 MHz, D_2O) δ 174.2 (Cq), 174.0 (Cq), 173.9 (Cq), 173.1 (Cq), 172.3 (Cq), 172.0 (Cq), 170.2 (Cq), 156.7 (Cq), 150.4 (CH), 150.2 (CH), 147.6 (Cq), 147.5 (Cq), 141.1 (CH), 141.0 (CH), 140.0 (CH), 139.7 (CH), 131.3 (Cq), 130.9 (Cq), 130.8 (Cq), 129.9 (Cq), 127.9 (2C, CH), 127.1 (CH), 125.9 (CH), 125.8 (CH), 125.7 (CH), 53.3 (CH), 52.9 (CH), 51.7 (CH), 49.9 (CH), 42.2 (CH_2), 40.5 (CH_2), 34.8 (CH_2), 32.6 (CH_3), 32.5 (CH_3), 27.6 (CH_2), 25.2 (2C, CH_2), 24.3 (CH_2), 21.6 (CH_3). ^{195}Pt (86 MHz, D_2O) δ -2520.
ESI-MS (m/z) $C_{40}H_{51}N_{15}O_8Pt$ calcd for $[M]^{2+}$ 532.2, found 532.4.

Synthesis of [Pt(5,6-Me$_2$-phen)Cl$_2$][31,32]

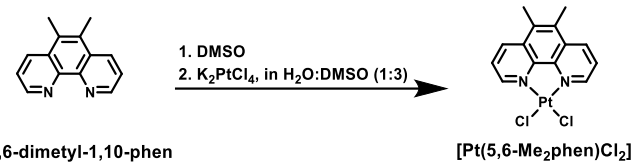

A hot solution of 5,6-Dimethyl-1,10-phenanthroline (35 mg, 0.1686 mmol, 1 equiv) in dimethyl sulfoxide (DMSO, 5 mL) was added to a hot solution of K_2PtCl_4 (70 mg, 0.1686 mmol, 1 equiv) in water (0.5 mL) and DMSO (1.5 mL). On cooling, a fine yellow precipitate of [Pt(5,6-Me$_2$-phen)Cl] formed. This was collected, washed with chilled 1 M HCl, water, ethanol and diethyl ether and then dried under vacuum at 110 °C for 2 h. [Pt(5,6-Me$_2$-phen)Cl] was obtained as yellow solid (77.5 mg, 97% yield).

[Pt(5,6-Me$_2$-phen) (10)](CF$_3$CO$_2$)$_2$, compound 5:

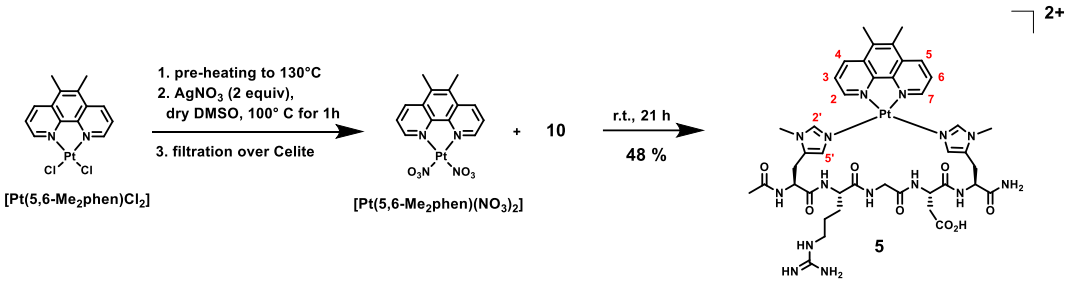

[Pt(phen)Cl$_2$] (10 mg, 0.02 mmoL, 1 equiv) was dissolved in a minimum amount of dry DMSO (500 µL) with heating at 130 °C. To this fine yellow suspension was added twice the stoichiometric amount of $AgNO_3$ (7.2 mg, 0.04 mmoL, 2 equiv), giving immediately a white-grey precipitate of AgCl and a yellow solution. The mixture was left to stir at 100 °C for 1 h, in the dark and nitrogen atmosphere, and then was filtered over Celite and the filter rinsed with dry DMSO (0.25 mL, 2 ×). The linear peptide **10** (17 mg, as TFA salt, 0.02 mmoL, 1 equiv) was then added as a solid to the filtrate and the mixture was degassed by nitrogen/ vacuum cycles (3 ×) and left to stir in the dark at room temperature for 21 h. The reaction was monitored by HPLC-MS

analysis and once no increase in conversion was observed, the reaction mixture was frozen and lyophilized. The resulting white solid was purified by preparative RP-HPLC (Solvent A: H_2O 0.1% TFA, Solvent B: CH_3CN 0.1% TFA, flow 20 mL/min, detection 210 nm) using the following gradient elution: 0 - 17 min, 5 -40% B; R_t = 11.4 min. The purified compound **3** was lyophilized and obtained as a white powder (13.3 mg, as TFA salt, 48% yield).

^{1}H NMR (400 MHz, D_2O) δ 8.91 (t, *J* = 9.2 Hz, 2H, H2 + H9), 8.16-8.10 (m, 2H, H2'+ H4 or H7), 8.06-7.96 (m, 2H, H7 or H4 + H2'), 7.93-7.82 (m, 2H, H3 + H8), 7.19 (s, 1H, H5'), 7.13 (s, 1H, H5'), 4.74 (m, 1H, Hα Hys_A), 4.65 (m, 1H, Hα Hα Hys_B), 4.55 (t, *J* = 7.0 Hz, 1H, Hα Asp), 4.24 (m, 1H, Hα Arg), 4.03 (d, *J* = 17.1 Hz, 1H, Hαa Gly), 3.72 (s, 3H, CH_3 Hys), 3.71 (s, 3H, CH_3 Hys), 3.59 (d, *J* = 17.1 Hz, 1H, Hαb Gly), 3.38-3.28 (m, 1H, Hβa Hys_A), 3.18-3.00 (m, 5H, Hβ Asp + Hδ Arg + Hβb Hys_A), 2.88-2.78 (dd, *J* = 17.1, 7.4 Hz ,1H, Hβa Hys_B), 2.72-2.63 (m, 7H, 2·CH_3 phen + Hβb Hys_B), 2.00 (s, 3H, CH_3 Ac), 1.75-1.39 (bm, 4H, Hβ Arg + Hγ Arg).

^{13}C NMR (100 MHz, D_2O) δ 174.2 (Cq), 174.0 (Cq), 174.0 (Cq), 173.2 (Cq), 172.4 (Cq), 172.0 (Cq), 170.3 (Cq), 156.7 (Cq), 148.9 (CH), 148.8 (CH), 146.3 (Cq), 146.3 (Cq), 139.9 (CH), 139.6 (CH), 138.0 (CH), 137.9 (CH), 132.8 (Cq), 132.7 (Cq), 131.4 (Cq), 131.1 (Cq), 131.0 (Cq), 130.1 (Cq), 127.0 (CH),125.8 (CH), 125.7 (CH), 125.5 (CH), 53.4 (CH), 52.9 (CH), 51.7 (CH), 50.0 (CH), 42.2 (CH_2), 40.4 (CH_2), 34.9 (CH_2), 32.6 (CH_3), 32.4 (CH_3), 27.7 (CH_2), 25.2 (2C, CH_2), 24.3 (CH_2), 21.6 (CH_3), 14.6 (2C, CH_3). ^{195}Pt (86 MHz, D_2O) δ -2538.
ESI-MS (m/z) $C_{42}H_{55}N_{15}O_8Pt$ calcd for $[M]^{2+}$ 546.2, found 546.1.

[Pt(en) (11)]$(CF_3CO_2)_2$, compound 6:

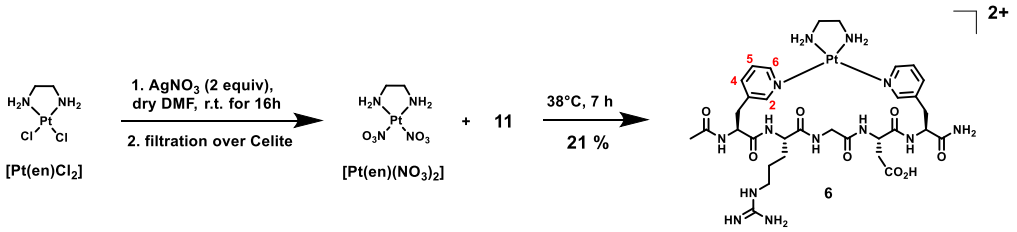

$[Pt(en)Cl_2]$ (6.1 mg, 0.02 mmoL, 1 equiv) was reacted with $AgNO_3$ (6.4 mg, 0.04 mmoL, 2 equiv) in dry DMF (0.2 mL) for 16 h in the dark and nitrogen atmosphere. The suspension was filtered over Celite and the filter rinsed with dry DMF (0.2 mL, 3 ×). The linear peptide **11** (15 mg, as TFA salt, 0.02 mmoL, 1 equiv) was then added as a solid to the filtrate and the mixture was degassed by nitrogen/ vacuum cycles (3 ×) and left to stir in the dark at 38 °C for 7 h. The reaction was monitored by HPLC-MS analysis and once no increase in conversion was observed, the reaction mixture was frozen and lyophilized. The resulting white solid was purified by preparative RP-HPLC (Solvent A: H_2O 0.1% TFA, Solvent B: CH_3CN 0.1% TFA, flow 20 mL/min, detection 210 nm) using the following gradient elution: 0 - 15 min, 5 -20% B; R_t = 8.2 min. The purified compound **3** was lyophilized and obtained as a white fluffy solid (4.6 mg, as TFA salt, 21% yield).

^{1}H NMR (400 MHz, D_2O) δ 8.80 (d, *J* = 1.5 Hz, 1H, $H2_A$), 8.55-8.41 (m, 3H, $H2_A$ + $H6_{A,B}$), 7.83-7.70 (m, 2H, $H4_{A,B}$), 7.44-7.34 (dd, *J* = 8.0, 5.9 Hz, 2H, $H5_{A,B}$), 4.75-4.64 (m, 2H, Hα $Ala_{A,B}$), 4.60 (t, *J* = 6.1 Hz, 1H, Hα Asp), 4.24-4.14 (m, 2H, Hα Arg + Hαa Gly), 4.00 (d, *J* = 16.7 Hz, 1H, Hαb Gly), 3.24-3.00 (m, 6H, Hβ Ala_A + Hδ Arg + Hβ Asp), 2.89-2.67 (m, 6H, Hβ Ala_B + 2·CH_2 (en)), 1.93 (s, 3H, CH_3 Ac), 1.86-1.53 (bm, 4H, Hβ Arg + Hγ Arg).

^{13}C NMR (100 MHz, D_2O) δ 174.3 (Cq), 174.2 (Cq), 173.9 (Cq), 173.8 (Cq), 171.9 (Cq), 171.8 (Cq), 170.9 (Cq), 156.8 (Cq), 152.3 (CH), 152.1 (CH), 150.6 (CH), 150.4 (CH), 141.8 (CH), 141.7 (CH), 136.4 (Cq), 135.9 (Cq), 126.9 (CH), 126.7 (CH), 53.5 (CH), 53.4 (CH), 52.8 (CH), 49.5 (CH), 47.5 (CH_2), 47.4 (CH_2), 43.3 (CH_2), 40.5 (CH_2), 34.6 (CH_2), 34.1 (CH_2), 33.7 (CH_2), 28.0 (CH_2), 24.4 (CH_2), 21.6 (CH_3). ^{195}Pt (86 MHz, D_2O) δ -2673.
ESI-MS (m/z) $C_{32}H_{49}N_{13}O_8Pt$ calcd for $[M]^{2+}$ 469.2, found 469.3.

Appendix of NMR Spectra

[Pt(en)(10)](CF_3CO_2)$_2$, compound 3:

^{1}H (400 MHz, D_2O)

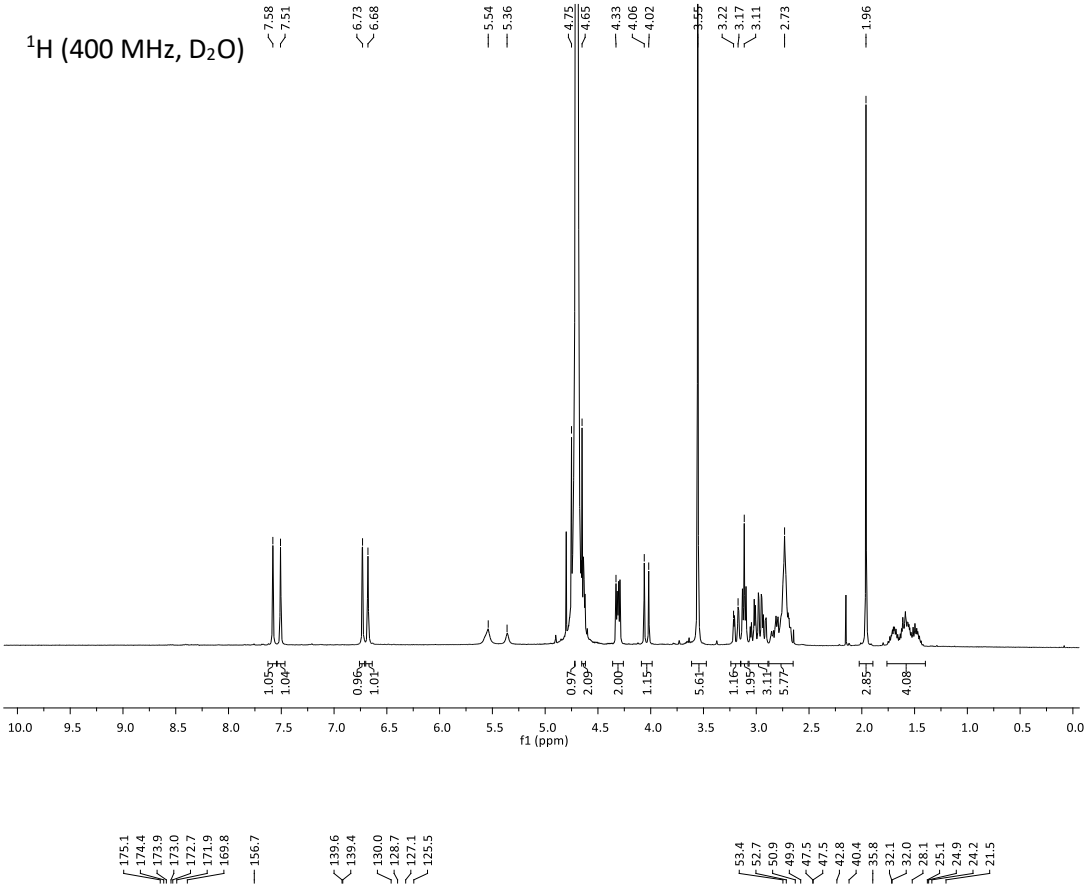

^{13}C (400 MHz, D_2O)

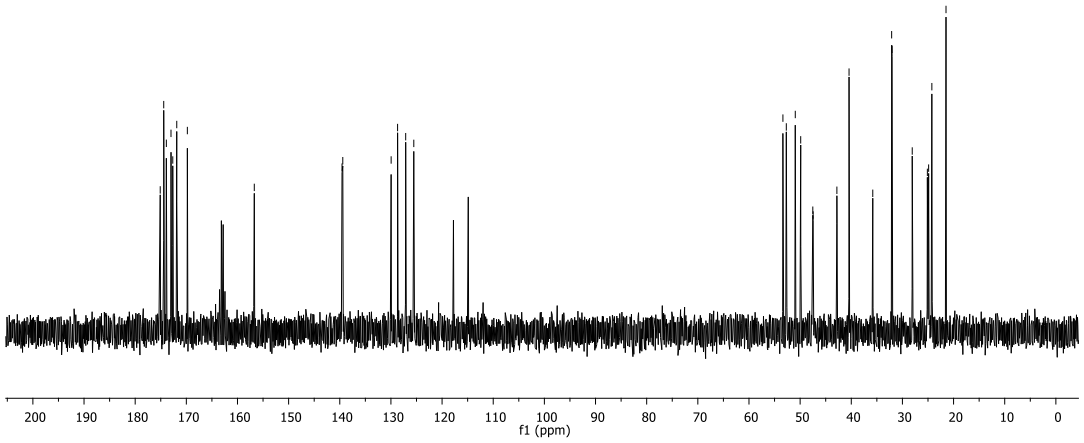

^{195}Pt (86 MHz, D_2O)

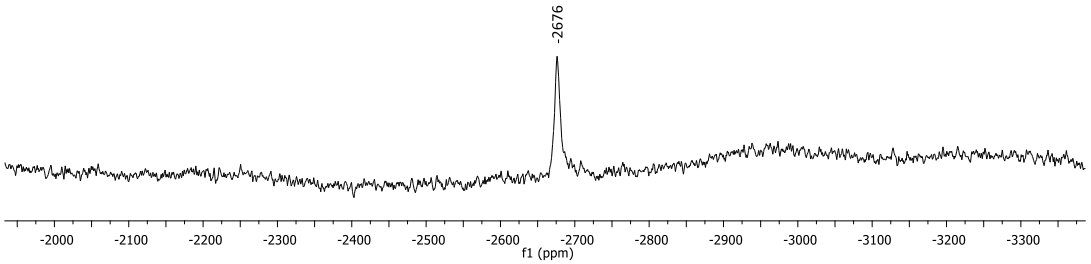

[Pt(phen)(10)]$(CF_3CO_2)_2$, compound 4:

^{1}H (400 MHz, D_2O)

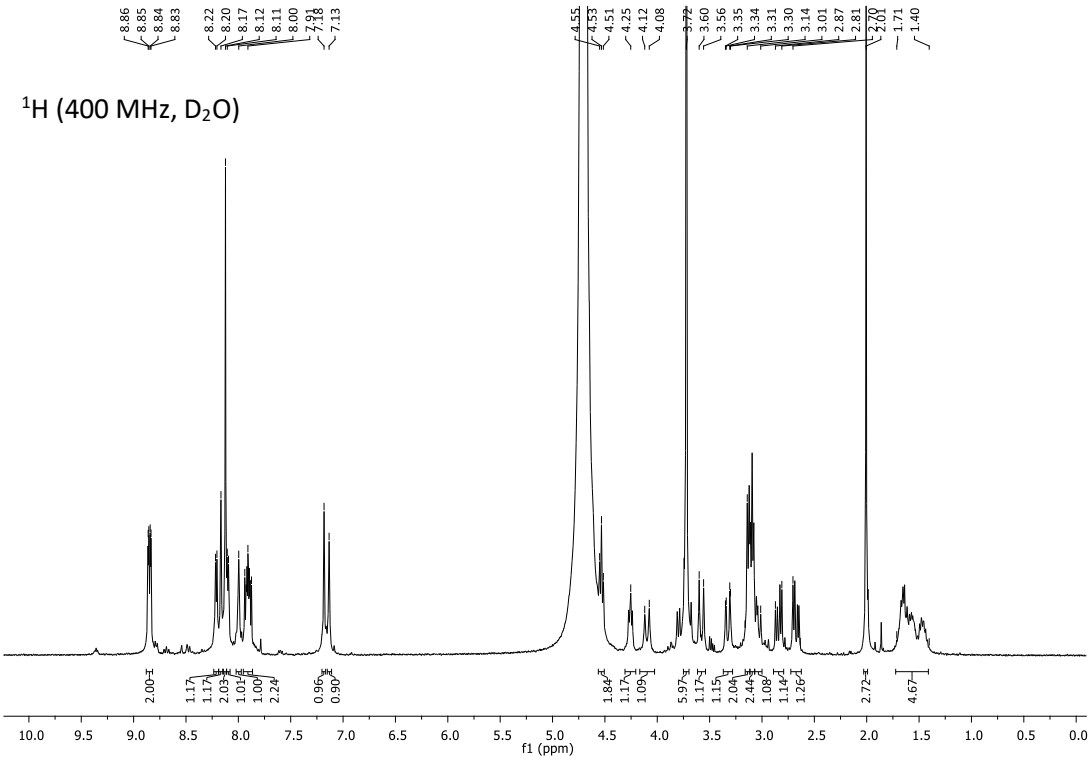

^{195}Pt (86 MHz, D_2O)

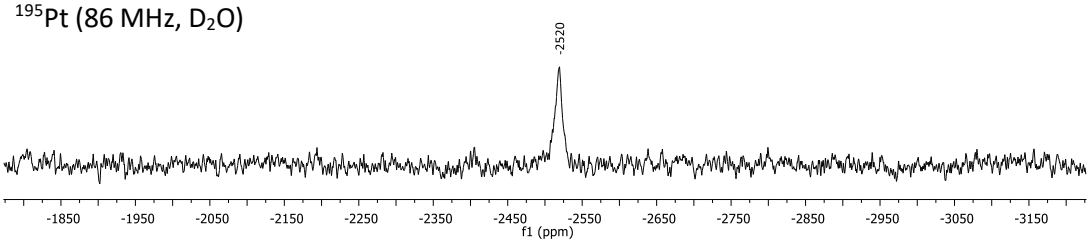

^{13}C (400 MHz, D_2O)

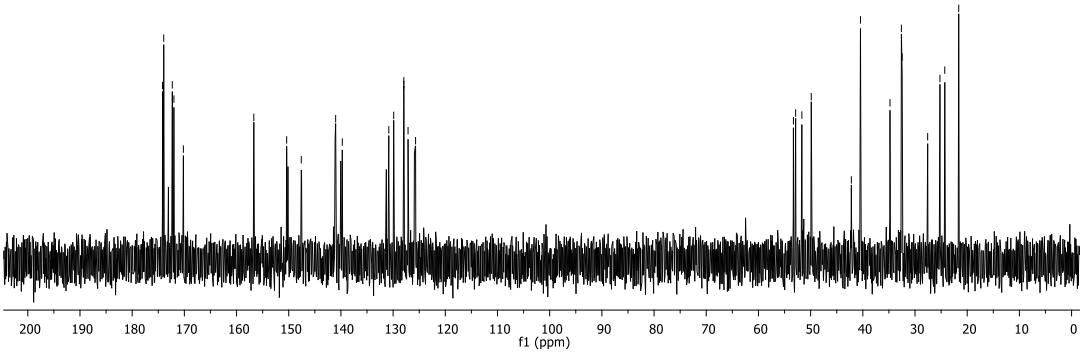

[Pt(5,6-Me_2-phen) (10)](CF_3CO_2)$_2$, compound 5:

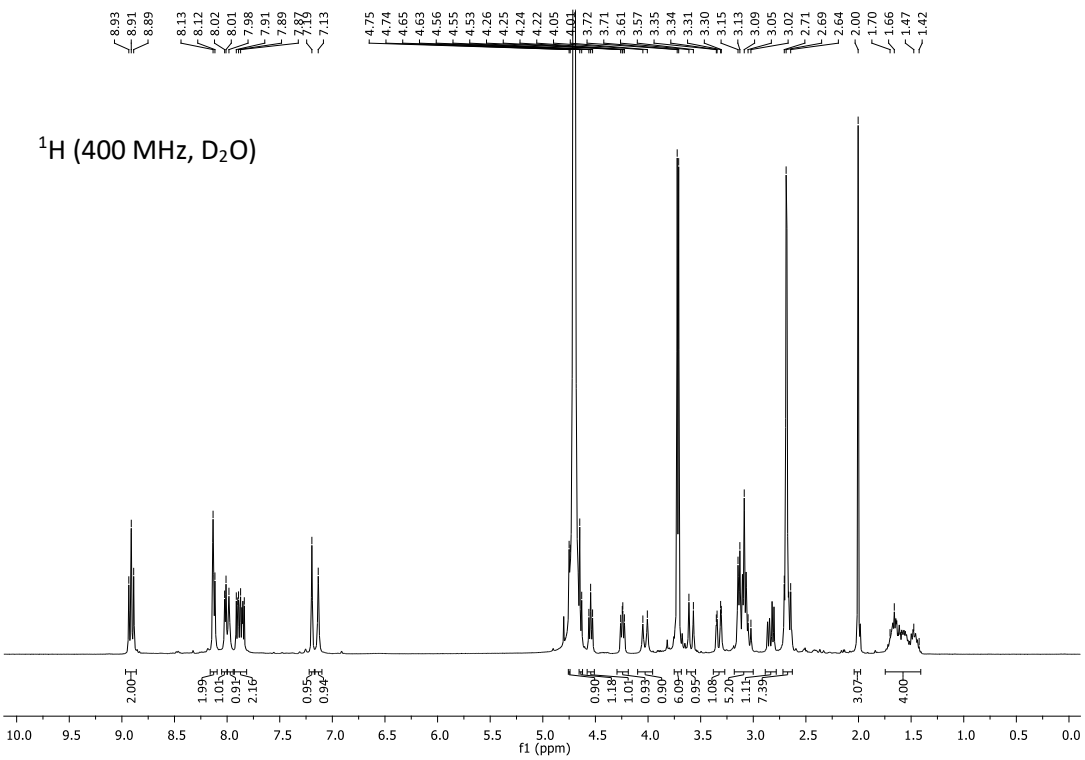

^{13}C (400 MHz, D_2O)

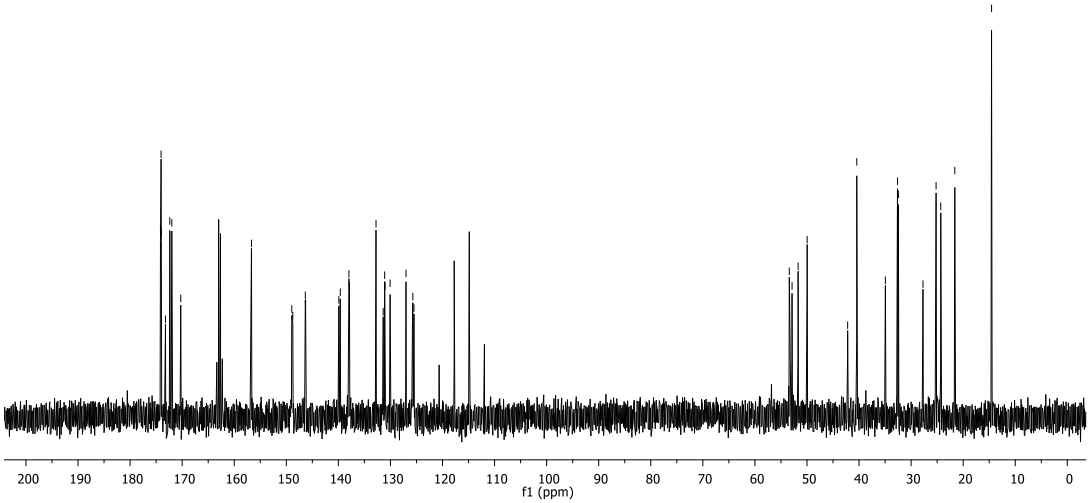

^{195}Pt (86 MHz, D_2O)

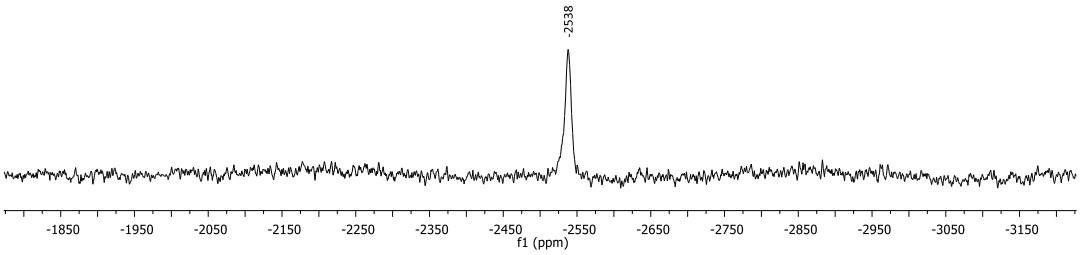

[Pt(en) (11)]$(CF_3CO_2)_2$, compound 6:

^{195}Pt (86 MHz, D_2O)

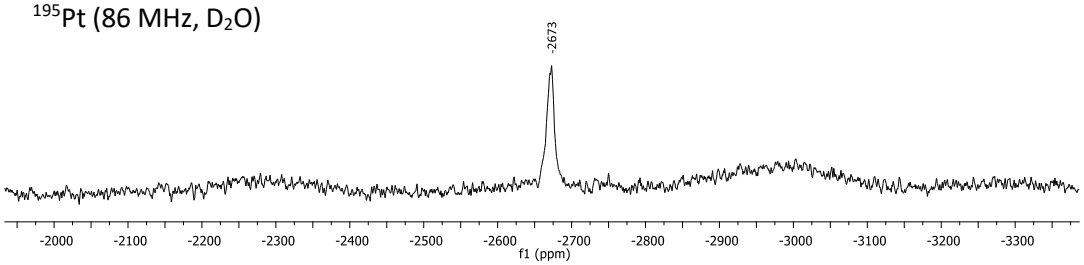

^{1}H (400 MHz, D_2O)

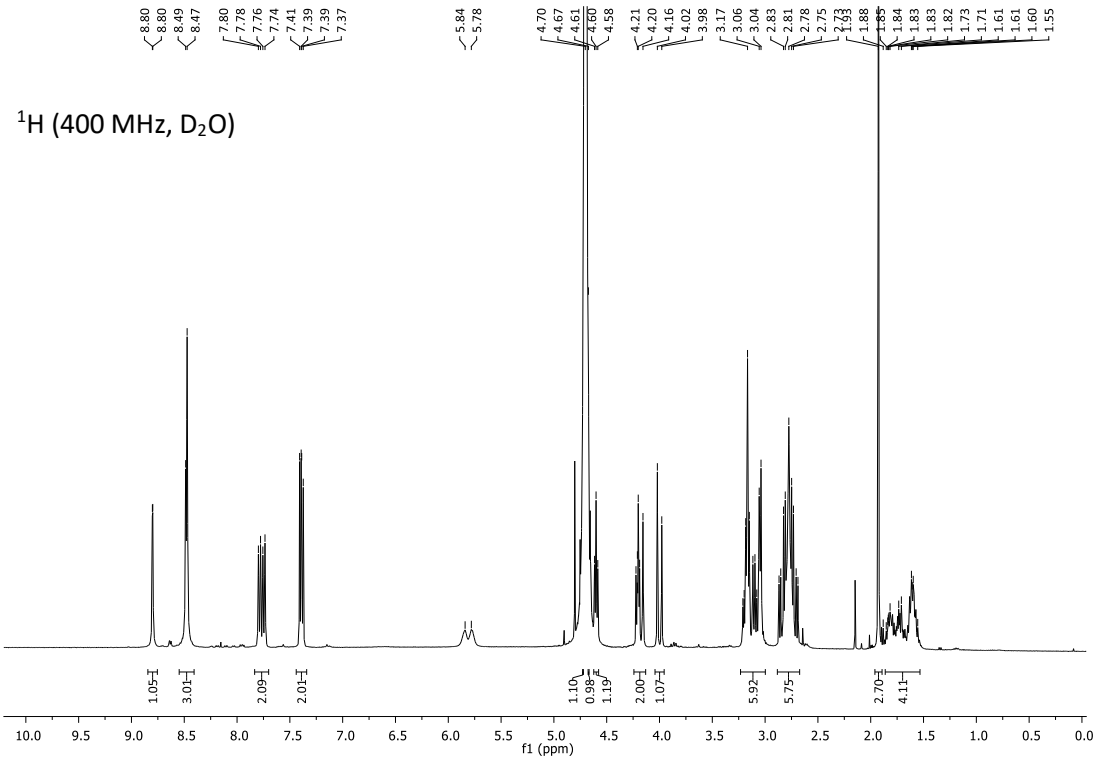

^{13}C (400 MHz, D_2O)

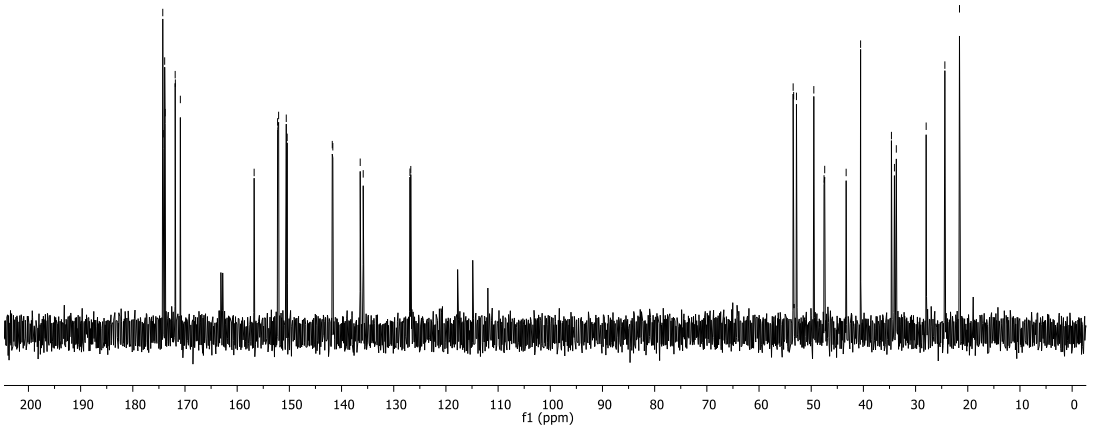

1*b*.6 References

(1) Johnstone, T. C.; Suntharalingam, K.; Lippard, S. J. *Chem. Rev.* **2016**, *116*, 3436–3486.
(2) U.S. National Library of Medicine, Cisplatin Injection. Accessed: 2015; http://www.nlm.nih.gov/medlineplus/druginfo/meds/a684036.html.
(3) Kelland, L. *Nat. Rev. Cancer* **2007**, *7* (8), 573–584.
(4) Timerbaev, A. R.; Hartinger, C. G.; Aleksenko, S. S.; Keppler, B. K. *Chem. Rev.* **2006**, *106* (6), 2224–2248.
(5) Moreno-Gordaliza, E.; Cañas, B.; Palacios, M. A.; Gómez-Gómez, M. M. *Talanta* **2012**, *88*, 599–608.
(6) Casini, A.; Mastrobuoni, G.; Temperini, C.; Gabbiani, C.; Francese, S.; Moneti, G.; Supuran, C. T.; Scozzafava, A.; Messori, L. *Chem. Commun.* **2007**, 156–158.
(7) Tsiveriotis, P.; Hadjiliadis, N. *J. Chem. Soc., Dalt. Trans.* **1999**, 459–465.
(8) Lempers, E. L. M.; Reedijk, J. *Inorg. Chem.* **1990**, *29* (10), 1880–1884.
(9) Dolman, M. E. (Emmy) M.; van Dorenmalen, K. M. A.; Pieters, E. H. E.; Sparidans, R. W.; Lacombe, M.; Szokol, B.; Orfi, L.; Keri, G.; Bovenschen, N.; Storm, G.; Hennink, W. E.; Kok, R. J. *Macromol. Biosci.* **2012**, *12*, 93–103.
(10) Harmsen, S.; Dolman, M. E. M.; Nemes, Z.; Lacombe, M.; Szokol, B.; Pato, J.; Keri, G.; Orfi, L.; Storm, G.; Hennink, W. E.; Kok, R. J. *Bioconjugate Chem.* **2011**, *22*, 540–545.
(11) Fretz, M. M.; Dolman, M. E. (Emmy) M.; Lacombe, M.; Prakash, J.; Nguyen, T. Q.; Goldschmeding, R.; Pato, J.; Storm, G.; Hennink, W. E.; Kok, R. J. *J. Control. Release* **2008**, *132* (3), 200–207.
(12) Gonzalo, T.; Beljaars, L.; van de Bovenkamp, M.; Temming, K.; van Loenen, A.-M.; Reker-Smit, C.; Meijer, D. K. F.; Lacombe, M.; Opdam, F.; Keri, G.; Orfi, L.; Poelstra, K.; Kok, R. J. *J. Pharmacol. Exp. Ther.* **2007**, *321* (3), 856–865.
(13) Waalboer, D. C. J.; Muns, J. A.; Sijbrandi, N. J.; Schasfoort, R. B. M.; Haselberg, R.; Somsen, G. W.; Houthoff, H.-J.; Van Dongen, G. A. M. S. *ChemMedChem* **2015**, *10*, 797–803.
(14) Driggers, E. M.; Hale, S. P.; Lee, J.; Terrett, N. K. *Nat. Rev.* **2008**, *7*, 608–624.
(15) Mallinson, J.; Collins, I. *Futur. Med. Chem.* **2012**, *4* (11), 1409–1438.
(16) Marsault, E.; Peterson, M. L. *J. Med. Chem.* **2011**, *54* (7), 1961–2004.
(17) White, C. J.; Yudin, A. K. *Nat. Chem.* **2011**, *3* (7), 509–524.
(18) Nielsen, D. S.; Shepherd, N. E.; Xu, W.; Lucke, A. J.; Stoermer, M. J.; Fairlie, D. P. *Chem. Rev.* **2017**, *117* (12), 8094–8128.
(19) Craik, D. J.; Fairlie, D. P.; Liras, S.; Price, D. *Chem. Biol. Drug Des.* **2013**, *81* (1), 136–147.
(20) Thakkar, A.; Trinh, T. B.; Pei, D. *ACS Comb. Sci.* **2013**, *15*, 120–129.
(21) Dharanipragada, R. *Futur. Med. Chem.* **2013**, *5* (7), 831–849.
(22) Frost, J. R.; Scully, C. C. G.; Yudin, A. K. *Nat. Chem.* **2016**, *8* (12), 1105–1111.
(23) Ma, X.; Jia, J.; Cao, R.; Wang, X.; Fei, H. *J. Am. Chem. Soc.* **2014**, *136*, 17734–17737.
(24) Arosio, D.; Casagrande, C. *Adv. Drug Deliv. Rev.* **2016**, *97*, 111–143.
(25) Bencini, A.; Lippolis, V. *Coord. Chem. Rev.* **2010**, *254*, 2096–2180.
(26) Accorsi, G.; Listorti, A.; Yoosaf, K.; Armaroli, N. *Chem. Soc. Rev.* **2009**, *38* (6), 1690.
(27) Garbutcheon-Singh, K. B.; Leverett, P.; Myers, S.; Aldrich-Wright, J. R. *Dalt. Trans.* **2013**, *42*, 918–926.
(28) Coyer, M. J.; Croft, M.; Chen, J.; Herber, R. H. *Inorg. Chem* **1992**, *31* (10), 1752–1757.
(29) Fröhling, C. D. W.; Sheldrick, W. S. *J. Chem. Soc. Dalt. Trans.* **1997**, No. 22, 4411–4420.
(30) Manka, S.; Becker, F.; Hohage, O.; Sheldrick, W. S. *J. Inorg. Biochem.* **2004**, *98* (11), 1947–1956.
(31) Brodie, C. R.; Collins, J. G.; Aldrich-Wright, J. R. *Dalt. Trans.* **2004**, 1145–1152.
(32) McFadyen, W. D.; Wakelin, L. P. G.; Roos, I. A. G.; Leopold, V. A. *J. Med. Chem.* **1985**, *28* (8), 1113–1116.

Chapter 2. Targeting integrin $\alpha_4\beta_1$

2.1 Introduction

2.1.1 α_4 integrin family

Integrins constitute a large class of heterodimeric cell surface molecules consisting of α and β-chains, each of which has a large extracellular domain and a short cytoplasmic tail. There are at least 18 different known α chains and 8 β-chains, which combine with each other in a non-covalent manner, to give 24 members of the integrin family. These members bind to specific protein ligands and are expressed on diverse cell types at different levels.[1] According to their corresponding natural ligands, the integrin subtypes can be roughly divided into four classes: (*i*) arginine-glycine-aspartate (RGD) receptors, representing the biggest subfamily, (*ii*) collagen receptors, (*iii*) leukocyte-specific receptors with, for example, the leucine-aspartate-valine (LDV) binding motif and (*iv*) laminin receptors (Fig. 1).[2]

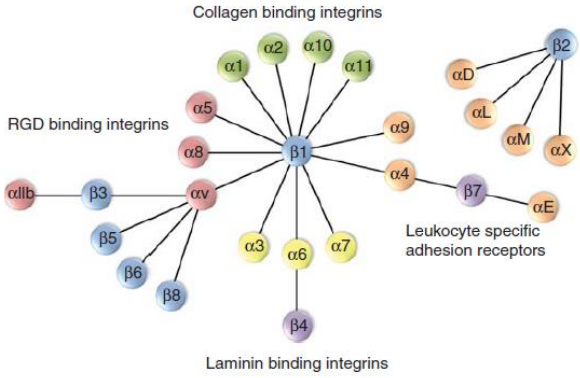

Figure 1. Classification of integrin subtypes according to their ligand-binding motifs: RGD receptors, collagen receptors, laminin receptors, leucocyte adhesion receptors, and their corresponding subtypes. Figure reprinted from ref.[2].

The α_4 integrin family belongs to the leukocyte integrin class, which is composed by ten members: all four β_2 integrins ($\alpha_L\beta_2$, $\alpha_M\beta_2$, $\alpha_X\beta_2$, $\alpha_D\beta_2$), the two β_7 integrins ($\alpha_E\beta_7$, $\alpha_4\beta_7$), $\alpha_4\beta_1$ and $\alpha_9\beta_1$ integrins, in addition to $\alpha_5\beta_1$ and $\alpha_v\beta_3$.[3] The α_4 subunit is able to associate with both β_1 and β_7 chains in order to build the integrin subtypes $\alpha_4\beta_1$ (also called very late antigen 4, VLA-4) and $\alpha_4\beta_7$ (Lymphocyte Peyer's Patch Adhesion Molecule). Natural ligands of both are (*i*) the vascular cell adhesion molecule-1 (VCAM-1) and (*ii*) the alternatively spliced portion of the connecting segment-1 (CS-1) of fibronectin (FN). In particular, the $\alpha_4\beta_1$ and $\alpha_4\beta_7$ integrins recognize FN via the Leu-Asp-Val (LDV) binding epitope, while interact with VCAM-1 via the homologous and essentially isosteric[4] binding sequence QIDSPL. A third ligand, the mucosal addressin cell adhesion molecule-1 (MAdCAM-1), binds to $\alpha_4\beta_7$ with relatively high selectivity. Since the expression of MAdCAM-1 is limited to high endothelial venules of gut-associated lymphoid organs and lamina propria venules, it is involved in the trafficking of $\alpha_4\beta_7$-bearing lymphocytes to these mucosal tissues.[1]

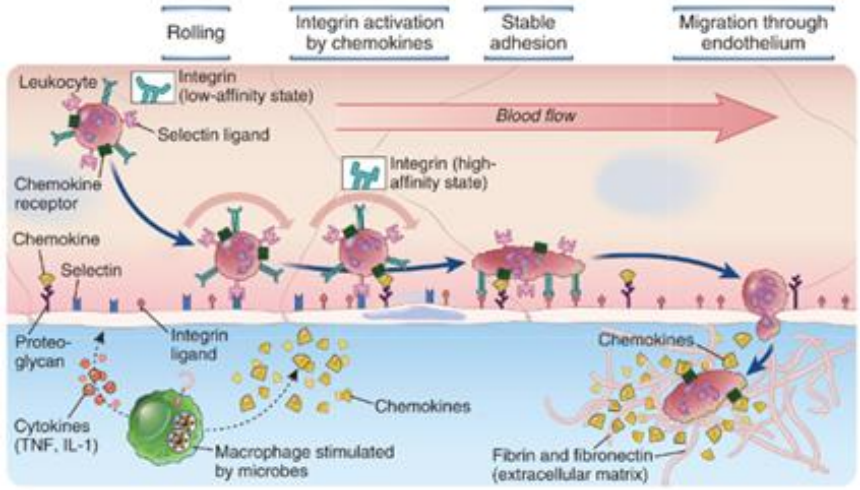

Figure 2. Multistep leukocyte-endothelial cell interactions mediating leukocyte recruitment into tissues. Figure reprinted from ref.[7].

In fact, $\alpha_4\beta_7$ is present on subpopulations of T- and B-lymphocytes and eosinophils,[5] while $\alpha_4\beta_1$ is mainly expressed on the surface of lymphocytes, eosinophils, monocytes, basophils and mast cells.[6] Neutrophils are also capable of expressing the $\alpha_4\beta_1$ integrin, but only after activation.[1] These two integrins play an important role in the immune response as they are involved in leukocyte adhesion, migration, and activation (Fig. 2).[2]

In response to locally released inflammatory stimuli, chemokines and cytokines (*i*) activate $\alpha_4\beta_1$ on the surface of circulating leukocytes and (*ii*) upregulate the expression of VCAM-1 on endothelial cells. While $\alpha_4\beta_1$ is constitutively expressed on leukocytes, CD-4$^+$ T cells and eosinophils, it may be upregulated in response to inflammation. Contacts between E-, L- and P-selectins on the endothelial surface and their carbohydrate ligands on leukocytes cause leukocytes to stick and roll when in contact with blood vessel walls. This process provides an opportunity for firm adhesion to occur between these leukocytes and VCAM-1 expressed on the endothelial cell surface, and leads to flattening of the cells followed by their transmigration from blood vessels to the extracellular matrix. Here, they bind to fibronectin and possibly other elements of the extracellular matrix before migrating along a chemokine gradient to the site of inflammation.[1,7]

As many inflammatory diseases are characterized by an influx of lymphocytes and leukocytes in the inflamed tissue, there is keen interest from the pharmaceutical research players (industry and academy) in finding and testing compounds that have the potential to attenuate this process.[1] Diseases associated with $\alpha_4\beta_1$ and $\alpha_4\beta_7$ are mainly inflammatory and autoimmune diseases that go along with a pathological accumulation of activated leukocytes in the affected tissues such as, for example, inflammatory bowel disease (IBD), Crohn's disease (CD), rheumatoid arthritis (RA), asthma and multiple sclerosis (MS).[1,8] Moreover, the $\alpha_4\beta_1$ integrin receptor demonstrated to play a pivotal role in tumor angiogenesis associated with chronic inflammation, since this condition may promote the angiogenetic switch in tumors.[9–11] $\alpha_4\beta_1$ is also involved in the recruitment of progenitor cells, the multipotent cells derived from bone marrow stem cells, in the formation of new blood vessels[12] and, because of its overexpression in melanoma cells, $\alpha_4\beta_1$ can be also considered a marker for predicting metastatic risk. [13] On these bases, molecules able to interfere in $\alpha_4\beta_1$ and/or $\alpha_4\beta_7$ binding may represent useful tools for chronic inflammations, autoimmune diseases and cancer therapy.

2.1.2 α_4 integrin ligands

2.1.2.1 Natalizumab

The first widely successful drug targeting leukocyte integrins was Natalizumab.[14] Natalizumab was the first humanized monoclonal antibody targeting the α_4-integrin subunit ($\alpha_4\beta_1$ and $\alpha_4\beta_7$) and it was approved by the FDA for the treatment of MS and CD in 2004. The unexpected development of a rare but potentially fatal complication, the progressive multifocal leukoencephalopathy (PML), in patients treated with Natalizumab triggered a voluntary withdrawal of the drug from the market in February 2005.[15] Since the benefits of this drug were so substantial, a re-evaluation of the FDA brought it back to the market in 2008 under the trade name Tysabri (Elan and Biogen) for patients with moderate to severe CD after an inadequate response to conventional therapies, and patients suffering from a severe form of MS with lack of alternative therapies. As the risk of PML is the limiting factor for the use of Natalizumab, the development of Vedolizumab, a humanized IgG1 monoclonal antibody, that selectively inhibits $\alpha_4\beta_7$ integrin by blocking its interaction with MAdCAM1, has effectively replaced Natalizumab in clinical practice for the treatment of Crohn's disease (CD) and ulcerative colitis. Up to now, only the anti-α_4 monoclonal antibody Natalizumab and the anti-$\alpha_4\beta_7$ antibody Vedolizumab have reached the market.[15] Focusing on Natalizumab, administered by monthly intravenous infusion, it exerts impressive inhibitory effects for the inflammatory aspects of multiple sclerosis, with >65% reduction in symptomatic attacks (relapses) during 2 years of treatment and >90% suppression of new inflammatory lesions.[16]

Multiple sclerosis is a chronic neuroinflammatory disease of the brain and spinal cord that is a common cause of serious physical disability in young adults, especially women.[17] This condition has heterogeneous clinical manifestations, such as sensory and visual disturbances, motor impairments, fatigue, pain and cognitive deficits, which are correlated with the spatiotemporal dissemination of lesional sites of pathology within the central nervous system (CNS) (Fig. 3). These lesions are a hallmark of multiple sclerosis and are caused by the infiltration of immune cells across the blood–brain barrier (BBB) that promotes inflammation, demyelination, gliosis and neuroaxonal degeneration, leading to disruption of neuronal signalling.

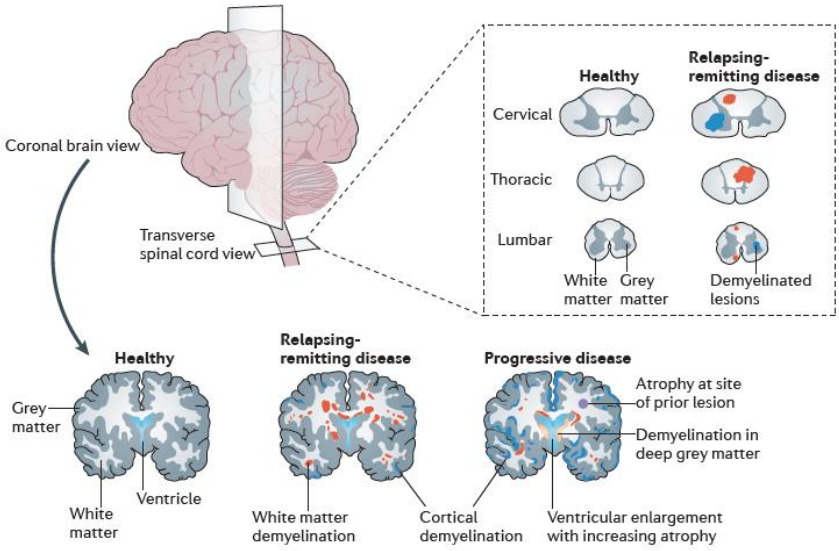

Figure 3. The pathology of multiple sclerosis. Demyelinated areas in the white and grey matter of the brain and spinal cord (called plaques or lesions) indicate a loss of myelin sheaths and oligodendrocytes and characterize the multiple sclerosis pathology. Figure reprinted from ref.[17].

The most common form of MS, affecting about 85% of patients, is the relapsing-remitting MS (RR-MS), which is characterized by recurring attacks of relapses followed by remission periods. Relapses are clinical exacerbations of neurological symptoms and coincide with focal CNS inflammation and demyelination, that are typically detectable using magnetic resonance imaging (MRI).[17] However, as previously said, the enthusiasm for the observed great efficacy of Natalizumab in the treatment of patients with RR-MS has been mitigated by the occurrence of the PML disease.[15,18] This condition is the result of reactivation of John Cunningham virus (JCV), a widespread commensal present in 55% of the population; the risk for developing PML after treatment with Natalizumab is about 2 in 1000 for patients treated for more than two years. There is no known treatment, prevention or cure for this condition and the infection leads to death or severe disability. The mechanism by which Natalizumab causes PML remains largely unknown;[19] Natalizumab/PML is not associated to generalized immunosuppression and it has been proposed, but not definitely proven, that it is mechanism-driven.[20] A biomarker measuring the individual JCV antibodies was developed, which proved highly predictive for PML susceptibility; nowadays routine and careful monitoring of this biomarker in any individual patient over time is at the base of any therapeutic decision.[21]

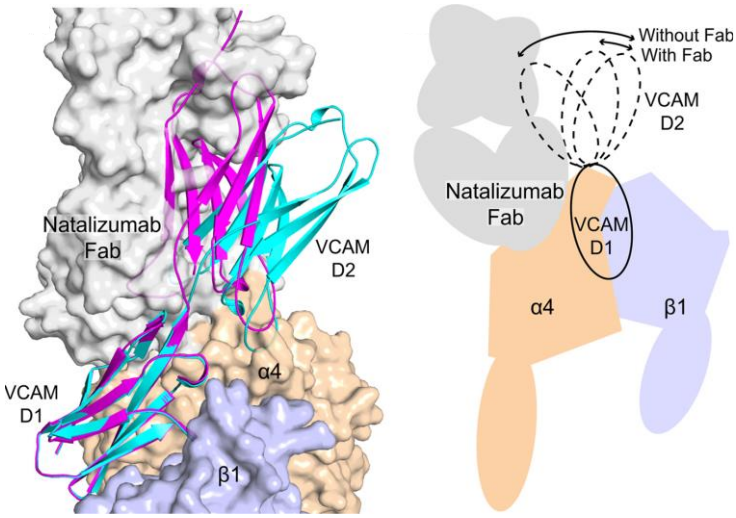

Quite surprisingly, the modality by which Natalizumab binds to α_4 integrins has been unravelled only recently (Fig. 4).[22] A crystal structure of the F_{ab} bound to an α_4 integrin subunit revealed that the epitope is adjacent to, but outside, the VCAM ligand binding groove formed at the interface of the α/β subunits. These studies proved that Natalizumab acts as a noncompetitive antagonist of the VCAM ligand and lowers its affinity to $\alpha_4\beta_1$ by limiting the number of VCAM conformations accessible for binding.

Figure 4. Model of VCAM binding to a Natalizumab Fab-$\alpha_4\beta_1$ complex. Figure reprinted from ref.[22]

Given the impressive effectiveness of Natalizumab in the treatment of patients with highly active RR-MS, a deeper understanding of the basic mechanisms of action could be of great importance in order to clarify: (*i*) how and to what extent blocking $\alpha_4\beta_1$-VCAM interaction may prevent migration of leukocytes across blood-brain barrier (BBB) into the CNS and (*ii*) whether and how such mechanism is associated to PML.

2.1.2.2 Small molecules

Aside monoclonal antibodies, a number of small molecules recognized as selective or dual ligands for $\alpha_4\beta_1$ and $\alpha_4\beta_7$ have been reported in the literature.[1,2,23,24] Indeed, since the mid-1990s, given the therapeutic relevance of the target, there has been great interest among pharmaceutical companies in discovering and evaluating new effective small molecules (SMs) alternative to antibodies, and a number of medicinal chemistry-driven researches flourished. The rationale behind these studies was the recognition of short aminoacidic sequences (LDS, IDS, ILDV) which were minimal consensus binding motifs shared by both VCAM-1 and CS-1 region of fibronectin.[25–27] Mimicking these sequences in SMs led to the creation of competitive antagonists which could likely fit in the groove at the interface between the α and β subunits.[28] Because of the similarity of the tripeptide recognition sequences, LDV for CS-1 peptide of fibronectin vs LDT for MAdCAM-1, small molecules designed starting from these fragments often showed dual affinity.[29]

Among the many small-molecule antagonists of the α_4 integrin discovered in the recent past,[1,21,22,28] just some examples will be herein reported, which include cyclic peptides and their peptidomimetic counterparts, the reference compound BIO1211 and some of its recently developed derivatives, focusing the attention toward ligands selective for $\alpha_4\beta_1$ as compared to $\alpha_4\beta_7$ and endowed with precise structural features.

- **Cyclic LDV derivatives**

Cyclization is a type of chemical modification designed to improve stability of a linear peptide of interest. In general, the cyclic analogues, in addition to being much more stable with respect to the native peptides toward enzymatic degradation, are conformationally more defined and possibly more selective towards the specific target.[31] Constrained peptide derivatives that contain the essential binding sequences found in VCAM-1 (IDS) and fibronectin (LDV) have afforded a variety of potent $\alpha_4\beta_1$ antagonists.[24] In 1997, Jackson et al.[32] reported the discovery of low nanomolar cyclic peptide $\alpha_4\beta_1$ antagonists, deriving from the binding epitope of VCAM-1 for $\alpha_4\beta_1$ and endowed with a X-CDPC core structure (Fig. 5).

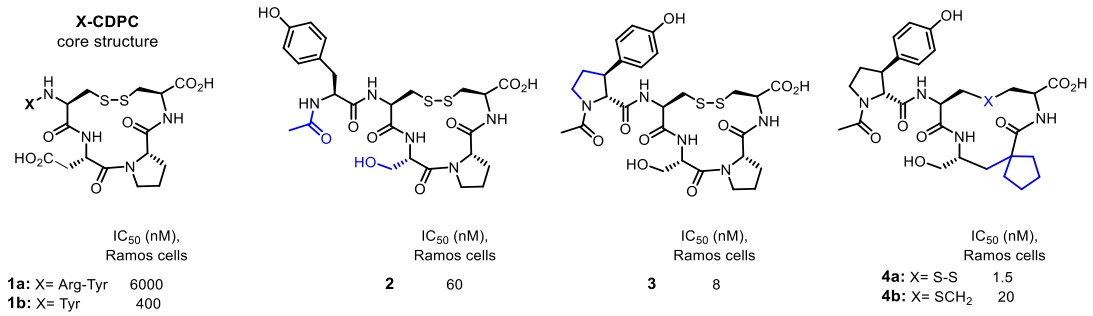

Figure 5. Cyclic peptides (**1**-**3**),[32] their peptidomimetic analogues (**4a**,**b**)[33] and indication of their binding affinity (IC_{50}) in $\alpha_4\beta_1$-overexpressing Ramos cells.

Cyclic X-CDPC peptides, such as compounds **1a** and **1b**, possess an Asp-Pro portion flanked by two Cys residues, involved in the formation of a disulfide bridge through their side chains, giving rise to cyclic tetrapeptides bearing various substitutions (X) at the *N*-terminus. Compound **1a** [YR*c*(CDPC)], substituted with the Tyr-Arg dipeptide, showed to inhibit the $\alpha_4\beta_1$/VCAM interaction at low micromolar concentration (IC_{50} = 6 μM, Ramos cell assay). Although previous mutagenesis studies of VCAM-1 integrin-binding epitope highlighted Arg and Asp as important contact residues,[24,32] the simple deletion of Arg led to compound **1b** [Y*c*(CDPC)], showing a 10-fold improved affinity (IC_{50} = 0.4 μM, Ramos cell assay). Moreover, the substitution of the Asp residue by serine in **1b**, and concomitant acylation of the *N*-terminal Tyr, produced compound **2** [Ac-Y*c*(CSPC)], which showed to inhibit the adhesion of $\alpha_4\beta_1$ integrin-expressing Ramos cells to VCAM-1 with an IC_{50} of 60 nM. A further improvement in affinity toward $\alpha_4\beta_1$ was obtained by introducing a constrained

tyrosine analogue, the (±)-*trans*-*N*-acetyl-3-(4-hydroxyphenyl) proline, at the *N*-terminus of the cyclic CSPC core that resulted in compound **3**. This latter compound showed to be almost 10 times more potent than compound **2**, with an IC_{50} of 8 nM (Ramos cell assay).

Since these cyclic peptides have a completely peptide nature and were obtained by formation of a disulfide bridge, which is sensitive to reduction, some efforts toward the development of peptidomimetic analogues were made to improve their metabolic stability. Although loss of activity was observed when both Asp and Pro were simultaneously replaced,[32] Fotohui and co-workers, in 2000, reported the synthesis of a class of spirocyclic disulfides, typified by **4a,**[34] and their thioether analogues, typified by **4b**,[33] in which the replacement of the Asp-Pro moiety with the achiral dipeptide mimetic 1-(2-aminoethyl)cyclopentane carboxylic acid led to potent inhibitors of the $\alpha_4\beta_1$/VCAM interaction. The introduction of the spirocyclopentyl Asp-Pro dipeptide-mimetic linker (**4a**, IC_{50} = 1.5 nM, Ramos cell assay) and the substitution of the disulfide bridge with a thioether group (**4b**, IC_{50} = 20 nM, Ramos cell assay) resulted in metabolically more stable and potent small molecule antagonists of $\alpha_4\beta_1$. Unluckily, for all these compounds (**1**-**4**), the selectivity toward $\alpha_4\beta_1$ with respect to the homologous $\alpha_4\beta_7$ integrin was not evaluated.

- **Linear LDV peptides and peptidomimetics**

In 1999, Adams's research group reported the synthesis of BIO1211 (MPUPA-LDVP),[4] a potent and selective $\alpha_4\beta_1$ antagonist, which showed to inhibit the $\alpha_4\beta_1$/VCAM-1 interaction with an IC_{50} of 4 nM (Jurkat cell assay) and a ~1000-fold selectivity for $\alpha_4\beta_1$ compared to $\alpha_4\beta_7$ integrin (IC_{50} $\alpha_4\beta_7$ = 2 µM, Jurkat cell assay). BIO1211 is formed by the peptide sequence Leu-Asp-Val-Pro (LDVP) simply substituted, at the *N*-terminus, with the 4-[(*N*-2-methylphenyl)ureido]-phenylacetyl group (MPUPA) (Fig. 6).

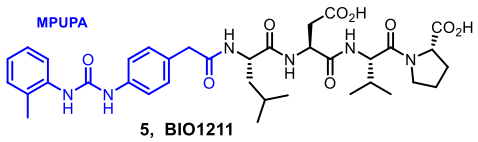

Figure 6. Structure of the linear peptide-LDV mimetic, **BIO1211** (**5**).

This compound was obtained starting from the Ile-Leu-Asp-Val (ILDV) sequence, the $\alpha_4\beta_1$-binding motif of fibronectin, which is a weak $\alpha_4\beta_1$ inhibitor (IC_{50} = 175 µM, Jurkat cell assay). After substitution of the *N*-terminal Ile with Tyr, a substantial improvement in the peptide inhibitor activity was observed. Further modifications on the terminal aromatic ring of Tyr led to the discovery of the best *N*-terminus capping group, the MPUPA functionality. This cap produced the major enhancement in the inhibitor activity over the starting peptide, also showing to possess selectivity for $\alpha_4\beta_1$ greater than 1000-fold with respect to the $\alpha_4\beta_7$ integrin. With the aim to enhance the enzymatic stability of the compound, a Pro residue was added at the *C*-terminus of the peptide sequence. This modification proved to maintain the high activity, but the residual peptidic nature of BIO1211 resulted in rapid enzymatic hydrolysis[35,36] and clearance *in* vivo.[37] Anyway, the *in vitro* efficacy and potency of BIO1211 were also confirmed *in vivo*.[38] When administered as an aerosol once daily (~0.1 mg/Kg), BIO1211 showed prophylactic effectiveness in a sheep model of allergic bronchoconstriction. The high level of *in vitro* and *in vivo* potency demonstrated by this nonsteroidal compound resulted in the first small-molecule VLA-4 antagonist to enter clinical trials.[38]

Given its potency and selectivity, BIO1211 was used as a reference compound in the studies aimed at developing new potent and selective $\alpha_4\beta_1$ antagonists. In order to overcome the enzymatic instability of BIO1211, a number of bioactive peptidomimetics have been prepared. In general, the large majority of the LDV peptidomimetics shares common structural features: (*i*) an aromatic cap at the *N*-terminus, (*ii*) a suitable spacer, and (*iii*) a β-carboxylate mimetic of Asp.[23,24,30] Recently, Gentilucci and co-workers developed new analogues of the $\alpha_4\beta_1$ integrin inhibitor BIO1211, obtained by retro-sequence strategy, which displayed a very good enzymatic stability, also due to the presence of a non-natural amino acid, a (*S*)-pyrrolidine-3-carboxylic acid (or β^2-Pro).[39] The general features of LDV peptidomimetics are maintained in these retro-sequences, which are composed by (*i*) an Asp or *iso*Asp residue equipped with an aromatic cap at the *N*-terminus, favouring the integrin binding,[23,24](*ii*) a β-amino acid (β^2-Pro), as spacer and constrained core exerting the

conformational control, and (*iii*) the 1-(4-(aminomethyl)phenyl)-3-(*o*-methylphenyl)urea (AMPUMP), the amino variant of the well-known α_4-targeting MPUPA group.

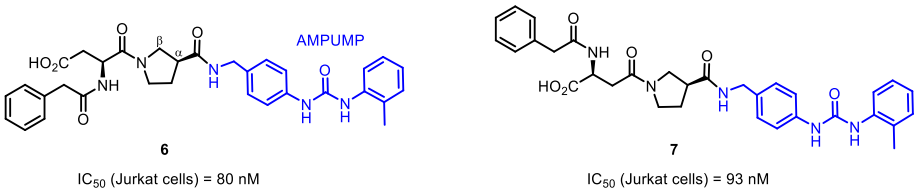

Figure 7. Structures of retro-sequences **6** and **7** containing β^2-Pro. IC_{50} values refer to $\alpha_4\beta_1$ integrin-expressing Jurkat cells.

The retro-sequences BnCO-Asp-β^2-Pro-AMPUMP **6**, and BnCO-*iso*Asp-β^2-Pro-AMPUMP **7** (Fig. 7), which possess the aromatic phenylacetyl group (BnCO) as *N*-cap, showed to inhibit the adhesion of $\alpha_4\beta_1$ integrin-expressing Jurkat cells to VCAM-1 with an IC_{50} of 80 nM and 93 nM, respectively. Apparently, these new compounds are less-potent integrin antagonists as compared to the reference BIO1211; however, due to their peptidomimetic nature, compounds **6** and **7** proved to be significantly more stable to enzymatic degradation in mouse serum than BIO1211. Indeed, after two hours, **6** was degraded only to a moderate extent (about 10%), and **7** was even more stable (<5% degradation), whereas BIO1211 was almost completely hydrolyzed under the same conditions.

β-proline core does not represent only a successful approach to overcome the low biovailability of natural peptides. The cyclic structure of proline is known to give particular conformational rigidity to peptides, inducing ordered spatial disposition of side chains, that are likely to facilitate binding with biological targets.[31]

Following a very common trend in bioactive peptide research, which exploit proline derivatives[40] as central cores in the synthesis of compounds showing high affinity profiles toward $\alpha_4\beta_1$ integrin, Tolomelli and co-workers, in 2015, developed completely non-peptidic BIO1211 mimetics containing a dehydro-β-proline ring (Fig. 8).[29]

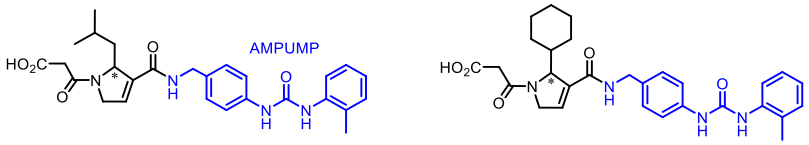

Figure 8. Structures of retro sequences **8** and **9**. IC_{50} values refer to $\alpha_4\beta_1$ integrin-expressing Jurkat cells.

As appendages to the central 3,4-dehydro-β-proline core were used: (*i*) a malonic acid chain, which contains a free carboxylate group as a fundamental handle for effective ligand-receptor interaction, (*ii*) the AMPUMP motif and (*iii*) two different lipophilic chains, such as the isobutyl and the cyclohexyl groups, which mimic the leucine side chain present in the LDV recognition sequence. The best integrin antagonist proved to be compound (*R*)-**8**, showing IC_{50} = 10 nM in the inhibition of adhesion between $\alpha_4\beta_1$ integrin expressing Jurkat cells and VCAM-1. This result highlighted the existence of a strong dependence of the binding competence on the stereochemistry of the heterocyclic core, suggesting a preferred disposition of the alkyl group for the (*R*) enantiomer, probably mimicking the spatial disposition of the lipophilic leucine or valine side chains in the LDV recognition sequence. Furthermore, compounds (*R*)-**8** and (*R*)-**9** showed modest activity toward the homologous integrin $\alpha_4\beta_7$, with an IC_{50} of 270 and 343 nM, respectively, while they did not display any activity toward $\alpha_5\beta_1$, $\alpha_L\beta_2$, and $\alpha_v\beta_3$ integrins.[29]

2.2 Aim of the work

In recent past years, our research unit exploited a proline derivative, the 4-aminoproline residue (Amp), in the development of a novel class of high-affinity RGD-based cyclopeptide antagonists[41,42] of $\alpha_V\beta_3$ and $\alpha_V\beta_5$ integrin receptors, known to be directly involved in the evolution and diffusion of metastatic tumor cells and angiogenesis.[43,44] The Amp scaffold (4-aminopyrrolidine-2-carboxylic acid) is a multifaceted molecular entity,[41] which can be grafted onto the peptide sequence of interest and foster the following intramolecular cyclization reaction, thanks to *cis*-configuration of the two carboxylic and the γ-amino functionalities. As already mentioned, the cyclic analogues are much more stable to enzymatic degradation with respect to the native peptides and they are also conformationally more defined, a feature that can impart higher target binding capability and selectivity.[31] Moreover, the Amp nucleus possesses a N^{α}-proline site free for covalent bonding to useful functional units.

Given its multifaceted nature, by adding the proper pharmacophoric groups, the Amp scaffold might be exploited to obtain a new class of small-molecule peptidomimetics as potential $\alpha_4\beta_1$ integrin antagonists. To explore this possibility, we decided to design and synthesize some cyclic aminoproline-based semipeptides, in which the Amp scaffold could be grafted onto suitable peptide sequences (LDV motif and its analogues) and functionalized at the N^{α}-proline site with the well-known aromatic cap, the α_4-targeting MPUPA group.

When studying the interactions between ligands and biological targets, the availability of the ligand-receptor X-ray crystallographic structure is of utmost importance, and it gives the opportunity to analyze plausible candidate ligands by massive *in silico* screenings, and to conduct highly detailed molecular docking analyses.[45] Since no X-ray analyses exist to date on the complete structure of the $\alpha_4\beta_1$ receptor, nor of the same receptor in complex with its SM ligand (or any other ligand), the design of these cyclic aminoproline-based peptidomimetics required the generation and validation of a $\alpha_4\beta_1$ receptor model by molecular modelling studies (vide infra). Using compound **12**, conceived by us as a potential ligand for $\alpha_4\beta_1$ receptor, docking simulation studies were performed, in order to investigate the possible binding modes of this ligand into the $\alpha_4\beta_1$ protein binding site.

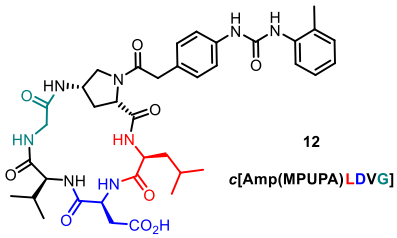

12

***c*[Amp(MPUPA)LDVG]**

The results of these docking analyses led to the design of six further cyclic aminoproline-based semipeptides. Aim of this part of the work was the design and synthesis of such products, and their evaluation as possible ligands of the $\alpha_4\beta_1$ integrin receptor by cell adhesion inhibition assays using Jurkat cells in the presence of VCAM-1. The development of potent and highly selective SM $\alpha_4\beta_1$ antagonists could be useful, in order to obtain: (*i*) lead compounds for therapeutic tool investigation, (*ii*) probes for crystallization attempts within the $\alpha_4\beta_1$receptor, with possible elucidation of the ligand-receptor interaction at the molecular level. Moreover, small molecule $\alpha_4\beta_1$ integrin antagonists could be attached to ancillary visualizing-diagnostic tools as active targeting probes, useful for the comprehension of the molecular mechanisms underlying the $\alpha_4\beta_1$/VCAM-mediated migration of lymphocytes, with possible future elucidation of the relationship between this mechanism and the $\alpha_4\beta_1$-dependent pathologies.

2.3 Results and Discussion

2.3.1 Design of $\alpha_4\beta_1$ ligands

- **Development and validation of the $\alpha_4\beta_1$ integrin structure**

The design of $\alpha_4\beta_1$ ligands by molecular modelling studies was performed by Dr. Agostino Bruno (Istituto FIRC di Oncologia Molecolare, IFOM, Milano). As confirmed by research in the Protein Data Bank (PDB), the worldwide archive of atomic coordinates describing the experimentally-determined structures of proteins and other important biological macromolecules, up to date, there are not structural data of the $\alpha_4\beta_1$ integrin receptor. However, the atomic coordinates of the single α_4 and β_1 subunits are available, obtained from other integrin complexes, such as $\alpha_4\beta_7$ e $\alpha_5\beta_1$. Since these integrins possess a high degree of structural conservation, a big-sized, solvent exposed ligand-binding site at the α/β interface and a divalent cation (Mg^{2+}) at the metal ion-dependent adhesion site (MIDAS), which may be involved in a coordinated bond with a carboxylate group of the ligand,[46,47] it was possible to generate the structure of the $\alpha_4\beta_1$ integrin complex starting from the available single subunits. In particular, the α_4 subunit was obtained by the $\alpha_4\beta_7$ complex (PDB code: 3V4V), while the β_1 subunit was derived from $\alpha_5\beta_1$ (PDB code: 3VI4). Using $\alpha_5\beta_1$ integrin complex as a template, the α_4 subunit was aligned with α_5 bound to β_1 ($\alpha_5\beta_1$), then the α_5 subunit was removed, giving a preliminary $\alpha_4\beta_1$ complex.

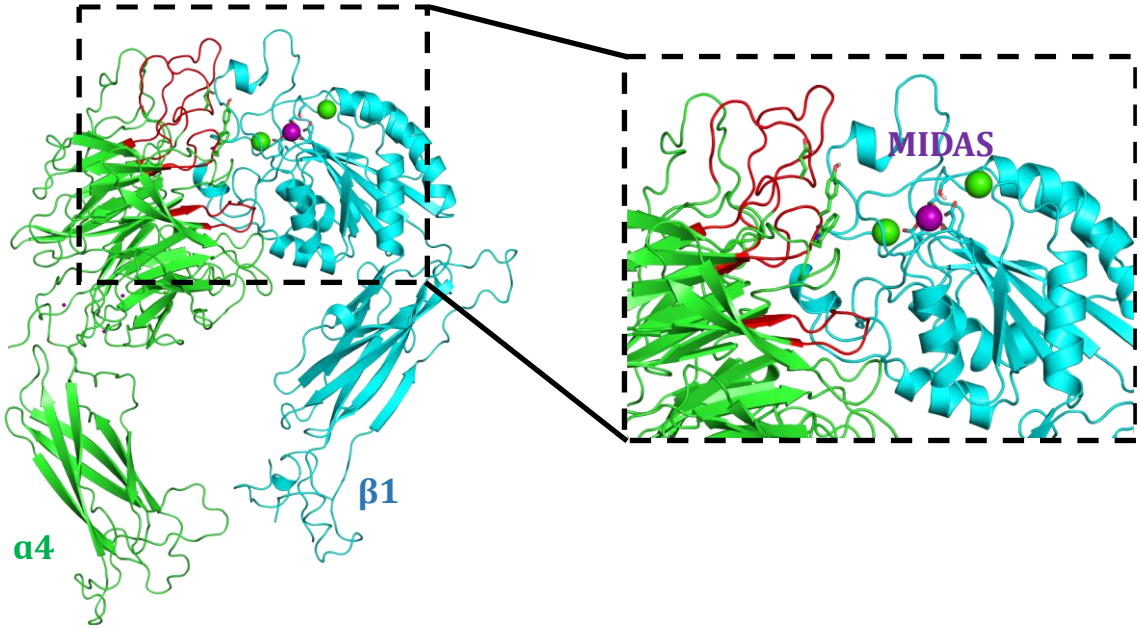

Figure 10. The final developed $\alpha_4\beta_1$ complex shows the classical structural organization of the integrin family; α_4 subunit (green cartoon), β_1 subunit (cyan cartoon). The Mg^{2+} ion of MIDAS is depicted as a purple ball.

The integrin complex thus obtained was refined using the Protein Preparation Wizard tool of Maestro9.1, optimized by a minimization protocol (Fig. 10), and then subjected to a validation procedure through docking studies using $\alpha_4\beta_1$ integrin antagonists including **1a** and **1b**, **3**, **4a** and **4b**, **BIO1211**, (*R*)-**8** and *(S)*-**8**. The structures of the investigated ligands are shown in the introduction of this chapter. For these docking experiments, we chose peptidic and peptidomimetic compounds with a high molecular diversity and inhibitory potencies ranging from micromolar to low nanomolar values.

For the sake of simplicity and clarity, the binding poses of just two compounds, **BIO1211** and (*R*)-**8**, are reported in Figure 11.

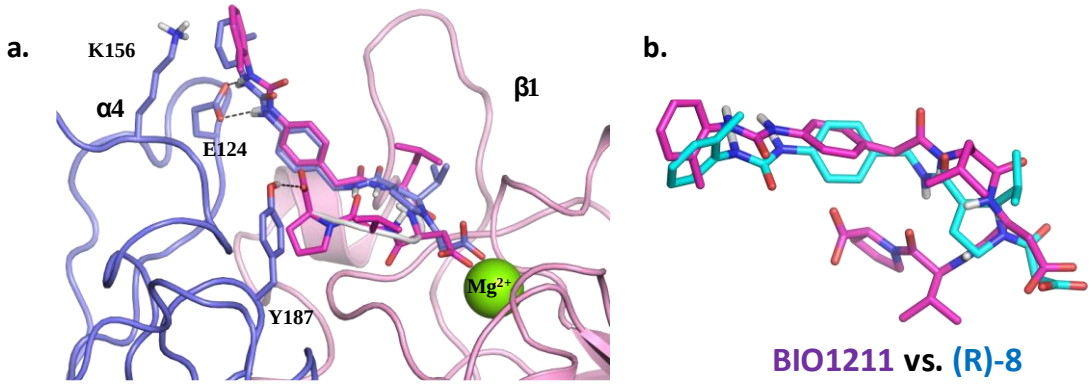

Figure 11. a. Binding poses of **BIO1211** (purple sticks) and (*R*)-**8** (blue sticks) in the binding site of $\alpha_4\beta_1$. The Mg^{2+} cation is reported as a green sphere. **b.** Overlapping of compounds **BIO1211** (purple sticks) e (*R*)**-8** (cyan sticks) obtained by docking studies. Note that the most important functional groups are perfectly superimposed.

From analysis of the binding poses, it can be noted that both compounds **BIO1211** and (*R*)-**8** interact with Mg^{2+} cation of the β subunit and share a common disposition within the binding pocket of the $\alpha_4\beta_1$ receptor, due to some common functional groups interacting with the same amino acid residues in the α subunit. In particular: (*i*) the ureido group of both compounds establishes a bidentate interaction with Glu124 (E124) residue, (*ii*) the aromatic ring of the phenyl-ureido group establishes a cation-π interaction with Lys156 (K156) residue, (*iii*) the isopropyl group of (*R*)-**8** assumes a spatial orientation similar to the valine side chain of **BIO1211**. This last observation would explain the experimental evidence for which its enantiomer (*S*)-**8** is considerably less active on $\alpha_4\beta_1$.[29] Furthermore, **BIO1211** establishes a hydrogen bond with Tyr187 (Y187), a very important interaction as highlighted by mutagenesis studies.[48]

Thus, the rationalization of the binding poses of the considered compounds proved to be in agreement with SAR studies reported in literature,[24,29] supporting the reliability of the developed receptor model. The validated model was used in the subsequent docking studies. The same experimental protocol was applied to identify the binding modes of possible $\alpha_4\beta_1$-antagonists bearing a cyclic aminoproline-based semipeptide structure, and their possible structural modifications to improve affinity toward $\alpha_4\beta_1$ integrin.

- **Docking studies of new potential $\alpha_4\beta_1$-antagonists**

The docking procedure developed during the validation process was used to evaluate compound **12**, also called *c*[Amp(MPUPA)LDVG], a new potential $\alpha_4\beta_1$-antagonist conceived in our research group. This compound is a cyclic aminoproline-based semipeptide, in which the multifaceted nature of the *cis*-4-amino-proline scaffold has been exploited as a scaffold to cyclize the LDVG tetrapeptide sequence. This compound presents the essential LDV recognizing motif with an additional Gly residue, and the N^{α}-proline site functionalized with the MPUPA group. In Figure 12 the binding poses of compound **12** are shown and compared to those of **BIO1211**.

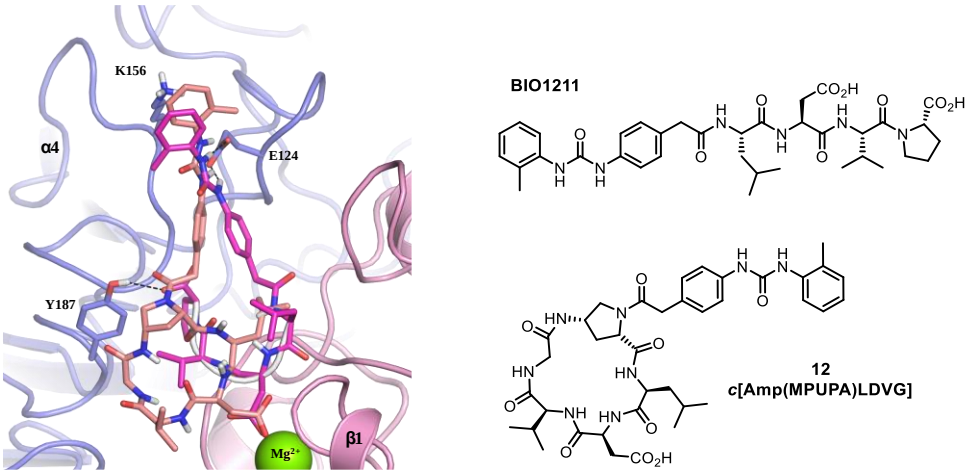

Figure 12. Binding poses of **12** (pink sticks) and of **BIO1211** (purple sticks) in the binding site of $\alpha_4\beta_1$.

From the analysis of the docking poses, we can claim that compound **12** (pink sticks) would be able to establish comparable interactions of **BIO1211** (purple sticks) in the binding pocket of the $\alpha_4\beta_1$ receptor model. Indeed, compound **12** is able to (*i*) chelate the divalent cation (Mg^{2+}) through the carboxylate group of the Asp residue and (*ii*) interact with the aminoacidic residues Tyr187, Lys156 e Glu124 in the same way as **BIO1211**. Moreover, its valine residue seems to assume the favorable spatial orientation as shown in **BIO1211**. Starting from compound **12**, which seems to possess all the required structural elements for a good integrin receptor affinity in a suitable conformational presentation, six further cyclic aminoproline-based semipeptide derivatives were designed, with the hope to discover compounds with high affinity profile. From the docking studies, a small collection of analogues of compound **12** was developed, with the following features: (*i*) lacking of Gly in a more constrained cyclic semipeptide, (*ii*) substitution of the Asp residue with Glu, allowing a better interaction of the carboxylate group at the end of the longer side chain with the divalent cation of MIDAS. Also, the corresponding retro sequences (VDL) were considered, together with the RGD derivative, to be used as negative controls during the binding assays (Fig. 13).

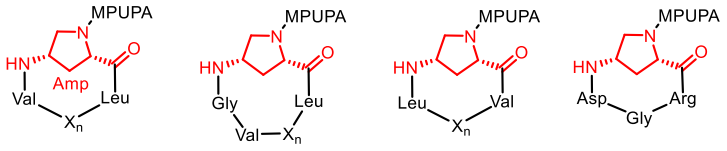

Figure 13. Cyclic aminoproline-based semipeptides **10-16** which were designed and synthesized in this work.

2.3.2 Synthesis of $\alpha_4\beta_1$ ligands

The designed compounds **10-16** were synthesized starting from the 4-aminoproline nucleus **18**, which was N^{α}-functionalized with the MPUPA moiety **19**, to give the desired *N*-Fmoc-Amp(MPUPA)-OH scaffold **17** (Scheme 1), suitable for SPPS Fmoc-strategy (Scheme 2). After cleavage from the resins, the synthesized linear peptides were cyclized, deprotected and purified by reverse phase HPLC, furnishing the desired cyclic aminoproline-based semipeptides **10-16**, to be finally evaluated by cellular assays.

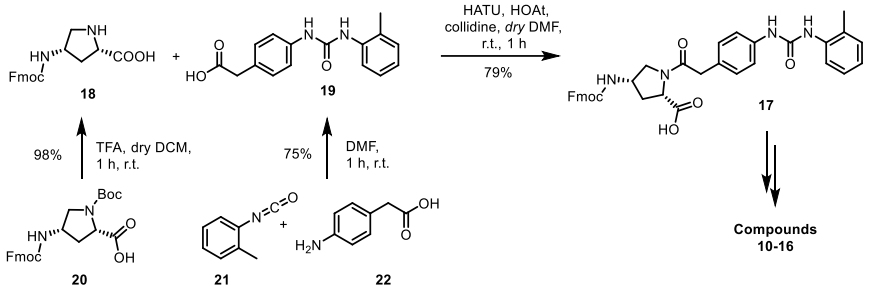

Scheme 1. Synthesis of *N*-Fmoc-Amp(MPUPA)-OH scaffold **17**.

In particular, the acidic treatment of the commercially available Fmoc-4-amino-1-Boc-pyrrolidine-2-carboxylic acid (**20**) produced the selective deprotection at N^{α}-proline site, giving compound **18**, as TFA salt, in high yield. The MPUPA portion (**19**) was instead synthesized starting from the commercially available precursors *o*-tolyl isocyanate (**21**) and 4-aminophenylacetic acid (**22**), following literature procedure.[4] Thus, the amino group of **22** reacted with the electrophilic carbon of the isocyanate group of **21** in DMF, producing the 4[(*N*-2-methylphenyl)ureido]-phenylacetyl scaffold (MPUPA, **19**) in a good 75% yield. Concerning the synthesis of the desired compound **17**, in order to avoid self-condensation reactions, since both compounds **18** and **19** possess a free carboxylic acid group, we decided to treat first the MPUPA unit **19** with the activating system HATU/HOAt/collidine in dry DMF. The following dropwise addition of the N^{α}-deprotected proline **18** to the reaction system led to the desired *N*-Fmoc-Amp(MPUPA)-OH scaffold **17** which was isolated, by reverse phase flash chromatography, in 79% yield.

For the synthesis of the linear precursors of compounds **10-16** we used the SPPS Fmoc-strategy exploiting acid-labile *o*-chlorotrityl chloride resins preloaded with three different amino acid residues: Asp(*t*Bu), Glu(*t*Bu) and Gly (Scheme 2).

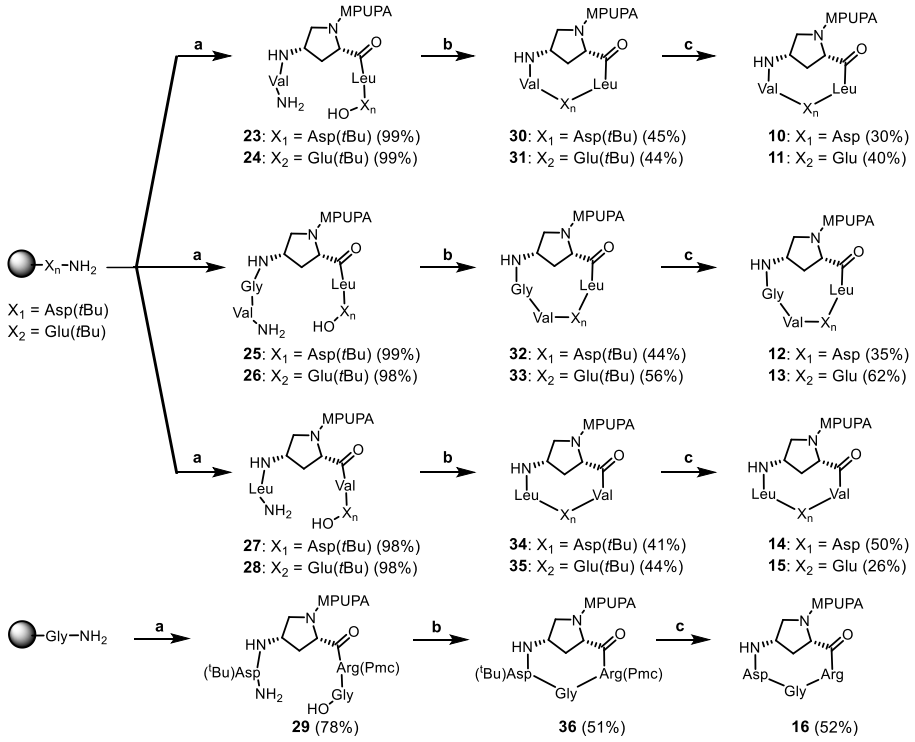

Scheme 2. a) ***Fmoc-SPPS*** **strategy:** (*Coupling*) Fmoc-amino acid, HATU, HOAt, collidine, DMF, rt, 4 h. (*Fmoc cleavage*) 20% piperidine in DMF, rt, 20 min. *Sequence of addition to obtain compounds*: (**23**, **24**) Fmoc-Leu-OH, **17**, Fmoc-Val-OH; (**25**, **26**) Fmoc-Leu-OH, **17**, Fmoc-Gly-OH, Fmoc-Val-OH; (**27**, **28**) Fmoc-Val-OH, **17**, Fmoc-Leu-OH; (**29**) Fmoc-Arg(Pmc)-OH, **17**, Fmoc-Asp(*t*Bu)-OH. (*Resin cleavage*) AcOH/TFE/DCM (1:1:3), rt, 20 min (2x). **b)** ***Cyclization*****:** HATU, HOAt, collidine, DCM/DMF, rt, 5 h. **c)** ***Deprotection*****:** TFA/TIS/H_2O (95:2.5:2.5), rt, 1 h.

Within all the peptide sequences to be synthesized, a critical role was played by the aminoproline scaffold; in fact, in all instances the Amp unit is positioned in a critical central position within the linear peptides, creating a local constraint that would likely preorganize the terminal chains toward the final macrocyclization step. Using standard Fmoc-SPPS chemistry, *N*-Fmoc-protected amino acids were coupled stepwise using the HATU/HOAt system in the presence of collidine. After each coupling, the Fmoc *N*-protecting group was easily removed by standard piperidine/DMF procedure and, once completed, the linear peptide sequences were readily cleaved from the resin using the usual AcOH/TFE/DCM system. This mild acidic treatment allowed to avoid the possible detachment of the acid-labile protecting groups *tert*-butyl (*t*Bu) and 2,2,5,7,8-pentamethylchroman-6-sulfonyl (Pmc) within the aspartic acid and arginine side chains, respectively. The crude linear peptides were obtained in yields ranging from 78 to 99% for the entire solid phase sequences.

The linear peptides **23**-**29** were then subjected to in-solution head-to-tail cyclization. As already mentioned in Chapter 1*a*, macrocyclization of peptides is generally considered a significant synthetic challenge.[49] Ring-closing (intramolecular) reactions are regularly plagued by low yields[50] and usually proceed much more slowly compared to intermolecular bond formations. Moreover, competing side reactions, such as dimerization of linear peptide precursors, often predominate for certain ring sizes. Since this problem can be minimized by carrying the reaction under high dilution conditions,[51] we performed the cyclization reaction by carefully keeping the linear peptide concentration quite low (3.3 mM) in a solution of dry DCM/DMF solvent mixture, in a 8:1 ratio. The expedient of keeping low the amount of the high boiling solvent (DMF), allowed for an easier evaporation of the solvent under vacuum after the completion of the reaction, thus avoiding high temperature and long times which can lead to the degradation of the cyclized product (e.g., oxidation to *N*-oxide proline ring derivatives, as observed in earlier works). Moreover, since the half-life of HATU under basic conditions is in the range of minutes,[51] we decided to previously dissolve the HATU/HOAt reagent couple in dry DCM/DMF solvent mixture (in a 10:1 ratio) and, after that, we added the solution of each linear peptide and collidine (predissolved in dry DCM/DMF, 5:1) to this reagent couple dropwise. In this way, the HATU coupling reagent should be reactive for more time and the slow addition of the linear peptide precursor would contribute to keep low its concentration in the reaction system. The crude cyclized peptides were purified by reverse phase flash chromatography [H_2O (0.1% TFA)/MeCN: linear gradient 80:20 to 20:80] furnishing the protected cyclized peptides in yields ranging from 41 to 56%. Finally, side-chain deprotection of the cyclic peptides was carried out under acidic conditions (TFA/TIS/ H_2O - 95:2.5:2.5). Compounds **10**-**16** were recovered, as TFA salts after RP-HPLC purification, in yields ranging from 30 to 60%, with global yields ranging from 11 to 26% for the cyclization/deprotection steps. Target compounds **10**-**16** were validated by high-resolution ESI mass spectrometry as well as various NMR techniques.

The biological assays on Jurkat cells are currently under investigation by researchers at the University of Florence (Dr. Francesca Bianchini, Dipartimento di Scienze Biomediche, Sperimentali e Cliniche “Mario Serio”, Università degli Studi di Firenze, Italy) and the results in terms of ligand binding affinity and selectivity towards the $\alpha_4\beta_1$ receptor will be collected and evaluated, with indications about possible structural refinement and optimization in future works.

2.4 Conclusions

The search for potent and selective integrin binders is a major topic of interest in current medicinal chemistry-driven projects. During this work, in particular, the synthesis of new potential $\alpha_4\beta_1$ integrin binders was targeted. Based on some computational suggestions, seven new cyclic semipeptides were synthesized, which were built upon a common aminoproline core scaffold and all bearing a MPUPA hexocyclic appendage. Future biological investigations will be carried out in order to evaluate their actual efficacy and selectivity as $\alpha_4\beta_1$ integrin binders.

2.5 Experimental Part

Experimental synthetic procedures and characterization data

General. All chemicals were of the highest commercially available quality and were used without further purification. Solvents were dried by standard procedures and reactions requiring anhydrous conditions were performed under nitrogen or argon atmosphere. H-Gly-2-ClTrt resin (loading 0.63 mmol/g), H-Asp(O*t*Bu)-2-ClTrt resin (loading 0.74 mmol/g), H-Glu(O*t*Bu)-2-ClTrt resin (loading 0.85 mmol/g) were purchased from Novabiochem, (2*S*,4*S*)-Fmoc-4-amino-1-Boc-pyrrolidine-2-carboxylic acid from PolyPeptide and all other reagents from Alfa Aesar, TCI and Sigma-Aldrich. Analytical thin layer chromatography (TLC) was performed on silica gel 60 F_{254} pre-coated plates with visualization under short-wavelength UV light and by dipping the plates with molybdate reagent (aqueous H_2SO_4 solution of ceric sulphate/ammonium molybdate) followed by heating. Flash column chromatography was performed using 40-63 µm silica gel and the indicated solvent mixtures. Automated flash column chromatography was carried out with the Biotage Isolera One system using Biotage KP-C18-HS cartridge (reverse phase flash chromatography). HPLC purifications were performed on a Prostar 210 apparatus (Varian, UV detection) equipped with C_{18}-10 µm column (Discovery BIO Wide Pore 21.2 × 250 mm). Routine NMR spectra were recorded on Avance 300 or 400 (Bruker) NMR spectrometers. Chemical shifts (δ) are reported in parts per million (ppm) with CD_2HOD resonance peak set at 3.31 ppm. Multiplicities are indicated as s (singlet), d (doublet), t (triplet), q (quartet), m (multiplet), and b (broad). Coupling constants, *J*, are reported in Hertz. ^{1}H NMR assignments are corroborated by 1D and 2D experiments (gCOSY sequences). Optical rotations were measured using a Perkin-Elmer model 341 polarimeter at ambient temperature using a 100 mm cell with a 1 mL capacity and are given in units of 10^{-1} deg cm^2 g^{-1}. High resolution mass analysis (ESI) was performed on LTQ ORBITRAP XL Thermo apparatus and are reported in the form of (*m/z*). Purity of all tested compounds was determined by analytical high-pressure liquid chromatography (HPLC) and was in the 96 - >99% range.

Abbreviations. Amp, 4-amino-L-proline; Boc, *tert*-butoxycarbonyl; Pmc, 2,2,5,7,8-pentamethylchroman-6-sulfonyl; Fmoc, 9-fluorenylmethoxycarbonyl; SPPS, solid phase peptide synthesis; DCM, dichloromethane; DMF, *N*,*N*-dimethylformamide; MeCN, acetonitrile; AcOH, glacial acetic acid ; TFA, trifluoroacetic acid; TFE, trifluoroethanol; HATU, *O*-(7-azabenzotriazol-1-yl)-*N*,*N*,*N*',*N*'-tetramethyluronium hexafluorophosphate; HOAt, 1-hydroxy-7-azabenzotriazole; TIS, triisopropylsilane; Fmoc-AA-OH, Fmoc-protected amino acids.

Starting Materials. H-Gly-2-ClTrt resin, H-Asp(*t*Bu)-2-ClTrt resin, H-Glu(*t*Bu)-2-ClTrt resin, *p*-aminophenylacetic acid (**22**), *o*-tolyl isocyanate (**21**), (2*S*,4*S*)-Fmoc-4-amino-1-Boc-pyrrolidine-2-carboxylic acid (**20**), Fmoc-Asp(*t*Bu)-OH; Fmoc-Arg (Pmc)-OH, Fmoc-Leu-OH, Fmoc-Val-OH, Fmoc-Gly-OH, HATU, HOAt, 2,4,6-collidine, piperidine, AcOH, TFE, TFA, TIS were commercially available and were used as such without further purification.

(2S,4S)-4-*N*-(9-Fluorenylmethoxycarbonyl)aminoproline (**18**) was prepared according to procedure reported in the Experimental Part (Chapter 1a), while 4-[[[(2-Methylphenyl)amino]carbonyl]amino]phenylacetic acid (MPUPA-OH) (**19**) was prepared according to literature procedure.[4]

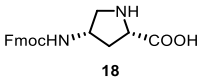

18

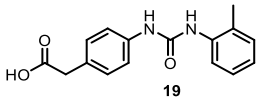

19

(2S,4S)-1-(MPUPA)-4-(Fmoc)aminoproline, or Fmoc-Amp(MPUPA)-OH (17)

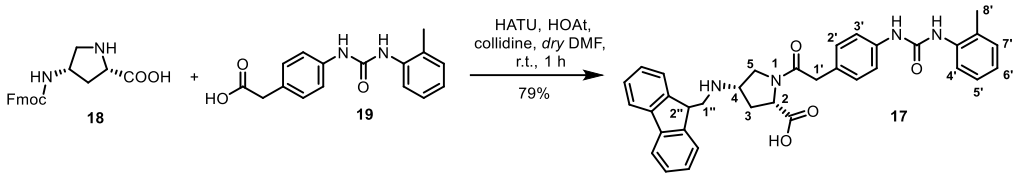

To a stirred solution of MPUPA-OH **19** (107 mg, 0.38 mmol, 1.1 equiv), HATU (144 mg, 0.38 mmol, 1.1 equiv) and HOAt (51 mg, 0.38 mmol, 1.1 equiv) in dry DMF (2 mL), 2,4,6-collidine (95 µL, 0.72 mmol, 2.1 quiv) was added and the system left to stir for 30 min, under argon at room temperature. To the reaction mixture it was then added dropwise (over 20 min) a stirred solution of compound **18** and 2,4,6-collidine (46 µL, 0.34 mmol, 1 equiv) in dry DMF (8 mL). The reaction went to completion in 40 min, and then treated with an aqueous solution of HCl (0.1 N) to precipitate the product. The crude residue was filtered and purified by reverse phase flash chromatography [H_2O (0.1% AcOH)/MeCN: linear gradient 80:20 to 20:80] furnishing compound **17** (168.2 mg, yield 79%) as withe glassy solid.

^{1}H NMR (MeOD, 400 MHz) δ 7.76 (d, *J* = 7.5 Hz, 2H, ArH Fmoc), 7.66-7.56 (m, 3H, ArH Fmoc and MPUPA), 7.42-7.33 (m, 4H, ArH Fmoc and MPUPA), 7.32-7.24 (bm, 2H, ArH Fmoc), 7.23-7.11 (m, 4H, ArH MPUPA), 7.01 (ddd, *J* = 7.4, 7.4, 1.0 Hz, 1H, H6' MPUPA), 4.40 (t, *J* = 6.8 Hz, 1H, H2 Amp), 4.31 (m, 2H, H1'' Fmoc), 4.24-4.14 (bm, 2H, H2'' Fmoc and H4 Amp), 3.94-3.86 (m, 1H, H5 Amp), 3.66 (d, *J* = 15.9 Hz, 1H, H1' MPUPA), 3.65 (d, *J* = 15.8 Hz, 1H, H1' MPUPA), 3.35 (m, 1H, H5 Amp), 2.60-2.49 (bm, 1H, H3 Amp), 2.25 (s, 3H, H8' MPUPA), 1.95-1.84 (bm, 1H, H3 Amp). ^{13}C NMR (MeOD, 400 MHz) δ 174.0, 171.3, 156.6, 154.4, 143.8, 141.2, 138.1, 136.5, 130.1, 129.7, 129.2, 128.3, 127.4, 126.8, 126.1, 124.8, 124.0, 123.0, 119.6, 119.0, 66.4, 57.8, 52.1, 51.3, 50.2, 40.4, 34.2, 16.7.

General procedure A: Fmoc-based SPPS

Linear peptides **23-29** were prepared according to the following general procedure, using the preloaded resins: (*i*) H-Asp(*t*Bu)-2-ClTrt resin (loading 0.74 mmol/g) (**23**, **25**, **27**); (*ii*) H-Glu(*t*Bu)-2-ClTrt resin (loading 0.85 mmol/g) (**24**, **26**, **28**); (*iii*) H-Gly-2-ClTrt resin (loading 0.63 mmol/g) (**29**).

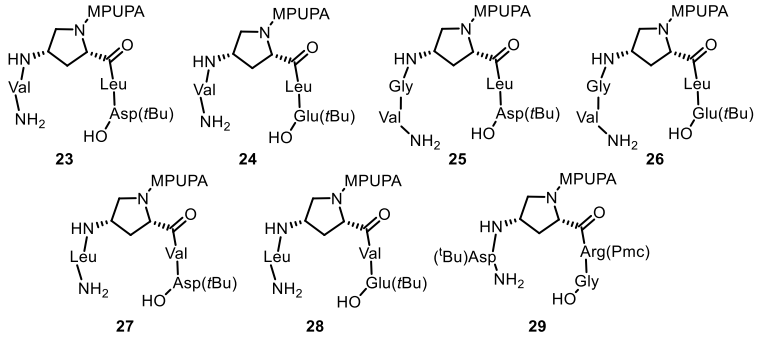

Resin swelling. The desired resin was swollen in a solid phase reaction vessel with dry DMF (2 mL) under mechanical stirring; after 40 min the solvent was drained and the resin was washed with DCM (2 ×) and DMF (2 ×).

Peptide coupling. A preformed solution of Fmoc-AA-OH (1.5 equiv with respect to the resin) in dry DMF (2 mL) was treated with HATU (2 equiv), HOAt (2 equiv) and 2,4,6-collidine (2 equiv), and stirred for 10 min before adding to the resin. The mixture was shaken at room temperature for 5 h. Completion of the reaction was checked by the Kaiser test (see Experimental Part, Chapter 1*a*). The solution was drained and the resin was washed several times with DMF (2 ×), *i*PrOH, (2 ×), Et_2O (2 ×), DCM (2 ×). The resin was then treated with 20% v/v piperidine in DMF (2 mL) and the mixture was stirred for 30 min (*Fmoc cleavage*). The solution was drained and the resin was washed with DMF (2 ×), *i*PrOH, (3 ×), Et_2O (2 ×), DCM (2 ×). The couplings of the further amino acids, in the proper sequence, were carried out under the same conditions.

Resin cleavage. After coupling of the last Fmoc-AA-OH, the resin was treated with 2 mL of the cleavage mixture DCM/TFE/AcOH (3:1:1) and kept under mechanical stirring for 20 min at room temperature. The solution was recovered and the resin was carefully washed with DCM (2 ×). This protocol was repeated twice. The combined solution was evaporated under reduced pressure (keeping temperature below 50 °C) affording desired linear peptide, which was used in the following synthetic step without further purification.

H-Val-1-(MPUPA)Amp-Leu-Asp(*t*Bu)-OH (23)

The synthesis of linear tetrapeptide **23** was performed following the general procedure A, using the preloaded H-Asp(*t*Bu)-2-ClTrt resin (60 mg, 0.044 mmol, 1 equiv) and the following Fmoc-amino acids: Fmoc-Leu-OH (23 mg, 0.06 mmol, 1.5 equiv), Fmoc-(MPUPA)Amp-OH **17** (40 mg, 0.06 mmol), Fmoc-Val-OH (22 mg, 0.06 mmol). The linear tetrapeptide **23** (34 mg, yield 99%) was obtained as a white glassy solid, and used in the following synthetic step without further purification. MS (ESI^+) *m/z* 780.4 $[M+H]^+$.

H-Val-1-(MPUPA)Amp-Leu-Glu(*t*Bu)-OH (24)

The synthesis of linear tetrapeptide **24** was performed following the general procedure A, using the preloaded H-Glu(*t*Bu)-2-ClTrt resin (51 mg, 0.043 mmol, 1 equiv) and the following Fmoc-amino acids: Fmoc-Leu-OH (23 mg, 0.06 mmol, 1.5 equiv), Fmoc-(MPUPA)Amp-OH **17** (40 mg, 0.06 mmol, 1.5 equiv), Fmoc-Val-OH (22 mg, 0.06 mmol, 1.5 equiv). The linear tetrapeptide **24** (34 mg, yield 99%) was obtained as a white glassy solid, and used in the following synthetic step without further purification. MS (ESI^+) *m/z* = 794.4 $[M+H]^+$.

H-Val-Gly-1-(MPUPA)Amp-Leu-Asp(*t*Bu)-OH (25)

The synthesis of linear tetrapeptide **25** was performed following the general procedure A, using the preloaded H-Asp(*t*Bu)-2-ClTrt resin (60 mg, 0.044 mmol, 1 equiv) and the following Fmoc-amino acids: Fmoc-Leu-OH (23 mg, 0.06 mmol, 1.5 equiv), Fmoc-(MPUPA)Amp-OH **17** (40 mg, 0.06 mmol, 1.5 equiv), Fmoc-Gly-OH (19 mg, 0.06 mmol, 1.5 equiv), Fmoc-Val-OH (22 mg, 0.06 mmol, 1.5 equiv). The linear tetrapeptide **25** (36 mg, yield 99%) was obtained as a white glassy solid, and used in the following synthetic step without further purification. MS (ESI^+) *m/z* = 837.4 $[M+H]^+$.

H-Val-1-(MPUPA)Amp-Leu-Glu(*t*Bu)-OH (26)

The synthesis of linear tetrapeptide **26** was performed following the general procedure A, using the preloaded H-Glu(*t*Bu)-2-ClTrt resin (51 mg, 0.043 mmol, 1 equiv) and the following Fmoc-amino acids: Fmoc-Leu-OH (23 mg, 0.06 mmol, 1.5 equiv), Fmoc-(MPUPA)Amp-OH **17** (40 mg, 0.06 mmol, 1.5 equiv), Fmoc-Gly-OH (19 mg, 0.06 mmol, 1.5 equiv), Fmoc-Val-OH (22 mg, 0.06 mmol, 1.5 equiv). The linear tetrapeptide **26** (36 mg, yield 98%) was obtained as a white glassy solid, and used in the following synthetic step without further purification. MS (ESI^+) *m/z* = 794.4 $[M+H]^+$.

H-Val-1-(MPUPA)Amp-Leu-Asp(*t*Bu)-OH (27)

The synthesis of linear tetrapeptide **27** was performed following the general procedure A, using the preloaded H-Asp(*t*Bu)-2-ClTrt resin (60 mg, 0.044 mmol, 1 equiv) and the following Fmoc-amino acids: Fmoc-Val-OH (22 mg, 0.06 mmol, 1.5 equiv), Fmoc-(MPUPA)Amp-OH **17** (40 mg, 0.06 mmol, 1.5 equiv), Fmoc-Leu-OH (23 mg, 0.06 mmol, 1.5 equiv). The linear tetrapeptide **27** (33 mg, yield 98%) was obtained as a white glassy solid, and used in the following synthetic step without further purification. MS (ESI^+) *m/z* = 780.4 $[M+H]^+$.

H-Leu-1-(MPUPA)Amp-Val-Glu(*t*Bu)-OH (28)

The synthesis of linear tetrapeptide **28** was performed following the general procedure A, using the preloaded H-Glu(*t*Bu)-2-ClTrt resin (51 mg, 0.043 mmol, 1 equiv) and the following Fmoc-amino acids: Fmoc-Val-OH (22 mg, 0.06 mmol, 1.5 equiv), Fmoc-(MPUPA)Amp-OH **17** (40 mg, 0.06 mmol, 1.5 equiv), Fmoc-Leu-OH (23 mg, 0.06 mmol, 1.5 equiv). The linear tetrapeptide **28** (34 mg, yield 98%) was obtained as a white glassy solid, and used in the following synthetic step without further purification. MS (ESI^+) *m/z* = 794.4 $[M+H]^+$.

H-Asp(*t*Bu)-1-(MPUPA)Amp-Arg(Pmc)-Gly-OH (29)

The synthesis of linear tetrapeptide **29** was performed following the general procedure A, using the preloaded H-Gly-2-ClTrt resin (70 mg, 0.044 mmol, 1 equiv) and the following Fmoc-amino acids: Fmoc-Arg(Pmc)-OH (43 mg, 0.06 mmol, 1.5 equiv), Fmoc-(MPUPA)Amp-OH **17** (40 mg, 0.06 mmol, 1.5 equiv), Fmoc-Asp(*t*Bu)-OH (27 mg, 0.06 mmol, 1.5 equiv). The linear tetrapeptide **23** (35 mg, yield 78%) was obtained as a white glassy solid, and used in the following step without further purification. MS (ESI$^+$) *m/z* = 1047.5 $[M+H]^+$.

General Procedure B: Cyclization reaction

Protected cyclic peptides **30-36** were prepared according to the following general procedure.

A solution of linear peptide (1 equiv) and 2,4,6-collidine (2.5 equiv) in dry DCM/DMF solvent mixture (5:1 ratio) was prepared. The mixture was stirred under argon at room temperature, and added dropwise to a solution of HATU (2 equiv) and HOAt (2 equiv) in dry DCM/DMF solvent mixture (10:1 ratio). The reaction mixture was degassed by argon/vacuum cycles (3 ×) and left to stir under argon at room temperature for 5 h. After reaction completion, the solution was concentrated under vacuum, treated with aq $NaHCO_3$ saturated solution and extracted with EtOAc (4 ×). The combined organic layers were dried with $MgSO_4$, filtered and evaporated under reduced pressure, keeping the temperature below 50 °C. The crude was purified by reverse phase flash chromatography [H_2O (0.1% TFA)/MeCN: linear gradient 80:20 to 20:80] furnishing the protected cyclic peptide as a solid.

General Procedure C: Deprotection reaction

Deprotected cyclic peptides **10-16** were prepared according to the following general procedure.

The protected cyclic intermediate (1 equiv) was dissolved in TFA/TIS/H_2O (95:2.5:2.5) mixture and stirred at room temperature for 1 h. Then the solvent was evaporated and the crude residue was thoroughly washed with Et_2O (4 ×) and petroleum ether (2 ×). Preparative RP-HPLC purification was performed [C_{18}-10 µm column, 21.2 × 250 mm; Solvent A: H_2O (0.1% TFA) and Solvent B: MeCN; flow rate 8 mL/min; detection 254 nm] using the following elution gradient: 0-1 min 10% B, 1-18 min 10-45% B, 18-25 min 45% B.

c[(MPUPA)AmpLDV] (10)

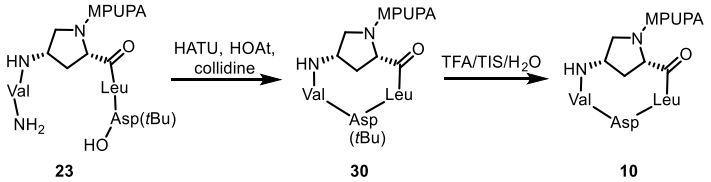

Compound **30** was prepared according to the general procedure B. A solution of linear peptide **23** (23 mg, 0.03 mmol) and 2,4,6-collidine (9.8 µL, 0.07 mmol) in dry DCM/DMF solvent mixture (1 mL /0.2 mL) was added dropwise to a solution of HATU (22 mg, 0.06 mmol) and HOAt (8 mg, 0.06 mmol) in dry DCM/DMF solvent mixture (4 mL /0.4 mL). After RP-flash chromatography, the protected cyclic peptide **30** (10 mg, yield 45%) was obtained as a white solid. MS (ESI$^+$) *m/z* = 762.4 $[M+H]^+$.

Compound **10** was prepared according to the general procedure C. The protected cyclic intermediate **30** (10 mg, 0.01 mmol, 1 equiv) was treated with 0.66 mL of TFA/TIS/H_2O (95:2.5:2.5) mixture and, after preparative RP-HPLC purification (R_t = 24.7 min), cyclic peptide **10** (2.7 mg, yield 30%) was obtained as a white glassy solid. MS (ESI$^+$) *m/z* = 706.4 $[M+H]^+$.

^{1}H NMR (MeOD, 400 MHz) δ 7.64 (dd, *J* = 8.0, 1.4 Hz, 1H, H4' MPUPA), 7.40 (m, 2H, H3' MPUPA), 7.22 (m, 2H, H2' MPUPA), 7.18 (m, 1H, H5' MPUPA), 7.13 (d, *J* = 8.5 Hz, 1H, H7' MPUPA), 7.04 (ddd, *J* = 7.5, 7.5, 1.0 Hz, 1H, H6' MPUPA), 4.67 (m, 1H, H4 Amp), 4.63 (d, *J* = 9.4 Hz, 1H, H2 Amp), 4.48 (t, *J* = 7.6 Hz, 1H, Hα Asp), 4.07 (t, *J* = 8.0 Hz, 1H, Hα Leu), 3.91 (dd, *J* = 11.9, 6.1 Hz, 1H, H5 Amp), 3.78 (d, *J* = 6.5 Hz, 1H, Hα Val), 3.70 (s, 2H, H1' MPUPA), 3.68 (m, 1H, H5 Amp), 3.00 (dd, *J* = 16.6, 7.5 Hz, 1H, Hβ Asp), 2.90 (dd, *J* = 16.6, 7.5 Hz, 1H, Hβ Asp), 2.50 (m, 1H, Hβ Val), 2.46 (m, 1H, H3 Amp), 2.31 (s, 3H, H8' MPUPA), 2.08 (d, *J* = 14 Hz, 1H, H3 Amp), 1.73 (m, 1H, Hγ Leu), 1.58 (m, 2H, Hβ Leu), 0.96 (m, 12H, 2CH_3 Val, 2CH_3 Leu). $[\alpha]_D^{25}$: –38 (*c* 1.0, MeOH)

c[(MPUPA)AmpLEV] (11)

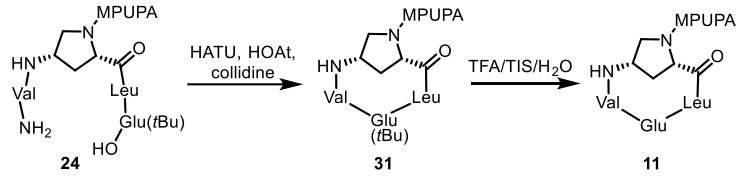

Compound **31** was prepared according to the general procedure B. A solution of linear peptide **24** (20 mg, 0.03 mmol) and 2,4,6-collidine (8.4 µL, 0.06 mmol) in dry DCM/DMF solvent mixture (1 mL /0.2 mL) was added dropwise to a solution of HATU (19 mg, 0.05 mmol) and HOAt (7 mg, 0.05 mmol) in dry DCM/DMF solvent mixture (4 mL /0.4 mL). After RP-flash chromatography, the protected cyclic peptide **31** (8.5 mg, yield 44%) was obtained as a white solid. MS (ESI$^+$) *m/z* = 776.4 $[M+H]^+$.

Compound **11** was prepared according to the general procedure C. The protected cyclic intermediate **31** (8 mg, 0.01 mmol) was treated with 0.55 mL of TFA/TIS/H_2O (95:2.5:2.5) mixture and, after preparative RP-HPLC purification (R_t = 24.6 min), cyclic peptide **11** (3.1 mg, yield 40%) was obtained as a white glassy solid. MS (ESI$^+$) *m/z* = 720.4 $[M+H]^+$.

^{1}H NMR (MeOD, 400 MHz) δ 7.64 (d, *J* = 8.0 Hz, 1H, H4' MPUPA), 7.41 (d, *J* = 8.5 Hz, 2H, H3' MPUPA), 7.21 (d, *J* = 8.6 Hz, 2H, H2' MPUPA), 7.18 (dd, *J* = 7.9, 7.9 Hz, 1H, H5' MPUPA), 7.13 (d, *J* = 8.5 Hz, 1H, H7' MPUPA), 7.04 (dd, *J* = 7.3, 7.3 Hz, 1H, H6' MPUPA), 4.71 (m, 1H, H2 Amp), 4.65 (m, 1H, H4 Amp), 4.60 (m, 1H, Hα Glu), 4.03 (m, 2H, Hα Leu, Hα Val), 3.93 (dd, *J* = 11.4, 6.3 Hz, 1H, H5 Amp), 3.70 (s, 2H, H1' MPUPA), 3.67 (m, 1H, H5 Amp), 2.47 (m, 1H, H3 Amp), 2.47 (m, 1H, Hβ Val), 2.36 (m, 2H, Hγ Glu), 2.31 (s, 3H, H8' MPUPA), 2.18 (m, 2H, Hβ Glu), 2.07 (d, *J* = 14.2 Hz, 1H, H3 Amp), 1.69 (m, 3H, Hβ Leu, Hγ Leu), 0.96 (m, 12H, CH_3 Leu, CH_3 Val). $[\alpha]_D^{25}$: –19 (*c* 1.0, MeOH)

c[(MPUPA)AmpLDVG] (12)

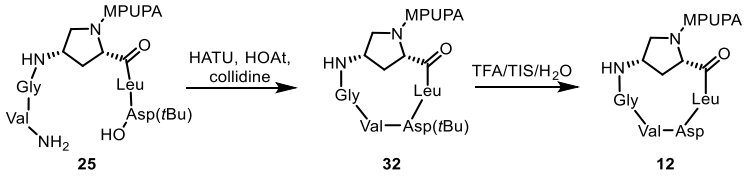

Compound **32** was prepared according to the general procedure B. A solution of linear peptide **25** (19 mg, 0.02 mmol) and 2,4,6-collidine (7.7 µL, 0.06 mmol) in dry DCM/DMF solvent mixture (1 mL /0.2 mL) was added dropwise to a solution of HATU (18 mg, 0.05 mmol) and HOAt (6 mg, 0.05 mmol) in dry DCM/DMF solvent mixture (4 mL /0.4 mL). After RP-flash chromatography, the protected cyclic peptide **32** (8.1 mg, yield 44%) was obtained as a white solid. MS (ESI$^+$) *m/z* = 818.4 $[M+H]^+$.

Compound **12** was prepared according to the general procedure C. The protected cyclic intermediate **32** (8 mg, 0.01 mmol) was treated with 0.55 mL of TFA/TIS/H_2O (95:2.5:2.5) mixture and, after preparative RP-HPLC purification (R_t = 24.6 min), cyclic peptide **15** (2.7 mg, yield 35%) was obtained as a yellowish glassy solid. MS (ESI$^+$) *m/z* = 763.4 $[M+H]^+$.

^{1}H NMR (MeOD, 400 MHz) δ 7.64 (d, *J* = 8.0 Hz, 1H, H4' MPUPA), 7.41 (d, *J* = 8.5 Hz, 2H, H3' MPUPA), 7.21 (d, *J* = 8.6 Hz, 2H, H2' MPUPA), 7.18 (dd, *J* = 7.9, 7.9 Hz, 1H, H5' MPUPA), 7.13 (d, *J* = 8.5 Hz, 1H, H7' MPUPA), 7.04 (dd, *J* = 7.3, 7.3 Hz, 1H, H6' MPUPA), 4.70 (dd, *J* = 10.3, 2.6 Hz, 1H, H2 Amp), 4.60 (dd, *J* = 6.9, 4.8 Hz, 1H, Hα Asp), 4.60 (m, 1H, H4 Amp), 4.13 (m, 1H, Hα Gly), 4.10 (m, 1H, Hα Leu), 4.02 (m, 1H, Hα Val), 3.95 (dd, *J* = 11.2, 6.6 Hz, 1H, H5 Amp), 3.72 (d, *J* = 15.3 Hz, 1H, H1' MPUPA), 3.69 (d, *J* = 15.6 Hz, 1H, H1' MPUPA), 3.54 (m, 1H, Hα Gly), 3.48 (m, 1H, H5 Amp), 3.05 (dd, *J* = 17.1, 7.2 Hz, 1H, Hβ Asp), 2.95 (dd, *J* = 17.0, 4.9 Hz, 1H, Hβ Asp), 2.62 (m, 1H, H3 Amp), 2.31 (s, 3H, H8' MPUPA), 2.24 (m, 1H, H3 Amp), 1.71 (m, 3H, Hβ Leu, Hγ Leu), 0.99 (m, 12H, CH_3 Leu, CH_3 Val). $[\alpha]_D^{25}$: –37 (*c* 1.0, MeOH)

c[(MPUPA)AmpLEVG] (13)

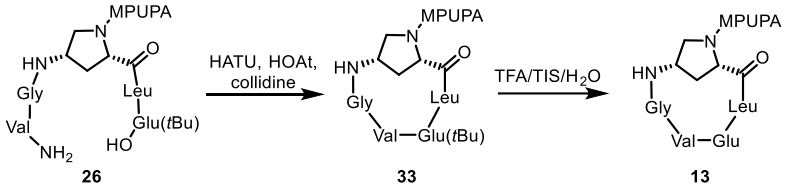

26 **33** **13**

Compound **33** was prepared according to the general procedure B. A solution of linear peptide **26** (27 mg, 0.03 mmol) and 2,4,6-collidine (11 µL, 0.08 mmol) in dry DCM/DMF solvent mixture (1.5 mL /0.3 mL) was added dropwise to a solution of HATU (25 mg, 0.07 mmol) and HOAt (9 mg, 0.07 mmol) in dry DCM/DMF solvent mixture (4 mL /0.4 mL). After RP-flash chromatography, the protected cyclic peptide **33** (14.5 mg, yield 56%) was obtained as a white solid. MS (ESI$^+$) *m/z* 833.5 $[M+H]^+$.

Compound **13** was prepared according to the general procedure C. The protected cyclic intermediate **33** (14.5 mg, 0.02 mmol) was treated with 0.9 mL of TFA/TIS/H_2O (95:2.5:2.5) mixture and, after preparative RP-HPLC purification (R_t = 24.5 min), cyclic peptide **13** (8.7 mg, yield 62%) was obtained as a white-yellow glassy solid. MS (ESI$^+$) *m/z* = 777.4 $[M+H]^+$.

^{1}H NMR (MeOD, 400 MHz) δ 7.64 (d, *J* = 8.0 Hz, 1H, H4' MPUPA), 7.41 (d, *J* = 8.5 Hz, 2H, H3' MPUPA), 7.21 (d, *J* = 8.6 Hz, 2H, H2' MPUPA), 7.18 (dd, J = 7.9, 7.9 Hz, 1H, H5' MPUPA), 7.13 (d, *J* = 8.5 Hz, 1H, H7' MPUPA), 7.04 (dd, J = 7.3, 7.3 Hz, 1H, H6' MPUPA), 4.70 (dd, *J* = 10.6, 3.3 Hz, 1H, H2 Amp), 4.62 (m, 1H, H4 Amp), 4.38 (dd, *J* = 9.1, 3.8 Hz, 1H, Hα Glu), 4.21 (d, *J* = 17.0 Hz, 1H, Hα Gly), 4.16 (dd, *J* = 9.4, 5.9 Hz, 1H, Hα Leu), 4.03 (dd, *J* = 11.0, 7.3 Hz, 1H, H5 Amp), 3.76 (d, *J* = 7.0 Hz, 1H, Hα Val), 3.71 (d, *J* = 3.9 Hz, 2H, H1' MPUPA), 3.47 (d, *J* = 17.1 Hz, 1H, Hα Gly), 3.45 (m, 1H, H5 Amp), 2.70 (ddd, *J* = 14.2, 9.4, 9.4 Hz, 1H, H3 Amp), 2.39 (m, 2H, Hγ Glu), 2.35 (m, 1H, H3 Amp), 2.31 (s, 3H, H8' MPUPA), 2.26 (m, 1H, Hβ Glu), 2.14 (m, 1H, Hβ Val), 2.05 (m, 1H, Hβ Glu), 1.77 (m, 1H, Hγ Leu), 1.69 (m, 2H, Hβ Leu), 1.02 (m, 6H, $2CH_3$ Val), 0.97 (m, 6H, $2CH_3$ Leu). $[\alpha]_D^{25}$: –38 (*c* 1.0, MeOH)

c[(MPUPA)AmpVDL] (14)

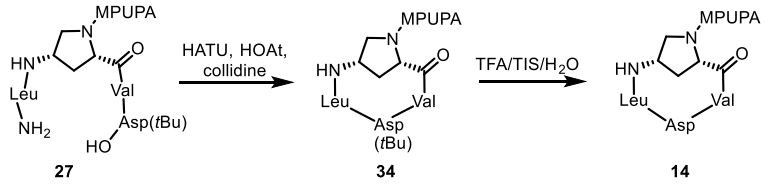

27 **34** **14**

Compound **34** was prepared according to the general procedure B. A solution of linear peptide **27** (20 mg, 0.03 mmol) and 2,4,6-collidine (8.5 µL, 0.06 mmol) in dry DCM/DMF solvent mixture (1 mL /0.2 mL) was added dropwise to a solution of HATU (20 mg, 0.05 mmol) and HOAt (7 mg, 0.05 mmol) in dry DCM/DMF solvent mixture (4 mL /0.4 mL). After RP-flash chromatography, the protected cyclic peptide **34** (8 mg, yield 41%) was obtained as a white solid. MS (ESI$^+$) *m/z* = 762.4 $[M+H]^+$.

Compound **14** was prepared according to the general procedure C. The protected cyclic intermediate **34** (8 mg, 0.01 mmol) was treated with 0.55 mL of TFA/TIS/H_2O (95:2.5:2.5) mixture and after preparative RP-HPLC purification (R_t = 24.3 min), cyclic peptide **14** (3.7 mg, yield 50%) was obtained as a white glassy solid. MS (ESI$^+$) *m/z* = 706.4 $[M+H]^+$.

^{1}H NMR (400 MHz, MeOD) δ 7.64 (dd, *J* = 8.0, 1.4 Hz, 1H, H4' MPUPA), 7.40 (m, 2H, H3' MPUPA), 7.22 (m, 2H, H2' MPUPA), 7.18 (m, 1H, H5' MPUPA), 7.13 (d, *J* = 8.5 Hz, 1H, H7' MPUPA), 7.04 (ddd, *J* = 7.5, 7.5, 1.0 Hz, 1H, H6' MPUPA), 4.69 (d, *J* = 9.6 Hz, 1H, H4 Amp), 4.68 (m, 1H, Hα Asp), 4.62 (dd, *J* = 8.9, 6.5 Hz, 1H, H2 Amp), 3.90 (dd, *J* = 11.9, 6.4 Hz, 1H, Hβ Asp), 3.82 (m, 1H, Hα Leu), 3.74 (dd, *J* = 8.5, 4.0 Hz, 1H, Hα Val), 3.69 (s, 2H, H1' MPUPA), 3.67 (d, *J* = 11.9 Hz, 1H, Hβ Asp), 3.00 (dd, *J* = 17.0, 8.8 Hz, 1H, H5 Amp), 2.69 (dd, *J* = 17.0, 6.4 Hz, 1H, H5 Amp), 2.48 (ddd, *J* = 14.3, 10.3, 6,7 Hz, H3 Amp), 2.31 (s, 3H, H8' MPUPA), 2.31 (m, 1H, Hβ Leu), 2.11 (d, *J* = 14.2 Hz, 1H, H3 Amp), 1.98 (m, 1H, Hβ Val), 1.87 (m, 1H, Hβ Leu), 1.70 (m, 1H, Hγ Leu), 1.10 (d, *J* = 6.8 Hz, 3H, CH_3 Val), 1.02 (d, *J* = 6.8 Hz, 3H, CH_3 Val), 0.92 (d, *J* = 6.8 Hz, 6H, $2CH_3$ Leu). $[\alpha]_D^{25}$:–24 (*c* 1.0, MeOH)

c[(MPUPA)AmpVEL] (15)

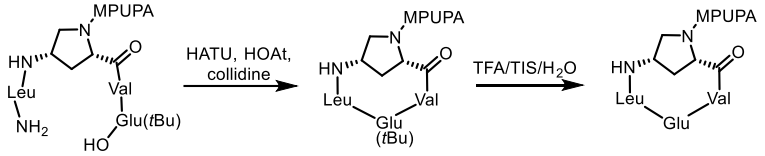

Compound **35** was prepared according to the general procedure B. A solution of linear peptide **28** (13 mg, 0.02 mmol) and 2,4,6-collidine (5.5 µL, 0.04 mmol) in dry DCM/DMF solvent mixture (0.5 mL /0.1 mL) was added dropwise to a solution of HATU (13 mg, 0.03 mmol) and HOAt (5 mg, 0.03 mmol) in dry DCM/DMF solvent mixture (2 mL /0.2 mL). After RP-flash chromatography, the protected cyclic peptide **35** (5.6 mg, yield 44%) was obtained as a white solid. MS (ESI$^+$) *m/z* = 776.4 $[M+H]^+$.

Compound **15** was prepared according to the general procedure C. The protected cyclic intermediate **35** (8 mg, 0.01 mmol) was treated 0.55 mL of TFA/TIS/H_2O (95:2.5:2.5) mixture and after preparative RP-HPLC purification (R_t = 24.6 min), cyclic peptide **15** (1.9 mg, yield 26%) was obtained as a white glassy solid. MS (ESI$^+$) *m/z* = 720.3 $[M+H]^+$.

^{1}H NMR (MeOD, 400 MHz) δ 7.64 (dd, *J* = 8.0, 1.4 Hz, 1H, H4' MPUPA), 7.40 (m, 2H, H3' MPUPA), 7.22 (m, 2H, H2' MPUPA), 7.18 (m, 1H, H5' MPUPA), 7.13 (d, *J* = 8.5 Hz, 1H, H7' MPUPA), 7.04 (ddd, *J* = 7.3, 7.3, 1.1 Hz, 1H, H6' MPUPA), 4.74 (m, 1H, H4 Amp), 4.68 (d, *J* = 9.8 Hz, 1H, H2 Amp), 4.31 (t, *J* = 8.4 Hz, 1H, Hα Glu), 3.93 (dd, J = 11.4, 6.3 Hz, 1H, H5 Amp), 3.85 (m, 1H, Hα Leu), 3.71 (m, 1H, Hα Val), 3.69 (s, 2H, H1' MPUPA), 3.69 (m, 1H, H5 Amp), 2.48 (m, 1H, H3 Amp), 2.31 (s, 3H, H8' MPUPA), 2.31 (m, 2H, Hγ Glu), 2.07 (m, 1H, H3 Amp), 2.02 (m, 2H, Hβ Glu), 2.01 (m, 1H, Hβ Val), 1.77 (m, 2H, Hβ Leu), 1.61 (m, 1H, Hγ Leu), 1.10 (m, 6H, $2CH_3$ Val), 0.93 (m, 6H, $2CH_3$ Leu). $[\alpha]_D^{25}$: –38 (*c* 1.0, MeOH)

c[(MPUPA)AmpRGD] (16)

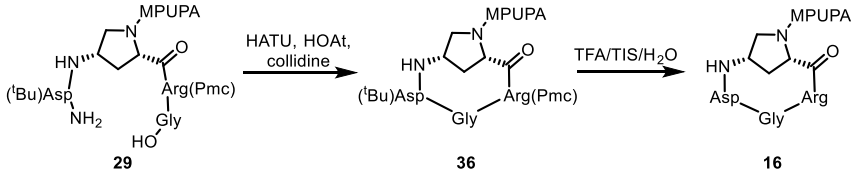

Compound **36** was prepared according to the general procedure B. A solution of linear peptide **29** (20 mg, 0.02 mmol) and 2,4,6-collidine (6.3 µL, 0.05 mmol) in dry DCM/DMF solvent mixture (1.5 mL /0.3 mL) was added dropwise to a solution of HATU (14 mg, 0.04 mmol) and HOAt (5 mg, 0.04 mmol) in dry DCM/DMF solvent mixture (4 mL /0.4 mL). After RP-flash chromatography, the protected cyclic peptide **36** (10.9 mg, yield 51%) was obtained as a white solid. MS (ESI$^+$) *m/z* = 1028.5 $[M+H]^+$.

Compound **16** was prepared according to the general procedure C. The protected cyclic intermediate **36** (10 mg, 0.01 mmol) was treated 0.55 mL of TFA/TIS/H_2O (95:2.5:2.5) mixture and after preparative RP-HPLC purification (R_t = 22.1 min), cyclic peptide **16** (3.6 mg, yield 52%) was obtained as a yellowish glassy solid. MS (ESI$^+$) *m/z* = 707.3 $[M+H]^+$.

^{1}H NMR (MeOD, 400 MHz) δ 7.64 (d, *J* = 8.0 Hz, 1H, H4' MPUPA), 7.41 (d, *J* = 8.5 Hz, 2H, H3' MPUPA), 7.21 (d, *J* = 8.6 Hz, 2H, H2' MPUPA), 7.18 (dd, J = 7.9, 7.9 Hz, 1H, H5' MPUPA), 7.13 (d, *J* = 8.5 Hz, 1H, H7' MPUPA), 7.04 (dd, *J* = 7.3, 7.3 Hz, 1H, H6' MPUPA), 4.71 (t, *J* = 5.6 Hz, 1H, Hα Asp), 4.66 (d, *J* = 9.5 Hz, 1H, H2 Amp), 4.59 (t, *J* = 6.0 Hz, 1H, H4 Amp), 4.19 (d, *J* = 13.8 Hz, 1H, Hα Gly), 4.09 (t, *J* = 6.8 Hz, 1H, Hα Arg), 3.93 (dd, *J* = 11.8, 6.4 Hz, 1H, H5 Amp), 3.70 (m, 3H, H1' MPUPA, H5 Amp), 3.42 (d, *J* = 13.8 Hz, 1H, Hα Gly), 3.20 (m, 2H, Hδ Arg), 2.81 (d, *J* = 5.7 Hz, 2H, Hβ Asp), 2.50 (m, 1H, H3 Amp), 2.31 (s, 3H, H8' MPUPA), 2.18 (d, *J* =14.4, 1H, H3 Amp), 1.76 (m, 2H, Hβ Arg), 1.65 (m, 2H, Hγ Arg). $[\alpha]_D^{25}$: –38 (*c* 1.0, MeOH)

2.6 References

(1) Tilley, J. W. *Expert Opin. Ther. Pat.* **2008**, *18* (8), 841–859.
(2) Kapp, T. G.; Rechenmacher, F.; Sobahi, T. R.; Kessler, H. *Expert Opin. Ther. Pat.* **2013**, *23* (10), 1273–1295.
(3) Arnaout, M. A. *F1000Research* **2016**, *5*, 1–13.
(4) Lin, K.; Ateeq, H. S.; Hsiung, S. H.; Chong, L. T.; Zimmerman, C. N.; Castro, A.; Lee, W.; Hammond, C. E.; Kalkunte, S.; Chen, L.; Pepinsky, R. B.; Leone, D. R.; Sprague, A. G.; Abraham, W. M.; Gill, A.; Lobb, R. R.; Adams, S. P. *J. Med. Chem* **1999**, *42*, 920–934.
(5) Erle, D. J.; Briskin, M. J.; Butcher, E. C.; Garcia-Pardo, A.; Lazarovits, A. I.; Tidswell, M. *J. Immunol.* **1994**, *153* (2), 517–528.
(6) Bochner, B. S.; Luscinskas, F. W.; Gimbrone, M. A.; Newman, W.; Sterbinsky, S. A.; Derse-Anthony, C. P.; Klunk, D.; Schleimer, R. P. *J. Exp. Med.* **1991**, *173*, 1553–1557.
(7) Abbas, A. K.; Lichtman, A. H.; Pillai, S. *Cellular and Molecular Immunology*, 9th ed.; Elsevier, Ed.
(8) Vanderslice, P.; Woodside, D. G. *Expert Opin. Investig. Drugs* **2006**, *15* (10), 1235–1255.
(9) Coussens, L. M.; Werb, Z. *Nature* **2002**, *420* (6917), 860–867.
(10) Garmy-Susini, B.; Jin, H.; Zhu, Y.; Sung, R.-J.; Hwang, R.; Varner, J. *J. Clin. Invest.* **2005**, *115* (6), 1542–1551.
(11) Shishido, S.; Bönig, H.; Kim, Y.-M. *Front. Oncol.* **2014**, *4* (99), 1–10.
(12) Jin, H.; Aiyer, A.; Su, J.; Borgstrom, P.; Stupack, D.; Friedlander, M.; Varner, J. *J. Clin. Invest.* **2006**, *116* (3), 652–662.
(13) Valcárcel, M.; Carrascal, T.; Crende, O.; Vidal-Vanaclocha, F. *J. Invest. Dermatol.* **2014**, *134* (2), 470–480.
(14) Steinman, L. *Nat. Rev. Drug Discov.* **2005**, *4* (6), 510–518.
(15) Ley, K.; Rivera-Nieves, J.; Sandborn, W. J.; Shattil, S. *Nat. Rev. Drug Discov.* **2016**, *15* (3), 173–183.
(16) Polman, C. H.; O'Connor, P.; Havrdova, E.; Hutchinson, M.; Kappos, L.; Miller, D. H.; Phillips, J. T.; Lublin, F. D.; Giovannoni, G.; Wajgt, A.; Toal, M.; Lynn, F.; Panzara, M. A.; Sandrock, A. *N. Engl. J. Med.* **2006**, *354* (9), 899–910.
(17) Dendrou, C. A.; Fugger, L.; Friese, M. A. *Nat. Rev. Immunol.* **2015**, *15* (9), 545–558.
(18) Winkelmann, A.; Loebermann, M.; Reisinger, E. C.; Hartung, H.-P.; Zettl, U. K. *Nat. Rev. Neurol.* **2016**, *12* (4), 217–233.
(19) Ransohoff, R. M. *Lancet Neurol.* **2010**, *9* (3), 231–233.
(20) Bloomgren, G.; Richman, S.; Hotermans, C.; Subramanyam, M.; Goelz, S.; Natarajan, A.; Lee, S.; Plavina, T.; Scanlon, J. V.; Sandrock, A.; Bozic, C. *N. Engl. J. Med.* **2012**, *366* (20), 1870–1880.
(21) Carson, K. R.; Focosi, D.; Major, E. O.; Petrini, M.; Richey, E. A.; West, D. P.; Bennett, C. L. *Lancet Oncol.* **2009**, *10* (8), 816–824.
(22) Yu, Y.; Schürpf, T.; Springer, T. A. *J. Biol. Chem.* **2013**, *288* (45), 32314–32325.
(23) Jackson, D. Y. *Curr. Pharm. Des.* **2002**, *8* (14), 1229–1253.
(24) Yang, G. X.; Hagmann, W. K. *Med. Res. Rev.* **2003**, *23* (3), 369–392.
(25) Desgrosellier, J. S.; Cheresh, D. *Nat. Rev. Cancer* **2010**, *10* (1), 9–22.
(26) Newham, P.; Craig, S. E.; Seddon, G. N.; Schofield, N. R.; Rees, A.; Edwards, R. M.; Jones, E. Y.; Humphries, M. J. *J. Biol. Chem.* **1997**, *272* (31), 19429–19440.
(27) Makarem, R.; Newham, P.; Askari, J. a; Green, L. J.; Clements, J.; Edwards, M.; Humphries, M. J.; Mould, a P. *J. Biol. Chem.* **1994**, *269* (6), 4005–4011.
(28) Yu, Y.; Zhu, J.; Mi, L. Z.; Walz, T.; Sun, H.; Chen, J. F.; Springer, T. A. *J. Cell Biol.* **2012**, *196* (1), 131–146.
(29) Tolomelli, A.; Baiula, M.; Viola, A.; Ferrazzano, L.; Gentilucci, L.; Dattoli, S. D.; Spampinato, S.; Juaristi, E.; Escudero, M. *ACS Med. Chem. Lett.* **2015**, *6* (6), 701–706.
(30) De Marco, R.; Tolomelli, A.; Juaristi, E.; Gentilucci, L. *Med. Res. Rev.* **2016**, *36* (3), 389–424.
(31) Gentilucci, L.; De Marco, R.; Cerisoli, L. *Curr. Pharm. Des.* **2010**, *16*, 3185–3203.
(32) Jackson, D. Y.; Quan, C.; Artis, D. R.; Rawson, T.; Blackburn, B.; Struble, M.; Fitzgerald, G.; Chan, K.; Mullins, S.; Burnier, J. P.; Fairbrother, W. J.; Clark, K.; Berisini, M.; Chui, H.; Renz, M.; Jones, S.; Fong, S. *J. Med. Chem.* **1997**, *40* (21), 3359–3368.
(33) Fotouhi, N.; Joshi, P.; Tilley, J. W.; Rowan, K.; Schwinge, V.; Wolitzky, B. *Bioorg. Med. Chem. Lett.* **2000**, *10*, 1167–1169.

(34) Fotouhi, N.; Joshi, P.; Fry, D.; Cook, C.; Tilley, J. W.; Kaplan, G.; Hanglow, A.; Rowan, K.; Schwinge, V.; Wolitzky, B. *Bioorganic Med. Chem. Lett.* **2000**, *10* (11), 1171–1173.
(35) Karanam, B. V; Jayraj, A.; Rabe, M.; Wang, Z.; Keohane, C.; Strauss, J.; Vincent, S. *Xenobiotica* **2007**, *37* (5), 487–502.
(36) Fisher, A. L.; DePuy, E.; Jayaraj, A.; Raab, C.; Braun, M.; Ellis-Hutchings, M.; Zhang, J.; Rogers, J. D.; Musson, D. G. *J. Pharm. Biomed. Anal.* **2002**, *27*, 57–71.
(37) Singh, J.; Van Vlijmen, H.; Liao, Y.; Lee, W. C.; Cornebise, M.; Harris, M.; Shu, I. H.; Gill, A.; Cuervo, J. H.; Abraham, W. M.; Adams, S. P. *J Med Chem* **2002**, *45* (14), 2988–2993.
(38) Lin, K. C.; Castro, A. C. *Curr. Opin. Chem. Biol.* **1998**, *2* (4), 453–457.
(39) Dattoli, S. D.; De Marco, R.; Baiula, M.; Spampinato, S.; Greco, A.; Tolomelli, A.; Gentilucci, L. *Eur. J. Med. Chem.* **2014**, *73*, 225–232.
(40) Setoguchi, M.; Iimura, S.; Sugimoto, Y.; Yoneda, Y.; Chiba, J.; Watanabe, T.; Muro, F.; Iigou, Y.; Takayama, G.; Yokoyama, M.; Taira, T.; Aonuma, M.; Takashi, T.; Nakayama, A.; Machinaga, N. *Bioorganic Med. Chem.* **2012**, *20*, 1201–1212.
(41) Zanardi, F.; Burreddu, P.; Rassu, G.; Auzzas, L.; Battistini, L.; Curti, C.; Sartori, A.; Nicastro, G.; Menchi, G.; Cini, N.; Bottonocetti, A.; Raspanti, S.; Casiraghi, G. *J. Med. Chem.* **2008**, *51* (6), 1771–1782.
(42) Battistini, L.; Burreddu, P.; Carta, P.; Rassu, G.; Auzzas, L.; Curti, C.; Zanardi, F.; Manzoni, L.; Araldi, E. M. V; Scolastico, C.; Casiraghi, G. *Org. Biomol. Chem.* **2009**, *7* (23), 4924–4935.
(43) Weis, S. M.; Cheresh, D. A. *Nat. Med.* **2011**, *17* (11), 1359–1370.
(44) Carmeliet, P.; Jain, R. K. *Nature* **2011**, *473* (7347), 298–307.
(45) Marinelli, L.; Lavecchia, A.; Gottschalk, K. E.; Novellino, E.; Kessler, H. *J. Med. Chem.* **2003**, *46* (21), 4393–4404.
(46) Carlevaro, C. M.; Martins-Da-Silva, J. H.; Savino, W.; Caffarena, E. R. *J. Theor. Comput. Chem.* **2013**, *12* (2), 1250108.
(47) Xiong, J.-P.; Stehle, T.; Zhang, R.; Joachimiak, A.; Frech, M.; Goodman, S. L.; Arnaout, M. A. *Science* **2002**, *296* (5565), 151–155.
(48) Irie, A.; Kamata, T.; Wilma, P.-M.; Takada, Y. *EMBO J.* **1995**, *14* (22), 5550–5556.
(49) Thakkar, A.; Trinh, T. B.; Pei, D. *ACS Comb. Sci.* **2013**, *15*, 120–129.
(50) Marsault, E.; Peterson, M. L. *J. Med. Chem.* **2011**, *54* (7), 1961–2004.
(51) Malesevic, M.; Strijowski, U.; Bächle, D.; Sewald, N. *J. Biotechnol.* **2004**, *112*, 73–77.

Acknowledgements

Firstly, I would like to acknowledge with gratitude my supervisor, Prof. Franca Zanardi, for giving me the opportunity to undertake the PhD study working in a really interesting research project. Thanks, Prof, for everything. Above all, for your kindness, patience and constant support.

I would also like to express my sincere gratitude to Prof. Andrea Sartori, my unofficial co-tutor, with whom I discussed any experimental problem during these years. His guidance, as well as for his precious suggestions, helped me in all the time of my doctorate.

I wish also to thank with deep gratitude Prof. Lucia Battistini and Prof. Claudio Curti, for sharing with me their time, experience and knowledge.

Special thanks to Dr. Nicoletta Brindani, because I could not have imagined having a better labmate.

I would also like to thank the Master's students with whom I was fortunate to collaborate in these three years as PhD student and who have contributed to this work. So, thanks are due to Valentina Beatrizzotti, Rocco Malavasi, Miriam Girardini and Andrea Ghidini.

I would like to thank all the scientists that collaborated and participated to this research work. In particular, I gratefully thank Dr. Francesca Bianchini (Università degli Studi di Firenze), Prof. Federica Vacondio (Università di Parma), Dr. Daniela Arosio (CNR-ISTM, Milano) and Dr. Agostino Bruno (Istituto FIRC di Oncologia Molecolare, IFOM, Milano).

I am grateful to Prof. Matteo Zanda (University of Aberdeen, Scotland, UK) for giving me the possibility to carry out a precious experience abroad, and meeting wonderful people: the Zanda's group members. Special thanks to Dr. Chiara Zanato, Dr. Sergio Dall'Angelo and Dr. Monica Piras for the scientific discussions, the help during lab work, and lunchtime conversations, always very funny. Thank you Ilaria Patruno, Beatrice Longo, Virginia Cristofori, Carlo De Dominicis, Alessandro Colombano, Dr. Manuele Musolino, Dr. Fernando Fernandez Diaz-Rullo, Dr. Chih-Chung Tseng and Dr. Debbie McLaggan, for making me feel at home from the first day and for leaving me a beautiful memory of this experience. I wish also to thank Michela Donnarumma for her friendship, and Dr. Massimiliano Baldassarre for his kindness, competence and fundamental assistance during the biological experiments.

I am also very grateful to Prof. Laura Belvisi (University of Milan) and Prof. Ernesto Occhiato (University of Florence), as external referees of my PhD thesis, for their painstaking revision work.

Grazie ad Anna Grazzi e Chiara Manzotti per essere amiche preziose, e a Mirco Lanzi per il suo costante ottimismo.

Grazie alla mia famiglia, che mi ha sempre supportato e sopportato in questi lunghi anni di studio.

FONDAZIONE CARIPARMA

Finally, I wish to thank with gratitude ***Fondazione Cariparma***, for having financed my PhD scholarship, allowing me to undertake this doctorate experience.